Aus der Augenklinik der Universität Rostock

Ex-vivo and In-vivo Characterization of Human Accommodation

Habilitationsschrift

zur

Erlangung des akademischen Grades

doctor rerum naturalium habilitatus / habilitata (Dr. rer. nat. habil.)

der Medizinischen Fakultät

der Universität Rostock

vorgelegt von
Oliver Stachs, geboren am 12.Oktober 1965 in Magdeburg
aus Rostock

Rostock, 15. Juni 2007

Gutachter:

- Herr Prof. Dr. med. Rudolf. F. Guthoff, Universität Rostock, Medizinische Fakultät, Augenklinik und Poliklinik
- Herr Prof. Dr. rer. nat. Thomas Gerber, Universität Rostock, Mathematisch-Naturwissenschaftliche Fakultät, Institut für Physik
- Herr Prof. Dr. Ing. Georg Bretthauer, Universität Karlsruhe, Institut für Angewandte Informatik / Automatisierungstechnik

Tag der Verteidigung: 24.06.2008

urn:nbn:de:gbv:28-diss2008-0093-2

TABLE OF CONTENTS

STUDY OBJECTIVES

Replacing the lens of a human eye by an artificial intraocular lens (IOL), either during cataract surgery or for other medical reasons, restores clear vision. Approximately 14 million IOL units were sold globally in 2005, producing 1.28 billion USD in total revenues. An aging global population, newly developed IOLs, and growing worldwide access to advanced medical technology are expected to produce a very high annual growth rate over the next years.

Efforts are being made on several fronts to develop even more advanced IOLs that mimic the natural lens, are injectable through a tiny incison, and restore accommodation. Today, technological developments with regard to phakic, accommodative, multifocal, adjustable and toric IOLs are being pursued along different tracks. The most immediate beneficiaries of new IOL designs are cataract patients seeking improved vision, thus eliminating the need to wear glasses. If these future IOLs perform according to expectation, cataract patients will experience significantly improved visual acuity and will be able to live without glasses. In order to surgically restore accommodation and to treat presbyopia, the process of accommodation and its loss in the aging eye must be understood. This is one objective of this contribution.

One of the greatest challenges of ophthalmology, especially of cataract surgery, is the restoration of accommodation in presbyopic eyes. There have been various attempts at solving this problem in order to enable far and near vision without glasses. However, optical or mechanical concepts have a limited accommodative ability. So far, the results of scleral or corneal techniques are doubtful. Concepts focusing on improved artificial lens materials are most promising, but are still at a very early experimental stage.

A completely satisfying approach to restoring accommodation still needs to be developed. Besides, there are considerable discrepancies between objective and subjective trials to evaluate the therapeutic success. A substantial biomechanical understanding of all structures and processes involved in accommodation as well as presbyopia are needed to develop promising new strategies. This contribution focuses on developing advanced imaging techniques (Ref. 1,2,13,14, 17)[A] to create a basic understanding of accommodation and presbyopia (Ref. 3, 4, 6, 7) and to evaluate existing concepts (Ref. 5,8-12,16) for restoring accommodation. Besides, the emphasis is also on replacing stiff presbyopic lenses by a material that imitates the young crystalline lens (Ref. 15).

To achieve the objectives, our research focused on the following aspects:

- Monitoring human ciliary muscle activity during accommodation
- Three-dimensional description of the structure of the human zonula
- Biomechanical modeling of the accommodative process
- Experimental simulation of accommodation
- Assessing accommodative biometric changes in phakic eyes
- Assessing potentially accommodating IOLs
- Drug-induced secondary cataract prevention in conjunction with lens refilling

[A] References 1-17 are found in the appendix and referred to in the text itself

INTRODUCTION

The eye as an optical instrument

Vision is indisputably one of our most important senses[B]. Impairment or loss of vision challenges the quality of life[C]. Besides, the visual system is extremely complex. Studies involving the eye therefore invariably cover various fields of science, including medicine, physics, pharmacology, and chemistry; a multidisciplinary approach is required in this context.

The eye is part of the body, it can not be understood without knowing about anatomy and physiology[1], not to forget chemistry and pharmacology[2]. The eye is an active optical instrument, its focusing ability (accommodation) cannot be understood without a background in physics, especially optics[3,4]. Fig. 1 shows Helmholtz' eye model, as modified by Laurence.

Retinal imaging is only one step of the visual process. The rod-and-cone system of the retina functions simultaneously to afford a kind of parallel processing; several pigments contribute to the cone reactions. Thus, the radiant energy of the incident light is transformed into electrical impulses that are passed on to the brain. The interaction of the retinal and neural processes is very complex and is currently being researched[5-7].

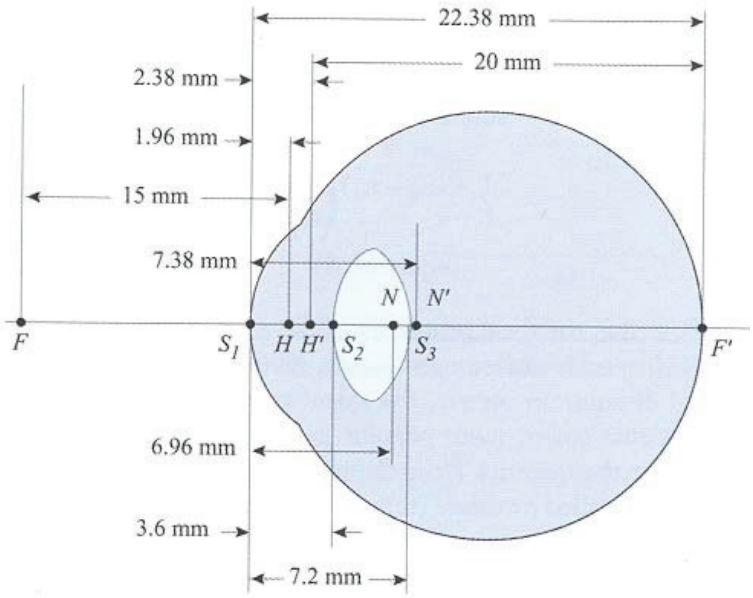

Fig. 1: Helmholtz' eye model as modified by Laurence[3]

[B] »Das Auge war vor allen anderen das Organ, womit ich die Welt fasste.«, Johann Wolfgang von Goethe, Dichtung und Wahrheit [The eye, in particular, was the organ through which I understood the world.] Goethe, Facts and Fiction

[C] »Das Auge gibt dem Körper Licht. Wenn dein Auge gesund ist, dann wird dein ganzer Körper hell sein. Wenn aber dein Auge krank ist, dann wird dein ganzer Körper finster sein.« [The eye gives light to the body. If your eye is healthy, then your entire body will be light. If, on the other hand, your eye is sick, then your whole body will be dark.] New Testament, Matthew 6,22-23 / Jesus: Sermon of the Mount

Human Accommodation and Presbyopia

Accommodation is a dynamic process, defined as an optical change of the power of the eye[8,9] originally described by Helmholtz in 1853[D] (Fig. 1). In the meantime, this theory has been confirmed by several authors[10-12].

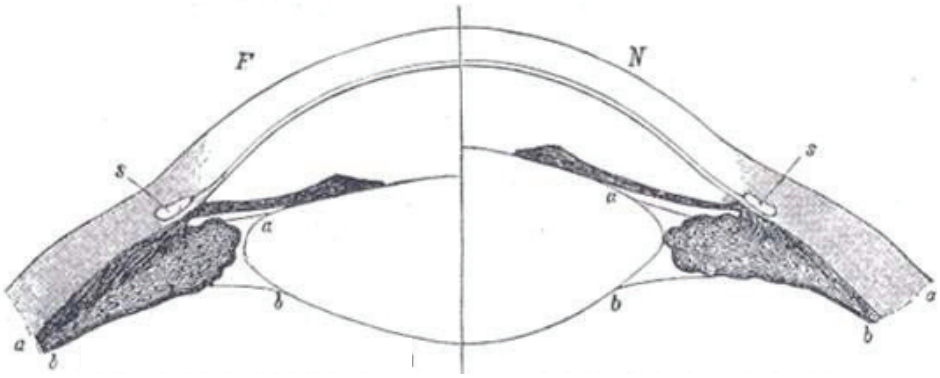

Fig. 2: Profile drawing of the lens in the accommodated and the unaccommodated state, respectively, according to Helmholtz's hypothesis described in 1853.

In a phakic eye of a young subject, contraction of the ciliary muscle moves the apex of the ciliary body to release at-rest zonular tension around the lens equator. Configuration changes of the ciliary muscle are shown in Fig. 14 as well as Refs. 2-4 and 6. These changes, together with the elastic lens capsule, allow the lens to assume the accommodative state[9,10].

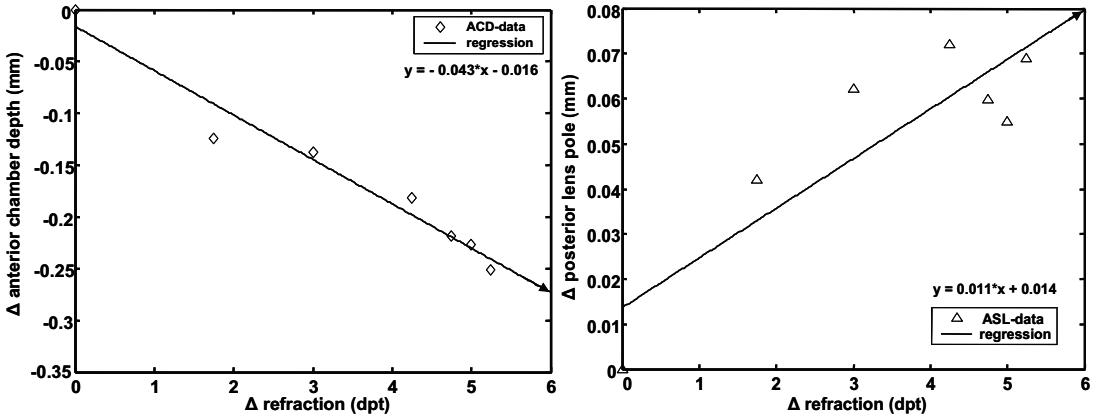

Fig. 3: Changes in anterior chamber depth and posterior lens pole position (measured by partial coherence interferometry) in relation to the refractive changes (measured with a Hartinger coincidence refractometer) of a 27-year-old subject (pharmacologically induced accommodation with 2% pilocarpine, negative values represent an anterior shift). Unpublished data.

During accommodation, the lens shows a decrease in equatorial diameter and an increase in axial thickness, associated with an anterior and posterior increase of the lens curvature[13-15]. These changes in lens thickness decrease the anterior chamber depth while increasing the

[D] »Ich halte es deshalb für wahrscheinlich, dass die Linse ihre Gestalt ändert, und beim Sehen in die Nähe nach vorn convexer wird. «, [I therefore consider it likely that the lens changes its shape, becoming more convex in front during near vision.] Bericht über die zur Bekanntmachung geeigneten Verhandlungen der Königl. Preus. Akademie der Wissenschaften zu Berlin [report on the publishable arguments of the Royal Prussian Academy of Sciences in Berlin] in the month of February, 1853

anterior segment length[14-16]. The optical power of the eye increases with the increasing lens surface curvature (see Figs. 3 and 4).

Presbyopia is loss of accommodation with age, an effect that has been attributed to alterations of the posterior attachment of the ciliary body[17,18], Young's modulus[19,20], and the geometry of the lens[21], respectively. Lens hardening is the generally accepted key factor of age-related loss of accommodation.

Concepts of Restoring Accommodation

During cataract surgery, an intraocular lens is implanted in the capsular bag. Despite excellent restoration of visual acuity and biocompatibility, no accommodation is detected in pseudophakic eyes, as the IOL optics change neither shape nor position in any way.

To restore accommodation in the human eye, the physiology of the accommodative structures must remain viable. Any residual activity needs to be utilized in order to design an implant to restore the accommodative ability.

Various attempts have been made to solve or bypass this problem:

- Monovision to correct presbyopia[22]
- Multifocal vision to correct presbyopia (lens-based[23,24], corneal[25])
- Laser treatment of the lens contents[26,27]
- Scleral expansion procedures[28,29]
- Accommodative intraocular lenses[30]
    - Single optic IOLs with flexible haptic support
    - Dual optic IOLs
    - Deformable Accommodating IOLs
    - Cubic optical elements (Alvarez principle)[31]
- Refilling the empty lens capsule (lens refilling, Phakoersatz)[32-36]
- Mechatronic concepts

These different attempts have met with varying success. Monovision is not physiological. Optical or mechanical concepts afford limited accommodative ability. Scleral or corneal concepts show doubtful results. Artificial lens material concepts are the most promising strategies, but they are still at a very early experimental stage.

All in all, todays' ophthalmologists have very limited means of helping their patients live without reading glasses. The list includes monovision, multifocality, and IOLs with flexible haptic support. Some techniques are associated with certain side effects in terms of contrast sensitivity. It is still impossible with these techniques to offer patients complete restoration of the accommodative eye function.

Accommodation and Pseudoaccommodation

Accommodation is a dynamic process, defined as optical change of the power of the eye. It is not the ability of distance-corrected eyes to have good near vision. The term pseudoaccommodation refers to the achievement of functional near vision in distance-corrected presbyopic eyes through nonaccommodating methods. These methods include multifocality, monovision, increased depth of field due to pupil size, and ocular aberrations. Pseudoaccommodation can provide functional near vision in a distance-corrected eye without effecting any physical changes in the refractive power of the eye. Objective methods distinguish true accommodative optical changes from pseudohakic effects that tend to improve near vision without accommodation.

The forward shift of so-called accommodative IOLs - such as the Crystalens™ - during accommodation is supposedly initiated by an increase in vitreous pressure as a result of mass redistribution during ciliary muscle contraction, as postulated by Coleman[37]. For example, the inventor claims that this lens[38] achieves excellent uncorrected far and near visual acuity on the basis of subjective evaluation methods. However, the validity of psychophysical methods of establishing true pseudophakic accommodation by optic shifts of accommodating IOLs is questionable because it depends mainly on depth of focus or pseudoaccommodation. The latter, in turn, correlates with numerous parameters, such as pupil size, astigmatism, and multifocality. The basic necessity for objective methods to assess IOL shifts or haptic angulation during ciliary muscle contraction is obvious. Objective accommodation measuring techniques[39] are certainly available. These include stimulating accommodation with trial lenses or pilocarpine and measuring the accommodative response with an objective optometer (Hartinger coincidence refractometer), partial coherence interferometry (AC-Master, Zeiss), or HF ultrasound.

METHODS

This chapter describes several techniques that were developed or were helpful in conjunction with this study.

Ultrasound in Ophthalmology

Ref. 17 contains a detailed overview about the history, the techniques, new developments, and clinical applications. The A-scan and B-scan formats have become, and remain, the bases of ophthalmic biometric applications and diagnostic imaging, respectively.

A-scans are displayed as a plot of echo amplitude along a single line. The distance to the tissue structure generating the echo can be determined by measuring the time interval between emission of the acoustic pulse and echo return. In 1957, Oksala and Lehtinen published a series of fundamental articles on the ophthalmic A-mode diagnostic method[40-42]. This method was further developed, especially in Europe[43], and was complemented by the diagnosis of orbital processes as well as biometry[44]. By the mid-1970s, ultrasound technology allowed the determination of the axial length in a clinical setting. This, in combination with corneal curvature measurements, gave rise to IOL power equations, several of which were proposed at that time. Currently, optical interferometry provides an alternative to ultrasound for the measurement of axial length. Optical techniques, while very accurate, cannot be used in the presence of opacities such as dense cataract.

The B-scan is a two-dimensional cross-sectional image created by mechanically sweeping the directional transducer axis around, covering an angle of typically 50 to 60º. G. Baum and J. Greenwood introduced their two-dimensional B-mode to ophthalmology[45]. Bronson[46] developed a hand-held contact B-mode transducer. This was the beginning of a sudden explosion of echographic diagnostic methods in ophthalmology. The real-time examination allows the evaluation of retinal detachment as well as vitreous membranes and makes it possible to visualize the pulsation of vessels in tumors.

In the early 1990s, ultrasound systems operating at 35–50MHz became available and were used for imaging the anterior segment of the eye, consisting of the cornea, the iris, the anterior chamber, the ciliary body, and the lens. Owing to the fact that attainable axial resolution is inversely related to the frequency, these systems provided a four- or five-fold improvement in resolution relative to the 10MHz scanners that had been used up until then. Since the first publication by Pavlin, Sherar, and Foster[47] on "*subsurface ultrasound microscopic imaging of the intact eye*" based on ophthalmic HF ultrasound in 1990, the cutting edge of ultrasound technology has been reached, which is still unsurpassed in terms of high-resolution ultrasound

imaging. The first commercial instrument manufactured by Zeiss-Humphrey was an upshot of research performed by Pavlin and Foster; it became a popular tool to investigate the pathology of the anterior segment, such as glaucoma, tumors, and cysts of the iris and ciliary body, hypotony, hyphaema, and trauma.

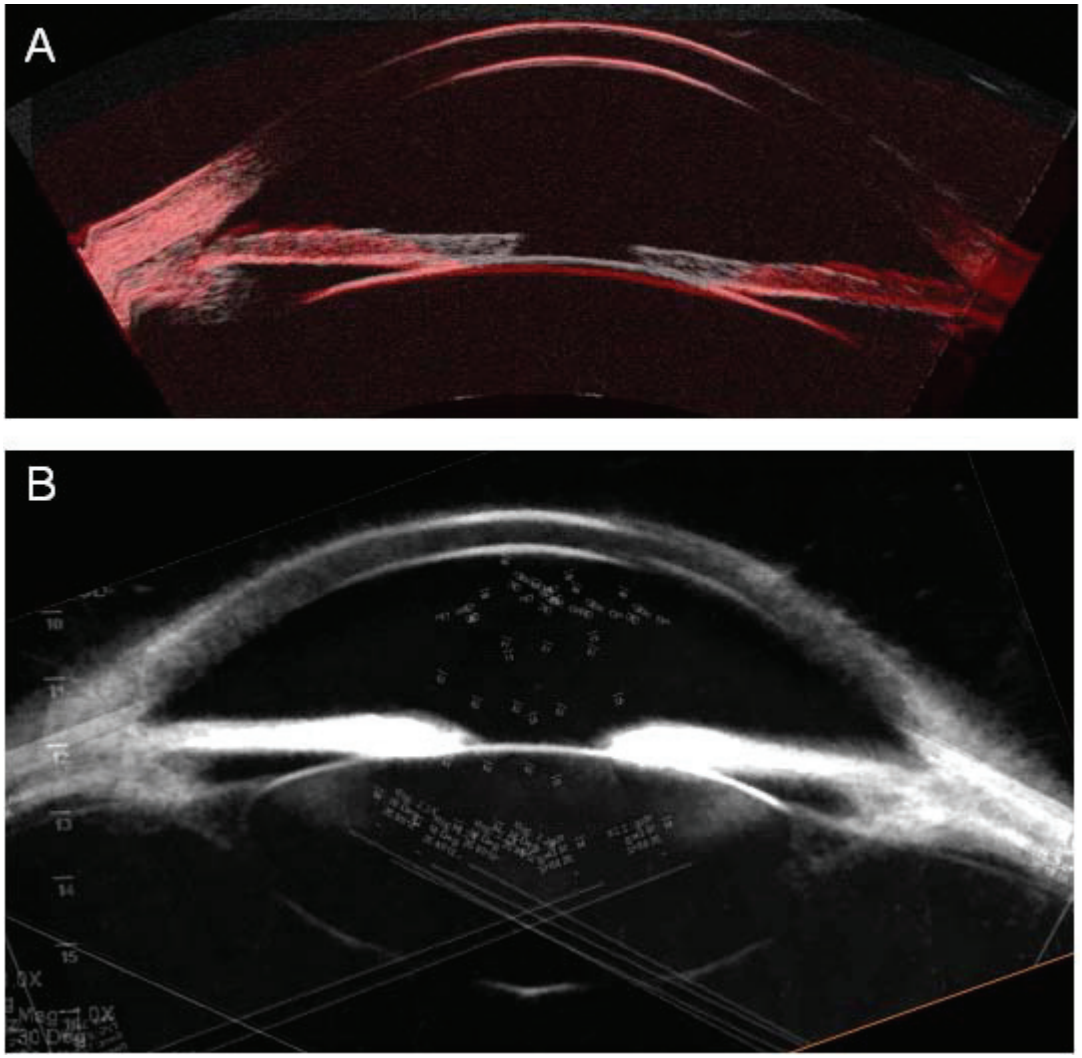

Fig. 4: A - Superimposition of cross-sections of the anterior segment during accommodation (gray) and disaccommodation (red), respectively; (Artemis-2, Ultralink). B – Superimposition of cross-sections for lens reconstruction (VuMax II, Sonomed). Unpublished data.

Refractive surgery presently is benefiting from results obtained by Coleman, Silverman, and Reinstein, based on the fact that high-frequency ultrasound arc scanning allows anterior segment imaging without any anamorphic distortion[48,49]. The authors developed an arc-shaped scan geometry allowing them to maintain constant range and a normal angle of incidence on the corneal surface[50]. This technology is called Artemis-2 and is manufactured by Ultralink LLC. The Artemis-2 not only makes it possible to quantitatively analyze the cornea, but it also helps to visualize the entire anterior segment in one single scan and is therefore useful for the measurement of angle-to-angle and sulcus-to-sulcus dimensions (that are crucial for the proper sizing of phakic lens implants) in conjunction with refractive correction. Fig. 4 exemplifies anterior lens shapes during accommodation and disaccommodation.

It has long been appreciated that three-dimensional ultrasonic images can be obtained from an ordered series of scan planes. Iezzi[51] first applied this technique to the anterior segment of the eye, which required considerable effort and ingenuity with regard to the instrumentation. Silverman[49] characterized the ciliary body, including the state of the ciliary processes of rabbits and normal human subjects using 3D high-resolution ultrasound. At the author's laboratory, an extension of the commercial Ultrasound Biomicroscope Model 840 (Humphrey Instruments, Carl Zeiss Group) was developed to obtain a user-friendly 3D- ultrasonic imaging system. In this case, 3D data sets consist of B-scan stacks of in-parallel planes with a defined distance between them. For 3D imaging, the computer-controlled scanning system moved the transducer perpendicularly (in z direction) to the B-scan plane (the xy plane) across the area being scanned. In conjunction with this movement, an additional miniature skid was mounted on the original linear motor of the UBM scanning device where the ultrasound transducer was attached. The video signal of the ultrasound unit was then digitized using a frame-grabber board (HaSoTec, Germany) synchronized with the z-motion control system. In other words, the z-movement is interrupted during image capturing and the image plane is oriented exactly perpendicularly to the z axis. AMIRA (TGS, San Diego, CA, USA) provides an interactive environment allowing features such as volume orientation for viewing planes and 3D perspectives, segmentation and determination of distances and surfaces. The modeling feature makes it possible to view anatomical structures in space and can be used for volume measurements.

Fig. 5, showing the anterior segment with the ciliary body, illustrates an example of 3D imaging. Several publications describe ex-vitro and in-vivo applications of these instruments[52-58] (Ref. 1-6,8,10). The investigations focus primarily on accommodation studies and the evaluation of so-called accommodative lenses.

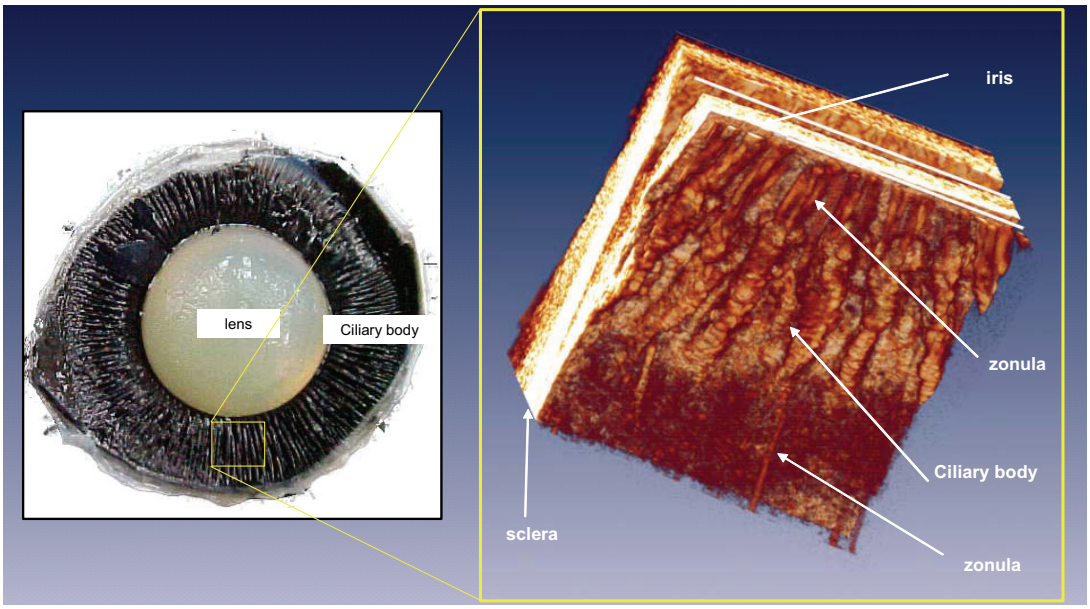

Fig. 5: 3D reconstruction of the human ciliary body (anterior segment viewed from behind).

Accommodation Measurement

The static accommodation response can be measured using a Hartinger coincidence refractometer (Fig. 6). This instrument is based on the Scheiner principle[59]. It requires subjective vernier alignment by the examiner but is totally objective with respect to the subject

and accurate to within 0.25 D[39]. The Hartinger is ideally suited to measure through small pupils larger than 2.0 mm in diameter. Negative-power trial lenses and pilocarpine can be used to subjectively and objectively stimulate accommodation when it is measured with the Hartinger. This instrument has been widely used to measure accommodation stimulated in a variety of ways in animals[10,11,60,61]and humans[39,62,62]. As shown in Fig. 7, this device was used on lens-refilled rabbit eyes in conjunction with a 2005 Rostock trial.

Dynamic accommodation can be measured using an infrared optometer, which operates according to the principle of a clinical retinoscope to measure the refractive power of the eye.

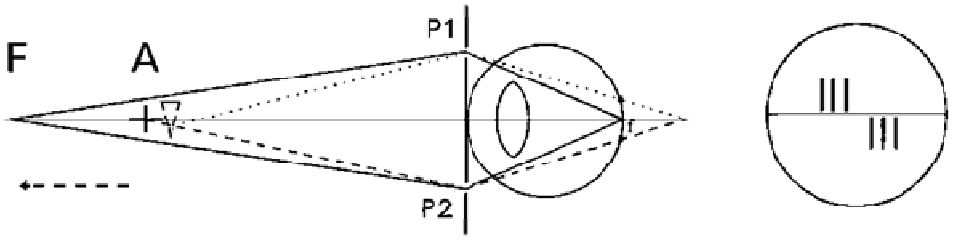

Fig. 6: Hartinger coincidence refractometer and the Scheiner principle. Above illustration shows a subject focused at F and viewing the target to align A. A prism placed at the upper half of target A gives rise to multiple light beams that are projected trough two pinholes. Two horizontal images are formed on the retina, as shown in the aligned target below. When A is shifted until it coincides with F, the two images are vertically aligned. The dial corresponding to the position of A provides a measure of the accommodation response that is accurate to within 0.25 D.

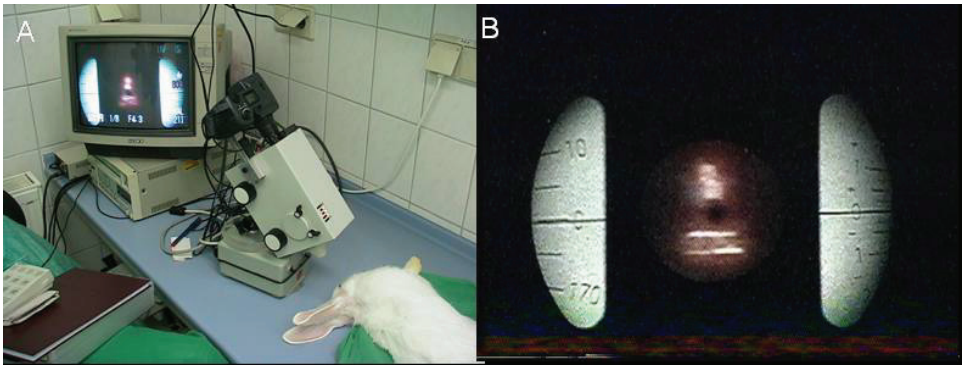

Fig. 7: Hartinger coincidence refractometer equipped with a CCD camera for rabbit experiments. Experimental setup (A), dial and aligned target in a rabbit eye, 12 weeks after lens refilling surgery (B).

Accommodation Simulation Device

The technique of mechanically stretching the lens to simulate accommodation can, of course, never precisely reflect the natural accommodation mechanism in the human eye. The results, however, may be used to design meaningful animal experiments.

Computer-controlled stretching devices were developed based on previous designs by Fisher, Glasser, Campbell, and Parel. Two designs devised in Rostock are shown in Figs. 8 and 9. Circumferential stretching is created by a stepper motor coupled to a digital outside micrometer for linear displacement and distance measurements. The instrument depicted in Fig. 9 is designed to measure the mechanical and optical properties of human donor lenses and refilled lenses.

The design shown in Fig. 8 was developed to investigate the performance of accommodative IOLs in an in authors laboratory developed artificial capsular bag. An IOL can be implanted in this capsular bag to simulate the accommodative process. The artificial capsular bag is shown in Fig. 7A. The main properties are summarized in Table 1.

Material	Nusil (Silicon Technology, France)
Equatorial internal diameter	9.5 mm
Capsular skin thickness	
Posterior	0.06 mm
Anterior	0.1 mm
Ring dimension	15.0 mm
Rhexis diameter	5.5 mm
Young's Modulus	0.25 MPa

Table1: Properties of the in-vitro capsular bag model (source: Ref. 8)

In order to analyze IOL performance, the artificial capsular bag is mounted in a simulation device (see Fig 8C). The arms of the fixture clamp the bag around its periphery, actually holding it at eight points. Rotation of the inner ring stretches or relaxes the bag. Inner ring rotation is accomplished by a stepping motor driving a worm gear. The amount of stretching correlates with the rotation of the inner ring. The entire arrangement is submerged in water for sonographic imaging. This device was used for the investigation of two commercially available IOL designs (AT45 and 1CU) published in Ref. 8 and 10.

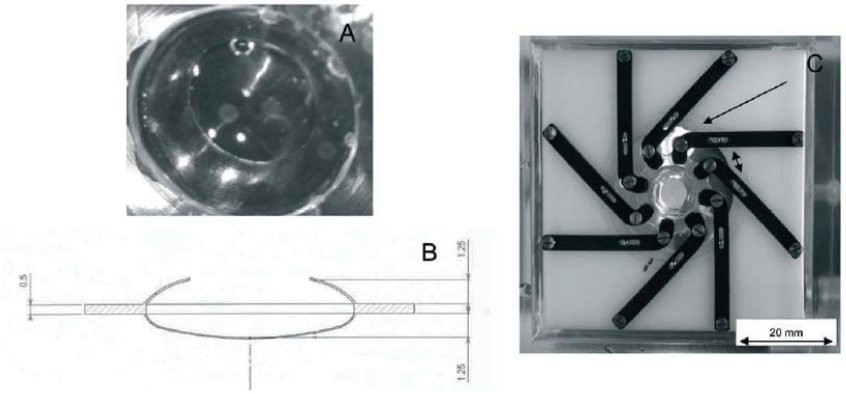

Fig. 8: A, B) Artificial capsular bag and C) stretching accommodation simulation device to investigate accommodative IOLs. The rotation of the inner ring with pins (indicated in image C) shifts the arms and stretches or relaxes the bag to simulate the force effects of the ciliary muscle. The 1CU IOL is implanted.

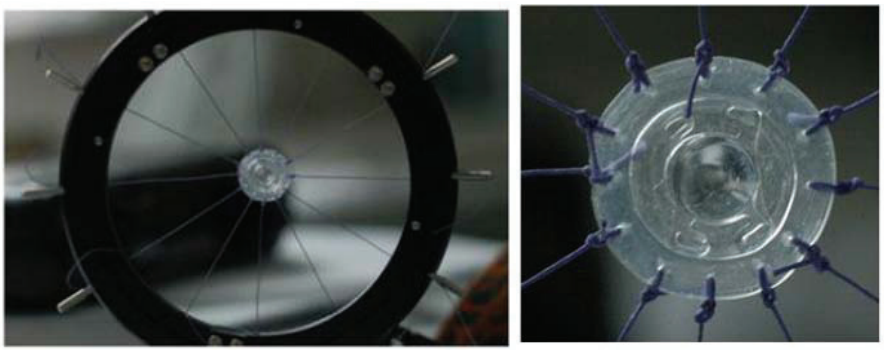

Fig.9: Second design of a stretching device based on previous designs by Fisher, Glasser, Campbell, and Parel

Scheimpflug Imaging

Scheimpflug systems are named after the inventor of the underlying optical principle, Theodor Scheimpflug, an Austrian general. This technique was patented in 1904. T. Scheimpflug invented the principle for adaptation in photographic cameras in order to take landscape photographs. Since then, the principle has been used in various contexts in conjunction with photography, especially to obtain a large depth of field.

In 1970, the first system for ophthalmic Scheimpflug imaging was developed based on results obtained by O. Hockwin. Mayer[63,64], for instance, published a detailed description of the Scheimpflug principle as used in ophthalmology. Since the first experiments with conventional photography, many researchers have applied digital imaging processing techniques to correct the images and to construct models of accommodation[65-67].

A new commercially available device (Pentacam, Oculus (Germany)) modeled on the Scheimpflug principle may be utilized for 3D imaging. While measuring and recording sectional images , the CCD camera rotates and provides sectional planes from the three spatial planes. The obtained measurements are then used to calculate a 3D model from which the anterior chamber depth, corneal pachymetry, and chamber angle can be computed.

In addition to its standard use in conjunction with human eyes, this instrument is also very useful for imaging the anterior segment in animal eyes (see Fig. 10), as it eliminates the need for interaction with the subject.

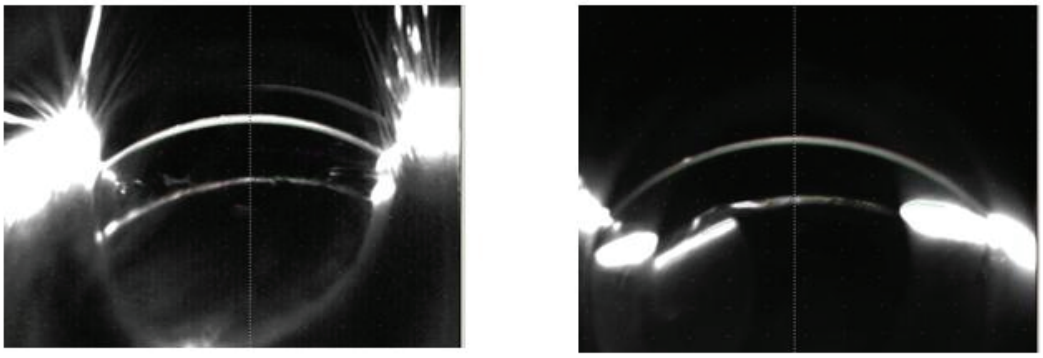

Fig. 10: Scheimpflug images of the anterior segment of two rabbit eyes after “lens refilling”, University of Rostock. Unpublished data.

Partial Coherence Interferometry

In the past few years, ultrasound has played a decisive role in the biometry of the anterior segment. Today there are various non-contact methods available. These are discussed in greater detail later in this text.

The highest axial resolution is achieved by partial coherence interferometry. The measuring principle in this case is derived from partially coherent interferometry and is implemented in an experimental device (AC-Master, Carl Zeiss Meditec (Germany)). A short coherence infrared laser beam is emitted by a luminescent diode and separated into two partial rays with different optical path lengths using a Michelson interferometer[68]. These partial rays are reflected onto different intraocular structures. An interference signal occurs and is recorded if the path difference between the partial rays is smaller than the coherence length. This instrument makes it possible to measure not only the anterior chamber depth but also the corneal and lens

thicknesses, measurements being obtained precisely along the optical axis[69,70]. For this purpose, the four Purkinje images resulting from reflection at the interfaces of the cornea and lens must be superimposed in conjunction with the measurement. During the examination the patient focuses on a mobile target inside the AC-Master, thus making it possible to superimpose the Purkinje images. A setup for simultaneously measuring the refraction (Hartinger) and the anterior segment biometry (AC Master) is given in Fig. 11.

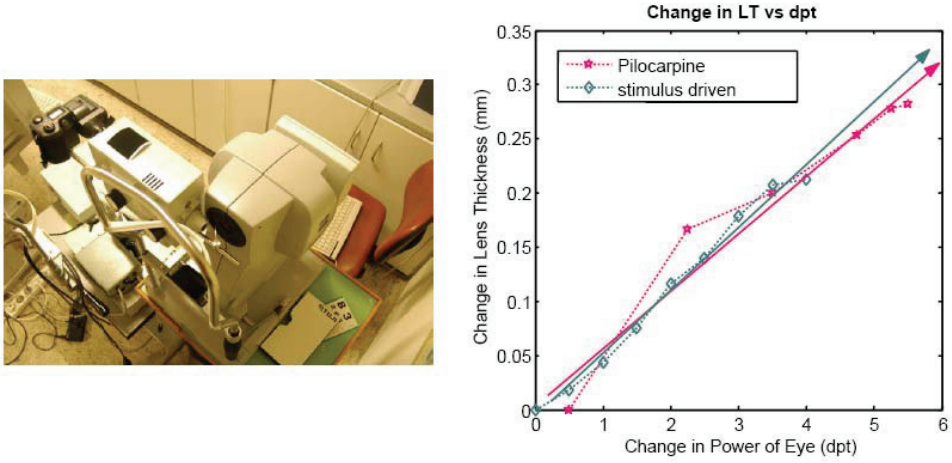

Fig. 11: Setup for simultaneously measuring the refraction (Hartinger) and the anterior segment biometry (AC Master) with a semitransparent mirror (left). The initial results are displayed on the right.

It should be pointed out that the IOL-Master (Carl Zeiss Meditec, Germany) uses PCI for axial length measurements but does not use partially coherent interferometry for measuring the anterior chamber depth (ACD). The ACD is measured by obtaining an "optical section" through the anterior chamber by means of a slit illumination system with subsequent image evaluation. The right eye is illuminated from the right-hand side, the left eye from the left. Measurements are obtained by image evaluation, illuminating the image at an angle of 30° relative to the optical axis. The standard biometrical anterior chamber depth is measured. Anatomically speaking, this is the anterior chamber depth plus the corneal thickness.

Anterior Segment Biometry

The exact measurement of the anterior chamber depth is of major importance in order to determine the actual position of the lens. This is of particular interest in conjunction with the assessment of accommodation-induced configurational changes of the phakic eye as well as potentially accommodative intraocular lenses based on the axial shift principle. Various intraocular lenses of this type were developed in recent years. Numerous studies focused on elucidating the accommodative ability of these lenses by measuring the anterior chamber depth[71-76]. A variety of methods were used, such as the IOLMaster[77], Orbscan[78], AC- Master[73-76], and the ultrasound technique[78]. Owing to this fact alone, different documented results are obtained on comparison of these studies[79,80].

In order to find out whether and in how far these methods are comparable in the first place, it is important to be aware of the optical interfaces detected by each approach, as well as the corrective factors utilized by the manufacturer specifically for the instrument in question as well as the pertinent technique.

Numerical Modeling of Accommodation

An understanding of lens changes during accommodation is fundamental for the development of these new generations of intraocular lenses for the treatment of presbyopia. Recently, attempts have been made to investigate human accommodation using numerical methods to model the optical performance of the eye. Significant studies were carried out using very simple models[37,81,82], while others used more complex models involving computer-aided design in combination with finite-element simulations[83-85].

Numerical modeling of biomechanical processes can, in general, lead to a better understanding of the processes being modeled. The sensitivity of the model with regard to the geometry as well as material properties can be quantified and used to fit experimental data. Numerical modeling, however, depends on the accuracy and quality of the data used in constructing the model. The material properties, the geometry, and the boundary condition assumptions are of particular importance. Thus, in creating a biomechanical model of the human accommodative system, the lens nucleus, the lens cortex, the lens capsule, the ciliary body, and the zonular fibers along with their geometrical and mechanical properties (e.g. Young's modulus, refraction index, stiffness) all have to be considered. Publications providing such data are few and far between, and there is very limited empirical information available on the required geometrical and material properties [83,84,86,87].

RESULTS AND DISCUSSION

This chapter presents the results in condensed form. For a better understanding, the results are discussed in their context here instead of a separate chapter.

Three-Dimensional Ultrasound Biomicroscopy to Study Accommodation

Ultrasound biomicroscopy has proven an important tool for investigating anterior segment structures with high spatial resolution. The first two-dimensional UBM investigations of the ciliary muscle in different accommodative states have been published[88-91]. The main problem and the primary source of error associated with two-dimensional ultrasonic imaging of the ciliary muscle in different states of accommodation lies in the dynamics of the accommodative process as well as the presence of the ciliary processes. These processes prevent precise quantification of the accommodative ciliary muscle changes. Additionally, differentiation is necessary to compare identical ciliary body sections. A 3D image analysis is necessary.

There is no commercially available device today for 3D high frequency ultrasonic imaging. The authors' laboratory developed a prototype scanning system for 3D imaging based on the Zeiss-Humphrey instrument into a user friendly 3D- ultrasonic imaging system. These systems, which generate high-resolution images, allowed the acquisition of scans in a series of ordered planes, ultimately affording 3-D images[55,57,58]. This principle is described in the publications 2 to 4. As an example, Fig. 12 shows an image of the anterior segment with the ciliary body and the zonula ciliaris. We will also show how to use this 3D technique in clinical routine work (Ref. 1) and to study the quantification of ciliary body function during accommodation (Refs. 2-4, 8, 10).

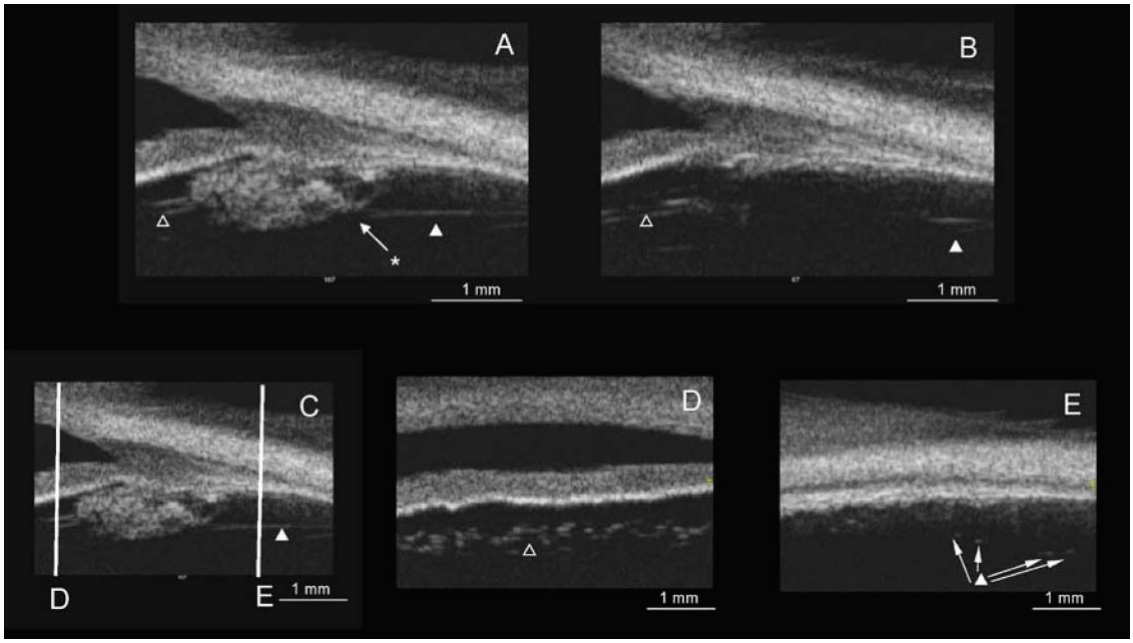

Fig. 12: Typical 3D-UBM sections across the human ciliary body. A section across the ciliary muscle with ciliary processes is shown in a, while only the ciliary muscle can be seen in the section depicted in b. Images d and e are the transverse sections marked in c. Zonular groups with differing orientations are marked (▲ ,△), Ref. 6

3D Ultrasound Biomicroscopy in Clinical Routine Work

Clinical UBM proves to be a highly powerful tool for the diagnosis of ocular diseases[92]. It has been used to investigate anatomical correlations with a variety of disorders, including anterior segment tumors, cysts, plateau iris, malignant glaucoma, and pigment dispersion syndrome.

Reference 1 shows the application of our developed technique for 3D imaging and points out the clinical benefit of this method in selected clinical cases. We demonstrated its value in three cases: zonulolysis after contusio bulbi, an iris tumor, and iris–ciliary body cysts; and we arrived at the conclusion that 3D UBM of the anterior eye segment provides clinically useful information regarding the size, the progress and the site of the existing pathology.

Monitoring Ciliary Muscle Activity During Accommodation

The mechanisms of human accommodation and the pathophysiology of presbyopia have been debated with surprising passion for nearly two centuries. Today we have two major approaches to intraocular presbyopia correction: first of all, attempts to develop accommodative IOL implants and, secondly, attempts at surgical restoration of accommodation. Before an artificial device to replace the lens can be developed, however, the influence of the aging ciliary muscle must be determined.

Table 2 provides an overview of studies concerning accommodation in human and monkey eyes. A variety of theories have been published and the question is all but settled. In general, many investigators agree with the Helmholtz explanation of accommodation[9].

While techniques for cataract surgery are constantly being improved, the exact accommodative mechanism and the cause of presbyopia remain to be elucidated. The possibility of surgical recovery of the power of accommodation makes it particularly interesting to study

accommodatively induced reactions. Besides, competitive hypotheses regarding the genesis of presbyopia, regression in accommodative amplitude caused by altered lens material properties as opposed to changed neuromuscular excitability, or contractibility of the ciliary muscle / the zonular fibers are still a matter of ongoing debate. The elusive details of the accommodative mechanism may primarily be attributed to the fact that direct observation of the ciliary muscle (see Fig. 13), due to its position behind the iris diaphragm, is very difficult. Observing the movement of the ciliary processes during accommodation, for instance by using a Scheimpflug camera, should not tempt us to conclude that the ciliary muscle necessarily also initiates this movement. It is possible to circumstantiate the ciliary muscle function using 3D-UBM (Ref. 2-4).

Study	Years	Method	Specimens	Ciliary muscle function
Stachs[93]	2002	UBM	10 persons 20-70 years	present with age-related decrease
Glasser[12]	2001	UBM, Video	Monkeys	present
Bacskulin[88]	2000	UBM	105 persons 10-91 years	present
Strenk[94]	1999	MRI	25 persons 22-83years	present
Bacskulin[89]	1996	UBM	10 persons 54-86 years	partially present
Kalman[95]	1993	Video	4 persons 16-48 years	present
Neider[67]	1990	Video	14 monkeys 1-24 years	present with age-related decrease
Lütjen-Drecoll [96,97]	1988	Morphological study	44 monkeys 0-35 years	muscle & nerve degeneration
Fischer[98]	1977	Model calculations	27 persons 15-55 years	present
Swegmark[99]	1969	Impedance cyclography	Persons up to 60 years of age	present

Table 2: Some of the studies concerning ciliary muscle activity published between 1996 and 2002

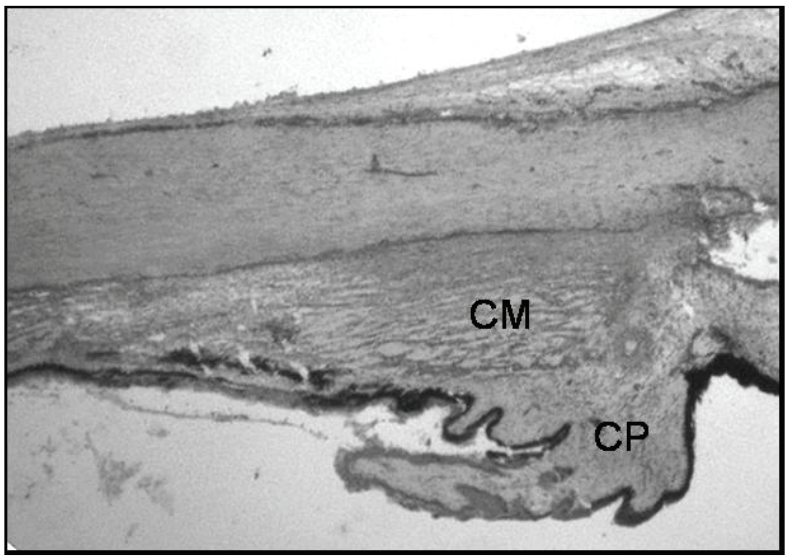

Fig. 13: The human ciliary body with the ciliary muscle (CM) and the ciliar processes (CP)

The possibility of differentiating between ciliary muscle sections with and without ciliary processes, respectively, proved that the muscle, during accommodation, effects a certain displacement in direction of the lens. The configurational differences of the muscle during accommodation and disaccommodation can be analyzed by contour recognition based on characteristic 2D parameters. Our investigations (Ref. 3) revealed significantly changing muscle configurations as well as changing characteristic positions on the ciliary muscle, demonstrating that this method allows in-vivo investigation and documentation of accommodative configurational changes of the ciliary muscle (Fig. 14). We have found a shift of the ciliary muscle center of gravity, which is a parameter reflecting the entire muscle contour in the direction of the lens equator. Values of this shift range between 0.04 and 0.26 mm, with a certain degree of individual variation and slightly decreasing tendency with age. This shift is diminished with increasing age, but it never disappears entirely. A certain degree of ciliary muscle activity is observed in young individuals as well as in those of presbyopic age. This muscle movement is less distinctive than muscle movements including ciliary processes; a fact that supports Hess and Fincham's early statements to the effect that the ciliary processes move in the direction of the lens during accommodation. This view was confirmed by Neider and Glasser, who studied iridectomized monkey eyes.

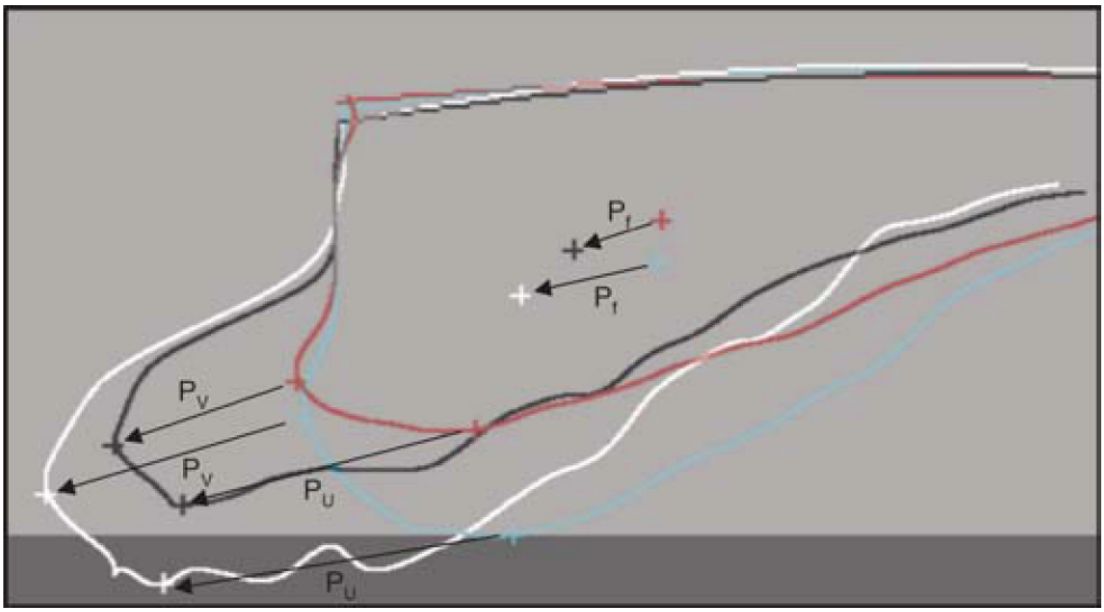

Fig. 14: Comparison of ciliary body contours during accommodation and disaccommodation, respectively (pharmacologically induced using 2% pilocarpine and 1% cyclopentolate). Accommodation shifts the ciliary muscle center of gravity toward the lens equator (ciliary muscle: red – disaccommodation, blue – disaccommodation; ciliary muscle with ciliary processes: black - accommodation, white – accommodation; (P_f center of gravity, P_v anterior contour point, P_u lower contour point)) (sources: Ref. 2-4).

Schachar[100], on the other hand, postulated that the valleculae of the ciliary body move away from the lens during accommodation. Our investigation published in Ref. 2-4 does not support Schachar's observation. We show a flattening of the valleculae which cannot be interpreted as a centrifugal movement away from the lens. This is also confirmed by analyzing the movement of the ciliary body center of gravity, which is the parameter describing the entire contour change.

Biomechanical Modeling of Accommodation

Our studies concerning the simulation of accommodation were to provide a more accurate description of the geometry and morphology of the zonula using three-dimensional ultrasound biomicroscopy and scanning electron microscopy to model the accommodative process. The results were published in Ref. 6.

Existing models provide a highly simplified and idealized description of the zonular apparatus. They are generally based on the assumptions of Farnsworth and Shyne[101], suggesting that three groups of zonular fibers exist: anterior, central, and posterior ones, at a ratio of 6:3:1. The movement of the ciliary muscle during accommodation was investigated[54,94], too, leading to the conclusion that there are age-related as well as inter-individual differences regarding the radius change of the ciliary body during accommodation. Very little information is available about the force exerted by the ciliary muscle on the zonular fibers. The position of the anchor point at the ciliary body of the zonular fibers is of particular importance with regard to the force transmission from the ciliary muscle to the lens.

Human eyes were examined without invasive manipulation using a custom-made 3D ultrasonic imaging technique that allows scanning of features with a spatial resolution of 30 µm. Environmental and conventional scanning electron microscopy (SEM) provided information to complement the ultrasonic images for use in the development of an anatomically more correct finite-element model of the zonular structures. This data, along with the material properties of the ocular tissue structures, was used to construct an advanced geometric model for finite-element simulation of the accommodative process.

Ciliary processes and zonular structures were clearly separated by both the 3D-UBM and the SEM methods. It was found that fibers inserting on the anterior and posterior lens capsule emerge from the anterior of the ciliary body. Fibers emerging near the pars plana insert on the lens and the ciliary body. No X-shaped crossing fibers were found.

This informative description of the accommodative apparatus, together with literature data, was used to construct numerical models of the human accommodative process. Thus, the models were based on the most up-to-date knowledge of the geometry and material properties of the tissue structures involved in accommodation. The FEM results indicate that a simplified model adequately describes the accommodative process under the given boundary conditions (Fig. 15). A more detailed zonular model produced comparable results. If numerical modeling is to be developed as a successfull approach to the investigation of presbyopia, then we will need high-quality experimental data (e.g., age-related mechanical and geometrical properties of the lens and zonules).

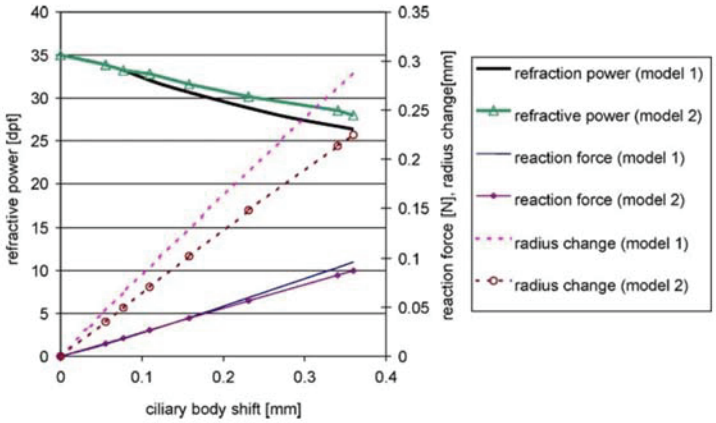

Fig 15: Calculated variation of refractive power, equatorial lens radius change, and total reaction force of the ciliary muscle with ciliary body movement in a 29-year-old lens. Model 1 assumes three sets of zonular fibers with a single anchor point; model 2 assumes ten sets of zonular fibers with multiple anchoring points (source: Ref. 6)

Evaluation of the Axial Shift Principle

IOLs were implanted in the capsular bag during cataract surgery. Despite excellent restoration of visual acuity and biocompatibility, these pseudophakic eyes show no accommodation, as the IOL optics alter neither their shape nor their position. Several attempts were made recently to achieve pseudophakic accommodation using different designs. The fundamental idea underlying all efforts to achieve potentially accommodating IOLs is to allow axial displacement of the IOL optics. The axial IOL movement induced by accommodation in human eyes has been quantified by ultrasound[78] and by dual-beam partial coherence interferometry[74-76]. However, high-frequency ultrasound is the only tool available to visualize the IOL haptic geometry hidden behind the iris diaphragm.

The first publication regarding this topic (Ref. 8) describes a trial where the described simulation device was used to study the IOL performance with an artificial capsular bag and a stretching device. The haptic region of the Akkommodative 1CU (HumanOptics AG) and CrystaLens AT-45 (Eyeonics Inc) was visualized in vitro in three dimensions. The simulation model revealed a maximum angulation change of 4.5° and 4.3° and a maximum forward shift of 0.33 mm and 0.28 mm for the AT-45 and the 1CU, respectively. The in-vitro results were then used to describe the in-vivo status of patients with accommodative implants (Ref. 8 and 10). In vivo, a change in haptic angulation <10° and a maximum forward shift of 0.50 mm were observed for the 1CU. These changes correspond to a theoretical approximate value of 0.50 diopters.

Another subsequent investigation (Ref. 12) aimed at determining pseudophakic accommodation in subjects implanted with the accommodative Human Optics 1 CU intraocular lens after drug-induced ciliary muscle stimulation by measuring the objective refraction and the changes in anterior chamber depth in comparison with a PMMA intraocular lens with rigid haptics. The 1 CU accommodative intraocular lens and the PMMA intraocular lens were implanted in 15 eyes of patients with an expected visual acuity of at least 0.7. Objective refraction under pilocarpine-stimulated ciliary muscle contraction was determined with a Hartinger coincidence refractometer. The anterior chamber depth was measured with Jäger's Haag–Streit slit-lamp attachment. The results reveal a mean anterior 1 CU shift of only 0.32 mm, with a maximum of 0.9 mm. The accommodative amplitudes measured with the Hartinger coincidence refractometer (mean value 0.47 D) correspond to these values.

We may conclude that the in-vitro mechanical performance of the investigated IOLs in these particular eyes does not appear to provide the range of accommodation that is needed for near vision. Results obtained with the AT 45 and the 1CU are discussed in detail in Ref. 8, 10, and 12. Ref. 8 was awarded with the 2005 Troutman Award of the IRS/AAO.

Evaluation of Biometric Methods of Measuring the Anterior Chamber Depth

Ref. 13 summarizes our observations regarding biometric methods of measuring the anterior chamber depth.

Basically, all these methods permit non-contact biometry of phakic eyes. The four methods in question differed systematically in terms of the median values of the anterior chamber depth (Fig. 16). The Bland–Altman plots (Ref. 13) for the combined data demonstrate the systematic differences between these four methods. There are no proportional or magnitude-related errors. The Pentacam generally measured the highest values, while the IOL-Master obtained the lowest values, with the slit-lamp pachymeter by Jaeger and the AC-Master operating approximately halfway between these two instruments with regard to ACD measurements.

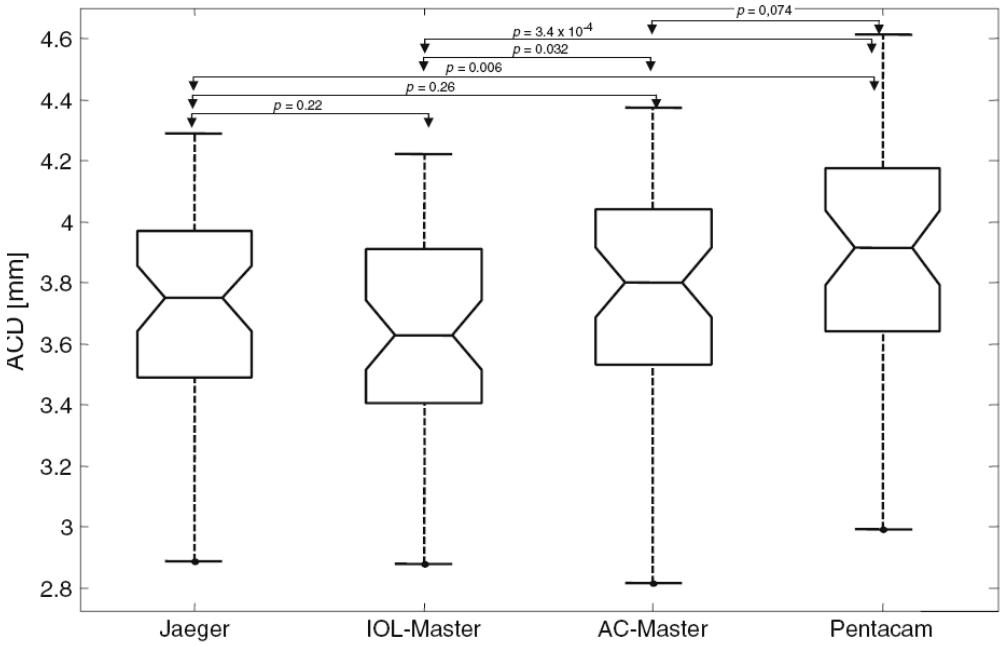

Fig 16: Box plots of the anterior chamber depths of 50 phakic eyes, measured with the slit-lamp pachymeter by Jaeger, the IOL-Master, the AC-Master, and the Pentacam, respectively. The graph shows the median values, the 25% and 75% quartiles, as well as the respective minimum and maximum values (source: Ref. 13).

The different physical measuring techniques and hence also instrument-specific corrective factors may possibly cause these systematic differences. Anterior chamber depth measurements with the IOL-Master are adapted to immersion ultrasound measurements by using corrective factors. In this context it should be noted that the IOL-Master does not use partial coherence interferometry, but employs a photographic technique to obtain ACD measurements instead. The AC-Master, which is based on partial coherence interferometry, utilizes the known refractive indices respectively the velocities of light in the ocular media at the relevant wavelengths. In this case, the values may be adapted to immersion ultrasound as well. Measurements with the Jaeger slit-lamp pachymeter are influenced by the corneal radius. Future identification of the optical interfaces detected by the various methods will be vital. It must be assumed, however, that the differences between the median and mean values obtained in this manner probably arise from the conversion of the original data. Basically, the velocity of light and sound in the respective ocular medium as well as their frequency distribution in the population, all of which need to be known, remain a challenge. Partial coherence interferometry involves measuring optical paths that are then converted into geometrical path lengths based on the refractive index. Ultrasound instruments, on the other hand, measure the transit time in the medium, and the geometric path is calculated via the sound velocity. The correlation with the results obtained in this context was not examined within the framework of this study.

Further investigations will be needed to elucidate this question. However, some of the studies available at this time show that optical measuring techniques like that of the IOL-Master are as independent of the researcher as possible[102]. With the Jaeger slit-lamp pachymeter, on the other hand, a certain subjective factor cannot be ruled out. The type of measuring axis can also create a bias. The AC-Master obtains all measurements along the optical axis, while the other instruments utilize the visual axis instead. All of the instruments used in this context had different targets fixed at infinite distance. It might, nevertheless, be possible to conclude different states of accommodation and, hence, different anterior chamber depths. Future

investigations should, if possible, also involve pharmacological deactivation, or the non-participating eye should focus on a fixed target which does not move.

With regard to reproducibility, it might be stated that the IOL-Master, the Pentacam and, above all, the AC-Master are very precise instruments for measuring the anterior chamber depth. Measurements with the AC-Master display by far the smallest standard deviation and are therefore highly reproducible. As an analog optical measuring method, the Jaeger slit-lamp pachymeter obtains the least reproducible results.

To summarize matters, our investigations show relatively large systematic deviations of the median of the empirically determined anterior chamber depths. This effect should be considered whenever anterior chamber measurements obtained by different techniques are to be compared. Anterior chamber depth measurements obtained with the IOL Master and the Pentacam require a relatively short learning curve and relatively little time. The slit-lamp pachymeter by Jaeger displays the lowest reproducibility and requires a certain degree of practice. The AC-Master necessitates a relatively high level of experience in the handling of the instrument and also calls for a high degree of patient compliance. This method benefits from its high precision as well as the fact that measurements are obtained along the optical axis.

Injectable Accommodative Lenses

The concept of replacing the stiff presbyopic lens with a material imitating the young crystalline lens is not a new one. A variety of pertinent publications are available.

Study	Specimens	Refilling material
Kessler[103]	Cadaver and rabbit	Immersion oil, silicone fluids, silastics
Agarwal[104]	-	Silicone elastomer
Parel[105]	Cadaver, cat, rabbit, monkey	Divinylmethylcyclosiloxane
Nishi[33,106-108]	Rabbit	Polymethyldisiloxane liquids
Stachs[109]	Rabbit	Polymer silicone material
Hettlich[34,110,111]	Rabbit	Monomer mixture (photopolymerization)
Haefliger[112,113]	Monkey	Silicone polymer gel
Koopmans[36,114]	Monkey	Polymer silicone material
Ravi[115,116]	Porcine cadaver	Polyethelene glycol-based hydrogels; acrylamide and bisacryloylhistamine-based hydrogels
de Groot[117]	In vitro	Isocyanate-crosslinked hydrogels derived from polyalcohols
Han[118]	In vitro, rabbit	Poloxamer hydrogel

Table 3: Fundamental studies regarding lens refilling procedures

In general, although each of the investigators (Table 3) successfully elucidated many of the ideal parameters, some major problems still remain:

- Creating a microcapsulorrhexis: An injectable gel lens requires a robust capsule and therefore a very small capsulorrhexis (< 2 mm), which necessitates innovative micro-instrumentation as well as extensive surgical training.
- Phacoemulsification through microcapsulorrhexis: Performing phacoemulsification through such a tiny capsulorrhexis presents a significant challenge. Although bimanual micro-incision techniques allow increasingly smaller incisions, performing the entire procedure through a sub 1 mm hole in the capsule requires an innovative approach.
- Sealing the microcapsulorrhexis: Sealing the microcapsulorrhexis to prevent leakage from the bag is a challenge.

- Polymer biocompatibility: Whatever gel material is selected, its biocompatibility is still essential and must be reliably established. Many of the materials used in current IOL designs have passed years of biocompatibility testing. This was accomplished by relying on materials that are used in other parts of the body as well; however, given the unique requirements of injectable gels, this is unlikely.
- Lens capsular volume variability: Lens capsular volumes vary widely among patients. In theory, only the optimum amount of gel allows the necessary changes in lens curvature. Controlling the injection of a gel with this much precision is a significant challenge.
- Polymer refraction: Achieving the desired refraction is not so easy, either. IOL lens power requirements vary widely among patients and determining the optimal amount of gel required to achieve the required power correction is a challenge.
- Preventing PCO: Finding a way to prevent PCO or ACO presents another significant challenge. With conventional IOLs, an Nd:YAG laser pulse can eliminate opacification; however, an injectable gel material would leak from the opening created with a laser.

The major problem seems to be PCO development because of the lens epithelial cells found on the inside of the capsular bag after phacoemulsification.

Opacification of the posterior capsule caused by postoperative proliferation of cells in the capsular bag remains the most frequent complication of cataract-intraocular lens surgery[119,120]. In addition to classic posterior capsular opacification (PCO, secondary cataract, after cataract), postoperative lens epithelial cell proliferation is also involved in the pathogenesis of anterior capsular opacification/fibrosis (ACO) as well as interlenticular opacification (ILO)[120-123]. Secondary cataract has been recognized since the origin of extracapsular cataract surgery and was noted by Ridley in conjunction with his very first IOL implantations[124,125]. This phenomenon was particularly common and severe in the early days of IOL surgery, when the importance of cortical cleanup was less appreciated. Through the 1980s and early 1990s, the incidence of PCO ranged between 25% and 50%[126,127]. PCO is a major problem in pediatric cataract surgery, where it occurs in almost 100% of all cases[128].

One of the crowning achievements of modern cataract surgery is the gradual, almost unnoticed decrease of this complication. The literature at present shows that with modern techniques and IOLs, the expected rate of PCO and the subsequent Nd: YAG laser posterior capsulotomy rate is now less than 10% .

There are a number of surgery-related and IOL-related factors to prevent posterior capsular opacification. Surgical factors include hydrodissection-enhanced cortical cleanup[129], in-the-bag (capsular) fixation[130], and the capsulorhexis edge on the IOL surface. Besides, there are basically three IOL-related factors to reduce PCO IOL biocompatibility[126], maximum IOL optic-posterior capsular contact[131,132], and the barrier effect of the IOL Optic[133,134]. But none of these techniques are suitable for lens refilling.

Another approach to prevent PCO involves the intraocular application of pharmacological agents[135,136]. For the 1980s, numerous investigators like Weller and Rieck[137,138] examined in cell culture studies the potential of pharmacological substances in order to successfully prevent LECs from proliferating and migrating. Pharmacologic agents that have been investigated include cytostatic drugs, such as 5-Fluorouracil[139,140], Daunomycin[137], Colchicine, Doxorubicin[141], Mitomycin C[139,142] , Methotrexate[143] , anti-inflammatory substances, such as Dexamethasone[144] and Diclofenac[144,145] , calcium-channel blockers, such as Mibefradil [146] and immunological agents, such as Cyclosporine A[147]. In addition adhesion inhibitors[148] and osmotic effective solutions [140] were tested. In several studies different drug delivery systems[149-152] were investigated in order to provide a longer and more effective impact on LECs.

The goal of the current study presented in paper 15 was to develop an ex vivo model by utilizing capsular rhexis specimens obtained during standard cataract surgery that can be tested for the ablation of LECs from the basal membrane. Since capsular rhexis specimens contain a

LEC layer on its natural substrate, the basal membrane, an effective cell ablation method established in the ex vivo model should also be effective in vivo.

To test the suitability of the model to differentiate drug effects on LECs of the capsular bag three pharmacological compounds known for their antiproliferative activity, Disulfiram, Methotrexate and Actinomycin D were tested for their effect on LEC ablation. Disulfiram, chemically tetraethylthiuramdisulfide (TETD), and its primary metabolite diethyldithiocarbamate are known to have in vitro antiproliferative effects on tumor cells, and inhibit several enzymes and cell proteins by formation of a metal complex or by reaction with functional sulfhydryl-groups. In addition it has been shown that a topical ocular drug delivery system containing TETD has anticataract effects in vivo on selenite-treated rats.

Methotrexate (MTX) is an antimetabolite drug used in treatment of cancer and autoimmune diseases. It acts by inhibiting the metabolism of folic acid. Based on research efforts in cancer chemotherapy, Hansen and co-workers[143] have found that a conjugate of MTX with an antibody specific for basement membrane collagen in the lens capsule is an effective inhibitor of LEC outgrowth in cell culture.

Actinomycin is any of a class of polypeptide antibiotics isolated from soil bacteria of the genus Streptomyces. As chemotherapeutic drug Actinomycin D (AM) intercalates into DNA, thereby interfering with the action of enzymes engaged in replication and transcription. Therefore it could be also an effective inhibitor of LEC viability.

Our in-vitro results regarding PCO preventation are summarized and discussed in detail in Ref. 15. Cultured capsular rhexis specimens from standard cataract surgery were used for these experiments. For the evaluation of the cell inhibitory and detaching potential of drugs the culture medium was replaced by different drug solutions. The specimens were incubated with these solutions for 5 minutes. The model drugs Disulfiram, Methotrexate and Actinomycin D were dissolved in pure water or were embedded in the hyaluronic acid (Healon^{TM}, AMO) in a drug concentration of 10µmol/l. After drug treatment the total number of residual cells on the surfaces of capsular rhexis specimens was assessed by use of microscopic methods. The residual viable and dead lens epithelial cells were differentiated by use of the Live-dead assay. Quantification of the lens epithelial cells was facilitated by staining with Hoechst-dye.

In summary, an ex vivo model was established which allows for the differentiation of drug action on lens epithelial cell ablation from the basal membrane. To estimate the effectiveness of drugs it was necessary to determine the cell numbers of untreated capsular rhexis specimens. The Live-dead assay on untreated capsular rhexis specimens has shown 1361 +/- 482 viable cells/mm^2. The treatment with Disulfiram, Methotrexate or Actinomycin D reduced the number of viable cells on capsular rhexis specimens drastically, because it ranges between 0.44 +/- 0.53 % (6.0 +/- 7.3 cells/mm^2) for Disulfiram, 0.27 +/-0.50 % (3.7 +/- 6.9 cells/mm^2) for Methotrexate and 0.07 +/- 0.19 % (0.1 +/- 0.27 cells/mm^2) for Actinomycin D. Of the three tested drugs Actinomycin D was slightly more potent in cell ablation than Disulfiram and Methotrexate.

Pure water is very effective with regard to in-vitro LEC cyclolysis and ablation. However, the in-vivo effectivity of pure water is known to be compromised by the diffusion of the body liquid, which is confirmed by our in-vivo observations of rabbit eyes. Fig. 17 shows rabbit eyes after lens refilling and pure water treatment (5 min) of the empty capsular bag in a study performed in Rostock. One month after surgery, the eyes were still clear, later to develop PCO three months postoperatively.

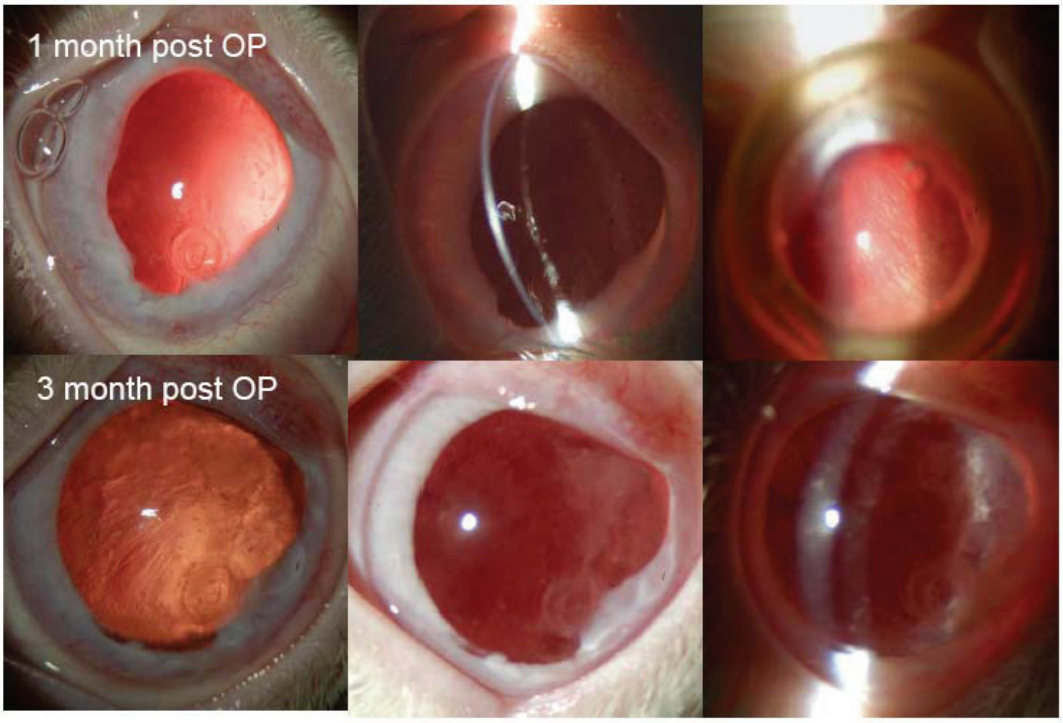

Fig. 17: Rabbit eye after lens refilling and capsular treatment with pure water, 1 month respectively 3 months postoperatively. Unpublished data.

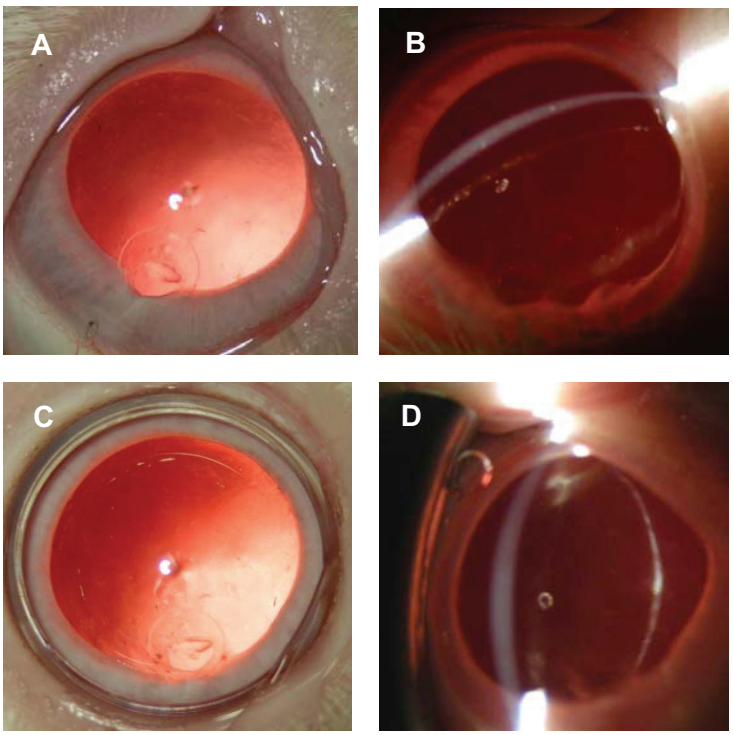

Fig. 18: Slit-lamp photographs of an eye with a refilled lens treated for 5 min with viscoelastic solution (Healon^{TM}, AMO) containing Actinomycin-D, obtained 9 (A,B) respectively 16 (C,D) months after surgery. No in-vivo leakage problems were observed. PCO and ACO were absent in all operated eyes. Unpublished data.

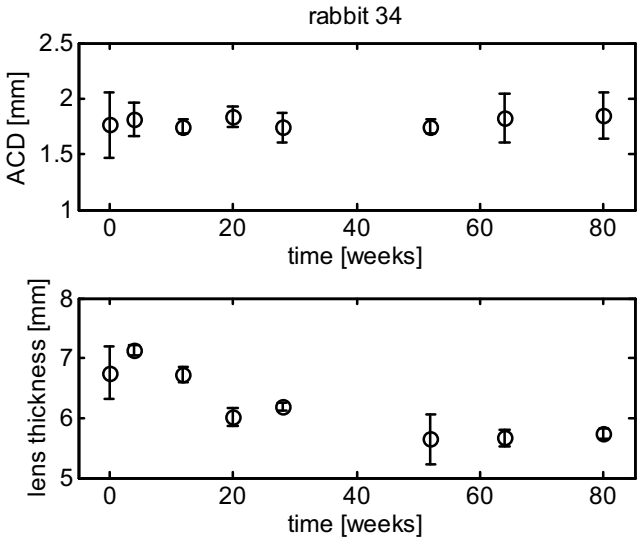

Fig. 19: Anterior chamber depth (ACD) and lens thickness (LT) of the refilled rabbit lenses from Fig. 18 during a follow-up period of up to 80 weeks. Unpublished data.

Based on the findings of paper 15 in several series of animal experiments, the empty capsular bag was exposed to a toxic Healon mixture for 5 min. After being 5 min treated with a viscoelastic solution (Healon^{TM}, AMO) containing Actinomycin-D, rabbit eyes - during the follow-up period of more than 16 months – show basically no PCO development (Fig. 18). PCO and ACO are absent in these operated eyes. No leakage problems were observed in vivo. Anterior chamber depth and lens thickness are shown in Fig. 19.

Another highly effective secondary cataract prevention technique involves treatment with a viscoelastic solution containing Methotrexate (MTX) and Actinomycin-D (AD). Up to 15 months after surgery, none of the eyes treated with an MTX + AD / Healon mixture show PCO or ACO development. There is a slight PCO in the rhexis and equatorial area (Fig. 20). Quite the reverse is true – within 6 weeks after surgery, rabbit eyes without capsular bag treatment develop considerable, if not massive PCO.

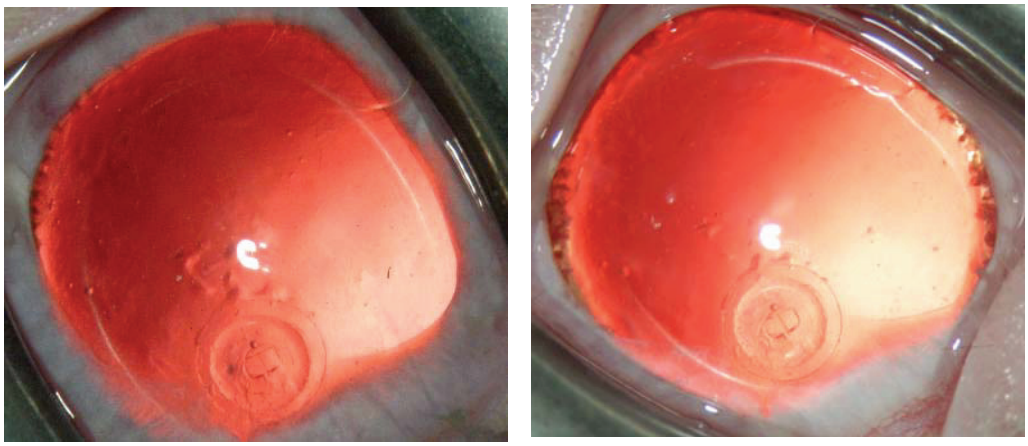

Fig. 20: Rabbit eye after lens refilling and capsular treatment with a viscoelastic solution containing D,L-Methotrexate (MTX) and Actinomycin-D (AD). The images were obtained 15 months postoperatively (left) respectively 2 years postoperatively (right). Unpublished data.

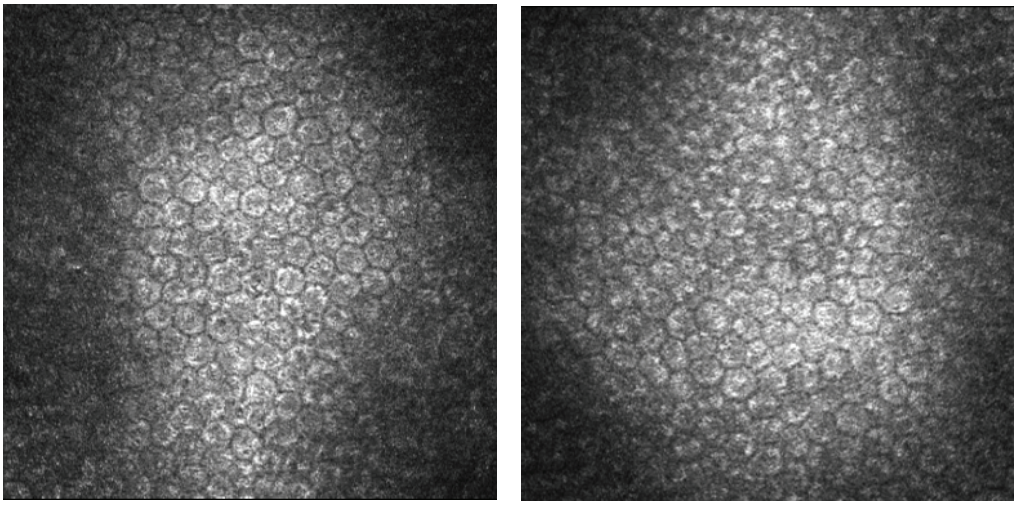

Fig. 21: Confocal microscopic images of the endothelium with the natural lens (left); the refilled lens was imaged 20 months after surgery (right). There is no difference with regard to the shape, the number, and the distribution of corneal endothelial cells. Unpublished data.

If the capsular bag is to be treated with a toxic agent, it is important to protect the corneal endothelium. In our rabbit experiments we used a viscoelastic agent (Healon^{TM}, AMO) as a carrier substance. As an indicator for a safe capsular bag treatment was investigated the corneal endothelium using an in house developed in vivo confocal microscopic technique[153]. Fig. 21 shows the endothelium in a natural rabbit eye respectively 20 months after lens refilling and MTX + AD tox treatment. Neither the shape nor the number and distribution of corneal endothelial cells had changed in any way preoperatively and postoperatively.

In general, rabbit eyes – without capsular bag treatment - are prone to considerable PCO development shortly after cataract surgery. These trials, performed with viscoelastic solution containing Actinomycin-D or Actinomycin-D and D,L-Methotrexate, were a good starting point for further mammal experiments. Further investigations involving non-human primates are needed to validate these results.

SUMMARY

These results suggest that accommodation can be restored and that new IOL designs, lens refilling techniques, or even entirely different approaches (e.g. mechatronic concepts, cubic optic elements) may improve lens performance and achieve clinical success in the future. We were able to demonstrate that the ciliary muscle remains active even at more advanced age. The results obtained by simulating accommodation based on our current knowledge of the pertinent biomechanical properties are compatible with Helmholtz' theory of accommodation, and they correspond to the empirical observations. We were also able to demonstrate that mechanical concepts based on the axial shift principle have very limited accommodative ability. This is consistent with the meta-analysis of peer-reviewed publications about these lenses. Thus, successful new concepts can only be developed with a thorough biomechanical understanding of all accommodative structures and processes as well as presbyopia. Sine qua non for all concepts is the control of the PCO problem.

Obviously, although subjective clinical results are important, objective methods really are essential to evaluate new design developments. A variety of instruments are available for objective accommodation measurements as well as mechanical performance.

To summarize matters, our study gave rise to the following conclusions:

- In order to surgically restore accommodation so as to treat presbyopia, we need to fully understand the loss of accommodation in the aging eye.
- When monitoring ciliary muscle activity, we need to differentiate between ciliary muscle sections with and without ciliary processes, respectively.
- During pharmacologically stimulated accommodation, the ciliary muscle moves centripetally in the direction of the lens, covering a distance between 0.04 and 0.26 mm, depending on the age and the subject.
- Accommodative ciliary muscle activity was observed even in presbyopic eyes, which goes to show that ciliary muscle activity is not the limiting factor in restoring accommodation.
- Attempts at restoring accommodation should be based on Helmholtz' theory of accommodation.
- The physiological magnitude of the refractive power changes can be explained by mathematical simulation according to Helmholtz' theory of accommodation.
- Artificial devices to simulate accommodation, including ocular tissue relevant for accommodation, may help us understand and evaluate new accommodative implants.
- To date, mechanical IOL concepts for so-called accommodative lenses have limited accommodative ability.
- New artificial lens materials (for lens refilling) are promising but are still at an early experimental stage.
- The capsular bag can be refilled with an artificial lens material, using a small opening. The capsular opacification problem, however, needs to be solved.
- In order to understand whether accommodation is restored by an artificial device, we need to demonstrate objectively that the eye undergoes an active change in optical refracting power during accommodation.
- In order to distinguish accommodation from pseudoaccommodation, we need objective methods to measure optical changes in refractive power or physical changes in the lens.

REFERENCES

1. Adler's Physiology of the Eye. Philadelphia, Pa, Mosby, 2003.
2. Clinical Ocular Pharmacology. Boston: Butterworth-Heinemann, 2001.
3. Arthur G B, Ronald B R. Bennett & Rabbetts' Clinical Visual Optics. Oxford: Butterworth-Heinemann, 1998.
4. Atchison D, Smith G. Optics of the human eye. Oxford: Butterworth-Heinemann, 2000.
5. Roska B, Molnar A, Werblin FS. Parallel processing in retinal ganglion cells: how integration of space-time patterns of excitation and inhibition form the spiking output. J Neurophysiol 2006;95:3810-3822.
6. Sjostrand FS. Contrast enhancement of the retinal image and image distortion associated with macular degeneration. J Submicrosc Cytol Pathol 2004;36:295-303.
7. Hartline HK. Visual receptors and retinal interaction. Science 1969;164:270-278.
8. Keeney A, Hagman R, Fratello C. Dictionary of Ophthalmic Optic. Newton, MA: Butterworth-Heinemann, 1995.
9. Helmholtz von H. Helmholtz's Treatise of Physiological Optics. New York, Dover: Southall JPC, 1909:143-173.
10. Glasser A, Kaufman PL. The mechanism of accommodation in primates. Ophthalmology 1999;106:863-872.
11. Croft MA, Glasser A, Kaufman PL. Accommodation and presbyopia. Int Ophthalmol Clin 2001;41:33-46.
12. Glasser A, Croft MA, Brumback L, Kaufman PL. Ultrasound biomicroscopy of the aging rhesus monkey ciliary region. Optom Vis Sci 2001;78:417-424.
13. Glasser A, Kaufman PL. The mechanism of accommodation in primates. Ophthalmology 1999;106:863-872.

14. Vilupuru AS, Glasser A. The relationship between refractive and biometric changes during Edinger-Westphal stimulated accommodation in rhesus monkeys. Exp Eye Res 2005;80:349-360.
15. Koeppl C, Findl O, Kriechbaum K, Drexler W. Comparison of pilocarpine-induced and stimulus-driven accommodation in phakic eyes. Exp Eye Res 2005;80:795-800.
16. Drexler W, Baumgartner A, Findl O, Hitzenberger CK, Fercher AF. Biometric investigation of changes in the anterior eye segment during accommodation. Vision Res 1997;37:2789-2800.
17. Lutjen-Drecoll E, Tamm E, Kaufman PL. Age-related loss of morphologic responses to pilocarpine in rhesus monkey ciliary muscle. Arch Ophthalmol 1988;106:1591-1598.
18. Tamm S, Tamm E, Rohen JW. Age-related changes of the human ciliary muscle. A quantitative morphometric study. Mech Ageing Dev 1992;62:209-221.
19. Heys KR, Cram SL, Truscott RJ. Massive increase in the stiffness of the human lens nucleus with age: the basis for presbyopia? Mol Vis 2004;10:956-963.
20. Glasser A, Campbell MC. Presbyopia and the optical changes in the human crystalline lens with age. Vision Res 1998;38:209-229.
21. Strenk SA, Strenk LM, Koretz JF. The mechanism of presbyopia. Prog Retin Eye Res 2005;24:379-393.
22. Azar D, Chang M, Kloek C, et al. Monovision refrative surgery for presbyopia. In Tsubota K, Boxer Wachler B, Azar D, Koch D, editors. Hyperopia & Presbyopia. New York, NY: Marcel Decker Inc., 2003:189-199.
23. Lane SS, Morris M, Nordan L, Packer M, Tarantino N, Wallace RB, III. Multifocal intraocular lenses. Ophthalmol Clin North Am 2006;19:89-105, vi.
24. Leyland M, Zinicola E. Multifocal versus monofocal intraocular lenses in cataract surgery: a systematic review. Ophthalmology 2003;110:1789-1798.
25. Baikoff G. Surgical treatment of presbyopia: scleral, corneal, and lenticular. Curr Opin Ophthalmol 2004;15:365-369.
26. Myers RI, Krueger RR. Novel approaches to correction of presbyopia with laser modification of the crystalline lens. J Refract Surg 1998;14:136-139.
27. Krueger RR, Kuszak J, Lubatschowski H, Myers RI, Ripken T, Heisterkamp A. First safety study of femtosecond laser photodisruption in animal lenses: tissue morphology and cataractogenesis. J Cataract Refract Surg 2005;31:2386-2394.
28. Schachar RA. Cause and treatment of presbyopia with a method for increasing the amplitude of accommodation. Ann Ophthalmol 1992;24:445-7, 452.
29. Mathews S. Scleral expansion surgery does not restore accommodation in human presbyopia. Ophthalmology 1999;106:873-877.
30. Dick HB. Accommodative intraocular lenses: current status. Curr Opin Ophthalmol 2005;16:8-26.
31. AN S, M R, G V, M L. Varifocal optics for a novel accommodative intraocular lens. Proceedings of SPIE 2006;6113.
32. Hara T, Sakka Y, Hayashi F. Electric double-sleeved vacuuming microtrephine for lens refilling. J Cataract Refract Surg 2000;26:1717-1721.
33. Nishi O, Nishi K, Mano C, Ichihara M, Honda T. Controlling the capsular shape in lens refilling. Arch Ophthalmol 1997;115:507-510.
34. Hettlich HJ, Lucke K, Kreiner CF. Light-induced endocapsular polymerization of injectable lens refilling materials. Ger J Ophthalmol 1992;1:346-349.
35. Kessler J. Lens refilling and regrowth of lens substance in the rabbit eye. Ann Ophthalmol 1975;7:1059-1062.
36. Koopmans SA, Terwee T, Haitjema HJ, Deuring H, Aarle S, Kooijman AC. Relation between injected volume and optical parameters in refilled isolated porcine lenses. Ophthalmic Physiol Opt 2004;24:572-579.
37. Coleman DJ. On the hydraulic suspension theory of accommodation. Trans Am Ophthalmol Soc 1986;84:846-868.
38. Cumming JS, Slade SG, Chayet A. Clinical evaluation of the model AT-45 silicone accommodating intraocular lens: results of feasibility and the initial phase of a Food and Drug Administration clinical trial. Ophthalmology 2001;108:2005-2009.
39. Wold JE, Hu A, Chen S, Glasser A. Subjective and objective measurement of human accommodative amplitude. J Cataract Refract Surg 2003;29:1878-1888.
40. Oksala A, Lehtinen A. Diagnostics of detachment of the retina by means of ultrasound. Acta Ophthalmol (Copenh) 1957;35:461-467.
41. Oksala A, Lehtinen A. Measurement of the velocity of sound in some parts of the eye. Acta Ophthalmol (Copenh) 1958;36:633-639.
42. Oksala A, Lehtinen A. Diagnostics of rupture of the sclera by means of ultrasound. Acta Ophthalmol (Copenh) 1958;36:37-42.
43. Ossoinig KC. Standardized echography: basic principles, clinical applications, and results. Int Ophthalmol Clin 1979;19:127-210.
44. Gernet H. [Ultrasonic biometry of the eye]. Klin Monatsbl Augenheilkd 1967;151:853-871.
45. Baum G, Greenwood I. Ultrasound in opthalmology. Am J Ophthalmol 1960;49:249-261.

46. Bronson, N., Fisher, Y., Pickering, N., and Trayner, N. Ophthalmic contact B-scan ultrasonography. 1976. Westport CT; Intercontinental.
Ref Type: Generic
47. Pavlin CJ, Sherar MD, Foster FS. Subsurface ultrasound microscopic imaging of the intact eye. Ophthalmology 1990;97:244-250.
48. Coleman DJ, Woods S, Rondeau MJ, Silverman RH. Ophthalmic ultrasonography. Radiol Clin North Am 1992;30:1105-1114.
49. Silverman RH, Rondeau MJ, Lizzi FL, Coleman DJ. Three-dimensional high-frequency ultrasonic parameter imaging of anterior segment pathology. Ophthalmology 1995;102:837-843.
50. Reinstein DZ, Silverman RH, Raevsky T, Simoni GJ, Lloyd HO, Najafi DJ, Rondeau MJ, Coleman DJ. Arc-scanning very high-frequency digital ultrasound for 3D pachymetric mapping of the corneal epithelium and stroma in laser in situ keratomileusis. J Refract Surg 2000;16:414-430.
51. Iezzi R, Rosen RB, Tello C, Liebmann J, Walsh JB, Ritch R. Personal computer-based 3-dimensional ultrasound biomicroscopy of the anterior segment. Arch Ophthalmol 1996;114:520-524.
52. Kirchhoff A, Stachs O, Guthoff R. Three-dimensional ultrasound findings of the posterior iris region. Graefes Arch Clin Exp Ophthalmol 2001;239:968-971.
53. Stachs O, Martin H, Terwee T, Schmitz K, Guthoff RF. 3d ultrasound biomicroscopy as a basis for fem simulations of the accommodation process. Invest Ophthalmol Vis Sci 2002;43:U82.
54. Stachs O, Martin H, Kirchhoff A, Stave J, Terwee T, Guthoff R. Monitoring accommodative ciliary muscle function using three-dimensional ultrasound. Graefes Arch Clin Exp Ophthalmol 2002;240:906-912.
55. Stachs O, Martin H, Behrend D, Schmitz KP, Guthoff R. Three-dimensional ultrasound biomicroscopy, environmental and conventional scanning electron microscopy investigations of the human zonula ciliaris for numerical modelling of accommodation. Graefes Arch Clin Exp Ophthalmol 2005;1-9.
56. Schneider H, Stachs O, Gobel K, Guthoff R. Changes of the accommodative amplitude and the anterior chamber depth after implantation of an accommodative intraocular lens. Graefes Arch Clin Exp Ophthalmol 2005.
57. Stachs O, Schneider H, Stave J, Guthoff R. Potentially accommodating intraocular lenses--an in vitro and in vivo study using three-dimensional high-frequency ultrasound. J Refract Surg 2005;21:37-45.
58. Stachs O, Schneider H, Beck R, Guthoff R. Pharmacological-induced haptic changes and the accommodative performance in patients with the AT-45 accommodative IOL. J Refract Surg 2006;22:145-150.
59. Fincham EF. The coincidence optometer. Proceedings of the Physical Society 1937;49:456-468.
60. Koretz JF, Bertasso AM, Neider MW, True-Gabelt BA, Kaufman PL. Slit-lamp studies of the rhesus monkey eye: II. Changes in crystalline lens shape, thickness and position during accommodation and aging. Exp Eye Res 1987;45:317-326.
61. Koretz JF, Neider MW, Kaufman PL, Bertasso AM, DeRousseau CJ, Bito LZ. Slit-lamp studies of the rhesus monkey eye. I. Survey of the anterior segment. Exp Eye Res 1987;44:307-318.
62. Koretz JF, Kaufman PL, Neider MW, Goeckner PA. Accommodation and presbyopia in the human eye--aging of the anterior segment. Vision Res 1989;29:1685-1692.
63. Mayer H, Irion KM. New approach to area image analysis of Scheimpflug photos of the anterior eye segment. Ophthalmic Res 1985;17:106-110.
64. Mayer H. Application of digital image analysis in cataract retroillumination photography. Ophthalmic Res 1987;19:266-270.
65. Norrby S. The Dubbelman eye model analysed by ray tracing through aspheric surfaces. Ophthalmic Physiol Opt 2005;25:153-161.
66. Dubbelman M, Van der Heijde GL, Weeber HA. Change in shape of the aging human crystalline lens with accommodation. Vision Res 2005;45:117-132.
67. Neider MW, Crawford K, Kaufman PL, Bito LZ. In vivo videography of the rhesus monkey accommodative apparatus. Age-related loss of ciliary muscle response to central stimulation. Arch Ophthalmol 1990;108:69-74.
68. Fercher A, Mengedoht K, Werner W. Eye-length measurement by interferometry with partially coherent light. Opt Lett 1988;186-188.
69. Drexler W, Baumgartner A, Findl O, Hitzenberger CK, Fercher AF. Biometric investigation of changes in the anterior eye segment during accommodation. Vision Res 1997;37:2789-2800.
70. Drexler W, Baumgartner A, Findl O, Hitzenberger CK, Sattmann H, Fercher AF. Submicrometer precision biometry of the anterior segment of the human eye. Invest Ophthalmol Vis Sci 1997;38:1304-1313.
71. Auffarth GU, Martin M, Fuchs HA, Rabsilber TM, Becker KA, Schmack I. [Validity of anterior chamber depth measurements for the evaluation of accommodation after implantation of an accommodative Humanoptics 1CU intraocular lens]. Ophthalmologe 2002;99:815-819.
72. Findl O, Kriechbaum K, Menapace R, Koeppl C, Sacu S, Wirtitsch M, Buehl W, Drexler W. Laserinterferometric assessment of pilocarpine-induced movement of an accommodating intraocular lens: a randomized trial. Ophthalmology 2004;111:1515-1521.
73. Findl O, Kiss B, Petternel V, Menapace R, Georgopoulos M, Rainer G, Drexler W. Intraocular lens movement caused by ciliary muscle contraction. J Cataract Refract Surg 2003;29:669-676.

74. Koeppl C, Findl O, Menapace R, Kriechbaum K, Wirtitsch M, Buehl W, Sacu S, Drexler W. Pilocarpine-induced shift of an accommodating intraocular lens: AT-45 Crystalens. J Cataract Refract Surg 2005;31:1290-1297.
75. Koeppl C, Findl O, Kriechbaum K, Drexler W. Comparison of pilocarpine-induced and stimulus-driven accommodation in phakic eyes. Exp Eye Res 2005;80:795-800.
76. Kriechbaum K, Findl O, Koeppl C, Menapace R, Drexler W. Stimulus-driven versus pilocarpine-induced biometric changes in pseudophakic eyes. Ophthalmology 2005;112:453-459.
77. Langenbucher A, Huber S, Nguyen NX, Seitz B, Gusek-Schneider GC, Kuchle M. Measurement of accommodation after implantation of an accommodating posterior chamber intraocular lens. J Cataract Refract Surg 2003;29:677-685.
78. Koranyi G, Lydahl E, Norrby S, Taube M. Anterior chamber depth measurement: a-scan versus optical methods. J Cataract Refract Surg 2002;28:243-247.
79. Kriechbaum K, Findl O, Kiss B, Sacu S, Petternel V, Drexler W. Comparison of anterior chamber depth measurement methods in phakic and pseudophakic eyes. J Cataract Refract Surg 2003;29:89-94.
80. Vetrugno M, Cardascia N, Cardia L. Anterior chamber depth measured by two methods in myopic and hyperopic phakic IOL implant. Br J Ophthalmol 2000;84:1113-1116.
81. Weale RA. Why we need reading-glasses before a zimmer-frame. Vision Res 2000;40:2233-2240.
82. Wyatt HJ. Application of a simple mechanical model of accommodation to the aging eye. Vision Res 1993;33:731-738.
83. Judge SJ, Burd HJ. Modelling the mechanics of accommodation and presbyopia. Ophthalmic Physiol Opt 2002;22:397-400.
84. Burd HJ, Judge SJ, Cross JA. Numerical modelling of the accommodating lens. Vision Res 2002;42:2235-2251.
85. Schachar RA, Bax AJ. Mechanism of human accommodation as analyzed by nonlinear finite element analysis. Compr Ther 2001;27:122-132.
86. Current aspects in human accommodation. Heidelberg: Kaden, 2001.
87. Current aspects in human accommodation II. Heidelberg: Kaden, 2003.
88. Bacskulin A, Martin H, Kundt G, Terwee T, Guthoff R. [Analysis of the dynamics of the ciliary muscle during accommodation]. Ophthalmologe 2000;97:855-859.
89. Bacskulin A, Gast R, Bergmann U, Guthoff R. [Ultrasound biomicroscopy imaging of accommodative configuration changes in the presbyopic ciliary body]. Ophthalmologe 1996;93:199-203.
90. Kano K, Kuwayama Y, Mizoue S, Hashitani T, Sasamoto Y, Horimoto K, Okamoto H. [Observation of physiological change in the human ciliary body using an ultrasound biomicroscope during accommodation]. Nippon Ganka Gakkai Zasshi 1999;103:297-300.
91. Ludwig K, Wegscheider E, Hoops JP, Kampik A. In vivo imaging of the human zonular apparatus with high-resolution ultrasound biomicroscopy. Graefes Arch Clin Exp Ophthalmol 1999;237:361-371.
92. Pavlin CJ, Harasiewicz K, Sherar MD, Foster FS. Clinical use of ultrasound biomicroscopy. Ophthalmology 1991;98:287-295.
93. Stachs O, Martin H, Kirchhoff A, Stave J, Terwee T, Guthoff R. Monitoring accommodative ciliary muscle function using three-dimensional ultrasound. Graefes Archive for Clinical and Experimental Ophthalmology 2002;240:906-912.
94. Strenk SA, Semmlow JL, Strenk LM, Munoz P, Gronlund-Jacob J, DeMarco JK. Age-related changes in human ciliary muscle and lens: a magnetic resonance imaging study. Invest Ophthalmol Vis Sci 1999;40:1162-1169.
95. Kalman A, Gloor B. Ciliary body motility and changes of anterior chamber depth during accommodation. Invest Ophthalmol 1993;34:1254.
96. Lutjen-Drecoll E, Tamm E, Kaufman PL. Age changes in rhesus monkey ciliary muscle: light and electron microscopy. Exp Eye Res 1988;47:885-899.
97. Lutjen-Drecoll E, Tamm E, Kaufman PL. Age-related loss of morphologic responses to pilocarpine in rhesus monkey ciliary muscle. Arch Ophthalmol 1988;106:1591-1598.
98. Fisher RF. The force of contraction of the human ciliary muscle during accommodation. J Physiol 1977;270:51-74.
99. Swegmark G. Studies with impedance cyclography on human ocular accommodation at different ages. Acta Ophthalmol (Copenh) 1969;47:1186-1206.
100. Schachar RA. The correction of presbyopia. Int Ophthalmol Clin 2001;41:53-70.
101. Farnsworth PN, Shyne SE. Anterior zonular shifts with age. Exp Eye Res 1979;28:291-297.
102. Vogel A, Dick HB, Krummenauer F. Reproducibility of optical biometry using partial coherence interferometry : intraobserver and interobserver reliability. J Cataract Refract Surg 2001;27:1961-1968.
103. Kessler J. Lens refilling and regrowth of lens substance in the rabbit eye. Ann Ophthalmol 1975;7:1059-1062.
104. Agarwal L, Narsimhan E, Mohan M. Experimental lens refilling. Orient Arch Ophthalmol 1967;5:205-212.
105. Parel JM, Gelender H, Trefers WF, Norton EW. Phaco-Ersatz: cataract surgery designed to preserve accommodation. Graefes Arch Clin Exp Ophthalmol 1986;224:165-173.

106. Nishi O, Hara T, Hara T, Sakka Y, Hayashi F, Nakamae K, Yamada Y. Refilling the lens with a inflatable endocapsular balloon: surgical procedure in animal eyes. Graefes Arch Clin Exp Ophthalmol 1992;230:47-55.
107. Nishi O, Nishi K. Accommodation amplitude after lens refilling with injectable silicone by sealing the capsule with a plug in primates. Arch Ophthalmol 1998;116:1358-1361.
108. Nishi O, Nishi K, Mano C, Ichihara M, Honda T. Lens refilling with injectable silicone in rabbit eyes. J Cataract Refract Surg 1998;24:975-982.
109. Stachs O, Schneider H, Stave J, Schmitz KP, Terwee T, Guthoff R. The anterior segment in rabbit eyes after lens refilling with injectable silicone polymer. Invest Ophthalmol Vis Sci 2003;44:U50.
110. Hettlich HJ, Lucke K, Kreiner CF. Light-induced endocapsular polymerization of injectable lens refilling materials. Ger J Ophthalmol 1992;1:346-349.
111. Hettlich HJ, Lucke K, siyo-Vogel MN, Schulte M, Vogel A. Lens refilling and endocapsular polymerization of an injectable intraocular lens: in vitro and in vivo study of potential risks and benefits. J Cataract Refract Surg 1994;20:115-123.
112. Haefliger E, Parel JM. Accommodation of an endocapsular silicone lens (Phaco-Ersatz) in the aging rhesus monkey. J Refract Corneal Surg 1994;10:550-555.
113. Haefliger E, Parel JM, Fantes F, Norton EW, Anderson DR, Forster RK, Hernandez E, Feuer WJ. Accommodation of an endocapsular silicone lens (Phaco-Ersatz) in the nonhuman primate. Ophthalmology 1987;94:471-477.
114. Koopmans SA, Terwee T, Haitjema HJ, Barkhof J, Kooijman AC. Effect of infusion bottle height on lens power after lens refilling with and without a plug. J Cataract Refract Surg 2003;29:1989-1995.
115. Murthy SK, Ravi N. Hydrogels as potential probes for investigating the mechanism of lenticular presbyopia. Curr Eye Res 2001;22:384-393.
116. Aliyar HA, Hamilton PD, Ravi N. Refilling of ocular lens capsule with copolymeric hydrogel containing reversible disulfide. Biomacromolecules 2005;6:204-211.
117. de Groot JH, van Beijma FJ, Haitjema HJ, Dillingham KA, Hodd KA, Koopmans SA, Norrby S. Injectable intraocular lens materials based upon hydrogels. Biomacromolecules 2001;2:628-634.
118. Han YK, Kwon JW, Kim JS, Cho CS, Wee WR, Lee JH. In vitro and in vivo study of lens refilling with poloxamer hydrogel. Br J Ophthalmol 2003;87:1399-1402.
119. Apple DJ. Influence of intraocular lens material and design on postoperative intracapsular cellular reactivity. Trans Am Ophthalmol Soc 2000;98:257-283.
120. Werner L, Pandey SK, Escobar-Gomez M, Visessook N, Peng Q, Apple DJ. Anterior capsule opacification: a histopathological study comparing different IOL styles. Ophthalmology 2000;107:463-471.
121. Gayton JL, Apple DJ, Peng Q, Visessook N, Sanders V, Werner L, Pandey SK, Escobar-Gomez M, Hoddinott DS, Van Der KM. Interlenticular opacification: clinicopathological correlation of a complication of posterior chamber piggyback intraocular lenses. J Cataract Refract Surg 2000;26:330-336.
122. Werner L, Pandey SK, Apple DJ, Escobar-Gomez M, McLendon L, Macky TA. Anterior capsule opacification: correlation of pathologic findings with clinical sequelae. Ophthalmology 2001;108:1675-1681.
123. Werner L, Apple DJ, Pandey SK, Solomon KD, Snyder ME, Brint SF, Gayton JL, Shugar JK, Trivedi RH, Izak AM. Analysis of elements of interlenticular opacification. Am J Ophthalmol 2002;133:320-326.
124. Ridley H. Long-term results of acrylic lens surgery. Proc R Soc Med 1970;63:309-310.
125. Ridley H. The origin and objectives of intraocular lenticular implants. Trans Sect Ophthalmol Am Acad Ophthalmol Otolaryngol 1976;81:OP65-OP66.
126. Apple DJ. Intraocular lens biocompatibility. J Cataract Refract Surg 1992;18:217-218.
127. Apple DJ, Solomon KD, Tetz MR, Assia EI, Holland EY, Legler UF, Tsai JC, Castaneda VE, Hoggatt JP, Kostick AM. Posterior capsule opacification. Surv Ophthalmol 1992;37:73-116.
128. Pandey SK, Wilson ME, Trivedi RH, Izak AM, Macky TA, Werner L, Apple DJ. Pediatric cataract surgery and intraocular lens implantation: current techniques, complications, and management. Int Ophthalmol Clin 2001;41:175-196.
129. Fine IH. Cortical cleaving hydrodissection. J Cataract Refract Surg 1992;18:508-512.
130. Ram J, Apple DJ, Peng Q, Visessook N, Auffarth GU, Schoderbek RJ, Jr., Ready EL. Update on fixation of rigid and foldable posterior chamber intraocular lenses. Part I: Elimination of fixation-induced decentration to achieve precise optical correction and visual rehabilitation. Ophthalmology 1999;106:883-890.
131. Linnola RJ, Werner L, Pandey SK, Escobar-Gomez M, Znoiko SL, Apple DJ. Adhesion of fibronectin, vitronectin, laminin, and collagen type IV to intraocular lens materials in pseudophakic human autopsy eyes. Part 2: explanted intraocular lenses. J Cataract Refract Surg 2000;26:1807-1818.
132. Linnola RJ, Werner L, Pandey SK, Escobar-Gomez M, Znoiko SL, Apple DJ. Adhesion of fibronectin, vitronectin, laminin, and collagen type IV to intraocular lens materials in pseudophakic human autopsy eyes. Part 1: histological sections. J Cataract Refract Surg 2000;26:1792-1806.
133. Nishi O, Nishi K, Menapace R, Akura J. Capsular bending ring to prevent posterior capsule opacification: 2 year follow-up. J Cataract Refract Surg 2001;27:1359-1365.
134. Nishi O, Nishi K, Akura J, Nagata T. Effect of round-edged acrylic intraocular lenses on preventing posterior capsule opacification. J Cataract Refract Surg 2001;27:608-613.

135. Auffarth GU, Rabsilber TM, Reuland AJ. New methods for the prevention of posterior capsule opacification. Ophthalmologe 2005;102:579-+.
136. Rabsilber TM, Auffarth GU. Pharmacological means to prevent secondary cataract. Klinische Monatsblatter fur Augenheilkunde 2006;223:559-567.
137. Weller M, Wiedemann P, Fischbach R, Hartmann C, Heimann K. Evaluation of daunomycin toxicity on lens epithelium in vitro. Int Ophthalmol 1988;12:127-130.
138. Rieck PW, Kriegsch J, Jaeckel C, Hartmann C. [Effect of suramin on proliferation and migration of lens epithelial cells in vitro]. Ophthalmologe 2004;101:73-79.
139. Ismail MM, Alio JL, Ruiz Moreno JM. Prevention of secondary cataract by antimitotic drugs: experimental study. Ophthalmic Res 1996;28:64-69.
140. Abdelwahab MT, Kugelberg M, Kugelberg U, Zetterstrom C. After-cataract evaluation after using balanced salt solution, distilled deionized water, and 5-fluorouracil with a sealed-capsule irrigation device in the eyes of 4-week-old rabbits. J Cataract Refract Surg 2006;32:1955-1960.
141. McDonnell PJ, Krause W, Glaser BM. In vitro inhibition of lens epithelial cell proliferation and migration. Ophthalmic Surg 1988;19:25-30.
142. Shin DH, Kim YY, Ren J, Weatherwax AL, Pearlman RB, Kim C, Glover KB, Muenk SB. Decrease of capsular opacification with adjunctive mitomycin C in combined glaucoma and cataract surgery. Ophthalmology 1998;105:1222-1226.
143. Hansen TJ, Tyndall R, Soll DB. Methotrexate-anticollagen conjugate inhibits in vitro lens cell outgrowth. Invest Ophthalmol Vis Sci 1987;28:1206-1209.
144. Symonds JG, Lovicu FJ, Chamberlain CG. Differing effects of dexamethasone and diclofenac on posterior capsule opacification-like changes in a rat lens explant model. Exp Eye Res 2006;83:771-782.
145. Cortina P, Gomez-Lechon MJ, Navea A, Menezo JL, Terencio MC, az-Llopis M. Diclofenac sodium and cyclosporin A inhibit human lens epithelial cell proliferation in culture. Graefes Arch Clin Exp Ophthalmol 1997;235:180-185.
146. Beck R, Nebe B, Guthoff R, Rychly J. Inhibition of lens epithelial cell adhesion by the calcium antagonist Mibefradil correlates with impaired integrin distribution and organization of the cytoskeleton. Graefes Arch Clin Exp Ophthalmol 2001;239:452-458.
147. Stamer L, Bohnke M, Vogelberg K, Arndt R. [Tissue levels of locally applied cyclosporin A in the rabbit eye]. Fortschr Ophthalmol 1989;86:540-542.
148. Nishi O, Nishi K, Mano C, Ichihara M, Honda T, Saitoh I. Inhibition of migrating lens epithelial cells by blocking the adhesion molecule integrin: a preliminary report. J Cataract Refract Surg 1997;23:860-865.
149. Kleinmann G, Apple DJ, Chew J, Hunter B, Stevens S, Larson S, Mamalis N, Olson RJ. Hydrophilic acrylic intraocular lens as a drug-delivery system for fourth-generation fluoroquinolones. J Cataract Refract Surg 2006;32:1717-1721.
150. Siqueira RC, Filho ER, Fialho SL, Lucena LR, Filho AM, Haddad A, Jorge R, Scott IU, Cunha AS. Pharmacokinetic and toxicity investigations of a new intraocular lens with a dexamethasone drug delivery system: a pilot study. Ophthalmologica 2006;220:338-342.
151. Kim HC, Hartner S, Behe M, Behr TM, Hampp NA. Two-photon absorption-controlled multidose drug release: a novel approach for secondary cataract treatment. J Biomed Opt 2006;11:34024.
152. Tetz MR, Ries MW, Lucas C, Stricker H, Volcker HE. Inhibition of posterior capsule opacification by an intraocular-lens-bound sustained drug delivery system: an experimental animal study and literature review. J Cataract Refract Surg 1996;22:1070-1078.
153. Stachs O, Knappe S, Stave J, Guthoff R. In vivo three-dimensional confocal laser scanning microscopy of the corneal nerve structure. Invest Ophthalmol Vis Sci 2005;46.

ACKNOWLEDGMENTS

This treatise is based on our research performed at the Department of Ophthalmology and the Institute for Biomedical Engineering, University of Rostock, Germany, between 2000 and 2007.

I would like to express my gratitude to my mentor, Prof. Dr. R.F. Guthoff. His commitment and enthusiasm provided me with a source of motivation that has been essential for my studies. I am also indebted to Prof. K.P. Schmitz, Prof. J. Stave, and Dr. H. Schneider for their support throughout the years and for their practical introduction to the facilities and equipment at the Department of Ophthalmology and the Institute for Biomedical Engineering. I am particularly grateful to Thom Terwee for his inspiration and creativity. In addition, I wish to thank my friends and colleagues who have – directly or indirectly - contributed to my studies.

Last but not least, I am forever indebted to my dear wife Angrit for her love, patience, and support without which this treatise would never have been written.

The research was supported by generous donations from:

- University of Rostock, Germany
- Deutsche Forschungsgesellschaft, Germany
- AMO, Gronningen, The Netherlands
- Carl Zeiss Meditec AG, Jena, Germany
- Steinbeis-Transferzentrum, Biomedizinische Technik und angewandte Pharmakologie in der Ophthalmologie, Rostock, Germany
- Bausch&Lomb, France
- AkkoLens, The Netherlands

CURRICULUM VITAE

Personal Data

- Name: Oliver Stachs
- Born: October 12, 1965 in Magdeburg
- Marital status: Married with Angrit Stachs, two children (Philipp und Anne Stachs)
- Institution: University of Rostock, Department of Ophthalmology
- Address: Doberaner Str. 140, 18055 Rostock, Germany
- Telephone: ++49/381/4948566
- Fax: ++49/381/4948502
- e-mail: oliver.stachs@med.uni-rostock.de

Education

- Ph.D. (Dr. rer. nat.), Physics (1996), University of Rostock (Germany)
- Graduate Physistist (1991), University of Rostock (Germany)

Professional Experience

- Present Position:
  - Research Assistant, University of Rostock, Department of Ophthalmology
- Previous Positions:
  - Research Associate, University of Rostock, Department of Physics, 1997 – 1999
  - Research Associate, Stanford University, Stanford Synchrotron Radiation Laboratory (USA), 1996-1997
  - Research Assistant, University of Rostock, Department of Physics, 1992 – 1984

Professional Activities

- Research fields:
  - Optic of the eye
  - Confocal microscopy
  - Ultrasonographical imaging
  - X-ray diffraction from amorphous materials
  - Material science
- Publications:
  - 6 book contributions
  - 26 refereed articles in peer-reviewed journals
  - 12 articles in other journals
  - 1 patent
- Extended Visits:
  - CEA, CEN (Saclay , France)
  - Stanford Synchrotron Radiation Laboratory , Stanford University (Stanford, USA)
  - Hamburger Synchrotronstrahlungslabor HASYLAB at the Deutsches Elektronen-Synchrotron DESY in Hamburg (Germany)
  - Michigan State University (East Lansing, USA)
- Journal Review:
  - British Journal of Ophthalmology
  - Journal of Refractive Surgery
  - Eye
  - Graefe Archive for Clinical and Experimental Ophthalmology
- Membership:
  - Association of Research in Vision and Ophthalmology
  - European Society of Cataract and Refractive Surgery

  - American Society of Cataract and Refractive Surgery
  - International Society of Refractive Surgery of the American Academy of Ophthalmology
  - Deutsche Ophthalmogische Gesellschaft
- Honors:
  - Scholarship holder of the „Deutschen Akademie der Naturforscher Leopoldina", Halle, Germany
  - Troutman Award, funded by the Microsurgical Research Foundation (ISRS/AAO), USA

LIST OF INCLUDED PUBLICATIONS

1. Kirchhoff A, Stachs O, Guthoff R. Three-dimensional ultrasound findings of the posterior iris region. Graefes Arch Clin Exp Ophthalmol 2001 Dec;239(12):968-71. ***Appendix page 1***

2. Stachs O. 3D ultrasonic imaging of the ciliary body region in Current Aspects of Human Accommodation, R. Guthoff and K. Ludwig (Eds.), Kaden Verlag 2001, 103-119. ***Appendix page 5***

3. Stachs O, Martin H, Kirchhoff A, Stave J, Terwee T, Guthoff R. Monitoring accommodative ciliary muscle function using three-dimensional ultrasound. Graefes Arch Clin Exp Ophthalmol 2002 Nov;240(11):906-12. ***Appendix page 20***

4. O. Stachs. Monitoring the human ciliary muscle function during accommodation in Current Aspects of Human Accommodation part II, R. Guthoff and K. Ludwig (Eds.), Kaden Verlag 2003, 105-118. ***Appendix page 27***

5. Stachs O, Schneider H, Stave J, Beck R, Guthoff RF. [Three-dimensional ultrasound biomicroscopic examinations for haptic differentiation of potentially accommodative intraocular lenses]. Ophthalmologe 2005 Mar;102(3):265-71. ***Appendix page 41***

6. Stachs O, Martin H, Behrend D, Schmitz KP, Guthoff R. Three-dimensional ultrasound biomicroscopy, environmental and conventional scanning electron microscopy investigations of the human zonula ciliaris for numerical modeling of accommodation. Graefes Arch Clin Exp Ophthalmol 2006 Jul 244(7):836-844. ***Appendix page 48***

   Schachar RA, Abolmaali A, Kamangar F. Comment on the publication "Three-dimensional ultrasound, biomicroscopy environmental and conventional scanning electron microscopy investigations of the human zonula ciliaris for numerical modeling of accommodation" by O. Stachs et al. Graefes Arch Clin Exp Ophthalmol 2006 Aug;244(8):1062-3. ***Appendix page 57***

7. Stachs O, Martin H. Reply to comment by R. Schachar et al. regarding our publication "Three-dimensional ultrasound biomicroscopy, environmental and conventional scanning electron microscopy investigations of the human zonula ciliaris for numerical modeling of accommodation" Graefes Arch Clin Exp Ophthalmol 2006 Aug;244(8):1064-5. ***Appendix page 59***

8. Stachs O, Schneider H, Stave J, Guthoff R. Potentially accommodating intraocular lenses--an in vitro and in vivo study using three-dimensional high-frequency ultrasound. J Refract Surg 2005 Jan;21(1):37-45. ***Appendix page 61***

   Stachs wins award for studies of potentially accommodating intraocular lenses J Refract Surg, 2005 Sep-Oct;21 (5): 505-505. ***Appendix page 70***

9. Schneider H, Stachs O, Guthoff R. [Evidence based observations on accommodative artificial lenses]. Klin Monatsbl Augenheilkd 2005 Apr;222(4):357-60. ***Appendix page 71***

10. Stachs O, Schneider H, Beck R, Guthoff R. Pharmacological-induced haptic changes and the accommodative performance in patients with the AT-45 accommodative IOL. J Refract Surg 2006 Feb;22(2):145-50. ***Appendix page 75***

    Cumming JS. Comment on the publication “Pharmacological-induced haptic changes

and the accommodative performance in patients with the AT-45 accommodative IOL." by O. Stachs et al. J Refract Surg 2006 Sep 22(7): 633-634. ***Appendix page 81***

11. Stachs O, Guthoff RF. Reply to comment by JS Cumming on the publication "Pharmacological-induced haptic changes and the accommodative performance in patients with the AT-45 accommodative IOL." by O. Stachs et al. J Refract Surg 2006 Sep 22(7): 634-635. ***Appendix page 82***
12. Schneider H, Stachs O, Gobel K, Guthoff R. Changes of the accommodative amplitude and the anterior chamber depth after implantation of an accommodative intraocular lens. Graefes Arch Clin Exp Ophthalmol 2006 Mar;244(3):322-9. ***Appendix page 84***
13. Meinhardt B, Stachs O, Stave J, Beck R, Guthoff R. Evaluation of biometric methods for measuring the anterior chamber depth in the non-contact mode. Graefes Arch Clin Exp Ophthalmol 2006 May;244(5):559-64. ***Appendix page 92***
14. Meinhardt B, Stachs O, Zhivov A, Guthoff RF. Evaluation of Biometric Methods for Measuring the Corneal Thickness in Comparison to Confocal Laser Scanning Microscopic Investigations, International Ophthalmology, submitted. ***Appendix page 98***
15. Sternberg K, Terwee T, Stachs O, Schneider H, Guthoff RF, Kramer S, Löber M, Henninghause G, Berhrend D, Schmidt KP. An in-vitro model for drug-induced secondary cataract prevention – Experimental results with Disulfiram, Methotrexate and Actinomycin D, Invest Ophthalmol, Vis Sci, submitted. ***Appendix page 106***
16. Stachs O. Intraocular behavior of accommodative IOLs. Master IOLs: principles and innovations. Jaypee Brothers Medical Publishers; 2006. p. 398-408. ***Appendix page 120***
17. Stachs O, Guthoff RF. Ultrasonography within the Framework of Ophthalmologic Differential Diagnosis. In: Agarwal A, Boyd S, Drews RC, editors. Diagnostic and Imaging Techniques in Ophthalmology. Highlights of Ophthalmology; 2006. p. 101-31. ***Appendix page 131***

COPIES OF INCLUDED PUBLICATIONS

Graefe's Arch Clin Exp Ophthalmol
(2001) 239:968–971

SHORT COMMUNICATION

DOI 10.1007/s004170100370

Alexander Kirchhoff
Oliver Stachs
Rudolf Guthoff

Three-dimensional ultrasound findings of the posterior iris region

Received: 14 February 2001
Revised: 15 May 2001
Accepted: 24 August 2001
Published online: 9 November 2001

A. Kirchhoff (✉) · O. Stachs · R. Guthoff
Universitätsaugenklinik Rostock,
Doberaner Strasse 140, 18057 Rostock,
Germany
e-mail:
alexander.kirchhoff@med.uni-rostock.de
Tel.: +49-381-4948501
Fax: +49-381-4948502

Abstract *Purpose:* The aim of this study was to assess the benefit of the three-dimensional ultrasound biomicroscopy in examination of the posterior iris and ciliary body. *Methods:* Three-dimensional visualisation of the anterior eye section was achieved through extension of the existing ultrasound biomicroscope system (Humphrey Instruments). Visualisation of posterior iris and ciliary body pathologies in three patients was performed with a three-dimensional reconstruction technique of B-scans. *Results:* The extended ultrasound system provided three-dimensional visualisation of alterations of the posterior iris region, i.e. iris cysts, ciliary body cysts and solid tumours of the ciliary body and iris. *Conclusions:* The three-dimensional ultrasound biomicroscopy yields extended diagnostic findings regarding iris and ciliary body pathology. This method offers an improved assessment of the posterior surface of the iris and the volume of the ciliary body. Furthermore, these data can be useful for procedures in computer simulation and calculation for a better understanding of the function of the ciliary body in the accommodation process.

Introduction

Ultrasound is the most widely used non-optical diagnostic tool for the imaging of the eye. Pavlin firstly described high-resolution ultrasound biomicroscopy (UBM) in 1990. The authors' results of a series of clinical cases have shown that this method can provide information unavailable with any other imaging technique. Thus, clinical UBM proved to be a tool with a significant potential in diagnoses of ocular diseases [7].

The ultrasound biomicroscope (UBM) provides high resolution and two-dimensional imaging of the anterior segment. It has been used in investigations of anatomic correlations of a variety of disorders, including anterior segment tumours, cysts, plateau iris, malignant glaucoma and pigment dispersion syndrome [1, 2, 5, 8, 9, 10, 11, 12]. The use of high-frequency transducers of ca. 50 MHz enabled high-resolution imaging of the anterior eye segment. This eye segment is a special case where attenuation by intervening tissue can be minimised by application of a fluid-coupling medium between eye and transducer.

Three-dimensional UBM was first described by Coleman et al. [3]. In this study we developed a new method of 3 D UBM and the clinical benefit of this method was demonstrated in a choice of clinical cases.

Patients and methods

Three patients of the University Eye Clinic Rostock were examined with the high-frequency UBM. One patient suffered from contusio bulbi, while the other two had iris tumours. The equipment and technique of the UBM have been described in detail elsewhere [4, 6, 7]. A 50-MHz transducer that achieves a resolution of approximately 50 μm was used. The field of view on screen is limited to 5×5 mm on the commercially available Humphrey unit. Eyecup immersion scanning was performed with a frame rate of 8 Hz.

Scanning was performed under topical anaesthesia with the patient in supine position. An eyecup filled with methylcellulose and

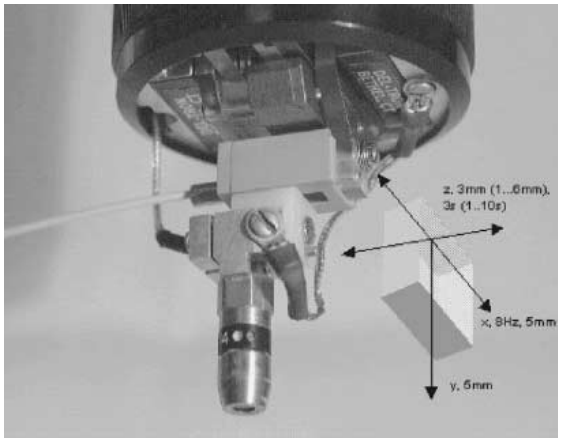

Fig. 1 The extended ultrasound biomicroscopy system – technical arrangement of the US probe

saline solution was inserted between the eyelids. Using a standard B-mode, the transducer was positioned at the centre of the ocular segment concerned. For 3D imaging, the computer-controlled scanning system moved the transducer at 90 deg to the plane of the 8-Hz sector motion (xy-plane) over the eye (z-direction). For this motion, a miniature skid was mounted on the 8-Hz scanning device. The technical arrangement of the US probe is depicted in Fig. 1.

The speed and distance adjustments of the z-motion are variable. The video display of the ultrasound unit was digitised with 8 Hz using a framegrabber board (Hasotec Fg30) synchronised with the motion control system. The acquisition time for a 3D sequence varied between 5 s and10 s; the latter should be the maximum time, considering movement by the patient and the examiner.

The motion control and data acquisition system was connected with a SGI workstation via a local area network for 3D reconstruction using VoxelView (Vital Images, Fairfield, Iowa, USA). This commercial volume-rendering software package provides an interactive environment allowing features such as volume orientation for viewing planes and 3D perspectives, segmentation and determination of distances and surfaces. To process one 3D data set a time of 30 min is necessary. The model-building feature allows the outline of anatomic structures in space and can additionally be used for volume measurements.

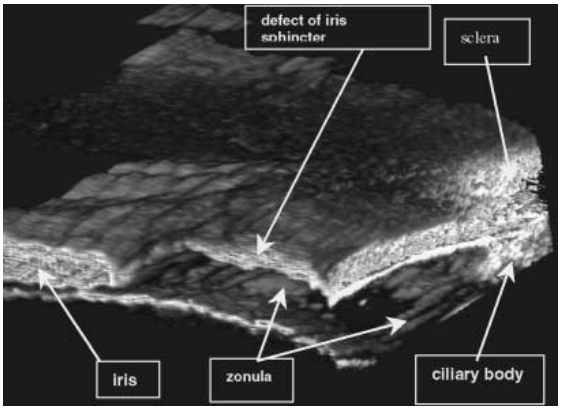

Fig. 2 3D-reconstructed volume of the iris sphincter defect, zonulolysis and prolapse of the vitreous body after contusio bulbi after 3D UBM

Case reports

Case 1

A 42-year-old woman with contusio bulbi was referred to the eye hospital. Physical examination revealed fine scratches on the corneal surface and a hyphema 1.5 mm high. Furthermore, a lesion of the iris sphincter and a prolapse of the vitreous body into the anterior chamber of the eye were observed. With the aid of 3D UBM, a sharply marginated defect of the zonules of Zinn leading to the prolapse of the vitreous body could be detected (Fig. 2). We defined these zonules as the structures between the ciliary body and the equator of the lens. Figure 3 shows the clinical situation after the resorption of the hyphema.

Case 2

A 27-year-old woman had a pigmented iris tumour at the base of the iris without contact to the corneal endothelium. 3D UBM was used to demonstrate tumour size and shape. These 3D images are useful in the long-term follow-up to determine increases in tumour volume and extent of tissue involvement. Figure 4 shows the clinical appearance, and Fig. 5 shows the 3D images in two slices in a variety of different planes.

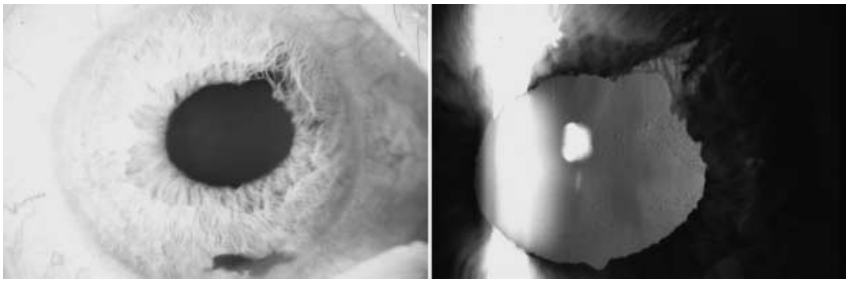

Fig. 3 Clinical pictures of a patient with contusio bulbi and traumatic iris sphincter defect and prolapse of the vitreous body

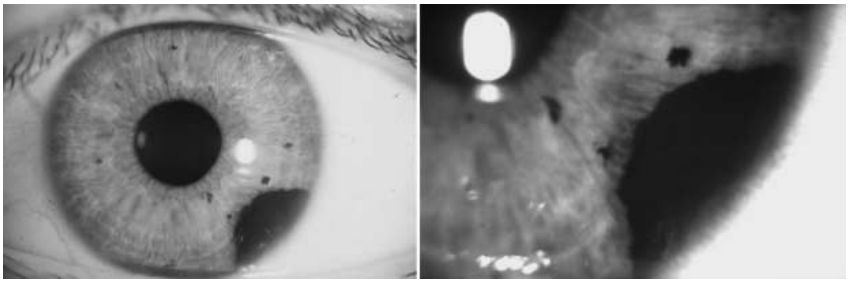

Fig. 4 Clinical pictures of an prominent iris naevus without retrocorneal contact

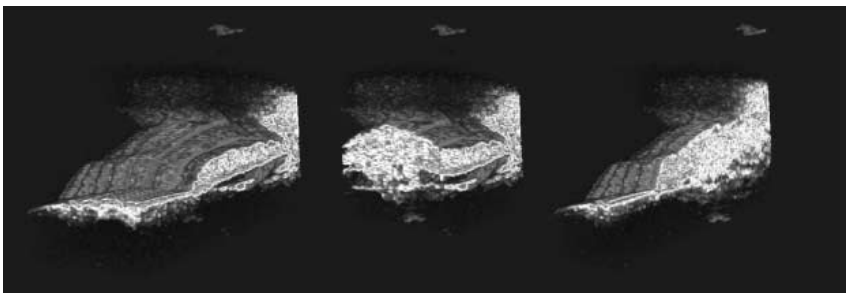

Fig. 5 3D-reconstructed volume of the iris naevus in 3D UBM and two different planes of the digitalised volume

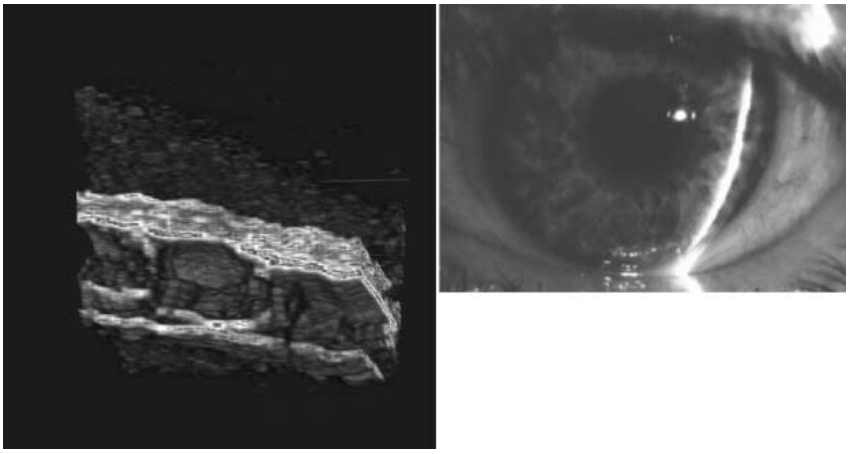

Fig. 6 A view into the volume of cysts of the iris and ciliary body in 3D UBM and the clinical picture

Case 3

A 35-year-old woman had a non-pigmented iris tumour at the base of the iris, in contact with the corneal endothelium. The finding was positive on transillumination. Therefore, the patient was suspected to have iris cysts. Using UBM, one large cyst could be demonstrated in the conspicuous area. Moreover, multiple small cysts were detected in the region of the iris and the ciliary body. Three-dimensional reconstruction, as shown in Fig. 6, revealed a precise visualisation of the cysts and their topographic relations that made it possible to document these findings exactly.

Discussion

This report describes techniques we developed for non-invasive characterisation of tissue microstructures by using high-frequency ultrasound, three-dimensional scanning and image reconstruction.

High-frequency ultrasound provides an axial resolution of approximately 50 μm and a lateral resolution of less than 100 μm in the focal plane. Through the design of a miniature skid we added the ability to acquire multi-

ple and parallel aligned slice images. The 2D sequential, parallel sections were reconstructed into three-dimensional voxel images.

We demonstrated this improved method in three different circumstances: zonulolysis after contusio bulbi, an iris tumour and iris–ciliary body cysts. In all cases, the demonstration with 3D UBM of defects in deeper regions of the eye was successfully performed. Regular monitoring of the bulb tension was recommended in case 1, and repeat 3D UBM every 6 months in case 2 and case 3.

We conclude that 3D UBM of the anterior eye segment provides clinically useful information regarding size, extension and site of the existing pathology. Furthermore, the expanded ultrasound system offers a non-invasive means of obtaining data on the ciliary body region in three dimensions at high resolution. The three-dimensional UBM system is a useful diagnostic tool that also allows volume measurement, distance spacing in volume and two-dimensional images in any plane of 3D volumes. The method improves diagnosis, monitoring and treatment planning. Furthermore, the reported data should be an useful tool for procedures in computer simulation and calculation to achieve a better understanding of the function of the ciliary body in the accommodation process.

References

1. Azuara-Blanco A (1999) Ultrasound biomicroscopy of ciliary body cysts. Am J Ophthalmol 128:259
2. Caronia RM, Liebmann JM, Stegman Z, Sokol J, Ritch R (1996) Increase in iris-lens contact after laser iridotomy for pupillary block angle closure. Am J Ophthalmol 122:53
3. Coleman KJ, Woods S, Rondeau MJ, Silverman RH (1992) Ophthalmic ultrasonography. Radiol Clin North Am 30:1105
4. Liebmann JM, Ritch R (1996) Ultrasound biomicroscopy of the anterior segment. J Am Optom Assoc 67:469
5. Marigo FA, Finger PT, McCormick SA, Iezzi R, Esaki K, Ishikawa H, Seedor J, Liebmann JM, Ritch R (1998) Anterior segment implantation cysts. Ultrasound biomicroscopy with histopathologic correlation. Arch Ophthalmol 116:1569
6. Pavlin CJ, Foster FS (1995) Ultrasound biomicroscopy of the eye. Springer, New York Berlin Heidelberg
7. Pavlin CJ, Harasiewicz K, Sherar MD, Foster FS (1991) Clinical use of ultrasound biomicroscopy. Ophthalmology 98:287
8. Pavlin CJ, Ritch R, Foster FS (1992) Ultrasound biomicroscopy in plateau iris syndrome. Am J Ophthalmol 113:390
9. Pavlin CJ, McWhae JA, McGowan HD, Foster FS (1992) Ultrasound biomicroscopy of anterior segment tumors. Ophthalmology 99:1220
10. Potash SD, Tello C, Liebmann J, Ritch R (1994) Ultrasound biomicroscopy in pigment dispersion syndrome [see comments]. Ophthalmology 101:332
11. Reminick LR, Finger PT, Ritch R, Weiss S, Ishikawa H (1998) Ultrasound biomicroscopy in the diagnosis and management of anterior segment tumors. J Am Optom Assoc 69:575
12. Sokol J, Stegman Z, Liebmann JM, Ritch R (1996) Location of the iris insertion in pigment dispersion syndrome. Ophthalmology 103:289

3-D Ultrasonic Imaging of the Ciliary Body Region

O. Stachs[1], A. Kirchhoff[1], H. Martin[2] and R. Guthoff[1]

The objective was to develop a three-dimensional high-resolution ultrasonic imaging technique to be utilized for in-vivo characterization of the ciliary body and the posterior iris. The results were to enhance the quantification of configurational changes of the ciliary body during accommodation by biomicroscopy. A standard ultrasound biomiscroscope (UBM Model 840 – Humphrey Instruments) with a frequency of 50 MHz and an axial resolution of 50 µm was upgraded by adding a computer-controlled linear scanning device, oriented at right angles to the B-scan plane of the US probe, to perform digital three-dimensional ultrasound measurements. This scanning system makes it possible to collect series of parallel slices. The resulting images were directly recorded and digitalized in on-line mode, a Silicon Graphics Workstation using VoxelViewgraphics software followed by three-dimensional visualisation and processing. After selection of relevant ciliary muscle cross-sections, characteristic 2D parameters of the ciliary muscle sections were used for approximation. In an in-vivo investigation of the ciliary body and the posterior region of the iris in human eyes, three-dimensional ultrasound images were obtained revealing accommodative changes of the ciliary body configuration. The technique of 3D visualization in combination with the option of obtaining any defined 2D images in any plane of the 3D volume make it possible to describe the accommodative ciliary muscle changes, including those of the ciliary processes. Evaluation of the 3D images allows a qualitative and quantitative assessment of configurational changes during accommodation and disaccommodation.

Introduction

The term 'accommodation' refers to the eye's ability to adjust to an object at varying distances so as to afford a sharp image on the retina. The refractive power of the eye as an opical system may be adjusted either by varying the distance of the plane of the image from the focal plane or by changing the focal length of the imaging system. Thus, parameters of accommodation include the changing distance between the retina and the lens, as well as the changing focal length by variation of the radius of curvature or the refractive indices of

[1] Universitäts-Augenklinik Rostock, Doberaner Straße 140, D–18055 Rostock, Germany

[2] Institut für Implantat-Technologie und Biomaterialien, Friedrich-Barnewitz-Straße 4, D–18119 Rostock,Germany

the structures involved in the imaging mechanism.

The numerous existing models of accommodation [6, 7, 10, 15, 16, 24, 31] express the ongoing search for a biomechanical model to describe the mechanism and the cause of accommodative phenomena as well as presbyopia.

Previous histological and ultrasound-biological investigations have revealed a variety of age-related changes occurring in the human ciliary muscle. The total muscle surface is reduced with time. In the age group between 30 and 85 years, the length of the ciliary muscle is shortened by almost half. While the longitudinal and the reticular portion of the ciliary muscle decrease, the circular portion, on the other hand, increases. Thus, some distance between the inner apex of the ciliary muscle and the scleral spur is lost. These results, published by Tamm [30] and Lütjen-Drecoll [18], suggest that the older ciliary muscle increasingly assumes the shape of a youthful ciliary muscle in the accommodated state. This conclusion is confirmed by our own two-dimensional ultrasound biomicroscopic investigations [2]. The results, however, do not allow a differentiated assessment of the eye's anatomy in the accommodated respectively the disaccommodated state; and neither do they afford a morphological elucidation of the accommodative dynamics.

Further investigation in conjunction with the above-mentioned theories, hypotheses and questions regarding the mechanism and cause of accommodation and presbyopia would very much benefit from a method allowing three-dimensional high-resolution imaging of the anterior portion of the eye; especially of the invisible areas behind the iris and, in particular, the ciliary muscle. This would make it possible to differentiate between the ciliary muscle and the ciliary processes and to observe the configurational changes of the muscle independently of the processes; considering that it is really the muscle itself that reflects the accommodation mechanism.

This study aims at developing a three-dimensional high-resolution imaging technique of the anterior portion of the eye by ultrasound biomicroscopy. Our focus, in particular, is on the behavior of the ciliary muscle during accommodation; in this context we are trying especially to determine the configurational and positional changes associated with accommodation. The newly developed three-dimensional ultrasound biomicroscopic technique affords data that add some new features to our understanding of the accommodative processes and the phenomenon of presbyopia. Besides, this approach also yields useful data for computer simulation (finite elements method); the pertinent results are utilized to develop a biomechanical model of the accommodative mechanism.

Methods and Measurements

Several authors [9, 11, 17, 19, 23] interpret the recovery of accommodative power as a long-term aim of cataract surgery. While surgical techniques used for cataract surgery are continuously being improved, the exact accommodative mechanism and the cause of presbyopia remains to be elucidated [1, 19, 32]. The possibility of surgical recovery of the accommodative power makes it particularly interesting to research accommodatively induced reactions. Besides, competitive hypotheses regarding the genesis of presbyopia, regression in accommodative amplitude caused by altered lens material properties [14] as opposed to changed neuromuscular excitability respectively contractibility of the ciliary muscle / the zonular fibers [1, 8, 29, 32] are still a matter of ongoing scientific debate.

The fact that the details of the accommodative mechanism remain unclear may primarily be attributed to the fact that direct observation of the ciliary muscle, due to its position behind the iris diaphragm, is very difficult. Ultrasound biomicroscopy, a high-resolution ultrasonic imaging technique, allows in-vivo microscopy of the ciliary body. This method has proven its value in the diagnostics of the anterior portion of the eye [2, 5, 12, 20-22].

At a sound frequency of approx. 50 MHz, which is commonly used in high-resolution ultrasound biomicroscopy, in combination with a penetration depth of 5 mm and a lateral expansion of 5 mm, a resolution of 50 µ may be attained [20]. Thus, measurements revealing the expansion of the pars plicata of the ciliary body as well as configurational changes of the presbyopic ciliary body were obtained at the Rostock Eye Clinic [2, 3, 13]. To determine the contours of the ciliary body, a software package allowing semi-automatic approximation of two-dimensional parameters was developed at the Rostock Eye Clinic in collaboration with the Institute for Biomedical Technology (Rostock University) [4]. Fig. 1 shows an example of an approximated ciliary body structure.

In order to understand the accommodative mechanism, we need precise information regarding the configurational changes of the ciliary muscle during accommodation. The main problem and the source of errors associated with two-dimensonal ultrasonic imaging of the ciliary muscle in various different states of accommodation arise from the dynamics of the accommodative process as well as the existence of the ciliary processes. Fig. 2 shows an ultrasound-biomicroscopic image of the ciliary body, seen in transverse direction, with clearly differentiated regions of the ciliary muscle with and without ciliany processes (Figs. 2 and 3).

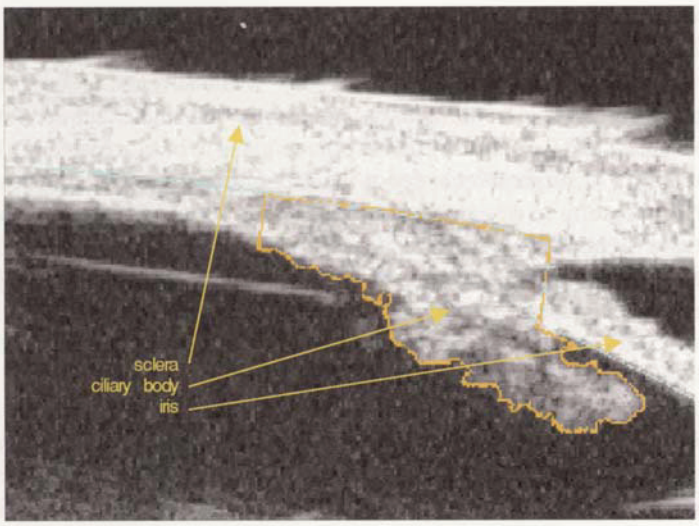

Figure 1. *Ultrasound biomicroscopic image of the ciliary body, radially oriented, with approximated contours of the ciliary body.*

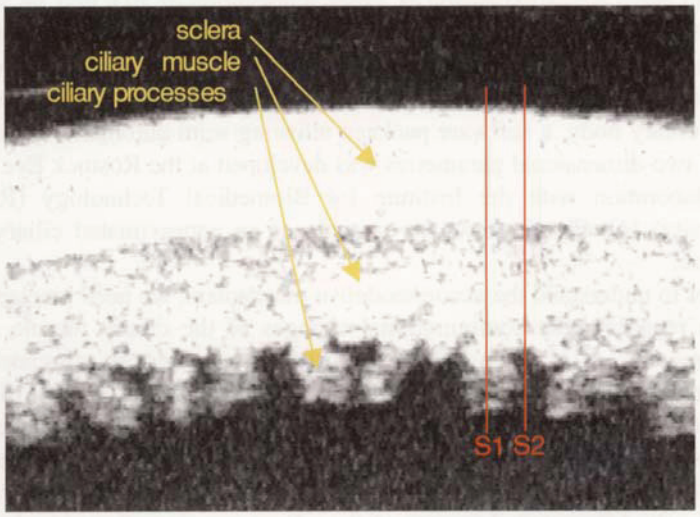

Figure 2. *Ultrasound biomicroscopic image of the ciliary body, transversally oriented, with sections S1 and S2.*

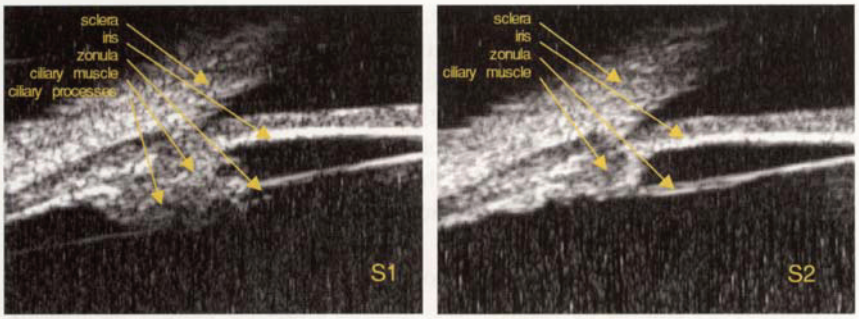

Figure 3. Various radial sections of a human ciliary body, including the sclera, the iris, the ciliary body, and the zonula. This figure shows sections through the ciliary muscle with ciliary processes (S1) and the ciliary muscle (S2), corresponding to the positions S1 and S2 in Fig. 2.

Radial sections in vicinal positions, such as S1 and S2, reveal significant differences with regard to the shape of the ciliary body. Fig. 3 shows two such radial sections through the ciliary body, corresponding to positions S1 and S2 in Fig. 2. A contour determination of the ciliary body in different accommodative states, the difference between sections such as S1 and S2 may exceed the expected accommodatively caused configurational changes of the muscle, since the processes deliver only a passive contribution to the deformation; thus preventing precise quantification of the corresponding characteristics of the ciliary muscle [2-4, 13].

Upgrading of the two-dimensional ultrasound biomicroscopy imaging technique to attain a three-dimensional approach would make it possible to gain much more information regarding the spatial localization and the orientation of structures in the anterior portion of the eye. When comparing the ciliary body in the accommodated resp. the disaccommodated state, sections containing no processes may thus be selected. In this case one might expect the remaining ciliary body volume to largely represent the ciliary muscle itself; which, after all, is the interesting element in this context. At this point in time there is no commercial ultrasonic system providing these necessary imaging qualities.

Three-dimensional ultrasonic in-vivo images obtained with an upgraded ultrasound biomicroscope (Humphrey UBM 840) were performed at the Rostock Eye Clinic. Figs. 4 and 5 show two examples of reconstructed objects. Fig. 4 shows the reconstruction of a phantom (suture material Vicryl, 6.0) in a water bath. Fig. 5 shows the volume segment of the ciliary body, including the scle-

ra and the iris, of an in-vivo human eye. The individual ciliary processes are to separate from the ciliary muscle. In this experimental setup, we equipped the ultrasound biomicroscope with an additional linear scanning device, oriented perpendicularly to the B-scan imaging plane. The B-scan imaging data, triggered to this additional direction of motion, are directly digitalized to serve as a basis for the 3D representation by the VoxelView program (Vital Images). Fig. 5 shows a reconstructed volumetric element 5 x 5 x 3 mm in size.

This may demonstrate the possibility of upgrading the Humphrey ultrasound biomicroscope and the potential of this method under 3D conditions, making it possible to selectively perform 2D and 3D calculations using reconstructed 3D elements.

Results

A specific approach of the question of accommodative configurational changes of the ciliary muscle involves obtaining defined sections through a three-dimensional reconstructed volume element of the ciliary body (Fig. 5), thus affording radial sections of the ciliary muscle without processes (Fig. 3, section S2).

In order to gain a preliminary three-dimensional impression of the configurational changes of the ciliary muscle, reconstructed 3D elements of the ciliary body were used to model the ciliary muscle contours along various 'valleys' in

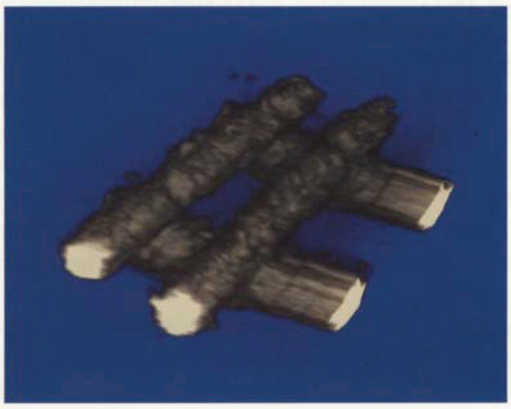

Figure 4. *Three-dimensional ultrasound biomicroscopic image of a phantom (crossed fibers (Vicryl, 6.0) in a water bath).*

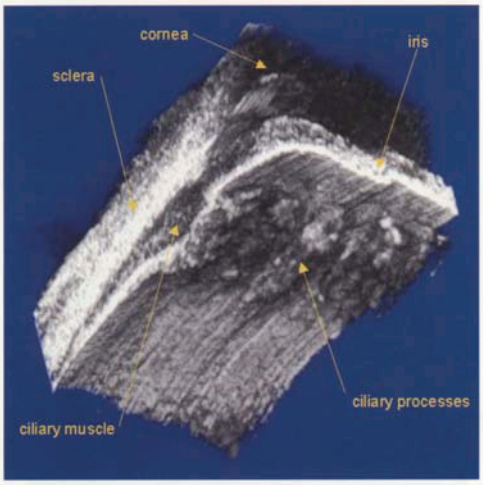

Figure 5. *Three-dimensional in-vivo image of a reconstructed 3D element of a ciliary body with the iris and the sclera.*

the disaccommodated and the accommodated state, respectively. Subsequently, the approximated peripheral muscular structures were modeled by a surface. Fig. 6 shows the 3D reconstruction of the ciliary bodies and the corresponding 3D models of the ciliary muscle. A quantitative analysis of these models clearly reveals muscular changes, especially with respect to the muscular thickness in the posterior area, toward the pars plana.

In an attempt to approach a preliminary quantitative calculation of the configurational changes, a large number of radial muscle sections were obtained from various 'valleys'. In the next step, the average contour was approximated and the resulting changes with regard to corresponding 2D parameters were analyzed. In this context, 10 sections obtained from the accommodated phase and the disaccommodated phase, respectively; these were then analyzed with a semi-automatic pattern recognition system [4]. The respective positions of the scleral spur and the ciliary muscular base were used to define a suitable coordinate system for the pattern recognition system. In addition, the posterior wall of the iris had to be differentiated from the neighboring ciliary muscle. The ciliary muscle base was approximated as a parable; while the posterior wall of the iris was approximated by a straight line. The scleral spur served as an origin of coordinates and as a center of rotation for the subsequent averag-

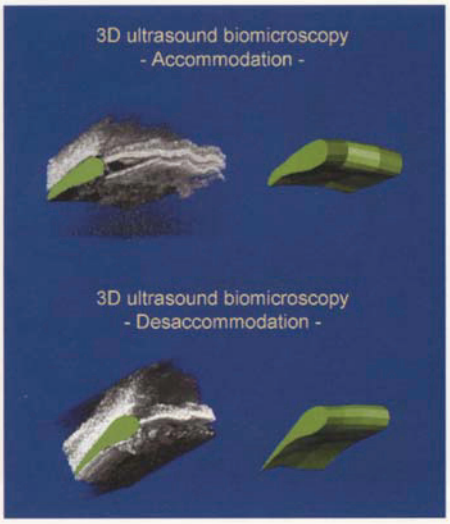

Figure 6. *3D reconstruction of the ciliary region and a model of the ciliary muscle during accommodation and disaccommodation, respectively, under pharmacological stimulation (test person with an accommodative range of 17 dpt).*

ing of the individual contours to afford a mean contour. A comparison was made on the basis of the mean outer contour; and a quantitative comparison was based on the defined 2D parameters - the center of gravity of the surface P_f, the anterior contour point P_v, and the lower contour point P_u. Fig. 7 shows a comparison of such contour approximations as well as the shift of the defined 2D parameters. This is a test person with an accommodative range of 17 dpt. at pharmacologically induced maximum acommodation (pilocarpine 2 %) respectively disaccommodation (cyclopentolate 1 %). These images reveal a configurational change of the entire muscle, both a shift of the center of gravity of the surface by approx. 0.3 mm; besides, the anterior point (approx. 0.5 mm) respectively the lower point (approx. 0.7 mm) is shifted toward the lens equator. In addition, the muscular thickness in the posterior region changes considerably in the direction of the pars plana. Fig. 8 shows the individual components of the coordinates and the shifts of individual 2D parameters as well as coordinate determination errors.

The question of in how far these ciliary muscle deformations affect the individual anterior and posterior zonulae and whether they cause deformation as

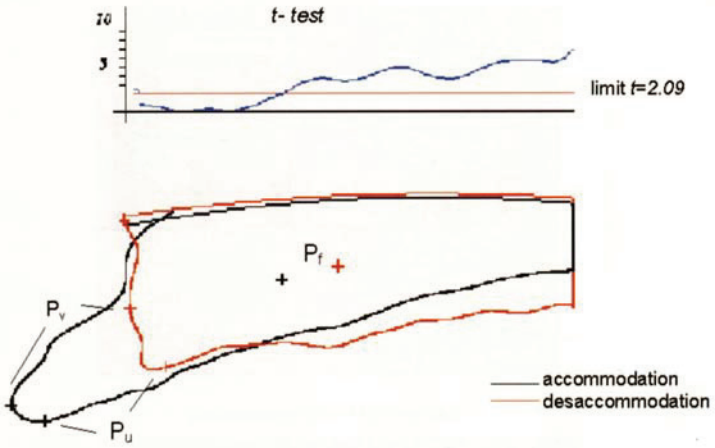

Figure 7. *Configuration of the ciliary muscle of a 17-year-old female test person (best corrected visual acuity 1.25, best corrected near vision Nd I/0.3, accommodative range 17 dpt, objective refractometry with unaffected pupil + 2.0 + 1.5 / 77°) during accommodation and disaccommodation, respectively; and comparison of the defined 2D parameters (center of gravity of the surface P_f, anterior contour point P_v, and lower contour point P_u).*

well as axial lens displacement remains to be elucidated by current investigations. In addition, the statistical significance of existing results ought to be enhanced by examining more test persons. The configurational changes calculated on the basis of the ciliary muscle contour approximations serve as a basis for computer simulations. In collaboration with the Institute for Biomedical Technology at Rostock University, an axially symmetric Finite Element Model of the human lens is currently being developed for this purpose; this instrument is used to investigate changes in refractive power of the lens during accommodation. This model allows for the rigidity of the zonular fibers, the variable thickness of the capsular bag, and the various material properties of the lens, the capsular bag, and the zonular fibers. Lens deformations are used to calculate the changes of refractive power of the lens during accommodation.

Discussion

These investigations aim at enhancing our understanding of the phenomena of accommodation and presbyopia. This was achieved by developing a three-dimensional high-resolution ultrasonic imaging technique that made it possible to analyze invisible areas of the anterior portion of the eye. Our particular

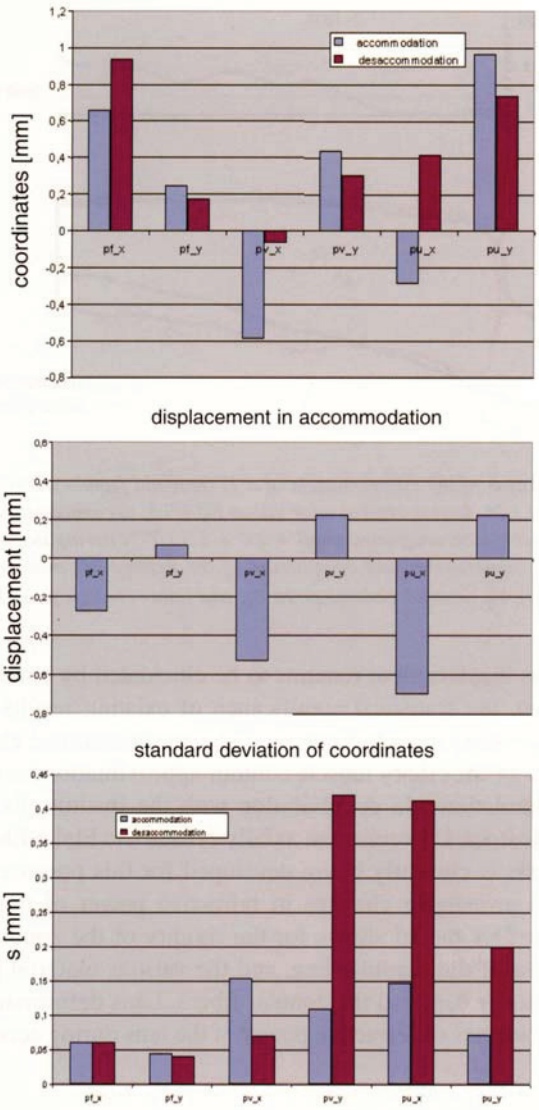

Figure 8. *Coordinate values, standard deviations and displacement of the x and y components of the defined 2D parameters (center of gravity of the surface P_f, anterior contour point P_v, and lower contour point P_u) of the ciliary muscle during accommodation and disaccommodation (see Fig. 7).*

emphasis was on the representation of configurational and positional changes of the ciliary muscle during accommodation.

The position of the ciliary muscle precludes direct optical observation. Ultrasound biomicroscopy, however, provides a high-resolution ultrasonic imaging technique of investigating these areas. The well-established 2D imaging technique (B mode) was upgraded such that it allows in-vivo acquisition of three-dimensional data.

This three-dimensional microscopic technique makes it possible to represent the ciliary body in various accommodative conditions. With these 3D data, radial sections of the ciliary body may be positioned such that the processes are avoided. The remaining ciliary body sections largely represent the ciliary muscle. The configurational differences of the muscle during accommodation and disaccommodation may be analyzed and discussed by contour recognition based on characteristic 2D parameters. Preliminary investigations revealed significant changes of the muscle configuration as well as changes of characteristic positions on the ciliary muscle; which demonstrates that this method allows in-vivo investigation and documentation of accommodative configurational changes of the ciliary muscle.

The following investigations will afford precise data regarding deformation of the ciliary muscle and will reveal correlations with existing accommodation ranges. These data – apart from explaining the accommodative processes – will also determine biological parameters in order to perfect simulation models of the lens and – as a future prospect - to develop suitable accommodative IOL materials. In order to use such accommodative lens implants, however, precise morphological imaging information is needed about the ciliary body, including quantitative data regarding the ciliary muscle activity during accommodation.

Acknowledgement

This research was supported in parts by BMBF grant no. 13N7238/3 as well as by Pharmacia.

The authors thank K. Muscheitis and P. Enzenross.

References

[1] Atchison, D.A.: Accommodation and presbyopia. Ophthal Physiol. Opt., 1995; 15: p. 255-277.

[2] Bacskulin, A.; Bergmann, U.; Horoczi, Z.; Guthoff, R.: Kontinuierliche ultraschallbiomikroskopische Darstellung der akkommodativen Veränderungen des humanen Ziliarkörpers. [*Continuous ultrasound-biomicroscopic representation of accommodative changes in the human ciliary body.*] Klin. Mbl. Augenheilk., 1995; p. 247-252.

[3] Bacskulin, A.; Gast, R.; Bergmann, U.; Guthoff, R.: Ultraschallbiomikroskopische Darstellung der akkommodativen Konfigurationsänderungen des presbyopen Ziliarkörpers. [*Ultrasound-biomicroscopic representation of accommodative configurational changes of the presbyopic ciliary body.*] Ophthalmologe 1996; 93: p. 199-203.

[4] Bacskulin, A.; Martin, H.; Terwee, T.; Guthoff, R.: Ein neues Bildverarbeitungssystem zur Quantifizierung der akkommodativ indizierten Formänderung des Ziliarmuskels. [*A new imaging system allowing quantification of the accommodatively induced deformation of the ciliary muscle.*] Klin. Mbl. Augenheilk.; submitted for publication.

[5] Bergmann, U.; Guthoff, R.: Klinische Entscheidungshilfen durch die Ultraschallbiomikroskopie. [*Clinical decision-making aid on the basis of ultrasound biomicroscopy.*] Klin. Mbl. Augenheilk., 1994; 205: p. 361-363.

[6] Coleman, D.J.: On the hydraulic suspension theory of accommodation. Trans. Am. Soc. Ophthalmol., 1986; 84: p. 846-868.

[7] Cramer, H.: Tijdschrift der Maatschappij voor Geneeskunde, 1851; 11: p. 115.

[8] Croft, M.A.; Kaufmann, P.L.; Crawford, K.S.; Neider, M.W.; Glasser, A.; Bito. L.Z.: Accommodation dynamics in aging rhesus monkeys. Am. J. Physiol., 1998; 275: p. 1885-1897.

[9] Cumming, J.S.; Kammann, J.: Experience with an accommodating IOL. J. Cataract Refract. Surg., 1996; 22: p. 1001.

[10] Descartes, R.: Traité de l'homme, 1677.

[11] Findl, O. ; Menapace, R.: Piggyback intraocular lenses. J. Cataract Refract. Surg., March 2000; 26: p. 308-309.

[12] Fischer, K.; Guthoff, R.: Neue Aspekte der Anwendung der Ultraschallbiomikroskopie. Klin Mbl Augenheilk., 1997; 211: p. 2.

[13] Fischer, K.; Krentz, H.; Guthoff, G.: Darstellung der Variationsbreite des Ziliarkörpers mittels Ultraschallbiomikroskopie. [*Representation of ciliary body variation by ultrasound biomicroscopy*] 96th DOG Congress, brief talk, 1998.

[14] Glasser, A.; Campbell, M.: Presbyopia and the optical changes in the human lens with age. Vis. Res., 1998; 38: p. 209-229.

[15] Gullstrand, A. : Der Mechanismus der Akkommodation. [*Accommodation mechanism*]. In: Handbuch der physiologischen Optik [*Handbook of physiological optics*]. (H. von Helmholtz, ed.) Third Edition, p. 327-353, 1909.

[16] von Helmholtz, H.: Über die Akkommodation des Auges. [*Accommodation of the eye*]. A.v. Graefe's Arch. Klin. Ophthalmol., 1855 (1); p. 1-74.

[17] Hettlich, H.J.; Lucke, K.; Asiyo-Vogel, M.N.; Schulte, M.; Vogel, A.: Lens refilling and endocapsular polymerization of an injectable intraocular lens: in vitro and in vivo study of potential risks and benefits. J. Cataract Refract. Surg., 1994; 20 (2): p. 115-123.

[18] Lütjen-Drecoll, E.; Tamm, E.; Kaufman, P.L.: Age-related loss of morphologic responses to pilocarpine in the rhesus monkey ciliary muscle. Arch. Ophthalmol., 1988; 106: p. 1591-1598.

[19] Nishi, O.; Nishi, K.: Accommodation amplitude after lens refilling with injectable silicone by sealing the capsule with a plug in primates. Arch. Ophthalmol., 1998; 116 (32): p. 1358-1361.

[20] Pavlin, C.J.; Foster, F.S.: Ultrasound biomicroscopy of the eye. Springer, Berlin, 1995.

[21] Pavlin, C.J.; Foster, F.S.: Ultrasound biomicroscopy. High-frequency ultrasound imaging of the eye at microscopic resolution. Radiol. Clin. North Am., 1998; 36: p. 1047-1058.

[22] Pavlin, C.J.; Foster, F.S.: Plateau iris syndrome: Changes in angle opening associated with dark, light, and pilocarpine administration. Am. J. Ophthalmol., 1999; 128: p. 288-291.

[23] Payer, H.: Ringwulstlinse mit Zoomwirkung zur Verstärkung einer Pseudoakkommodation und deren Erklärung aus erweiterter Akkommodationstheorie. [*Annular ring lens with a zoom function to enhance pseudo-accommodation and its explanation on the basis of extended accommodation theory*]. Spktr. Augenheilk., 1997; 11: p. 81-89.

[24] Rohen, J.W.: Der Ziliarkörper als funktionelles System. [*The ciliary body as a functional system*]. Morph. Jahrbuch, 1952; 92: p. 415.

[25] Rohen, J.W.; Rentsch, F.J.: Der konstruktive Bau des Zonularapparates beim Menschen und dessen funktionelle Bedeutung. [*The construction of the zonular apparatus in the human eye and its functional impact*]. A.v. Graefe's Arch. Klin. Exp. Ophthalmol., 1969; 178: p. 1-19.

[26] Schachar, R.A. : Cause and treatment of presbyopia with a method for increasing the amplitude of accommodation. Ann. Ophthalmol., 1992; 24: p. 445-452.

[27] Schachar, R.A.: Pathophysiology of accommodation and presbyopia. J. Florida M.A., 1994; 81: p. 268-271.

[28] Schachar, R.A.; Anderson, D.A.: The mechanism of ciliary muscle function. Ann. Ophthalmol., 1995; 27: p. 126-132.

[29] Tamm, E.; Lütjen-Drecoll, E; Jungkunz, W.; Rohen, J.W.: Posterior attachment of ciliary muscle in young, accommodating old, presbyopic old monkeys. Invest. Ophthalmol. Vis. Sci., 1991 ; 32 : p. 1678-1692.

[30] Tamm, S. ; Tamm, E. ; Rohen, J.W. : Age-related changes of the human ciliary muscle. A quantitative morphometric study. Mech. Ageing and Development, 1992; 62: p. 209-211.

[31] Tscherning, M.: H.v. Helmholtz et la théorie de l'accommodation. [*von Helmholtz and the accommodation theory*]. 1909, Paris.

[32] Weale, R.: Presbyopia towards the end of the 20th century. Surv. Ophthalmol., 1989; 34: p. 15-30.

Graefe's Arch Clin Exp Ophthalmol
(2002) 240:906–912

CLINICAL INVESTIGATION

DOI 10.1007/s00417-002-0551-2

Oliver Stachs
Heiner Martin
Alexander Kirchhoff
Joachim Stave
Thom Terwee
Rudolf Guthoff

Monitoring accommodative ciliary muscle function using three-dimensional ultrasound

Received: 27 February 2002
Revised: 1 July 2002
Accepted: 6 August 2002
Published online: 9 October 2002

O. Stachs (✉) · A. Kirchhoff · J. Stave
R. Guthoff
Department of Ophthalmology,
University of Rostock,
Doberaner Strasse 140, 18055 Rostock,
Germany
e-mail: oliver.stachs@med.uni-rostock.de
Tel.: +49-381-4948565
Fax: +49-381-4948502

H. Martin
Institute for Biomedical Engineering,
University of Rostock, Rostock, Germany

T. Terwee
Pharmacia und Upjohn, Groningen,
The Netherlands

Abstract *Background:* Our objective was to develop a three-dimensional high-resolution ultrasonic imaging technique to be utilized for in-vivo characterization of the ciliary body and the posterior iris. The benefit of this imaging in enhancing the quantification of the configurational changes in the ciliary body during accommodation is demonstrated. *Methods:* Sequential ultrasound biomicroscopic images of the ciliary body region were obtained with a computer-controlled scanning device designed for use with a standard ultrasound biomicroscope for 3D imaging. Custom-made software allows online data collection, data analysis and 3D reconstruction in conjunction with commercially available VoxelView software. *Results:* The three-dimensional presentation allows a close approximation of the ciliary muscle inside the ciliary body in vivo. We are able to distinguish and to analyze the changes in the muscle contour in different accommodation states. During accommodation a shift in the ciliary muscle center of gravity in a range of 0.04–0.26 mm (mean 0.13±0.06 mm) in the direction of the lens equator, with an interindividual variation and a small decrease with age, was observed. *Conclusions:* High-resolution ultrasound is a well established technique for in-vivo investigation of the anterior segment. Three-dimensional ultrasound biomicroscopy allows an assessment of the individual ciliary muscle activity in consideration of the ciliary processes. In combination with a contour analysis tool we improved the muscle contour determination during different accommodation states. The investigation showed an activity of the ciliary muscle in young volunteers as well as those of presbyopic age.

Introduction

The mechanisms of human accommodation and the pathophysiology of presbyopia have been debated with surprising passion for nearly two centuries. Today there exist two major forms of intraocular presbyopia correction: first, the attempts to create accommodative IOL implants [28, 30] and second, to surgically restore accommodation [36]. Before the development of an artificial accommodative lens-replacing material with accommodative capabilities can become feasible, the influence of the aging ciliary muscle must be determined.

In recent years various imaging techniques have been developed to improve identification, characterization and quantification of ophthalmologic diagnosis [17, 18, 22, 26]. Ultrasound biomicroscopy (UBM) has proven an important tool for investigating anterior segment structures with high spatial resolution [23, 31, 32, 33].

The first two-dimensional UBM investigations of the ciliary muscle in different accommodation states [4, 13, 20, 24] have been published. The main problem and source of error associated with two-dimensional ultrasonic imaging of the ciliary muscle in different states of accommodation lies in the dynamics of the accommoda-

tive process as well as the presence of the ciliary processes. The existence of the processes prevents precise quantification of the accommodative ciliary muscle changes. Additionally, differentiation is necessary to compare identical ciliary body sections.

It has long been appreciated that three-dimensional (3D) ultrasonic images can be produced from an ordered series of scan planes. This technique was first applied to the anterior segment of the eye by Iezzi et al. [19] and required considerable effort and ingenuity with regard to apparatus [6, 9, 35]. Iezzi et al. used a scanning control arm for a continuous z-movement and stored the data on videotape for subsequent digitalization. Silverman et al. [37] characterized the ciliary body including the state of the ciliary processes of rabbits and normal human subjects using 3D high-resolution ultrasound. There the scanning system consist of two orthogonal linear stages with a computer-controlled stepping motor.

In this paper a simple and low-cost extension of the commercial Ultrasound Biomicroscope Model 840 (Humphrey Instruments, Carl Zeiss Group) into a user-friendly 3D- ultrasonic imaging system is described. Currently Paradigm Medical Industries is the manufacturer of the latest UBM generation. Furthermore, we will show how we are using this 3D technique to study the quantification of ciliary body function during accommodation.

Materials and methods

The principle of the UBM has been described in detail previously [32]. Iezzi et. al. and Coleman et. al. used a technique for 3D ultrasound [6, 9, 19, 35], whose application is already demonstrated [5, 29, 38, 39, 41].

In this study a 3D imaging method using an standard UBM in combination with an 3D extension is used [21]. Here 3D data sets consist of B-scan stacks of in-parallel planes with a defined distance between them. Patients were scanned with the ultrasound probe coupled to the eye with Methocel (Ciba Vision) and a normal saline water bath. The examiner positioned the transducer in the center of the ocular segment of interest using standard B-mode. For 3D imaging the computer-controlled scanning system moved the transducer perpendicular (*z*-direction) to the B-scan plane (*xy*-plane) over the area being scanned. For this motion an additional miniature skid was mounted on the original linear motor of the UBM scanning device where the ultrasound transducer is attached (Fig. 1). Because of its weight it is not possible to attach also the drive of this skid. Therefore the skid is powered from an external stepping motor via a Bowden wire. The technical arrangement of the ultrasound probe is shown in Fig. 1.

The video signal of the ultrasound unit is digitized using a frame-grabber board (HaSoTec, Germany) synchronized with the *z*-motion control system. That means during image capturing the *z*-movement is stopped and the image plane is exactly perpendicular to the *z*-axis. For the investigations presented here, 10 s acquisition time with a scanning range of 2.5 mm was used for all subjects, which is thought to be the maximum considering patient and examiner movements. Thus, all 3D scans have the same sampling density. The original UBM raw data (256 scan lines × 1024 samples per line, 256-level grayscale) pictured on the UBM display with 880×440 pixels were converted into 440×440 pixels (256-level gray scale) during capturing by the frame grabber. No degradation of the image quality is observable and the influence of the conversion is negligible compared with the movement artifacts and contour finding.

The motion control and data acquisition system is connected with an SGI workstation via a local area network for 3D reconstruction using VoxelView (Vital Images, Fairfield, Iowa, USA). This commercial volume rendering software package provides an interactive environment allowing features such as volume orientation for viewing planes and 3D perspectives, segmentation and determination of distances and surfaces. The feature of model building allows outlining of anatomic structures in space and can be used for volume measurements.

Accommodative studies have been carried out using pharmacologically induced accommodation (pilocarpine 2%, left eye) or disaccommodation (cyclopentolate 1%, right eye). The ciliary body regions of 12 volunteers were scanned 30 min after pharmacological treatment, and for contour determination a differentiation between sections with and without ciliary processes was made using VoxelView. The configuration of the differently stimulated ciliary bodies was analyzed using the following procedure for contour determination. The respective positions of the scleral spur and the ciliary muscular base were used to define a suitable coordinate system for the pattern recognition system. In addition, the posterior wall of the iris had to be differentiated from the neighboring ciliary muscle. The ciliary muscle base was approximated as a parabola, while the posterior wall of the iris was approximated as a straight line. The scleral spur served as an origin of coordinates

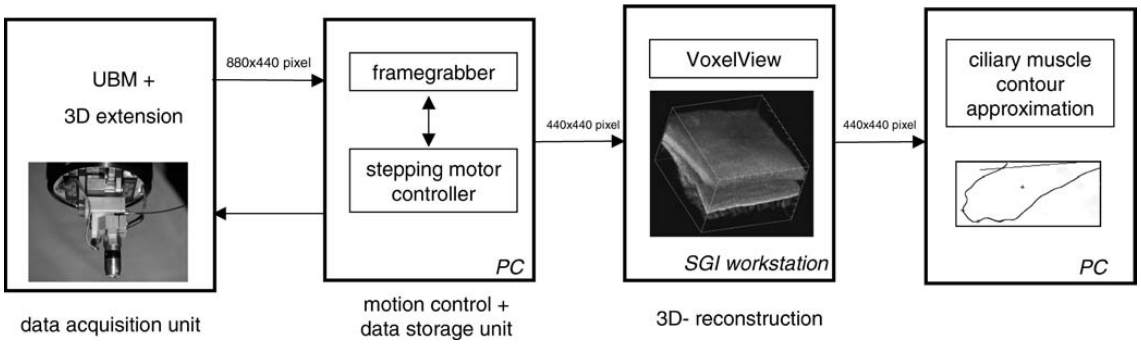

Fig. 1 Schematic representation of the modified ultrasound biomicroscope (*UBM*) for three-dimensional imaging and the principle of data evaluation for ciliary muscle approximation

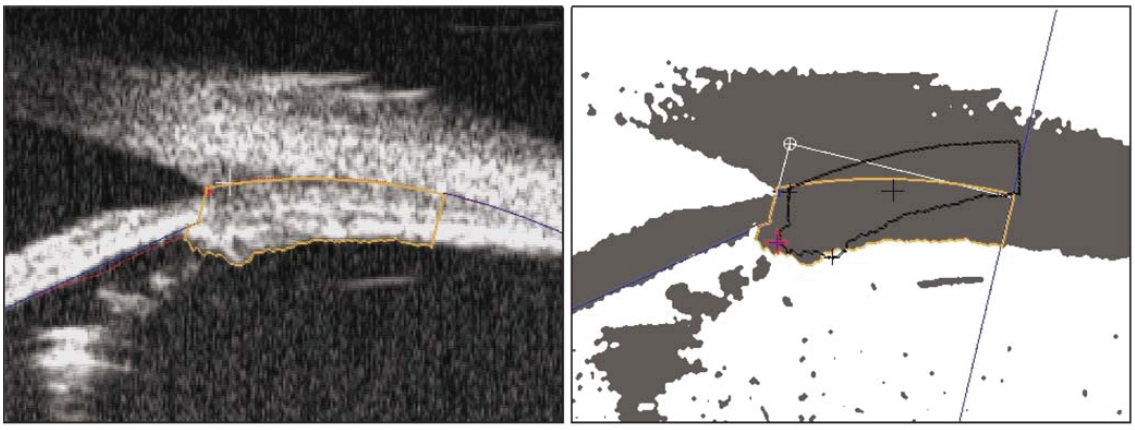

Fig. 2 Ultrasound biomicroscopic sectional image of the ciliary body extracted from a 3D data set. After manual marking of the scleral spur, the posterior surface of the iris and the base of the ciliary body(*blue*), the outer contour of the ciliary body is approximated (*yellow*)

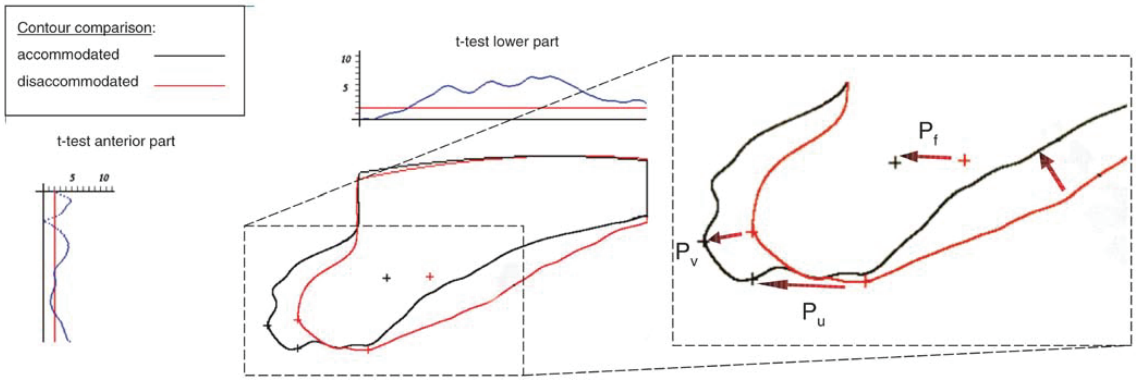

Fig. 3 An example of quantification of the contour changes of the ciliary muscle during accommodation. The outer contour after superposition and averaging of 10 individual contour approximations in accommodation (*black*) and disaccommodation (*red*) as well as the defined characteristic contour points (P_f center of gravity, P_v anterior contour point, P_u lower contour point) are shown

and as a rotation center for the subsequent averaging of the individual contours to afford a mean contour. Figure 2 shows the principle of segmentation. The outer contour of the ciliary body was found using a fixed threshold value in the gray-scale images. For contour comparison ten comparable radial sections through the ciliary body were selected, approximated and averaged. A comparison was made on the basis of the mean outer contour, and a quantitative comparison was based on the defined 2D parameters – the center of gravity of the surface P_f, the anterior contour point P_v and the lower contour point P_u (Fig. 3). The contour-finding procedures were carried out by one examiner for the whole study. Using a sample image and five individual independent contour findings the average error in the center of gravity is 3.3%.

An example of quantification of the contour changes of the ciliary muscle during accommodation is shown in Fig. 3. The outer contours in accommodation and disaccommodation are shown, as is the shift of defined characteristic contour points (center of gravity P_f, anterior contour point P_v and lower contour point P_u).

Results

A 3D-UBM image of the anterior segment is given in Fig. 4, depicting the ciliary body region of a normal volunteer. The volumetric reconstruction shows the sclera, cornea, iris and the ciliary body with ciliary processes. The ciliary body is composed of two parts, the pars plicata and the pars plana. The pars plicata contains a series of about 70 radially oriented projections, the so-called ciliary processes, and makes up the anterior 2 mm of the ciliary body. The pars plana is contiguous with the anterior pars plicata and the posterior choroid. In this figure, the ciliary processes can clearly be differentiated.

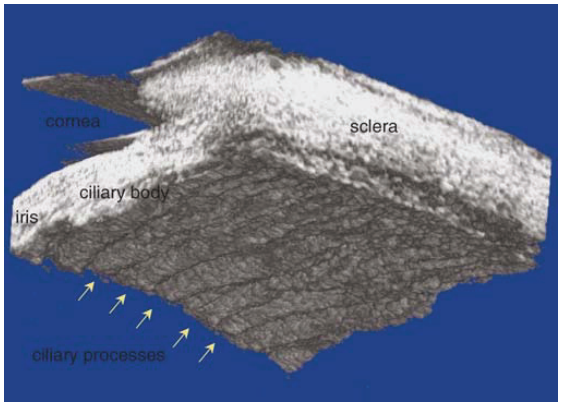

Fig. 4 Reconstruction of the ciliary body region in vivo. *Arrows* ciliary processes

In order to understand the accommodative mechanism, precise information is needed regarding the configurational changes of the ciliary muscle during accommodation. The main problem and the source of errors associated with 2D ultrasonic imaging of the ciliary muscle in various different states of accommodation lies in the dynamics of the accommodative process as well as the presence of the ciliary processes. The existence of these ciliary processes prevents precise quantification of the corresponding characteristics of the ciliary muscle. Figure 5 shows a UBM image of the ciliary body with clearly differentiated regions of the ciliary muscle with and without ciliary processes as well as corresponding sections S, S1 and S2. Radial sections in neighboring positions, such as S1 and S2, reveal significant differences with regard to the shape of the ciliary body. Two such radial sections through the ciliary body are shown in Fig. 5 right. The difference between sections such as S1 and S2 may exceed the expected accommodatively caused configurational changes of the muscle, since the processes contribute only passively to the deformation, thus preventing precise quantification of the corresponding characteristics of the ciliary muscle [2, 3, 4, 12].

In this context, accommodative studies have been carried out. A 17-year-old volunteer in states of pharmacologically induced accommodation and of disaccommodation was scanned using 3D-UBM. In an attempt at quantitative calculation of the configurational changes, a number of sections were selected from various regions of the ciliary body: the ciliary muscle with ciliary processes, and only the ciliary muscle. In the next step, the average contour was approximated and the resulting changes with regard to corresponding 2D parameters were analyzed. In Fig. 6 a contour comparison of the ciliary body during accommodation and disaccommodation corresponding to the slice positions S1 and S2 is shown. It should be emphasized that by occurrence of an accommodation stimulus a configurational change of the entire contours S1 and S2 is shown. Both in S1 (ciliary muscle with ciliary processes) and S2 (ciliary muscle) a shift of P_f, P_v and P_u in direction of the lens equator is observable, whereby the displacement for S1 is larger than S2 (Table 1).

For comparison of the ciliary muscle activity of young volunteers and subjects of presbyopic age, the anterior segment of one subject in each of these age categories was scanned. For accommodation stimulus, scanning and analysis the same procedure as described above was used. A contour comparison of the ciliary muscle of an young (34 years) and an old (71 years) volunteer, together with the changes of the muscle contour during an accommodation stimulus, is shown in Fig. 7. In both subjects activity of the ciliary muscle, i.e., a shift in the ciliary muscle center of gravity P_f as well as anterior

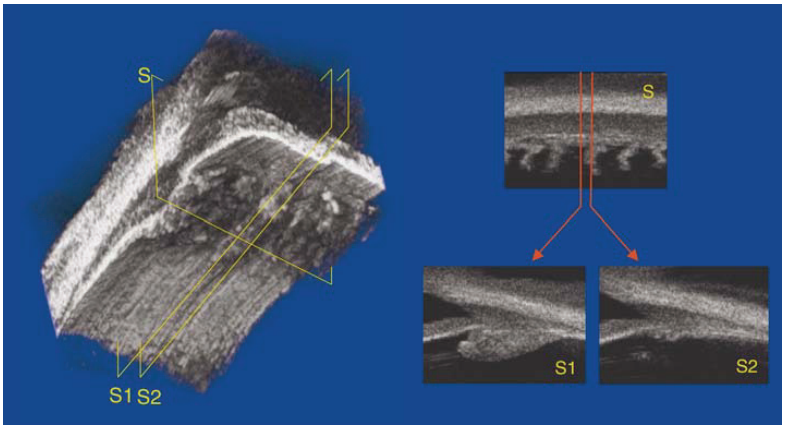

Fig. 5 Different sections across the human ciliary body are shown. Depicted are sections in transverse direction (*S*) across the ciliary muscle with ciliary processes (*S1*) and only the ciliary muscle (*S2*)

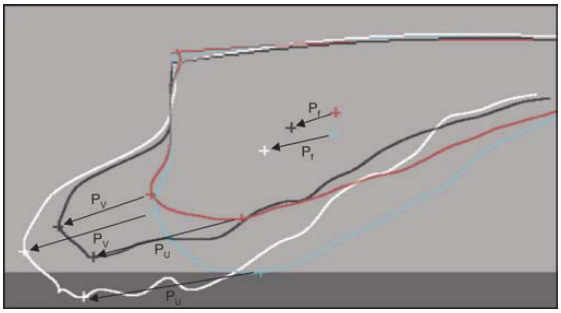

Fig. 6 Contour comparison of the ciliary body during accommodation and disaccommodation corresponding to the slice positions S1 and S2 in Fig. 5. By occurrence of an accommodation stimulus a shift of the contour points (P_f center of gravity, P_v anterior contour point, P_u lower contour point) in direction to the lens equator takes place. Ciliary muscle in disaccommodation (*red*) and accommodation (*black*); ciliary muscle with ciliary processes in disaccommodation (*blue*) and accommodation (*white*)

Table 1 Shift (absolute value of the displacement vector) of the characteristic contour points using ciliary muscle with ciliary processes and ciliary muscle corresponding to the contour approximation in Fig. 6

Contour point	Ciliary muscle with ciliary processes (S1)	Ciliary muscle (S2)
Center of gravity P_f	0.26 mm	0.16 mm
Anterior contour point P_v	0.47 mm	0.33 mm
Lower contour point P_u	0.60 mm	0.51 mm

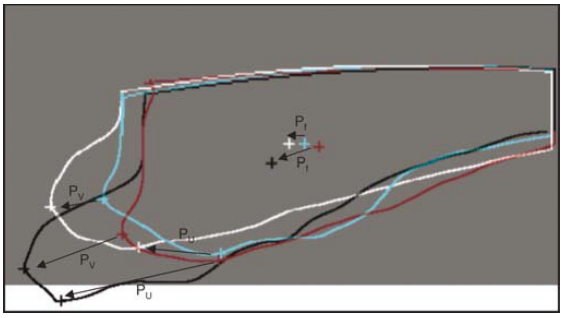

Fig. 7 Contour comparison of the ciliary muscle of a young (age 34 years) and an old (71 years) volunteer as well as the changes in the muscle contour during an accommodation stimulus. Young subject in disaccommodation (*red*) and accommodation (*black*); old subject in disaccommodation (*blue*) and accommodation (*white*)

point P_v and lower point P_u in the direction of the lens equator, can be detected (Table 2). The displacement of characteristic contour points in the young volunteer was greater than in the old volunteer. It is of interest that the

Table 2 Shift of the characteristic contour points during accommodation using the ciliary muscle of a young volunteer (age 34 years) and an old volunteer (age 71 years) corresponding to the contour approximation in Fig. 7

Contour point	Age of volunteers	
	34 years	71 years
Center of gravity P_f	0.17 mm	0.05 mm
Anterior contour point P_v	0.36 mm	0.18 mm
Lower contour point P_u	0.56 mm	0.28 mm

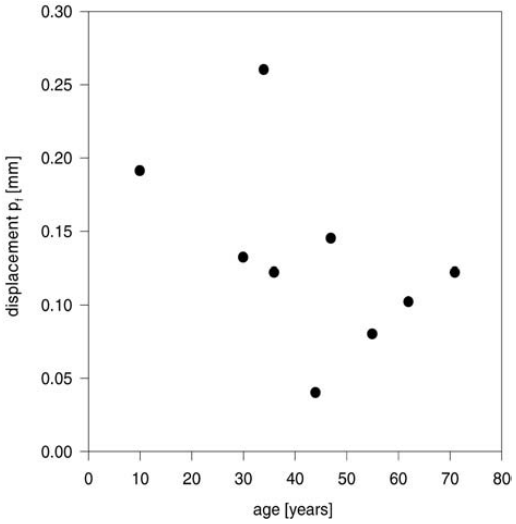

Fig. 8 The absolute value of the displacement vector of the ciliary muscle center of gravity P_f during accommodation depending on the age of the volunteer

investigations show activity of the ciliary muscle in young volunteers as well as in presbyopic age.

As a matter of principle, the contour points P_f, P_v and P_u are able to specify and quantify the individual ciliary muscle activity. The disadvantage is the need to analyze a large number of parameters. In this respect, simplification is necessary. As a parameter which describes the entire muscle contour, utilization of the displacement vector of the center of gravity P_f is preferable. Figure 8 shows the absolute values of the displacement vector P_f of the ciliary muscle center of gravity during accommodation depending on the age of the volunteers. Values of P_f ranged between 0.04 and 0.26 mm (mean 0.13±0.06 mm) with interindividual variation and a small decrease with age.

Discussion

Accommodation has been the subject of scientific discussion for more than 100 years. A number of different theories have been published and still there is ongoing debate. In general, many investigators agree with the Helmholtz explanation of accommodation.

Several authors [8, 11, 16, 28, 34] interpret the recovery of accommodative power as a long-term aim of cataract surgery. While surgical techniques used for cataract surgery are continuously being improved, the exact accommodative mechanism and the cause of presbyopia remains to be elucidated [1, 28, 42].

The possibility of surgical recovery of the power of accommodation makes it particularly interesting to study accommodatively induced reactions. Besides, competitive hypotheses regarding the genesis of presbyopia, regression in accommodative amplitude caused by altered lens material properties [14] as opposed to changed neuromuscular excitability or contractibility of the ciliary muscle / the zonular fibers [1, 7, 40, 42] are still a matter of ongoing debate.

The fact that the details of the accommodative mechanism remain unclear may primarily be attributed to the fact that direct observation of the ciliary muscle, due to its position behind the iris diaphragm, is very difficult. The observation of movement of the ciliary processes during accommodation, for instance by using a Scheimpflug camera, does not stringently allow one to conclude that the ciliary muscle is initiator of the movement. It is possible to circumstantiate the ciliary muscle function using 3D-UBM. The possibility of a differentiation between ciliary muscle sections with and without ciliary processes proved that the muscle realized a displacement in direction of the lens during accommodation, illustrated in Fig. 6. This movement of the muscle is smaller than those of the muscle including ciliary processes. It supports the early statements of Hess and Fincham [10, 15] that the ciliary processes move in the direction of the lens during accommodation. This view has been supported by the work of Neider [27] and Glasser [13] in iridectomized monkey eyes. On the contrary, Schachar postulated [36] that the valleculae of the ciliary body move away from the lens during accommodation. Our investigation does not support this observation. Figures 6 and 7 show a flattening of the valleculae which cannot be interpreted as a centrifugal movement away from the lens. This is also documented by analysis of the movement of the ciliary body center of gravity as the parameter which describes the entire contour change.

Detailed investigations of ciliary muscle contour changes were carried out by Lütgen-Drecoll using enucleated monkey eyes [25]. The study showed that all ciliary muscle regions contract during accommodation. The scleral spur is the fixed anchor point. The posterior muscle sections move in the direction of the lens due to the mobility (relocatability) over the sclera or choroid. Thereby, the anterior section of the muscle (nearest to the lens) is shifted in anterior direction. The anterior circular section of the muscle pulls the apex of the ciliary muscle circularly inwardly and increases the girth of the muscle abdomen. These results using anatomic animal investigations can be confirmed by our 3D-UBM investigations in vivo, exemplified in Figs. 6 and 7.

Upgrading of the 2D-UBM imaging technique to attain a 3D approach would make it possible to gain much more information regarding the spatial localization of the ciliary muscle. When comparing the ciliary body in the accommodated and the disaccommodated state, sections containing no ciliary processes may thus be selected. In this case one might expect the remaining ciliary body volume to largely represent the ciliary muscle itself, which, after all, is the interesting element in this context.

The configurational differences of the muscle during accommodation and disaccommodation may be analyzed and discussed by contour recognition based on characteristic 2D parameters. Our investigations revealed significant changes in the muscle configuration as well as changes in characteristic positions on the ciliary muscle, demonstrating that this method allows in-vivo investigation and documentation of accommodative configurational changes of the ciliary muscle. Recapitulating the findings illustrated in Fig. 8, we have found a shift of the ciliary muscle center of gravity, as a parameter which describes the entire muscle contour, in the direction of the lens equator. Values of this shift range between 0.04 and 0.26 mm with an individual variation and a small decrease with age. Bacskulin et al. [4] found an anterior shift of the anterior contour point ranging between 0.45 and –0.1 mm during accommodation, yielding an average shift of 0.05 mm of the ciliary muscle center of gravity anteriorly. In our study an average value of P_f=0.13 mm was found. The data of Bacskulin et al. agree with our finding that an excursion of center of gravity occurs at all ages. This shift decreases with increasing age, but never disappears. There is a certain activity of the ciliary muscle in young individuals as well as in those of presbyopic age.

These investigations aimed at enhancing the quantification of individual ciliary muscle activity. This was achieved by developing a three-dimensional high-resolution ultrasonic imaging technique that made it possible to analyze invisible areas of the anterior part of the eye. Particular emphasis was placed on the representation of configurational and positional changes of the ciliary muscle during accommodation.

Acknowledgements This research was supported by DFG grant no. GU 263/7-1. The authors thank K. Muscheites and P. Enzenross for technical assistance as well as A. Haubold for his critical comments.

References

1. Atchison DA (1995) Accommodation and presbyopia. Ophthalmic Physiol Opt 15:255–277
2. Bacskulin A, Bergmann U, Horoczi Z, Guthoff R (1995) Kontinuierliche ultraschallbiomikroskopische Darstellung der akkommodativen Veränderungen des humanen Ziliarkörpers. Klin Mbl Augenheilkd 247–252
3. Bacskulin A, Gast R, Bergmann U, Guthoff R (1996) Ultraschallbiomikroskopische Darstellung der akkommodativen Konfigurationsänderungen des presbyopen Ziliarkörpers. Ophthalmologe 93:199–203
4. Bacskulin A, Martin H, Kundt G, Terwee T, Guthoff R (2000) Analysis of the dynamics of the ciliary muscle during accommodation. Ophthalmologe 97:855–859
5. Coleman DJ (1995) Evaluation of ciliary body detachment in hypotony. Retina 15:312–318
6. Coleman DJ, Silvermann RH, Daly SW (1998) Advances in ophthalmic ultrasound. Radiol Clin North Am Imaging Ophthalmol 36:1073–1082
7. Croft MA, Kaufmann PL, Crawford KS, Neider MW, Glasser A, Bito LZ (1998) Accommodation dynamics in aging rhesus monkeys. Am J Physiol 275:1885–1897
8. Cumming JS, Kammann J (1996) Experience with an accommodating IOL. J Cataract Refract Surg 22:1001
9. Cusumano A, Coleman DJ, Silvermann RH, Reinstein DZ, Rondeau MJ, Ursea R, Daly SM (1998) Three dimensional ultrasound imaging – clinical applications. Ophthalmology 105:300–306
10. Fincham EF (1937) The mechanism of accommodation. Br J Ophthalmol [Monogr Suppl] VIII:1–80
11. Findl O, Menapace R (2000) Piggyback intraocular lenses. J Cataract Refract Surg 26:308–309
12. Fischer K, Krentz H, Guthoff R(1998) Darstellung der Variationsbreite des Ziliarkörpers mittels Ultraschallbiomikroskopie. 96th DOG Congress, short presentation
13. Glasser A (2001) Edinger-Westphal stimulated accommodation in monkeys. In: Guthoff, Ludwig (eds) Current aspects of accommodation. Kaden, pp 53–69
14. Glasser A, Campbell M (1998) Presbyopia and the optical changes in the human lens with age. Vis Res 38:209–229
15. Hess C (1904) Beobachtungen über den Akkommodationsvorgang. Klin Mbl Augenheilkd 42:309–315
16. Hettlich HJ, Lucke, K, Asiyo-Vogel MN, Schulte M, Vogel A (1994) Lens refilling and endocapsular polymerization of an injectable intraocular lens: in vitro and in vivo study of potential risks and benefits. J Cataract Refract Surg 20:115–123
17. Hockwin O, Wergekin E, Laser H, Dragomirescu V (1983) Scheimpflug photography. Ophthalmic Res 15:102–108
18. Hoerauf H, Wirbelauer C, Scholz C, Engelhardt R, Koch P, Laqua H, Birngruber R (2000) Slit-lamp-adapted optical coherence tomography of the anterior segment, Graefes Arch Clin Exp Ophthalmol 238:8–18
19. Iezzi R, Rosen RB, Tello C, Liebmann J, Walsh JB, Ritch R (1996) Personal computer-based 3-dimensional ultrasound biomicroscopy of the anterior segment. Arch Ophthalmol 114:520–524
20. Kano K, Kuwayama Y, Mizoue S, et al. (1999) Observation of physiological change in the human ciliary body using an ultrasound biomicroscope [in Japanese]. Nippon Ganka Gakkai Zasshi 103:297–300
21. Kirchhoff A, Stachs O, Guthoff R (2001) Three-dimensional ultrasound findings of the posterior iris region. Graefes Arch Clin Exp Ophthalmol. 239:968–971
22. Liebmann JM, Ritch R (1986) Ultrasound biomicroscopy of the anterior segment. J Am Optom Assoc 67:469–479
23. Lizzi FL, Rourke MC, Sokil-Melgar JB, et al (1992) Interfacing very-high frequency transducers to digital-acquisition scanning systems. SPIE Proc 1773:313–321
24. Ludwig K, Wegscheider E, Hoops JP, Kampik A (1999) In vivo imaging of the human zonular apparatus with high-resolution ultrasound biomicroscopy. Graefes Arch Clin Exp Ophthalmol 237:361–371
25. Lütjen-Drecoll E (2001) Edinger-Westphal stimulated accommodation in monkeys. In: Guthoff, Ludwig (eds) Current aspects of accommodation. Kaden, pp 25–35
26. Mashima Y, Oshitari K, Imamura Y, Momoshima S, Shiga H, Oguchi Y (1996) High-resolution magnetic resonance imaging of the intraorbital optic nerve and subarachnoid space in patients with papilledema and optic atrophy. Arch Ophthalmol 114:1197–1203
27. Neider MW, Crawford K, Kaufman PL, Bito LZ (1990) In vivo videography of the rhesus monkey accommodative apparatus. Arch Ophthalmol 108:69–74
28. Nishi O, Nishi K (1998) Accommodation amplitude after lens refilling with injectable silicone by sealing the capsule with a plug in primates. Arch Ophthalmol 116:1358–1361
29. Nouby-Mahmoud G, Colemann DJ (1993) Using high-frequency ultrasound to characterize intraocular foreign bodies. Ophthalmic Surg 24:944–999
30. Parel JM, Gelender H, Trefers WF, Norton EW (1986) Phaco-Ersatz: cataract surgery designed to preserve accommodation. Graefes Arch Clin Exp Ophthalmol 224:165–173
31. Pavlin CJ, Foster FS (1992) Ultrasound biomicroscopy in glaucoma. Acta Ophthalmol 204 [Suppl]:7–9
32. Pavlin CJ, Foster FS (1995) Ultrasound biomicroscopy of the eye. Springer, New York Berlin Heidelberg
33. Pavlin CJ, Sherar MD, Foster FS (1990) Subsurface ultrasound microscopic imaging of the intact eye. Ophthalmology 97:244–250
34. Payer H (1997) Ringwulstlinse mit Zoomwirkung zur Verstärkung einer Pseudoakkommodation und deren Erklärung aus erweiterter Akkommodationstheorie. Spektrum Augenheilkd 11:81–89
35. Reinstein DZ, Raevsky T, Colemann DJ (1997) Improved system for ultrasonic imaging and biometry J Ultrasound Med 16:117–124
36. Schachar RA (2001) The correction of presbyopia [review]. Int Ophthalmol Clin 41:53–70
37. Silverman RH, Lizzi FL, Ursea BG, Rondeau MJ, Eldeen NB, Kaliscz A, Lloyd HO, Coleman DJ (2001) High-resolution ultrasonic imaging and characterization of the ciliary body. Invest Ophthalmol Vis Sci 42:885–894
38. Silvermann RH, Rondeau MJ, Lizzi FL, Coleman DJ (1995) Three dimensional ultrasonic parameter imaging of anterior segment pathology. Ophthalmology 102:837–843
39. Silvermann RH, Folberg R, Boldt HC, Lloyd HO, Rondeau MJ, Mehaffey MG, Colemann DJ (1997) Correlation of ultrasound parameter imaging with microcirculatory pattern in uveal melanoma. Ultrasound Med Biol 23:573–581
40. Tamm E, Lütjen-Drecoll E, Jungkunz W, Rohen JW (1991) Posterior attachment of ciliary muscle in young, accommodating old, presbyopic old monkeys. Invest Ophthalmol Vis Sci 32:1678–1692
41. Ursea R, Coleman DJ, Silvermann RH, Lizzi FL, Harrison W (1998) Correlation of high frequency ultrasound backscatter with tumor microstructure on iris melanoma. Ophthalmology 105:906–912
42. Weale R (1989) Presbyopia towards the end of the 20th century. Surv Ophthalmol 34:15–30

Monitoring the Human Ciliary Muscle Function During Accommodation

O. Stachs[1]

Quantification of ciliary muscle function is expected to gain importance for two reasons - it will enhance our basic understanding of the accommodation process, including presbyopia, and it will serve as a basis for the development of suitable accommodative lens-replacing materials.The location of the accommodative apparatus - behind the iris and the sclera - presents an elementary disadvantage for investigations of human accommodation. It precludes studying the entire lens in different accommodative states and under in-vivo conditions. Animal models based on completely iridectomized eyes, histological preparation, or Edinger-Westphal stimulation [12, 15, 16, 20, 25, 28, 29, 36, 37] might help circumvent this problem. Nevertheless, these difficulties may have contributed to the fact that accommodation is interpreted by a variety of mutually exclusive theories [1, 6, 9, 22, 37, 38, 39, 44, 45].

Ultrasound Techniques

In recent years, various imaging techniques have been developed to improve the identification, characterization and quantification of the morphology of the eye [18, 23. 27, 34, 33, 31, 2, 19]. Ultrasound is the most widely used non-optical technique for ocular analysis. The resolution of ultrasound images is related to the frequency of the transducer. The utilization of the polyvinylidene fluoride transducer technique [34, 33] permits a very high ultrasound scanning frequency. At this frequency, resolutions of 30 microns axially by 60 microns laterally were obtained. While attenuation limits the use of this technique to the anterior segment of the eye (cornea, lens, iris, ciliary body), very high-frequency ultrasound has had a major impact on accommodation studies [24, 16]. Three-dimensional ultrasound is an extension of B-scan imaging and comprises data acquisition, graphical reconstruction, visualization, and biometry. It has long been appreciated that three-dimensional ultrasonic images consist of series of neatly stacked two-dimensional scans [7, 11, 35, 21].

This article describes an attempt to quantify the ciliary body function during accommodation by 3D sonographic analysis; it also demonstrates the value of this technique for the assessment of individual ciliary muscle activity.

[1] Eye Clinic of the University of Rostock, Doberaner Straße 140, D-18055 Rostock, Germany

Materials and Methods

Scanning system and imaging

The UBM principle has been described in detail [32]. Coleman et. al. used a more complicated 3D ultrasound technique [7, 11, 35], which is described in the literature [8, 41, 43, 40, 30].

For the study presented in this chapter a simple, previously described [21, 42] 3D imaging method is used. In this context, 3D data sets consist of stacks of B-scans in parallel planes at a defined distance. For 3D imaging, the computer-controlled scanning system moved the transducer orthogonally (in z direction) to the plane of the 8 Hz motion (xy plane) above the area being scanned. Scanning time and scanning range in conjunction with the travel along the z axis in the third dimension are variable. In this case, accommodation investigations were based on a scanning time of 10 sec with a scanning range of 2.5 mm in z direction. This is thought to be the optimum, considering movement-related artefacts and resolution. The video signal of the ultrasound unit was digitized using a framegrabber board (HaSoTec, Germany); and storage was synchronized with the z motion. The motion control and data acquisition system was connected to a SGI workstation via LAN network for 3D reconstruction using *VoxelView* (Vital Images, USA). Fig.1 shows an example of 3D reconstruction with the above-mentioned scanning parameters. This volume-rendering software package provides an interactive environment allowing features such as volume orientation for viewing planes and 3D perspectives, segmentation, and determination of distances and surfaces.

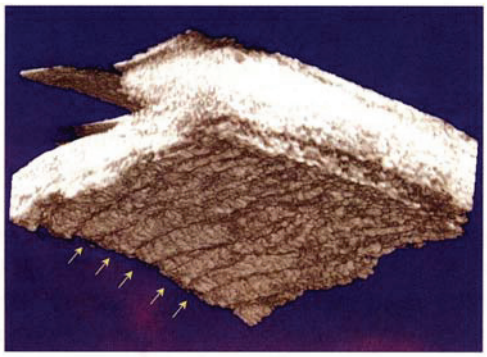

Figure 1.
Three-dimensional image of the ciliary body area; the arrows indicate the ciliary processes.

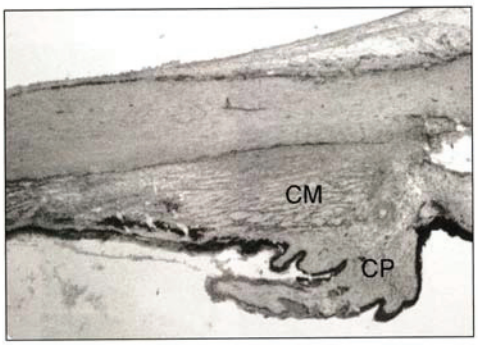

Figure 2. *The human ciliary body with the ciliary muscle (CM) and the ciliary processes (CP).*

This system makes it possible to extract sectional B-images in any plane of the 3D volume so as to distinguish the ciliary muscle structures (fig.3).

Patients

This investigation complied with the Declaration of Helsinki. All of the participants, after receiving appropriate instruction and explanation of the nature and the possible consequences of this research, signed the informed consent form to confirm their agreement with the non-invasive investigative technique. This investigation was based on 3D UBM studies of the anterior segment of 7 healthy volunteers between 10 and 71 years of age. Scanning was performed under topical anesthesia, with the patient in supine position. An eyecup filled with methylcellulose and saline solution was inserted between the eyelids.
The ciliary body regions of the volunteers' eyes were scanned at maximum far and near accommodation. Accommodative studies involved pharmacologically induced accommodation with pilocarpine 2 %; cyclopentolate 1 % was administered for disaccommodation.

Results

The main problem and the primary source of errors associated with two-dimensonal ultrasonic imaging of the ciliary muscle in various different states of accommodation arise from the dynamics of the accommodative process as well as the existence of the ciliary processes (figs.2 and 3). These ciliary processes preclude any precise quantification of the corresponding characteristics of the ciliary muscle. An investigation of radial sections in vicinal positions, such as S1 and S2 in fig.3, reveals significant differences with regard to

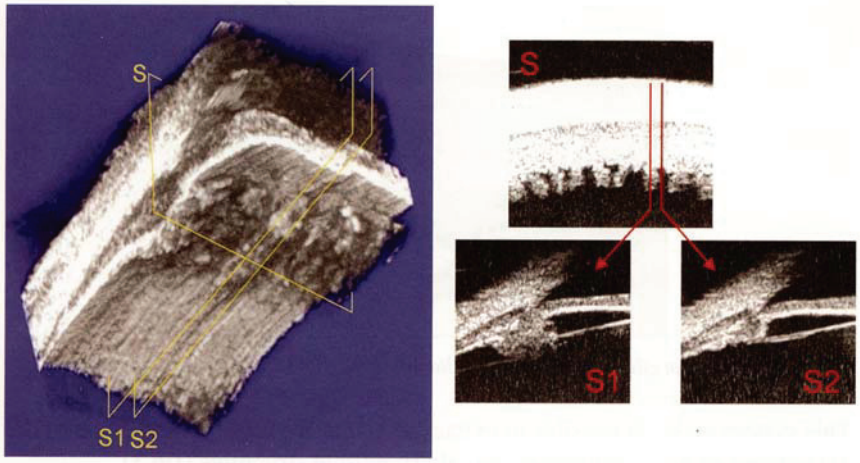

Figure 3. *A three-dimensional image of the human ciliary body; slices S, S1 and S2 are indicated. Note that ciliary muscle separation is possible. The smaller images present various sections of the human ciliary body. Sections are shown in transversal direction (S) across the ciliary muscle, including the ciliary processes (S1); S2 contains only the ciliary muscle.*

the shape of the ciliary body. Determining the contours of the ciliary body, especially those of the ciliary muscle in different accommodative states, demonstrates that the difference between sections such as S1 and S2 in fig.3 may exceed the expected accommodatively caused configurational changes in the muscle. In this case the ciliary processes only contribute passively to the deformation, thus preventing precise quantification of the corresponding characteristics of the ciliary muscle [3, 4, 5, 14].

Thus, sectional B-images corresponding to the S2 sections (fig.3) were used to approximate the contours of the ciliary muscle. For accommodation studies, ten of these sections were selected in the accommodated and in the disaccommodated phase, respectively; these were then analyzed with a semi-automatic pattern recognition system (fig. 4 and [5]). The respective positions of the scleral spur and the ciliary muscular base were used to define a suitable coordinate system for the pattern recognition system. In addition, the posterior wall of the iris had to be differentiated from the neighboring ciliary muscle.

***Figure 4**. Ultrasound biomicroscopic sectional image of the ciliary body, obtained from a 3D data set, corresponding to fig.3, Section s2. After marking the scleral spur, the posterior surface of the iris and the base of the ciliary body(blue), the outer contour of the ciliary body is approximated (yellow).*

The ciliary muscle base was approximated by a parabolic shape, while the posterior wall of the iris was approximated by a straight line. The scleral spur, by definition, coincided with the origin of coordinates and also served as a center of rotation for the subsequent averaging of the individual contours to afford a mean contour. A comparison was made on the basis of the mean outer contour; and a quantitative comparison was performed based on the center of gravity of the surface P_f, the anterior contour point P_V, and the lower contour point P_u (see fig.5 for definition). Fig.5 shows an example of a contour approximation after main value determination of 10 individual contour approximations corresponding to fig.4.

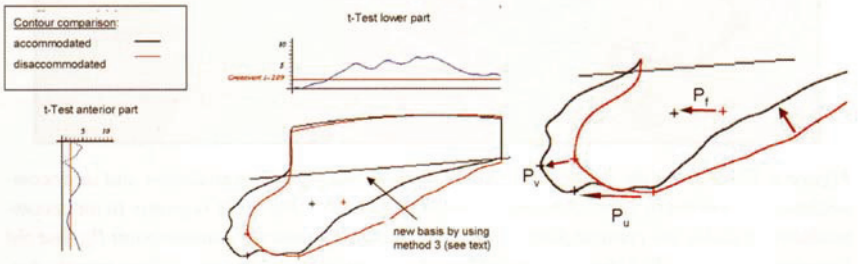

***Figure 5.** Quantifying the contour changes of the ciliary muscle during accommodation. This image shows the outer contour after superposition of 10 individual contour approximations (see Fig. 4) during accommodation (black) and disaccommodation (red), respectively. The defined characteristic contour points (center of gravity P_f, anterior contour point P_V, and the lower contour point P_U) are clearly indicated.*

Discussion

The ciliary muscle, which is the 'engine' powering the mechanism of accommodation, is optically invisible. In iridectomized eyes, observation is limited to the anterior vascularized ciliary processes in lens direction. These ciliary processes, together with the zonular fibers, passively contribute to ciliary muscle movement. This mechanism can be confirmed by 3D ultrasound biomicroscopy [42], making it possible to distinguish between ciliary muscle sections with and without ciliary processes (fig.3) and analyzing contour changes during accommodation (figs.6, 7). Observation of the ciliary processes during accommodation, for instance by using a Scheimpflug camera, reveals an accommodative movement which does not necessarily point to the ciliary muscle causing this movement. However, the ciliary muscle function may be confirmed by 3D ultrasound biomicroscopy. Distinguishing between ciliary muscle sections with and without ciliary processes, respectively, reveals the (albeit less drastic) shift of these ciliary processes in the direction of the lens (fig.6).

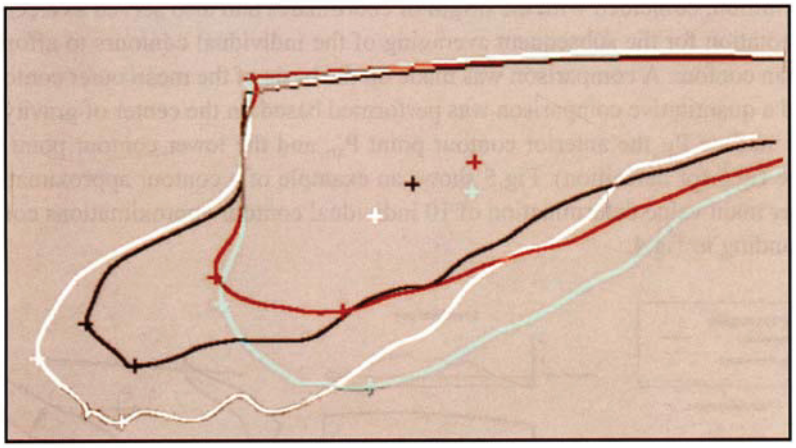

***Figure 6**. Comparing the contours of the ciliary body during accommodation and disaccommodation, respectively, corresponding to slices S1 and S2 in Fig. 4. In response to an accommodative stimulus, the contour points (center of gravity P_f, anterior contour point P_v, and the lower contour point P_u) show a noticeable shift toward the lens equator (ciliary muscle during disaccommodation (red) and accommodation (black), respectively; ciliary muscle with ciliary processes during disaccommodation (blue) and accommodation (white), respectively).*

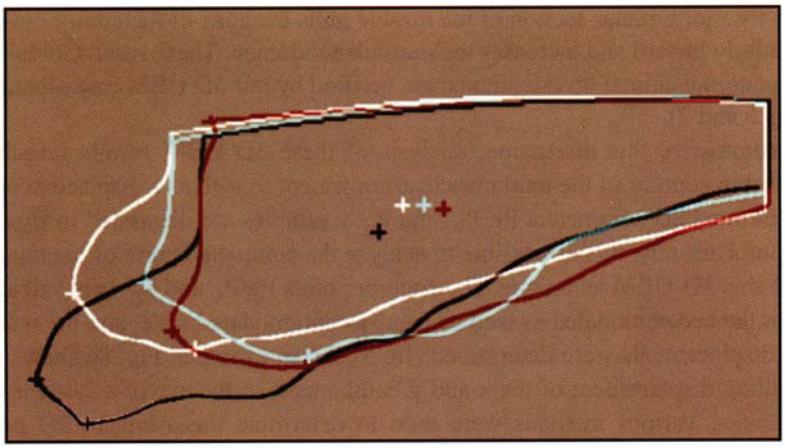

Figure 7. *Comparison of the ciliary muscle contours in a young eye (volunteer 34 years of age) versus an older eye (71 years). Changing muscle contours caused by an accommodative stimulus. This reveals the activity of the ciliary muscle in the eyes of young volunteers and in the presbyopic eye (young subject during disaccommodation (red) and accommodation (black), respectively; old subject during disaccommodation (blue) and accommodation (white), respectively).*

This evidence substantiates earlier results published by Hess and Fincham [17, 13], claiming that the ciliary processes approach the lens during accommodation. This concept is also supported by Neider [29] and Glasser [16] who investigated iridectomized monkey eyes. Contrasting results were obtained by Schachar who, in 1994, postulated that the cilliary body valleys move away from the lens during accommodation. Our own investigations, however, do not confirm Schachar's observation. Figs.6 and 7 show a flattening of the valleys which cannot be interpreted as a centrifugal movement away from the lens. In addition, dynamic analysis of the center of gravity of the ciliary body, being the parameter reflecting the entire contour change, corroborates this mechanism.

Lütgen-Drecoll performed detailed investigations of ciliary muscle contour changes in enucleated monkey eyes [26]. This investigation suggests that all ciliary muscle regions contract during accommodation. The scleral spur, being the anchor point, remains fixed. The posterior muscle sections move in the direction of the lens due to the mobility (relocatability) over the sclera respectively the choroid. Thus, the anterior section of the muscle (the one closest to the lens) shifts in anterior direction.

The anterior circular section of the muscle pulls the apex of the ciliary muscle circularly inward and increases the muscular abdomen. These results, obtained by anatomic animal investigations, are verified by our 3D UBM investigations (figs.6 and 7).

To summarize this discussion, analysis of these 3D UBM results reveals a changing contour of the total muscle arrangement as well as a displacement of the defined 2D parameters P_f, P_V, and P_u. Examples are illustrated in figs. 5-7. Unfortunately, it is impossible to analyze the complete length of the muscle with this 3D-UBM technique. The contour points P_f, P_V and P_u were calculated in the accommodated as well as the disaccommodated state, and the resulting displacements were determined (fig.5). As an example, Fig. 8a shows the resulting displacement of the x and y components in the eye of a 22-year-old volunteer. Various methods were used to determine the averaged 2D point locations based on individual ciliary muscle contours corresponding to fig. 4. The first approach involved outer contour determination, followed by point determination with averaging. According to the second approach, the outer contour was found by averaged contour determination, followed by point determination. The third approach was derived from the second one, with changed bases (fig.5). This third approach reveals enhanced sensitivity for contour changes at the center of gravity. The standard deviation of coordinate values determined by the third approach is shown in fig. 8b.

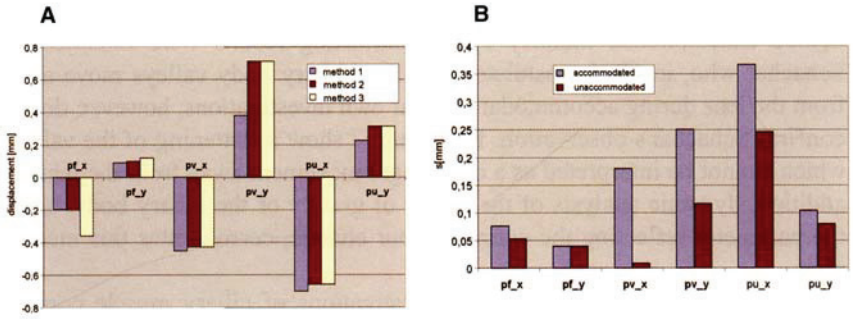

Figure 8. *A - Shift along the coordinate (x, y); determination of defined 2D parameters (center of gravity P_f, anterior contour point P_V, and the lower contour point P_u) of the ciliary muscle in the eye of a 22-year-old subject during accommodation; B - standard deviation of the coordinate values (x, y) (determined by the third approach) during accommodation and disaccommodation, respectively.*

The contour points P_f, P_v and P_u were selected for their specific position; i. e., they reflect the individual ciliary muscle activity which can thus be specified and quantified. This analysis, however, has the disadvantage of involving a large number of parameters. Hence it had to be simplified. When evaluating the standard deviation with regard to the determination of the x and y components P_f, P_v and P_u (fig.8b), one should preferably use the displacement vector of the center of gravity. Fig.9 shows the absolute values regarding P_f displacement of the center of gravity of the ciliary muscle during accommodation in relation to the volunteer's age. Values are between 0.04 and 0.26 mm, with a certain variation between individuals, which decreases slightly with age. If the absolute value of the displacement vector is used the direction of the movement is lost. Representing the displacement vector in a polar coordinate system offers a simple, effective technique of assessing and quantifying the individual accommodation (fig.10). In this case the point of origin is at the center of gravity of the ciliary muscle during disaccommodation; while the green dots represent the center of gravity during accommodation. An analysis of the angle of the displacement vectors, as well as the corresponding values, provides information on the individual ciliary muscle activity. Investigations demonstrate that this angle is somewhere between 130° and 210°; with values of up to 0.26 mm.

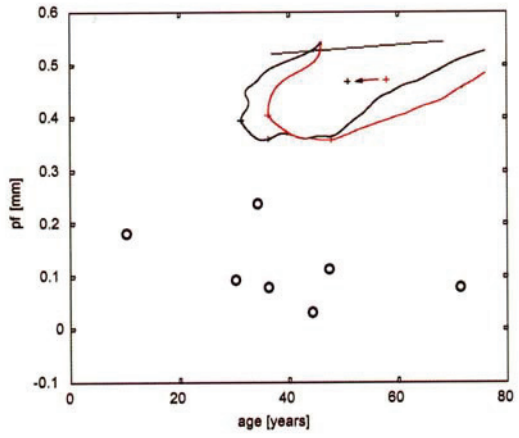

Figure 9. *Absolute displacement of the center of gravity of the ciliary muscle during accommodation in relation to the volunteer's age.*

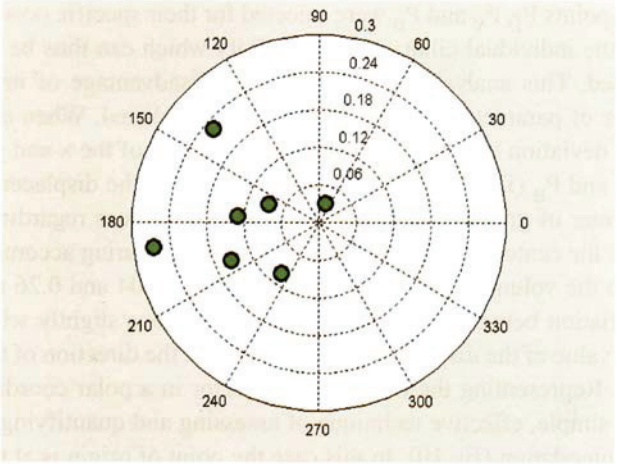

Figure 10. *Displacement vector (in polar coordinates) of the center of gravity of the ciliary muscle during accommodation. The point of origin represents the disaccomodated state; the green points reveal the accommodation of individual eyes.*

Results regarding individual ciliary muscle activity may be summarized as follows: Upgrading the two-dimensional ultrasound biomicroscopic imaging technique and turning it into a three-dimensional approach would provide much more comprehensive information regarding the behavior of the ciliary muscle in space.

The described three-dimensional microscopic technique makes it possible to represent the ciliary body in various accommodative states. Based on these 3D data, radial sections of the ciliary body may be selected so as to avoid the ciliary processes. The remaining ciliary body sections represent the ciliary muscle. The differences between muscular configuration during accommodation and disaccommodation, respectively, may be analyzed and discussed by contour recognition based on characteristic 2D parameters. Pertinent investigations revealed significant changes of the muscle configuration as well as the characteristic positions on the ciliary muscle. They confirm that this is a suitable method for in-vivo investigation and documentation of accommodative configurational changes of the ciliary muscle. This investigation points to ciliary muscle activity in young as well as presbyopic eyes. Presentation of the displacement vector in a polar coordinate system is preferable if one is to study individual ciliary muscle activity.

Acknowledgment

This research was supported by DFG grant no. GU 263/7-1.

The author also expresses his gratitude to P. Enzenross, K. Hornich, A. Kirchhoff, H. Martin, K. Muscheitis, J. Stave and H. Schneider.

References

[1] Atchison, D.A.: Accommodation and presbyopia. Ophthal. Physiol. Opt., 1995; 15: p. 255-277.

[2] Auffarth, G.U.; Biazid, Y.; Tetz, M.R.; Völcker. H.E.: Reliabilität der Vorderkammertiefenmessungen mit dem Orbscan-Topographiegerät. [*Reliability of the anterior chamber depth measurements obtained with the Orbscan topographic instrument*]. In: (Ohrloff, C., ed.) 11. Kongreß der DGII 1997, p. 125-130. Springer, Berlin, Heidelberg, New York, 1997.

[3] Bacskulin, A.; Bergmann, U.; Horoczi, Z.; Guthoff, R.: Kontinuierliche ultraschallbiomikroskopische Darstellung der akkommodativen Veränderungen des humanen Ziliarkörpers. [*Continuous ultrasound-biomicroscopic representation of accommodative changes in the human ciliary body*]. Klin. Mbl. Augenheilk., 1995; p. 247-252.

[4] Bacskulin, A.; Gast, R.; Bergmann, U.; Guthoff, R.: Ultraschallbiomikroskopische Darstellung der akkommodativen Konfigurationsänderungen des presbyopen Ziliarkörpers [*Ultrasound-biomicroscopic representation of accommodative configurational changes of the presbyopic ciliary body*]. Ophthalmologe, 1996; 93: p. 199-203.

[5] Bacskulin, A.; Martin, H.; Kundt, G.; Terwee, T.; Guthoff, R.: Analysis of the dynamics of the ciliary muscle during accommodation. Ophthalmologe, 2000; 97 (12): p. 855-859.

[6] Coleman, D.J.: On the hydraulic suspension theory of accommodation. Trans. Am. Soc. Ophthalmol., 1986; 84: p. 846-868.

[7] Coleman, D.J.; Silvermann, R.H.; Daly, S.W.: Advances in Ophthalmic Ultrasound. Radiologic Clinics of North America. Imaging in Ophthalology, 1998; 36: p. 1073-1082.

[8] Coleman, D.J.: Evaluation of ciliary body detachment in Hypotony. Retina, 1995; 15 (4): p. 312-318.

[9] Croft, M.A.; Glasser, A.; Kaufman, P.L.: Accommodation and presbyopia. Int. Ophthal. Clin., 2001; 41 (2): p. 33-46.

[10] Croft, M.A.; Kaufmann, P.L.; Crawford, K.S.; Neider, M.W.; Glasser, A.; Bito, L.Z.: Accommodation dynamics in aging rhesus monkeys. Am. J. Physiol., 1998; 275: p. 1885-1897.

[11] Cusumano, A.; Coleman, D.J.; Silvermann, R.H.; Reinstein, D.Z.; Rondeau, M.J.; Ursea, R.; Daly, S.M.: Three-dimensional ultrasound imaging - clinical applications. Ophthalmology, 1998; 105 (2): p. 300-306.

[12] Farnsworth, P.N.; Burke, P: Three-dimensional architecture of the suspensory apparatus of the lens of the rhesus monkey. Exp. Eye Res., 1977; 25: p. 563-576.

[13] Fincham, E.F.: The mechanism of accommodation. Brit. J. Ophthal. Monograph Suppl., 1937; VIII: p. 1-80.

[14] Fischer, K.; Krentz, H.; Guthoff, R.: Darstellung der Variationsbreite des Ziliarkörpers mittels Ultraschallbiomikroskopie. [*Representation of ciliary body variation by ultrasound biomicroscopy*] 96th DOG Congress 1998, short presentation.

[15] Glasser, A.; Campbell, M.: Presbyopia and the optical changes in the human lens with age. Vis. Res., 1998; 38: p. 209-229.

[16] Glasser, A.; Croft, M.A.; Brumback, L.; Kaufman, P.L.: Ultrasound biomicroscopy of the aging rhesus monkey ciliary region. Opt. Vis. Sci., 2001; 78 (6): p. 417-24.

[17] Hess, C.: Beobachtungen über den Akkommodationsvorgang. [*Observations regarding the accommodative process*]. Klin. Mbl. Augenheilk., 1904; 42: p. 309-315

[18] Hockwin, O.; Wergekin, E.; Laser, H.; Dragomirescu, V.: Scheimpflug photography. Ophthal. Res., 1983; 15: p. 102-108.

[19] Hoerauf, H.; Wirbelauer, C.; Scholz, C.; Engelhardt, R.; Koch, P.; Laqua, H.; Birngruber, R.: Slit-lamp-adapted optical coherence tomography of the anterior segment. A. v. Graefe's Arch. Clin. Exp. Ophthalmol., 2000; 238: p. 8-18.

[20] Kaufman, P.L.; Rohen, J.W.; Bµrµny, E.H.: Hyperopia and loss of accommodation following ciliary muscle disinsertion in the cynomolgus monkey: physiologic and scanning electron microscopic studies. Invest. Ophthalmol. Vis. Sci., 1979; 18: p. 665-673.

[21] Kirchhoff, A.; Stachs, O.; Guthoff, R.: Three-dimensional ultrasound findings of the posterior iris region. A. v. Graefe's Arch. Clin. Exp. Ophthalmol., 2001; 239 (12): p. 968-71.

[22] Koretz, J.F.; Handelman, G.H.: Model of the accommodative mechanism in the human eye. Vis. Res., 1982; 22: p. 917-927.

[23] Liebmann, J.M.; Ritch, R.: Ultrasound biomicroscopy of the anterior segment. J. Am. Optom. Assoc., 1986; 67: p. 469-479.

[24] Ludwig, K.; Wegscheider, E.; Hoops, J.P.; Kampik. A.: In vivo imaging of the human zonular apparatus with high-resolution ultrasound biomicroscopy. A. v. Graefe's Arch. Clin. Exp. Ophthalmol., 1999; 237 (5): p. 361-71.

[25] Lütjen-Drecoll, E.; Tamm, E.; Kaufman, P.L.: Age-changes in the ciliary muscle. Light and electron microscopy. Exp. Eye Res., 1988; 47: p. 885-899.

[26] Lütjen-Drecoll, E.: Morphology and age-related changes of the Accommodation Apparatus in Current Aspects of Human Accommodation, p. 25-36. Kaden Verlag, 2001.

[27] Mashima, Y.; Oshitari, K.; Imamura, Y.; Momoshima, S.; Shiga, H.; Oguchi, Y.: High-resolution magnetic resonance imaging of the intraorbital optic nerve and subarachnoid space in patients with papilledema and optic atro-phy. Arch. Ophthalmol., 1996; 114: p. 1197-1203.

[28] McCulloch, C.: The zonule of Zinn: its origin, course and insertion, and its relation to neighbouring structures. Trans. Am. Ophthalmol. Soc., 1954; 52: p. 525-585.

[29] Neider, M.W.; Crawford, K.S.; Kaufman, P.L.: In vivo videography of the rhesus monkey accommodative apparatus. Arch. Ophthalmol., 1990; 108: p. 69-74.

[30] 30, G.; Coleman, D.J.: Using high-frequency Ultrasound to characterize intraocular foreign Bodies. Ophthalm. Surg., 1993; 24 (2): p. 944-999.

[31] Pavlin, C.J.; Foster, F.S.: Ultrasound biomicroscopy in glaucoma. Acta Ophthalmol, 1992; 204 (suppl.); p. 7-9.

[32] Pavlin, C.J.; Foster, F.S.: Ultrasound biomicroscopy of the eye. Springer, New York, 1995.

[33] Pavlin, C.J.; Harasiewicz, K.; Sherar, M.D.; Foster, F.S.: Clinical use of ultrasound biomicroscopy. Ophthalmology, 1991; 98: p. 287-295.

[34] Pavlin, C.J.; Sherar, M.D.; Foster, F.S.: Subsurface ultrasound microscopic imaging of the intact eye. Ophthalmology, 1990; 97: p. 244-50.

[35] Reinstein, D.Z.; Raevsky, T.; Coleman, D.J.: Improved system for ultrasonic imaging and biometry. J. Ultra. Med., 1997; 16: p. 117-124.

[36] Rohen, J.W.: Scanning electron microscopic studies of the zonular apparatus in human and monkey eyes. Invest. Ophthalmol. Vis. Sci., 1979; 18: p. 131-144.

[37] Rohen, J.W.; Rentsch, F.J.: Der konstruktive Bau des Zonulaapparats beim Menschen und dessen funktionelle Bedeutung. [*The construction of the zonular apparatus in the human eye and its function*]. A. v. Graefe's Arch. Clin.Exp. Ophthalmol., 1969; 178: p. 1-19.

[38] Schachar, R.A.: Pathophysiology of accommodation and presbyopia. J. Florida Med. Assoc., 1994; 81: p. 268-271.

[39] Schachar, R.A.: Zonular function: a new hypothesis with clinical implications. Ann. Ophthalmol., 1994; 26: p. 36-38.

[40] Silvermann, R.H.; Folberg, R.; Boldt, H.C.; Lloyd, H.O.; Rondeau, M.J.; Mehaffey, M.G.; Coleman, D.J.: Correlation of ultrasound parameter imaging with microcirculatory pattern in uveal melanoma: Ultra. Med. Biol., 1997; 23 (4): p. 573-581.

[41] Silvermann, R.H.; Rondeau, M.J.; Lizze, F.L.; Coleman, D.J.: Three dimensional ultrasonic parameter imaging of anterior segment pathology. Ophthalmology, 1995; 102 (5): p. 837-843.

[42] Stachs, O.; Kirchhoff, A.; Terwee, T.; Guthoff, R.: Monitoring the accommodative ciliary body function using three-dimensional ultrasound. A. v. Graefe's Arch. Clin. Exp. Ophthalmol., 2002: Submitted.

[43] Ursea, R.; Coleman, D.J.; Silvermann, R.H.; Lizzi, F.L.; Harrison, W.: Correlation of high frequency ultrasound backscatter with tumor microstructur on iris melanoma, Ophthalmology, 1998; 105 (5): p. 906-912.

[44] von Helmholtz, H.: Über die Akkommodation des Auges. [*About the accommodation of the eye*] A. v. Graefe's Arch. Ophthalmol., 1855; 1: p. 1-74.

[45] Weale, R.: Presbyopia towards the end of the 20th century. Surv. Ophthalmol., 1989; 34: p. 15-30.

Ophthalmologe 2005 · 102:265–271
DOI 10.1007/s00347-004-1122-1
Online publiziert: 19. Oktober 2004

O. Stachs · H. Schneider · J. Stave · R. Beck · R. F. Guthoff
Augenklinik, Universität Rostock

3D-ultraschallbiomikroskopische Untersuchungen zur Differenzierung der Haptiken von potenziell akkommodationsfähigen Intraokularlinsen

Während einer Kataraktoperation wird eine Intraokularlinse in den Kapselsack implantiert. Postoperativ verursachen Kapselfibrose und Kapselsackschrumpfung eine „Verfestigung" der IOL-Optik und -Haptik in der erhaltenen Kapsel. Trotz exzellenter Möglichkeiten der Wiederherstellung der Sehschärfe besitzen dann die pseudophaken Augen kein objektives Akkommodationsvermögen, da die implantierte IOL-Optik weder ihre Form noch ihre axiale Position ändern kann.

Perspektivisch könnte eine pseudophake Akkommodation durch das Ersetzen der verhärteten Linse durch ein flexibles Material mit einem entsprechenden Brechungsindex erreicht werden („Lens refilling"). Hier existieren eine Reihe von experimentellen Ansätzen [1, 11, 13, 19, 20, 24, 26], welche sich bisher ausschließlich im tierexperimentellen Stadium befinden.

Bis heute kann eine pseudophake Akkommodation nur durch den Einsatz von bi- bzw. multifokalen Linsen oder durch eine axiale Verschiebung der IOL-Optik erreicht werden. Letztere könnte über eine durch den Ziliarmuskel induzierte Haptikänderung hervorgerufen werden. Gegenwärtig existieren eine Reihe von Ansätzen unter Nutzung unterschiedlicher Linsen- und Haptikgeometrien [3, 9, 10, 15, 17, 23], um eine derartige pseudophake Akkommodation zu erreichen.

Eine Quantifizierung dieser akkommodativ bedingten axialen IOL-Bewegung ist durch die Nutzung von Ultraschall [8, 10, 18, 22] und insbesondere durch die partielle Kohärenzinterferometrie [4, 5, 6, 7] mit sehr hoher Genauigkeit möglich. Mit der Ultraschallbiomikroskopie steht eine Methode zur Verfügung, diese gemessenen axialen Verschiebungen mit der Änderung der Haptikgeometrie zu korrelieren. Die Interpretation derartiger ultraschallbiomikroskopischer Aufnahmen der Haptiken gestaltet sich jedoch schwierig, wenn nur eine B-Scan-Ebene zur Verfügung steht, sodass hier auf eine dreidimensionale Darstellung zurückgegriffen werden sollte. Das Ziel der hier dargestellten Untersuchungen ist die Evaluierung von akkommodativ bedingten Änderungen der Haptikgeometrie unter Nutzung der dreidimensionalen Ultraschallbiomikroskopie.

Material und Methode

Die Eigenschaften der beiden untersuchten Linsen (1CU (HumanOptics) und CrystaLens AT45 (C&C Vision)) sind in **Tabelle 1** zusammengefasst. Um eine Akkommodation zu simulieren, wurden die Linsen in einen künstlichen Silikonkapselsack (DE Patent 197 38 101.4) implantiert, dessen Eigenschaften bereits beschrieben wurden [2].

Dreidimensionale Ultraschallbiomikroskopie

Zur Evaluierung der IOL-Position und der Haptikkonfiguration wurde ein eigenentwickeltes 3D-Ultraschallbiomikroskop verwendet [25]. Dabei wird ein kommerzielles Ultraschallbiomikroskop (Ultrasound Biomicroscope Model 840, (Humphrey Instruments, Carl Zeiss Group)) mit einer 3D-Erweiterung genutzt, welche eine präzise Bewegung der B-Scan Ebene in Z-Richtung ermöglicht und somit sowohl In-vitro- als auch In-vivo-Messungen erlaubt. Dabei bestehen 3D-Datensätze aus parallelen B-Scans mit einem definierten Abstand zueinander.

Die 3D-Rekonstruktion wurde mit „VoxelView" (Vital Images, Fairfield, USA) und „Amira" (TGS, San Diego, USA) durchgeführt. In vitro treten keine Bewegungsartefakte auf, sodass eine hochauflösende artefaktfreie 3D-Darstellung unter Nutzung von 160 individuellen B-Scans möglich ist. Die entsprechenden 3D-Volumina werden genutzt, um die tangentiale Ebene der anterioren Grenzfläche der Haptik bzw. Optik zu finden und einen senkrecht zu dieser Ebene verlaufenden Schnitt durch den Haptik-Optik-Bereich zu legen. Dieser wird für die eigentliche biometrische Analyse genutzt. Somit kann in vitro ein Fehler durch Verkippungseffekte ausgeschlossen werden. Zur

Tabelle 1

Eigenschaften der untersuchten Linsen

Modell	Aufbau	Gesamtdurchmesser [mm]	Haptikmaterial	Haptikdesign	Optikdurchmesser [mm]	Optikmaterial
1CU (HumanOptics)	einteilig	9,5	Acryl	Platte	5,5	Acryl
AT-45 (C&C Vision)	mehrteilig	11,5	Silikon und Polyimid	Platte	4,5	Silikon

Tabelle 2

Postoperative Parameter 4 Monate nach Implantation einer 1CU-IOL postoperativ

Patient	Alter [Jahre]	Visus prä	IOL [Dpt]	VF post sc	VF post cc	VN post sc	VN post cc	Nahaddition [Dpt]
1	66	0,5	+18,0	1,25	1,25	0,3	1,25	3
2	66	0,6	+19,0	0,8	1,25	0,4	1,5	2
3	72	0,5	+20,5	0,9	1,25	0,3	1,0	3
4	74	0,4	+24,0	0,8	1,25	0,4	1,25	2,5

Visus prä: *präoperativer Visus,* IOL: *Dioptrien der implantierten IOL,* VF post sc: *unkorrigierter postoperativer Fernvisus,* VF post cc: *bestkorrigierter postoperativer Fernvisus,* VN post sc: *postoperativer Nahvisus mit Fernkorrektur,* VN post cc: *bestkorrigierter Nahvisus (35 cm, Birkhäuser).*

Berechnung der Haptikanwinkelung und der axialen Verschiebung kommt „ImageJ" (NIH, USA) zum Einsatz.

Simulation der Akkommodation

Zur In-vitro-Analyse der akkommodativen Fähigkeiten dieser Linsen wurde der Kapselsack in eine Dehnungseinrichtung eingespannt (**Abb. 1**). Diese ermöglicht eine Simulation der Akkommodation ähnlich der im humanen Auge. Die Arme der Einrichtung halten die künstliche Kapsel an 8 peripheren Punkten. Eine über einen Schrittmotor angesteuerte Rotation des inneren Rings der Dehnungseinrichtung spannt bzw. entspannt den Kapselsack. Der Betrag der Spannung bzw. Entspannung des Kapselsacks ist proportional zur Rotation des inneren Rings. Zur sonografischen Untersuchung befindet sich die gesamte Anordnung im Wasserbad.

Zur Beurteilung von akkommodativ bedingten Haptikänderungen wurde der Winkel zwischen IOL-Optik und -Haptik unter Nutzung der anterioren Grenzflächen der IOLs analysiert. Dabei dienen die Punkte # in **Abb. 2** bzw. 3 als Rotationszentren für die Bestimmung der Haptikanwinkelung. Dazu wurde jeweils eine der untersuchten IOL-Typen (20 Dpt) in 3 verschiedene Kapselsäcke implantiert. Für jedes Kapselsack-Linsen-Ensemble wurden 2 Dehnungsversuche durchgeführt. Für jeden dieser Versuche wird in 3 Dehnungszuständen (0, 0,25 mm und 0,5 mm) ein 3D-Volumen berechnet, aus welchem die biometrischen Daten über eine Auswertung der entsprechenden B-Scans erhoben werden.

In-vivo-Messungen

Die In-vivo-Messungen wurden unter pharmakologisch induzierter Ziliarmuskelkontraktion (Cyclopentolat 1% und Pilocarpin 2%) 4 Monate postoperativ an 2 aufeinanderfolgenden Tagen durchgeführt. Dabei erfolgte bei 10 Patienten jeweils 30 min nach Medikamentenapplikation eine Untersuchung der Ziliarkörperregion und der zentralen Vorderkammer mit der 3D-Ultraschallbiomikroskopie. Aus den erhaltenen 3D-Volumina wurden jeweils 6 verschiedene Schnitte durch die Haptik für den akkommodierten bzw. desakkommodierten Zustand ausgewählt und nach Mittelwertbildung Änderungen der haptischen Elemente sowie die axiale IOL-Verschiebung analysiert. Positive Werte für die axiale Verschiebung repräsentieren dabei eine Bewegung nach anterior. Zur Beurteilung von akkommodativ bedingten Haptikänderungen wurde wiederum der Winkel zwischen IOL-Optik und -Haptik unter Nutzung der anterioren Grenzflächen der IOLs analysiert. Dabei dienen analog zu den In-vitro-Experimenten die Punkte # in **Abb. 2** bzw. 3 als Rotationszentren für die Bestimmung der Haptikanwinkelung.

Ergebnisse

Die dreidimensionalen Rekonstruktionen und eine interaktive Auswahl von Schnitten durch die Haptik der untersuchten IOLs im künstlichen Kapselsack sind in **Abb. 2** und 3 dargestellt. Für die 1CU (**Abb. 2**) sind Optik (*O*) und Haptik (*H*) gut differenzierbar. Der Spot (*) in der äquatorialen Region des Kapselsacks repräsentiert den charakteristischen Steg der Haptik der 1CU. Die posteriore Seite der Optik ist durch Laufzeiteffekte verfälscht dargestellt. Der Punkt # wirkt als Gelenk bei einer evtl. möglichen Haptikanwinkelung und wird als Rotationspunkt bei der Bestimmung der Anwinkelung genutzt. Das Gelenk der AT45 ist ebenfalls markiert (**Abb. 3**; Punkt #). Optik (*O*) und Haptik (*H*) sind gut differenzierbar, wobei die Strukturen (*) durch die Polyimidkonstruktion der Plattenhaptik der AT45 verursacht werden. Die posteriore Linsenfläche ist nicht darstellbar.

In **Abb. 4** sind B-Scans dargestellt, die exemplarisch ein Akkommodationsexperiment mit der 1CU zeigen, wobei für die äquatoriale Dehnung bzw. Entspannung ein Wert vom max. 0,5 mm angesetzt wurde. Eine Radiusänderung des Kapselsacks verursacht eine Änderung in der Haptikanwinkelung von 10,4±1,3° und eine axiale Verschiebung von 0,36±0,03 mm für die 1CU, entsprechend für die AT45 9,3±1,0° Haptikan-

winkelung und 0,50±0,03 mm axiale Verschiebung (siehe **Abb. 5**).

Die Kenntnis über die Echocharakteristik des Haptikbereichs wurde genutzt, um die In-vivo-Situation von Patienten mit akkommodativen Implantaten quantitativ zu beschreiben. Die 3D-UBM-Untersuchungen wurden 4 Monate postopertiv durchgeführt, wobei der postoperative Status 12 Wochen nach IOL-Implantation erhoben wurde. Eine detaillierte Analyse der Haptikanwinkelung unter verschiedenen Akkommodationstimuli konnte für 4 Patienten durchgeführt werden, deren prä- und postoperativer Status in **Tabelle 2** dargestellt ist. Die Analyse der Haptikanwinkelung der anderen untersuchten Patienten war aufgrund der Echocharakteristik dieser Haptiken nicht eindeutig möglich. Exemplarisch zeigt **Abb. 6** eine 3D-Rekonstruktion und die entsprechende Bildanalyse der 1CU-Haptik eines 75 Jahre alten Patienten in Desakkommodation, 4 Monate nach der Operation. Hier wurde eine Haptikanwinkelung von 6±1,9° gegenüber der entspannten IOL-Haptik gefunden. Zu beachten ist in diesem Beispiel wie in **Abb. 1** der Steg am äußeren Rand der Haptik (*), über den sich die anteriore Kapsel spannt. In **Abb. 7** ist der Effekt von Cyclopentolat (*links*) und Pilocarpin (*rechts*) in einem weiteren Fall gezeigt. Für dieses Beispiel wurde unter Cyclopentolat im Vergleich zur entspannten Haptik eine Anwinkelung von 4±2,1° beobachtet. Die Gabe von Pilocarpin verursachte eine zusätzliche Anwinkelung von 10±1,8°. Die Resultate dieser Analysen der Haptikanwinkelung und der Änderung der Vorderkammertiefe mit den entsprechenden Standardabweichungen sind in **Abb. 8** zusammengefasst. In Desakkommodation ist generell eine Haptikanwinkelung zwischen 2° und 4° zu beobachten. Die Gabe von Pilocarpin verursachte eine zusätzliche Anwinkelung von maximal 10° für die 1CU. In einem Fall wurde eine Haptikverbiegung gefunden (**Abb. 9**). Hier verursachte Pilocarpin einen posteriore Verschiebung der IOL-Optik.

Diskussion

Zunächst wurde die Hinterkammerlinse 1CU untersucht, deren Funktionsprinzip auf „Finite-Elemente-Simulationen“ von

Zusammenfassung · Abstract

Ophthalmologe 2005 · 102:265–271
DOI 10.1007/s00347-004-1122-1

O. Stachs · H. Schneider · J. Stave · R. Beck · R. F. Guthoff

3D-ultraschallbiomikroskopische Untersuchungen zur Differenzierung der Haptiken von potenziell akkommodationsfähigen Intraokularlinsen

Zusammenfassung

Hintergrund. Der Wirkmechanismus von potenziell akkommodationsfähigen Kunstlinsen nach dem „Optic-shift-Prinzip“ wird derzeit kontrovers diskutiert. Ziel dieser Untersuchung ist eine dreidimensionale ultraschallbiomikroskopische Analyse dieses Wirkmechanismus.

Methode. Es wurde eine Testkammer zur In-vitro-Untersuchung der Konfigurationsänderungen der Haptiken akkommodativer IOLs entwickelt. Die Ergebnisse werden auf die In-vivo-Situation bei Patienten mit akkommodativen Implantaten übertragen.

Ergebnisse. Die dreidimensionale Ultraschallbiomikroskopie erlaubt eine Separation der haptischen Elemente von potenziell akkommodationsfähigen IOLs. Sowohl in vitro als auch in den ausgewählten In-vivo-Fällen konnte eine Haptikanwinkelung bis 10° verbunden mit einer IOL-Verschiebung von max. 0,5 mm ermittelt werden.

Schlussfolgerungen. Das entwickelte Simulationsmodell in Kombination mit der 3D-Ultraschallbiomikroskopie ist gut geeignet, potenziell akkommodationsfähige Kunstlinsen unterschiedlichen Designs auf ihre Veränderungen im Haptikbereich in vitro zu beurteilen und diese Informationen für die Evaluierung der In-vivo-Situation zu nutzen.

Schlüsselwörter

Akkommodationsfähige Kunstlinsen · IOL-Haptik · Optic-shift-Prinzip · 3D-Ultraschallbiomikroskopie · In-vitro-Untersuchung · Konfigurationsänderung

Three-dimensional ultrasound biomicroscopic examinations for haptic differentiation of potentially accommodative intraocular lenses

Abstract

Purpose. The principal ability of potentially accommodative IOLs is based on an axial shift of the IOL optics induced by the ciliary body action in interaction with a reversible change in haptic angulation. The aim of this study was to investigate the accommodative performance of this new IOL generation.

Method. The authors have designed a test device to study IOL performance experimentally. These results were extrapolated to the in vivo situation in patients with accommodative implants.

Results. The 3D high-resolution presentation of the anterior segment of the eye allows a separation of the IOL haptic elements. In vitro and in the selected in vivo cases a change in haptic angulation <10° in combination with a maximal IOL shift of 0.5 mm was found.

Conclusions. The simulation model used in combination with 3D ultrasound biomicroscopy provides information about the potential of accommodative IOL designs. Conclusions corresponding to changes in haptic angulation during accommodation can be drawn and applied to the in vivo situation.

Keywords

Accommodative IOL · IOL haptics · Optical shift principle · Three-dimensional ultrasound biomicroscopy · In vitro examination · Change in configuration

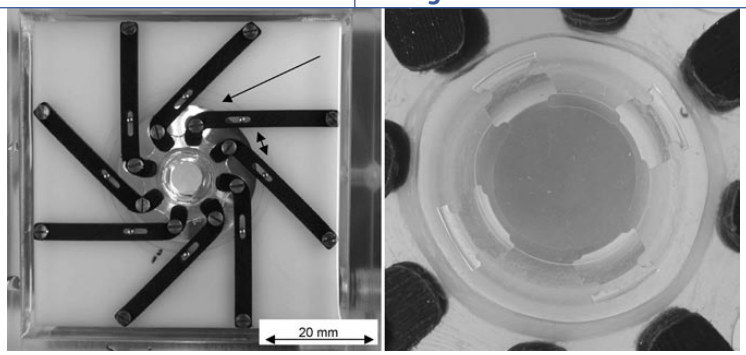

Abb. 1 ▲ **Instrumentierung zur Simulation der Akkommodation. Die Arme halten den künstlichen Kapselsack (Silikon) im Äquatorbereich, in den die IOL implantiert wird**

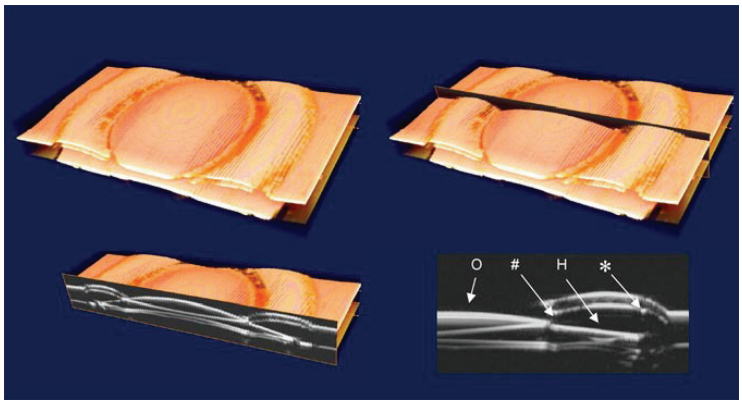

Abb. 2 ▲ **3D-ultraschallbiomikroskopische Darstellung und B-Bild der 1CU im künstlichen Kapselsack. Optik (*O*) und Haptik (*H*) differenzierbar. Spot (*) am äußeren Rand der Haptik, hervorgerufen durch Steg der Haptikkonstruktion der 1CU**

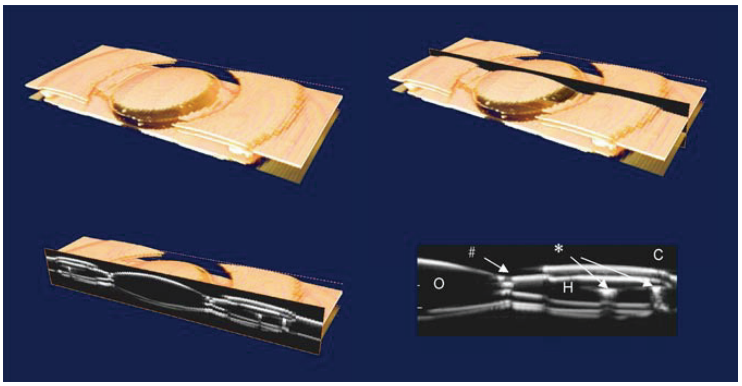

Abb. 3 ▲ **Dreidimensionale ultraschallbiomikroskopische Darstellung und B-Bild der CrystaLens AT-45 im künstlichen Kapselsack. Optik (*O*), Haptik (*H*) und Scharnier (*#*) der Haptik differenzierbar. Posteriore Linsenfläche nicht darstellbar**

Hanna [15] basiert. Als theoretischer Wirkmechanismus wird hier angenommen, dass eine Kontraktion des Ziliarmuskels, welche zu einer Entspannung der Zonula führt, den Kapselsack erschlaffen lässt. Dies soll zu veränderten Kräfteverhältnissen führen, in deren Folge sich die Haptik der Linse anwinkelt und zu einer entsprechenden axialen Verschiebung führt. Unsere In-vitro-Experimente zeigen einen vergleichbaren Effekt. Für die Dehnung bzw. Entspannung wurde eine Radiusänderung des Kapselsacks von 0,5 mm angenommen. In früheren Untersuchungen wurden mit der dreidimensionalen Ultraschallbiomikroskopie [25] eine maximale Verschiebung von 0,26 mm und mit Magnetresonanztomographie [27] ein Wert von 0,30 mm (für ein 40-jähriges Auge) ermittelt. Mit diesem maximalen Wert von 0,5 mm fanden wir eine axiale Verschiebung von 0,36±0,03 mm für die 1CU, verursacht durch eine Haptikanwinkelung von 10,4±1,3°. Eine für diese Linse theoretisch vorhergesagte Änderung der Haptikanwinkelung von 30° konnten wir nicht finden. Bei der Nutzung von Gullstrand's Augenmodell verursacht eine anteriore Verschiebung um 1 mm einer 20-Dpt-IOL im Kapselsack eine Änderung der Brillenkorrektur um 1,9 Dpt [12]. Eine Anteriorverschiebung um 0,36 mm bewirkt entsprechend eine Änderung der Brillenkorrektur um 0,68 Dpt. Sollte sich die IOL weiter anterior im Strahlengang befinden, ist die Änderung der Brillenkorrektur, abhängig von der exakten IOL-Position, entsprechend kleiner.

Für die AT45 wurde in vitro eine maximale Axialverschiebung von 0,5±0,03 mm bei 9,3±1,0° Änderung der Haptikanwinkelung gefunden. Wiederum unter Nutzung von Gullstrand's Augenmodell bedeutet dies eine Refraktionsänderung kleiner als 0,95 Dpt. Diese gemessene axiale Verschiebung korrespondiert nicht vollständig mit dem theoretischen Wirkprinzip der AT45. Sie wurde entwickelt, um die Ziliarmuskelaktivität direkt über die Haptik und über eine Veränderung des Glaskörperdrucks in eine axiale Bewegung zu übertragen. Unser Simulationsmodell kann jedoch Variationen des Drucks im Bereich des Glaskörpers nicht simulieren. Dies bedeutet, dass das In-vivo-Potenzial dieser Linse größer sein könnte, falls diese Druckän-

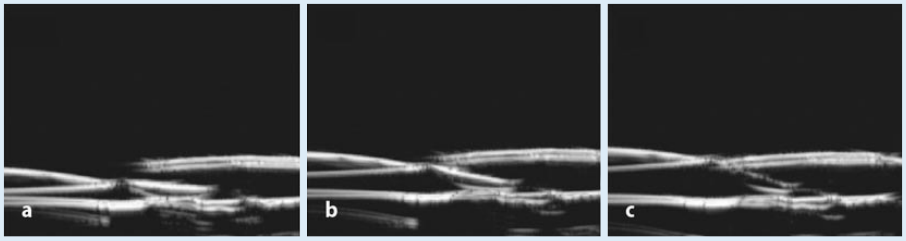

Abb. 4 ◀ **Ultraschallbiomikroskopische Abbildungen der 1CU-Kunstlinse nach unterschiedlicher Dehnung des Kapselsacks (Δr=0,5 mm, a hohe Spannung (Desakkommodation), c Entspannung (Akkommodation), b Zwischenposition)**

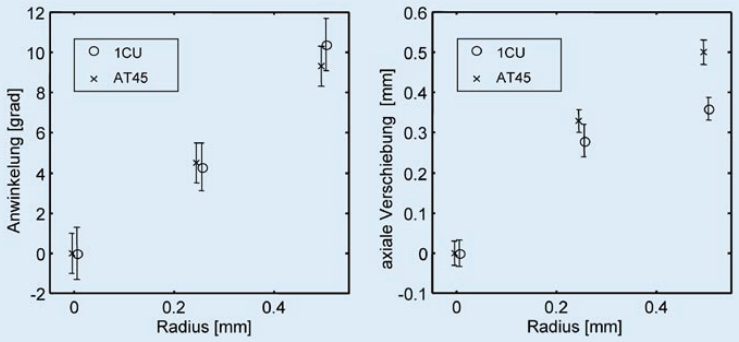

Abb. 5 ◀ **Änderung der Haptikanwinkelung (*links*) und axiale Verschiebung der Optik (*rechts*) der untersuchten IOLs bei äquatorialer Dehnung bzw. Entspannung des künstlichen Kapselsacks**

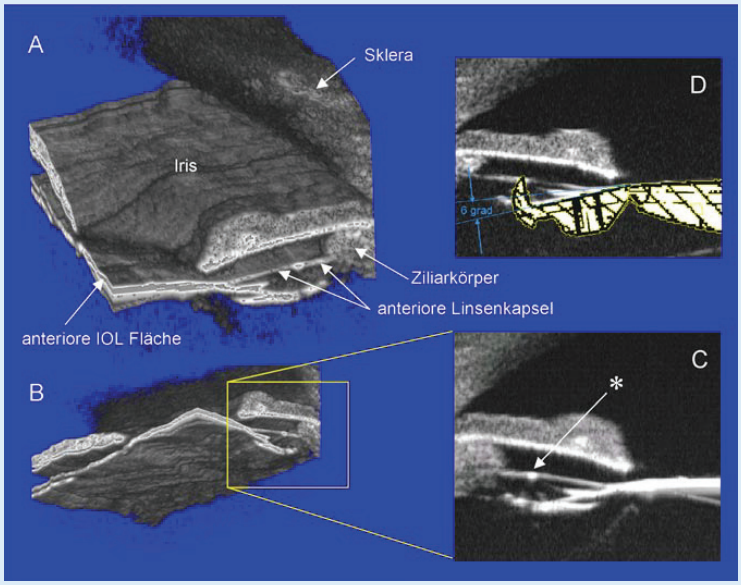

Abb. 6 ◀ **Dreidimensionale Rekonstruktion (a anteriorer und b posteriorer Blick) und Bildanalyse (c, d mit Modell) der Haptikregion der 1CU-IOL in vivo (4 Monate postoperativ, 75 Jahre) unter Cyclopentolat 1%**

derungen in den entsprechenden Größenordnungen auftreten.

Die Kenntnis der Echocharakteristik der Haptik der 1CU kann genutzt werden, um die In-vivo-Situation an Patienten mit diesem potenziell akkommodationsfähigen Implantat im Detail zu beschreiben. Kritisch zu diskutieren ist die Genauigkeit der In-vivo-Untersuchungen im Gegensatz zu den In-vitro-Experimenten, bei welchen eine exakte Ausrichtung der Schnittebenen durch den Haptik-Optik-Bereich möglich ist. Eine Verfälschung der biometrischen Resultate durch Verkippung ist hier auszuschließen. In-vivo-Experimente sind anfälliger für derartige Fehler. Dies zeigt sich auch in der größeren Standardabweichung von maximal ±2,5° für die Bestimmung der Anwinkelung. Es ist jedoch festzustellen, dass die im Rahmen der hier durchgeführten Studie genutzte Methode der dreidimensionalen Ultraschallbiomikroskopie die einzige ist, die derartige Analysen von Haptikänderungen überhaupt zulässt. Unter bewusster Kenntnis der möglichen auftretenden Fehler – und damit einer Vermeidung von Überinterpretationen – ist eine Analyse von pharmakologisch stimulierten Haptikveränderungen jedoch durchaus möglich.

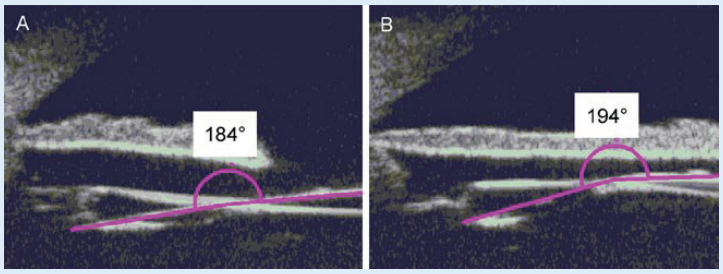

Abb. 7 ▲ **Änderung der Haptikanwinkelung bei der Gabe von** a **Cyclopentolat und** b **Pilocarpin , 4 Monate postoperativ, 67 Jahre. Bereits in Desakkommodation Anwinkelung von 4°. In Akkommodation zusätzliche 10°**

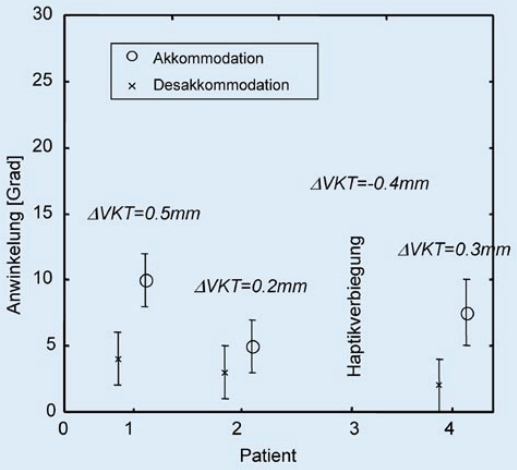

Abb. 8 ◀ **Haptikanwinkelung und Vorderkammertiefe in unterschiedlichen Akkommodationszuständen (1CU). Posteriore Werte für die Vorderkammertiefe repräsentieren eine anteriore Verschiebung der IOL**

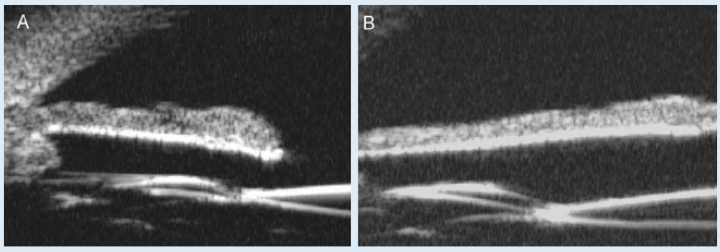

Abb. 9 ▲ **Haptikverbiegung unter** a **Cyclopentolat und** b **Pilocarpin , 4 Monate postoperativ, 78 Jahre**

Die ◘ **Abb. 7** und 9 zeigen die Änderung der Haptikanwinkelung und der Vorderkammertiefe unter Cyclopentolat und Pilocarpin anhand zweier ausgewählter Beispiele. Zunächst verursacht die Kapselsackschrumpfung bereits eine gewisse Haptikanwinkelung in Desakkommodation (4° in ◘ **Abb. 7**). In diesem beobachten Fall induziert Pilocarpin eine zusätzliche Anwinkelung von 10°. Hier kann zu diesem postoperativen Zeitpunkt von einem akkommodativen Potenzial gesprochen werden. Wird der in ◘ **Abb. 9** dargestellte Fall analysiert, so ist eine Verbiegung der Plattenhaptik zu beobachten, die bei der Gabe von Pilocarpin zu einer posterioren Verschiebung der Optik führt. Die beobachtete Haptikverbiegung kann sowohl auf eine Schrumpfung des Kapselsacks als auch auf einen präoperativ kleineren Kapselsack zurückgeführt werden.

Nach unseren Ergebnissen verursacht die Kapselsackschrumpfung in den analysierten Patienten bereits in Desakkommodation eine Haptikanwinkelung zwischen 2° und 4°. Pilocarpin induziert eine zusätzliche Anwinkelung zwischen 5° und 10°, was eine Änderung der Vorderkammertiefe zwischen 0,2 mm und 0,5 mm bewirkt. Unter Nutzung von Gullstrand's Augenmodell und abhängig von der exakten IOL-Position ergibt dies Refraktionsänderungen in der Brillenebene kleiner als 0,38 Dpt für 0,2 mm Axialbewegung bzw. 0,95 Dpt für 0,5 mm Bewegung. Die gefunden Änderungen in der Vorderkammertiefe sind kleiner als die von Langenbucher [16] gefundenen Werte mit einer durchschnittlichen Abnahme der Vorderkammertiefe von 0,78 mm unter Nutzung des IOL-Master bzw. 0,63 mm unter Nutzung der Ultraschallbiomikroskopie. Hier ist darauf hinzuweisen, dass die Vermessung von pseudophaken Augen mit dem konventionellen IOL-Master nicht korrekt möglich ist [14]. Die interferometrischen Messungen von Findl [4, 5, 6, 7] zeigen unter Pilocarpin eine moderate anteriore Bewegung der 1CU, was zu einer mittleren Akkommodationsamplitude von 0,5 Dpt führt. Die dort gefundenen Werte liegen im Bereich der im Rahmen unserer Arbeit ermittelten Werte.

Eine theoretisch mögliche, für die 1CU vorhergesagte Haptikanwinkelung von 30° konnte von uns nicht festgestellt werden. Selbst unter der Annahme, dass in vivo die biometrische Analyse von Haptikveränderungen einem relativ großen Messfehler unterliegt, ist davon auszugehen, dass derartige Werte in vivo nicht erreicht werden können.

Fazit für die Praxis

Das entwickelte Simulationsmodell in Kombination mit der 3D-Ultraschallbiomikroskopie ist gut geeignet, potenziell akkommodationsfähige Intraokularlinsen unterschiedlichen Designs hinsichtlich ihrer akkommodativen Performance in vitro zu beurteilen und für eine Evaluierung der In-vivo-Situation zu nutzen. Die Kenntnis der Echocharakteristik der Haptiken kann genutzt werden, um die In-vivo-Situation an Patienten mit potenziell akkommodationsfähigen Implanta-

ten im Detail zu beschreiben. Neben Haptikverbiegungen kann die Kapselsackschrumpfung bereits in Desakkommodation zu einer Haptikanwinkelung beim 1CU-Implantat führen. Unter Pilocarpin ergeben sich maximale Änderungen der Haptikanwinkelung von 10°. Die akkommodative Performance der untersuchten Linsen reicht nicht aus, um die Lesebrille zu ersetzen.

Korrespondierender Autor

Dr. O. Stachs

Augenklinik der Medizinischen Fakultät der Universität Rostock,
Doberaner Straße 140, 18055 Rostock
E-Mail: oliver.stachs@med.uni-rostock.de

Interessenkonflikt: Keine Angaben

Literatur

1. Agarwal LP, Narsinhan EC, Mohan M (1967) Experimental lens refilling. Orient Arch Ophthalmol 5:205–212
2. Beck R, Pfeiffer K, Stave J, Guthoff R (2000) A 3-D capsular bag model for describing biomechanical properties of neu intraocular lenses. Ophthalmologe 97:546–551
3. Cumming JS, Kamman J (1996) Experience with an accommodating IOL. J Cataract Refract Surg 22:1001
4. Findl O, Drexler W, Menapace R et al. (1998) Accurate determination of effective lens position and lens-capsule distance with 4 intraocular lenses. J Cataract Refract Surg 24:1094–1098
5. Findl O, Kriechbaum K, Köppl C, Menapace R, Drexler W (2003) Laser interferometric measurements of IOL movement with accommodating IOI's. Proc ASCRS 2003, San Francisco, 80
6. Findl O, Menapace R, Kriechbaum K, Köppl C, Drexler W (2003) Laser interferometric measurements of movement of an„accommodating" IOL. In: Guthoff R, Ludwig K (eds) Current Aspects in Accommodation II. Kaden, Heidelberg, S 211–221
7. Findl O, Kiss B, Petternel V, Menapace R, Georgopoulos M, Rainer G, Drexler W (2003) Intraocular lens movement caused by ciliary muscle contraction. J Cataract Refract Surg 29:669–676
8. Gandolfi SA, Marchini G, Tosi R, Mora P, Pedrotti E, Sartori P, Manzotti F (2003) UBM changes during accommodation in eyes implanted with Crystalens AT 45 and 1CU IOL. A pilot study. Invest Ophthalmol Vis Sci 44: E-Abstract 252
9. Hara T, Yasuda A, Yamada Y (1990) Accommodative intraocular lens with spring action. Part 1. Design and placement in an excised animal eye. Ophthalmic Surg 21:128–133
10. Hardman Lea SJ, Rubinstein MP, Snead MP, Haworth AM (1990) Pseudophakic accommodation? A study of the stability of capsular bag supported, one piece, rigid tripod, or soft flexible implants. Br J Ophthalmol 74:22–25
11. Hettlich HJ, Lucke K, Asiyo-Vogel M, Schulte M, Vogel A (1994) Lens refilling and endocapsular polymerization of an injectable intraocular lens: in vitro and in vivo study of potential risks and benefits. J Cataract Refract Surg 20:115–123
12. Holladay JT (1993) Related Articles, Links Abstract Refractive power calculations for intraocular lenses in the phakic eye. Am J Ophthalmol 116:63–66
13. Kessler J (1964) Experiments in refilling the lens. Arch Ophthalmol 71:412–417
14. Kriechbaum K, Findl O, Kiss B, Sacu S, Petternel V, Drexler W (2003) Comparison of anterior chamber depth measurement methods in phakic and pseudophakic eyes. J Cataract Refract Surg 29:89–94
15. Küchle M, Nguyen NX, Langenbucher A, Gusek-Schneider GC, Seitz B, Hanna KD (2002) Implantation of a new accommodative posterior chamber intraocular lens. J Refract Surg 18:208–216
16. Langenbucher A, Huber S, Nguyen NX, Seitz B, Gusek-Schneider GC, Kuchle M (2003) Measurement of accommodation after implantation of an accommodating posterior chamber intraocular lens (1). J Cataract Refract Surg 29:677–685
17. Legeais JM, Werner L, Abenhaim A, Renard G (1999) Pseudoaccommodation: BioComFold versus a foldable silicone intraocular lens. J Cataract Refract Surg 25:262–267
18. Nakazawa M, Ohtsuki K (1984) Apparent accommodation pseudophakic eyes after implantation of posterior chamber intraocular lenses: optical analysis. Invest Ophthalmol Vis Sci 25:1458–1460
19. Nishi O, Hara T, Sakka Y, Hayashi F, Nakamae K, Yamada Y (1992) Refilling the lens with an inflatable endocapsular balloon: surgical procedure in animal eyes. Graefes Arch Clin Exp Ophthalmol 230:47–55
20. Parel JM, Gelender H, Treffers WF, Norton EW (1986) Phaco-ersatz: cataract surgery designed to preserve accommodation. Graefes Arch Clin Exp Ophthalmol 224:165–173
21. Pavlin CJ, Foster FS (1992) Ultrasound biomicroscopy in glaucoma. Acta Ophthalmol 204 [Suppl]:7–9
22. Ravalico G, Baccara F (1990) Apparent accommodation in pseudophakic eyes. Acta Ophthalmol (Copenh) 68:604–606
23. Sarfarazi FM (2003) Optical and mechanical design for human implantation of the Sarfarazi Elliptical Accommodatin IOL. Proc ASCRS 2003, Abstract #738
24. Schneider H, Stave J, Terwee T, Guthoff R (2003) Intraoperative refraction control of injectable lenses. In: Guthoff R, Ludwig K (eds) Current Aspects of Accommodation II. Kaden, Heidelberg, S 155–162
25. Stachs O, Martin H, Kirchhoff A, Stave J, Terwee T, Guthoff R (2002) Monitoring accommodative ciliary muscle function using three-dimensional ultrasound. Graefes Arch Clin Exp Ophthalmol 240:906–912
26. Stachs O, Schneider HJ, Stave J, Schmitz KP, Terwee T, Guthoff R (2003) The anterior segment in rabbit eyes after lens refilling with injectable silicone polymer. ARVO Meeting Abstracts, 44:273
27. Strenk SA, Semmlow JL, Strenk LM, Munoz P, Gronlund-Jacob J, DeMarco JK (1999) Age-related changes in human ciliary muscle and lens: a magnetic resonance imaging study. Invest Ophthalmol Vis Sci 40:1162–1169

Fachnachrichten

Deutsche Ärzte im Ausland gesucht

Viele deutsche Ärzte haben Interesse an Stellen im Ausland: Sie klagen über die Belastung durch Stress und die Vielzahl administrativer Aufgaben in Deutschland. Demgegenüber steht die schlechte Bezahlung - verglichen mit z. B. anderen europäischen Staaten. Gerade in Skandinavien und Saudi-Arabien oder den Vereinigten Arabischen Emiraten werden zurzeit Ärzte vor allem aus Deutschland gesucht, um den dort herrschenden Ärztemangel zu beheben.

Saudi-Arabien will die medizinischen Versorgung weiter verbessern und sucht deshalb qualifizierte Fachärzte und Fachärztinnen aus Deutschland, vor allem Kardiologen, Neurologen, Internisten, Pädiater, Radiologen, Rheumatologen, Orthopäden, HNO-Ärzte, Gynäkologen, Chirurgen, Notfallärzte, Anästhesisten, Pathologen und Zahnärzte. Da ausländische Ärzte in erster Linie als Ober- und Chefärzte arbeiten sollen, wird eine fünfjährige Facharzt-Tätigkeit vorausgesetzt – wie auch die Beherrschung der englischen Sprache. Die monatlichen Gehälter liegen zwischen 8.000 und 10.000 US Dollar und die Kosten für Unterkünfte und Flüge werden vom Arbeitgeber übernommen.

Auch in den skandinavischen Ländern herrscht ein beachtlicher Ärztemangel. Mediziner, die dort bereits arbeiten, loben insbesondere die guten Arbeitsbedingungen und das Mindestmaß an Bürokratie. Hier werden Ärzte aller Fachgebiete gesucht.

Weitere Infomationen erhalten Sie bei:
Universitas, Tel: 08721-120253,
Fax: 08721-120352,
E-Mail:universitas-int@web.de.

Quelle: Fa. Universitas, Eggenfelden

Graefe's Arch Clin Exp Ophthalmol
DOI 10.1007/s00417-005-0126-0

LABORATORY INVESTIGATION

Oliver Stachs
Heiner Martin
Detlef Behrend
Klaus-Peter Schmitz
Rudolf Guthoff

Three-dimensional ultrasound biomicroscopy, environmental and conventional scanning electron microscopy investigations of the human zonula ciliaris for numerical modelling of accommodation

Received: 17 June 2005
Revised: 2 August 2005
Accepted: 5 August 2005

Presented in part at the 101st Meeting of the Deutsche Ophthalmologische Gesellschaft, 2003, Berlin, Germany

O. Stachs (✉) · R. Guthoff
Eye Clinic, University of Rostock,
Doberaner Strasse 140,
18055 Rostock, Germany
e-mail: oliver.stachs@med.uni-rostock.de
Tel.: +49-381-4948566
Fax: +49-381-4948502

H. Martin · D. Behrend · K.-P. Schmitz
Institute for Biomedical Engineering,
University of Rostock,
Rostock, Germany

Abstract *Purpose:* Biomechanical modelling of the accommodation process is a useful tool for studying the mechanism of accommodation and presbyopia and can aid in the development of accommodative lens-replacing materials. Existing biomechanical models, however, use a very simplified zonula structure. The aim of this study was to use three-dimensional ultrasonic imaging and scanning electron microscopy to provide a more detailed, three-dimensional description of the structure of the human zonula to improve the modelling of accommodation. *Methods:* Five human eyes were examined without invasive manipulation using a custom-made three-dimensional ultrasonic imaging technique that allows scanning of features with a spatial resolution of 30 μm. Environmental and conventional scanning electron microscopy (SEM) provided information to complement the ultrasonic images for use in development of a more anatomically correct finite-element model of the zonula structures. These data along with the material properties of the ocular tissue structures were used to construct an advanced geometric model for finite-element simulation of the accommodation process. *Results:* Images were obtained through three-dimensional ultrabiomicroscopy (3D-UBM) of anatomical features heretofore not directly imagable in their native state. Ciliary processes and zonula structures were clearly separated by both the 3D-UBM and the SEM methods. It was found that fibres inserting on the anterior and posterior lens capsule emerge anteriorly at the ciliary body. Fibres emerging near the pars plana insert on the lens and the ciliary body. No X-shaped crossing fibres were found. Modelling of the accommodation process with both the simple and the more complex geometric models produced refractive power changes comparable with in vivo findings. *Conclusions:* The 3D-UBM allowed examination of zonula structures in their native state with minimized preparation artefacts. While these data were incorporated into a complex and more anatomically correct finite-element simulation of intraocular features including lens, zonular system and ciliary body it was found that a simplified zonular model is sufficient for the numerical simulation of the accommodation process.

Keywords Accomodation · 3D ultrasound biomicroscopy · Scanning electron microscopy · Numerical modelling

Introduction

Two approaches for the correction of presbyopia, namely lens refilling [1, 15, 17, 22, 23, 28, 30] and intraocular lenses based on the optical shift principle [6, 12, 13, 19, 20, 26, 28], have been reported. An understanding of lens changes during accommodation is fundamental for the development of these new generations of intraocular lenses for the treatment of presbyopia. Recently, attempts have been made to investigate human accommodation using numerical methods to model the optical performance of the eye. Significant studies have been carried out using very simple models (e.g. [5, 33, 34]) while others have used more complex models involving computer-aided design in combination with finite-element simulations (e.g. [3, 27]).

Numerical modelling of biomechanical processes can, in general, lead to a better understanding of the processes being modelled. The sensitivity of the model to geometry and material properties can be quantified and used to fit experimental data. Numerical modelling, however, is dependent on the accuracy and quality of the data used in constructing the model. The material properties, geometry and boundary condition assumptions are of particular importance. Thus, in the development of a biomechanical model of the human accommodation system, the lens nucleus, lens cortex, lens capsule, ciliary body and zonular fibres along with their geometrical and mechanical properties (e.g. Young's modulus, refraction index, stiffness) all have to be considered. These data exist for only a few selected cases in the literature, and limited experimental information on the required geometrical and material properties is available [3, 10, 11].

Existing models have described the zonular apparatus in a very simplified and idealized manner. The assumptions of Farnsworth and Shyne [9] have generally been used. They suggest that three groups of zonular fibres exist: anterior, central and posterior, in the ratio 6:3:1. The movement of the ciliary muscle during accommodation has been investigated [29, 32]. These investigations led to the conclusion that there is age dependence and inter-individual difference in radius change of the ciliary body during accommodation. There is little knowledge on the force of the ciliary muscle on the zonular fibres. The position of the anchor point at the ciliary body of the zonular fibres is of particular importance with regard to the force transmission from the ciliary muscle to the lens.

The purpose of the current work was to obtain a more accurate description of the geometry and morphology of the zonula, using three-dimensional ultrasound biomicroscopy (3D-UBM) and scanning electron microscopy (SEM), for use in modelling the accommodation process. The data are used to construct a model of the accommodation apparatus including lens and zonular fibres to investigate the mechanical and optical performance of the eye.

Materials and methods

Five freshly enucleated human eyes (age 31–73 years) were available for the experimental part of the study. None of the eyes had a previous history of intraocular surgery in the anterior segment. All eyes were enucleated for ocular pathologies in the posterior segment [primary large choroidal melanomas (three cases) or recurrent melanomas after treatment (two cases)].

Informed consent was obtained from all subjects before participation. Procedures adhered to the tenets of the Declaration of Helsinki, and the protocol was approved by the ethics committee of the University of Rostock.

The anterior segment between lens equator and ciliary body was scanned using 3D-UBM shortly after enucleation (not later than 6 h) without further invasive manipulation. Eye segments for SEM were prepared by bisecting the eyes in the equatorial region with a scalpel. The remaining vitreous humour was completely removed from the posterior face of the anterior segment. The anterior segment was fixed with pins to avoid tissue deformation. A 90° section of the sclera and cornea was removed to provide a lateral view of the contained structures. These sections, without further manipulation, were examined in an environmental scanning microscope followed by conventional SEM examination.

Three-dimensional ultrasound biomicroscopy

The freshly enucleated human eyes were examined using the 3D ultrasound biomicroscope previously described by Stachs et al. [29]. No modifications were required for ex vivo use. With this microscope, 3D data sets consisting of stacks of B-scans in parallel planes at a defined distance were obtained. The computer-controlled scanning system moves the table with the eye holder perpendicular (z direction) to the B-scan plane. The video signal of the ultrasound unit is digitized using a frame-grabber board (HaSoTec, Germany) synchronized with the z-motion control system. For the z-movement a distance of 5 mm is scanned in 20 s acquisition time. All 3D scans have the same sampling density with 160 frames. The original UBM raw data (256 scan lines×1024 samples per line, 256-level grey scale) pictured on the UBM display with 880×440 pixels were converted into 440×440 pixels (256-level grey scale) during capture by the frame grabber. No degradation of the image quality was observable, and the influence of the digital conversion was negligible. The voxel size is 0.011×0.011×0.031 mm. The motion control and data acquisition system is connected with a Windows NT workstation via a local area network for 3D reconstruction using AMIRA (TGS, San Diego, CA, USA). This commercial volume-rendering software package provides an interactive environment allowing features such as volume orientation for viewing planes and 3D perspectives, segmentation and determination of distances and surfaces.

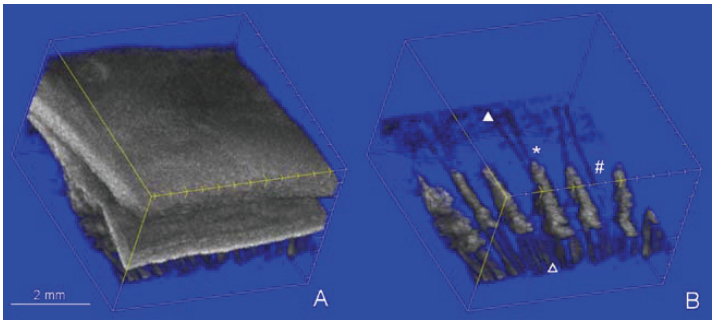

Fig. 1 3D-UBM reconstruction of the human ciliary body region ex vivo. **a** The unmodified scan volume; **b** digital subtraction of the sclera and iris from the same volume exposes the ciliary processes and zonular fibre groups. Different zonular groups and anchor points are marked (▲, △,*,#)

Scanning electron microscopy

On completion of the 3D UBM examination, segments of the eyeballs were prepared as described above and were examined twice, firstly in their native state using an environmental scanning electron microscope (ESEM XL 30, Philips) and secondly, after gold coating (Sputter Coater 103, Baltec, Germany), by conventional SEM (HV-mode, DSM 960 A, Zeiss, Germany).

Model building

For simulation of the accommodation, a finite-element model (FEM) was created for a 29-year-old lens based on the data of Brown [2]. The model is assumed to be stress free in the accommodated state (Fig. 7). The deformed lens, i.e. the unaccommodated state, was achieved by a prescribed radial displacement at the end of the zonular fibres according to the linear regression data of Strenk et al. [32]. For our basic model three sets of zonular fibres are assumed to connect the lens with the ciliary body at a single point and the numbers of anterior, posterior and central fibres are in the ration 6:3:1 [9]. The axial displacement of the zonular fibre ends was fixed. The lens consists of the capsular bag, which was modelled by one-dimensional axisymmetric shell elements. The capsular bag content (nucleus and cortex) was modelled by two-dimensional axisymmetric elements. The radial displacements at the optical axis of the lens were fixed. In principle, the basic model (Fig. 7a) utilizes the same source data for the model geometry and material properties as used by Burd et al. [3].

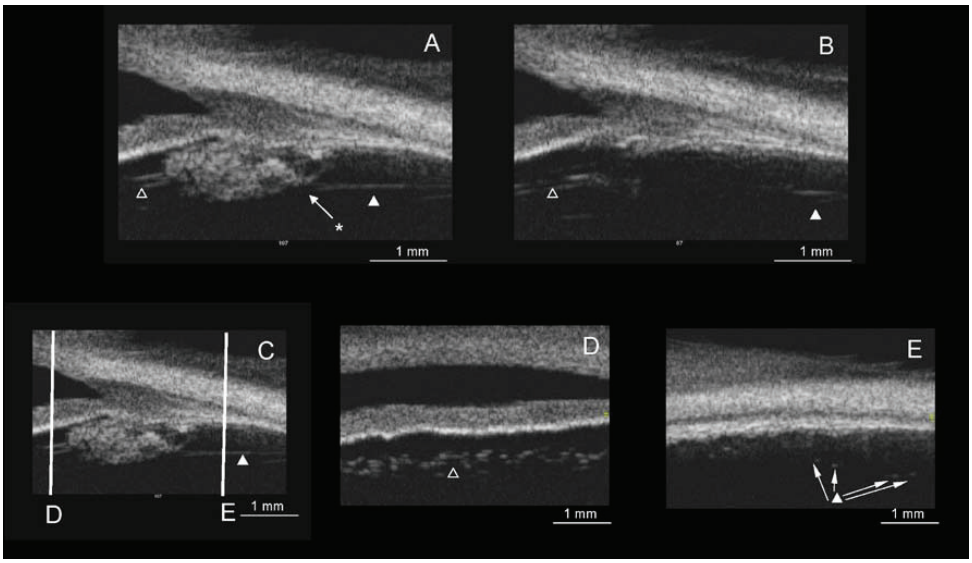

Fig. 2 Typical 3D-UBM sections across the human ciliary body. A section across the ciliary muscle with ciliary processes is shown in **a**, while only the ciliary muscle can be seen in the section depicted in **b**. Images **d** and **e** are the transverse sections marked in **c**. Zonular groups with differing orientations are marked (▲, △)

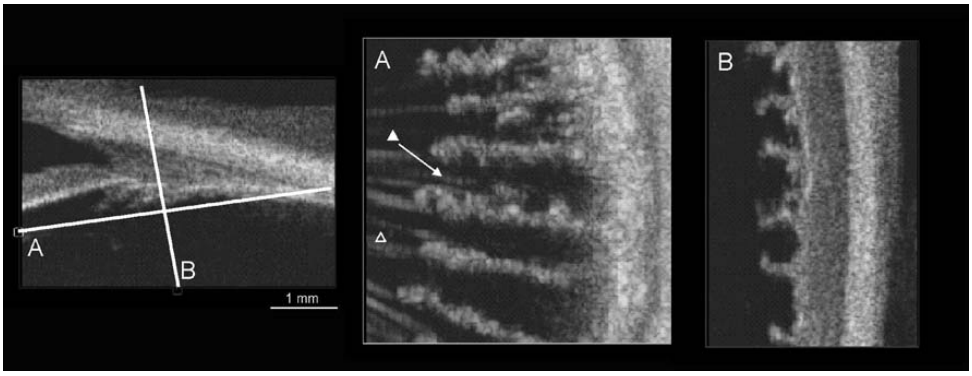

Fig. 3 Orthogonal sections across the human ciliary body. **a** A section in the transverse direction between the lens and a ciliary body: zonular fibres are marked (▲, △). **b** An orthogonal section across the ciliary body: ciliary processes can clearly be separated by 3D-UBM

This model is very well documented and was used as the basis for our FEM analyis.

The more complex model incorporated the course, attachment points and structure of the zonular fibres as determined by 3D-UBM and augmented by the ESEM and SEM findings. Oblique sections across the ciliary body with zonular fibres, or across the lens with zonular fibres, were selected using AMIRA. The configuration of the ciliary body was analysed using the following procedure for contour determination previously described by Stachs et al. [29]. The respective positions of the scleral spur and the ciliary muscular base were used to define a suitable coordinate system for the pattern recognition system. In addition, the posterior wall of the iris had to be differentiated from the neighbouring ciliary muscle. The ciliary muscle base was approximated as a parabola, while the posterior wall of the iris was approximated as a straight line. The scleral spur served as an origin of coordinates and as a rotation center for the subsequent averaging of the individual contours to afford a mean contour. The outer contour of the ciliary body was found using a fixed threshold value in the grey-scale images. For contour finding, ten comparable radial sections through the ciliary body were selected, approximated and averaged. The shape of the lens

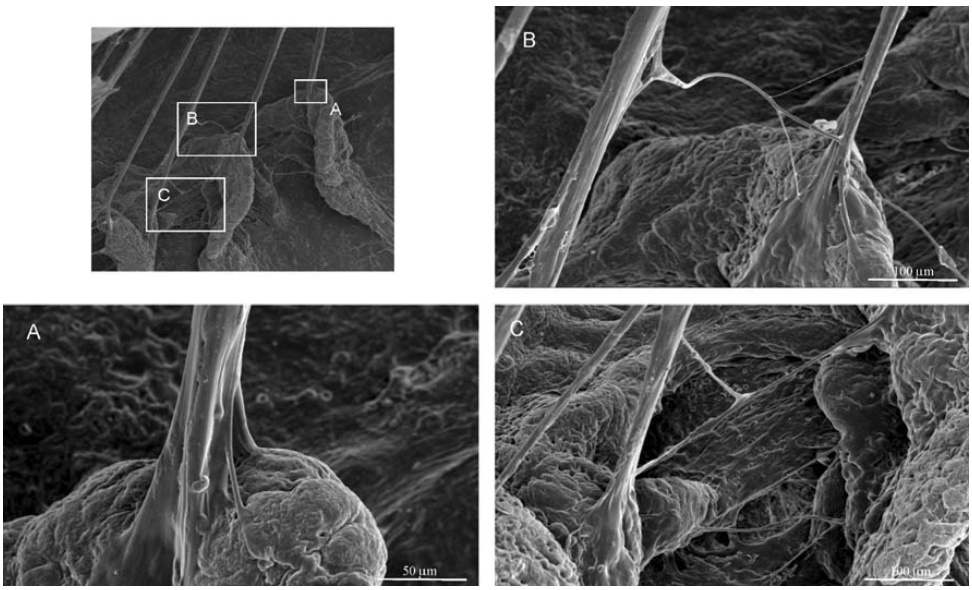

Fig. 4 Scanning electron micrograph of a typical specimen. **a**, **b** Fibres originating at the ciliary body ridges. **c** Intra-ciliary fibres that connected between neighbouring ciliary processes were found in the ciliary body valleys

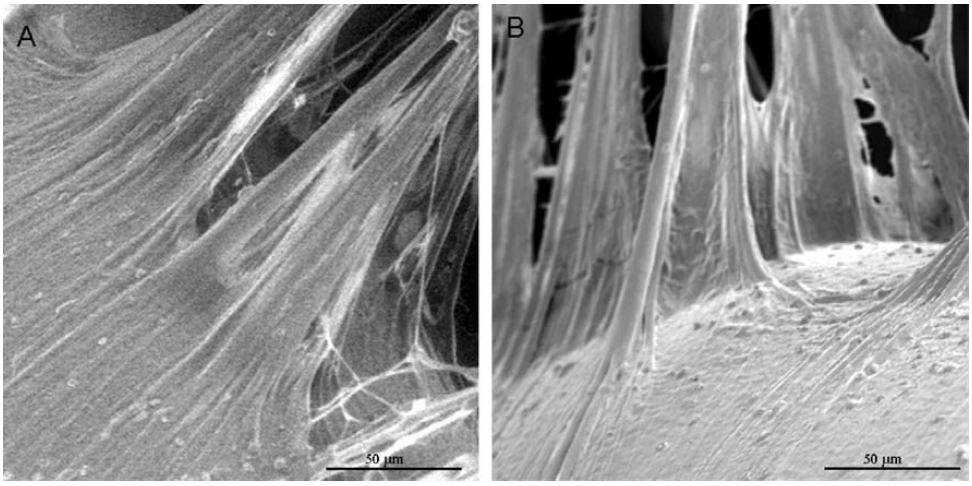

Fig. 5 Typical dorso-lateral views of zonular fibre insertion on the lens obtained with ESEM (**a**) and conventional SEM (**b**)

is calculated according to the least-square polynomials given and discussed in detail by Burd et al. [3]. Typical zonular traversing patterns between lens and ciliary body were analysed and integrated in a geometric model shown in Fig. 6b. For model building a differentiation between the five investigated eyes was not conducted.

Finite-element modelling

The calculations were performed nonlinearly considering large displacements using the finite-element software package Abaqus 6.2–7 (Abaqus, Providence, RI, USA).

The finite-element analysis produces the deformed contours of the anterior and the posterior lens surfaces from which the refractive power can be calculated. For this purpose, a least-square approximation of the anterior and the posterior lens contour by circular arcs is performed. This approximation is done in the central region of the lens with a radius of 0.8 mm.

The refractive power D can be calculated from the anterior and the posterior curvature radii R_a and R_f as follows:

$$D = D_f + D_b - \frac{t_c}{n_l} D_f D_b$$

$$D_f = \left(n_l - n_{aq}\right)/R_f; D_b = \left(n_{aq} - n_l\right)/R_b$$

D_f refractive part of the anterior lens surface
D_b refractive part of the posterior lens surface
n_l refractive index of the lens (n_l=1.42)
n_{aq} refractive index of the aqueous (n_{aq}=1.336)
t_c lens thickness

The lens and the aqueous are assumed to be optically homogeneous. Furthermore, the refractive indices of the lens and the aqueous were assumed to be constant. Age-related changes of these indices are not considered. This paper deals only with the refractive power change due to deformation of the lens and the resulting curvature change.

Results

Three-dimensional UBM can visualize zonular fibre groups hidden behind the iris. As shown in Fig. 1, digital subtraction of the sclera and iris from the scanned volume

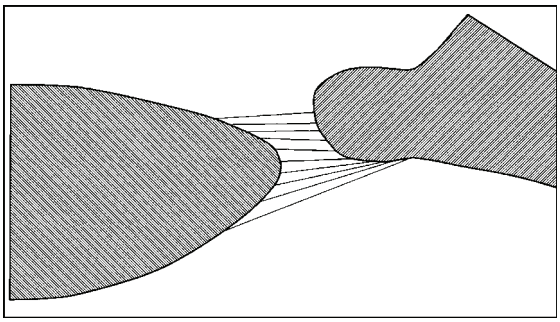

Fig. 6 The more complex model with ten sets of zonular fibres and multiple anchor points based on the contour approximation procedure

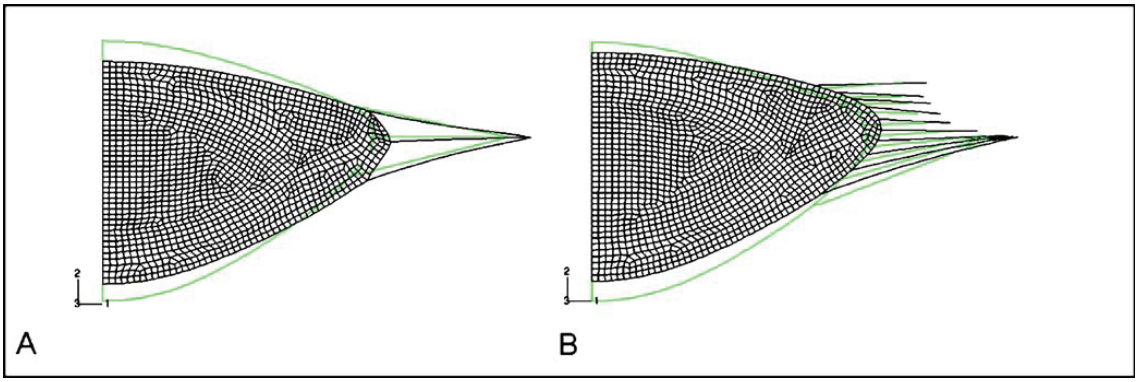

Fig. 7 Finite-element meshes for the 29-year-old lens. **a** The simple model with three sets of zonular fibres and a single anchor point. **b** The more complex model with ten sets of zonular fibres and multiple anchor points. The accommodated (reference) state is outlined in *green*, while the unaccommodated state (deformed mesh) is shown in *black*

of intact human eyes exposed the ciliary processes and zonular fibre groups. Single fibres, however, cannot be displayed with the current spatial resolution of 3D-UBM. Nevertheless, individual fibres could be seen in the two types of SEM used in this study. Additional structural and geometric data obtained from the two types of SEM complemented the findings from 3D-UBM.

All observed zonular fibres ran from different regions of the ciliary body to the equatorial zone of the lens (Figs. 1–5). There were no significant differences among the samples with respect to the overall arrangement and the total number of observable fibres. The results for all five eyes were similar.

Fibres were found to originate at the pars plana of the ciliary body (Figs. 1b▲, 2a▲,b▲,c▲,e▲). These fibres ran in the direction of the ciliary body, reached the pars plicata of the ciliary body, and followed their course through the ciliary body valleys (Figs. 1b#, 2b△, 3a▲). Fibres entered the valleys in two ways. Firstly, some fibres touched the ciliary body tangentially along the lateral walls of valleys and the dorsal ends of the ciliary processes (Figs. 1b*, 2a*). This attachment or anchoring may be responsible for a change of the direction of these fibres. Secondly, some of the zonular fibres crossed the ciliary body valleys without contact and ran directly towards the lens (Figs. 1b#, 3a▲). In this case, no change in fibre direction was observed. It cannot be stated that these fibres ended at preferred regions at the lens (anteriorly or posteriorly).

The main part of the observed fibres originated at the lateral walls and at the top of the ciliary processes (Figs. 1b△, 2a△, 3a△, 4a,b) and ran straight in the direction of the lens. These fibres were present in all zonular layers (posterior, equatorial and anterior) inserted on the lens surface (Fig. 5). Typical dorso-lateral views of zonular fibre insertion on the lens obtained with ESEM and conventional SEM are shown in Fig. 5a and Fig. 5b respectively. No X-shaped zonular groups crossing between the ciliary body and the lens were found. Additionally, some

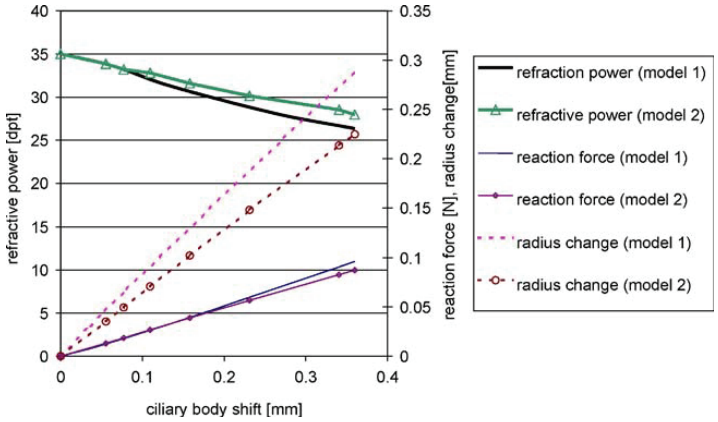

Fig. 8 Calculated variation of refractive power, equatorial lens radius change and total reaction force of the ciliary muscle with ciliary body movement for a 29-year-old lens. Model 1 assumes three sets of zonular fibres with a single anchor point; model 2 assumes ten sets of zonular fibres vwith multiple anchoring points

Table 1 FEM results for both models (model 1: three sets of zonular fibres with a single anchor point; model 2: ten sets of zonular fibres with multiple anchoring points) at a radial displacement of ciliary body of 0.36 mm

	Model 1	Model 2
Refraction power unacc. (dpt)	26.3	27.9
Reaction force (N)	0.096	0.087
Radius change (mm)	0.288	0.225

intraciliary fibres that ran between neighbouring ciliary processes were found in the ciliary body valleys (Fig. 4c).

Based on the 3D-UBM and ESEM/SEM images, typical zonular traversing patterns between lens and ciliary body were analysed and integrated in a geometric model shown in Fig. 6. This figure shows the advanced model with lens, approximated ciliary body and the zonular structure with 10 idealized fibre groups representing the findings in B-scan image data and SEM/SEM patterns. Both models (single anchor point, multiple anchor points) were used for finite-element modelling of accommodation. FEM calculations were carried out using the axisymmetric meshes shown in Fig. 7. The deformed lenses for both models are shown in Fig. 7 for a ciliary body displacement corresponding to the unaccommodated state. Also shown in Fig. 7 is an outline of the lenses in the accommodated state.

In Fig. 8, the results of the FEM simulations (refractive power, equatorial lens radius change and total reaction force) are shown. The maximum values for these magnitudes at a ciliary body radial displacement of 0.36 mm are given in Table 1.

Discussion

The human lens is attached to the ciliary muscle by the zonular fibres that originate at the pars plana and are anchored to the ciliary body before connecting to the lens. There are few detailed studies concerning the zonular geometry and the attachment to the ciliary body [4, 9, 21, 25]. For the numerical simulation of the accommodation process, the positions of the zonular fibre anchor points at the ciliary body are fundamental because these anchor points affect the amplitude and direction of force transmission from the ciliary muscle via the zonular fibres to the lens. Heretofore, the investigation of the anchor points has been difficult because these structures are hidden behind the iris. Direct optical visualization of these structures was not possible and examination by SEM can introduce preparation artefacts.

A combination of a 3D-UBM and ESEM examination of native structures without preparation artefacts in conjunction with conventional SEM experiments allowed a precise description of the zonula traversing pattern (e.g. Fig. 1). 3D-UBM clearly showed the ciliary process and zonular fibre groups normally hidden behind the iris. The ESEM examination of the zonula geometry in native samples showed that the preparation necessary for conventional SEM produces artefacts. Figure 5 shows images of the equatorial region of the lens by the two electron microscopic techniques. The SEM image is much sharper than the ESEM image. However, the SEM preparation results in alteration (shrinkage) of the zonula geometry. In addition, comparison with the native zonula geometry found using 3D-UBM leads to the realization that the dehydration induces a bundling of single fibres into broad threads. Thus the SEM preparation, taken alone, can lead to wrong conclusions regarding the structure and traversing patterns of the fibres.

A number of studies [9, 16, 25, 31] report that the zonular fibres originate exclusively at the pars plana. In this study, it was also observed that fibres originate at the pars plana. In addition fibres were found to originate at the lateral wall of the ciliary processes. This is in agreement with the results of Raviola [24]. Fibres were also observed to originate at the ciliary ridges as described by Davanger [7]. Using advanced imaging techniques, the findings of these earlier two studies were confirmed. However, the question remains of whether these are independent fibres or fibres emerging near the pars plana with an anchor point at the ciliary processes. Our investigations cannot give a clear answer; however, this question has, as a first approximation, a subordinated importance for FEM simulation.

We have found that the main part of the zonular fibres originate or have an anchor point at the lateral walls or at the top of the ciliary processes and run directly to the lens. An advanced geometric model was created using the newly defined zonular fibre traversing patterns. The advanced FEM for simulation of accommodation is shown in Fig. 7b in comparison to the simpler geometry in Fig. 7a. Both models were created with the same mesh and the same geometric and mechanical properties of the lens. The zonular fibres are modelled by axisymmetric shell elements. They form conical sheets around the lens. These sheets represent individual fibres. A material model was used in which the circumferential stiffness of these fibres is zero.

The FEM calculations were carried out using the two models. In each case, a displacement was applied in increments to the points representing the ciliary body. A displacement of 0.36 mm for maximal relaxation/stretching was used. This maximum displacement value encompasses the in vivo determined shifts of the ciliary muscle centre of gravity found using 3D-UBM [29] (max. 0.26 mm) and that found using magnetic resonance imaging [32] (Δr [mm]=0.5129–0.00525*age[years]). The resulting geometry of the lens was computed using the solution algorithm of Abaqus.

From the schematics of the two models shown in Fig. 7 it can be seen that the paraxial anterior surface is flatter in the

unaccommodated state than in accommodation. This is consistent with the Helmholtz theory of accommodation [14]. In both models, with accommodation, the anterior lens pole moves forward and the posterior lens pole moves backwards. This behaviour is also consistent with the theoretical calculations of Burd et al. [3] and agrees quantitatively with the experimental findings of Drexler and colleagues [8, 18].

In Fig. 7, the results of the FEM simulations are shown. It can clearly be seen that there are only small difference between the results from the two FEMs. The model with ten sets of zonular fibres shows a slightly lower radius change as the load is transferred by more zonular fibres. The calculated total circumferential reaction force at the ciliary body is nearly the same for the two models. The refractive power change calculated by the two models is also similar. This latter finding can be explained by the fact that the applied load has an influence on lens deformation only in the immediate region around the application point. The optical axis, where the optical power is calculated, is relatively far from the load application point, so there is very little influence of the zonula model on the optical power.

In conclusion, 3D-UBM and ESEM/SEM provided detailed information about the morphology of the zonules. With 3D-UBM, zonular fibre groups, normally hidden behind the iris, were made visible. This new, descriptive information on the accommodation apparatus and literature data were used to construct numerical models of the human accommodation process. Thus, the models were based on the most current knowledge of the geometry and material properties of the tissue structures involved in accommodation. Both models show good agreement with published data. The FEM results indicate that the simplified model adequately describes the accommodation process under the given boundary conditions. The more detailed zonula model produced comparable results. If numerical modelling is to be developed as a successful approach in the study of presbyopia, then this will rely on high-quality experimental data (e.g. age-related mechanical and geometric properties of the lens and zonules) becoming available in the future.

Acknowledgement The authors thank Prof. Axel Haubold for his helpful advice and editorial assistance in the preparation of this manuscript.

References

1. Agarwal LP, Narsinhan EC, Mohan M (1967) Experimental lens refilling. Orient Arch Ophthalmol 5:205–212
2. Brown N (1973) The change in shape and internal form of the lens of the eye on accommodation. Exp Eye Res 15:441–459
3. Burd HJ, Judge SJ, Cross JA (2002) Numerical modelling of the accommodating lens. Vision Res 42:2235–2251
4. Canals M, Costa-Vila J, Potau JM, Merindano MD, Ruano D (1996) Scanning electron microscopy of the human zonule of the lens (zonula ciliaris). Acta Anat 157:309–314
5. Coleman DJ (1986) On the hydraulic suspension theory of accommodation. Trans Am Soc Ophthalmol 84:846–868
6. Cumming JS, Kamman J (1996) Experience with an accommodating IOL. J Cataract Refract Surg 22(8):1001
7. Davanger M (1975) The suspensory apparatus of the lens. The surface of the ciliary body. A scanning electron microscopic study. Acta Ophthalmol 53 (1):19–33
8. Drexler W, Baumgartner A, Findl O, Hitzenberger CK, Fercher AF (1997) Biometric investigation of changes in the anterior eye segment during accommodation. Vision Res 37: 2789–2800
9. Farnsworth PN, Shyne SE (1979) Anterior zonular shifts with age. Exp Eye Res 28:291–297
10. Guthoff R, Ludwig K (2001) Current aspects in human accommodation I. Kaden, Heidelberg
11. Guthoff R, Ludwig K (2003) Current aspects in human accommodation II. Kaden, Heidelberg
12. Hara T, Hara T, Yasuda A, Yamada Y (1990) Accommodative intraocular lens with spring action. 1. Design and placement in an excised animal eye. Ophthalmic Surg 21:128–133
13. Hardman Lea SJ, Rubinstein MP, Snead MP, Haworth AM (1990) Pseudophakic accommodation? A study of the stability of capsular bag supported, one piece, rigid tripod, or soft flexible implants. Br J Ophthalmol 74:22–25
14. von Helmholtz H (1909) Physiological optics, vol. 1. Dover, New York, 1962, pp 143–172; English translation by JPC Southall for the Optical Society of America (1924) from the 3rd German edition of Handbuch der Physiologischen Optik, Voss, Hamburg
15. Hettlich HJ, Lucke K, Asiyo-Vogel M, Schulte M, Vogel A (1994) Lens refilling and endocapsular polymerization of an injectable intraocular lens: in vitro and in vivo study of potential risks and benefits. J Cataract Refract Surg 20(2):115–123
16. Hogan MJ, Alvarado JA, Wedell JE (1971) Histology of the human eye. Saunders, Philadelphia, pp 272–652
17. Kessler J (1964) Experiments in refilling the lens. Arch Ophthalmol 71:412–417
18. Kriechbaum K, Findl O, Kiss B, Sacu S, Petternel V, Drexler W (2003) Comparison of anterior chamber depth measurement methods in phakic and pseudophakic eyes. J Cataract Refract Surg 29(1):89–94
19. Küchle M, Nguyen NX, Langenbucher A, Gusek-Schneider GC, Seitz B, Hanna KD (2002) Implantation of a new accommodative posterior chamber intraocular lens. J Refract Surg 18 (3):208–216
20. Legeais JM, Werner L, Werner L, Abenhaim A, Renard G (1999) Pseudoaccommodation: BioComFold versus a foldable silicone intraocular lens. J Cataract Refract Surg 25 (2):262–267
21. Ludwig K, Wegscheider E, Hoops JP, Kampik A (1999) In vivo imaging of the human zonular apparatus with high-resolution ultrasound biomicroscopy. Graefes Arch Clin Exp Ophthalmol 237:361–371

22. Nishi O, Hara T, Hara T, Sakka Y, Hayashi F, Nakamae K, Yamada Y (1992) Refilling the lens with an inflatable endocapsular balloon: surgical procedure in animal eyes. Graefes Arch Clin Exp Ophthalmol 230:47–55
23. Parel JM, Gelender H, Treffers WF, Norton EW (1986) Phaco-ersatz: cataract surgery designed to preserve accommodation. Graefes Arch Clin Exp Ophthalmol 224:165–173
24. Raviola G (1971) The fine structure of the ciliary zonule and ciliary epithelium. With special regard to the organization and insertion of the zonular fibrils. Invest Ophthalmol 10 (11):851–869
25. Rohen JW (1979) Scanning electron microscopic studies of the zonular apparatus in human and monkey eyes. Invest Ophthalmol Vis Sci 18:133–144
26. Sarfarazi FM (2003) Optical and mechanical design for human Implantation of the Sarfarazi Elliptical Accommodative IOL. Proceedings of the ASCRS 2003, Abstract #738
27. Schachar RA, Bax AJ (2001) Mechanism of accommodation as analyzed by nonlinear finite element analysis. Ann Ophthalmol Clin 33(2):103–112
28. Schneider H, Stave J, Terwee T, Guthoff R (2003) Intraoperative refraction control of injectable lenses. In Guthoff R, Ludwig K (eds) Current aspects of accommodation II. Kaden, Heidelberg, pp 155–162
29. Stachs O, Martin H, Kirchhoff A, Stave J, Terwee T, Guthoff R (2002) Monitoring accommodative ciliary muscle function using three-dimensional ultrasound. Graefes Arch Clin Exp Ophthalmol 240:906–912
30. Stachs O, Schneider H, Stave J, Schmitz KP, Terwee T, Guthoff R (2003) The anterior segment in rabbit eyes after lens refilling with injectable silicone polymer. ARVO, Meet Abstr 44:273
31. Streeten BW (1994) Anatomy of the zonular apparatus. In Duane TD, Jaeger EA (eds) Biomedical foundations of ophthalmology, vol 1, chapter 14. Harper & Row, New York
32. Strenk SA, Semmlow JL, Strenk LM, Munoz P, Gronlund-Jacob J, DeMarco JK (1999) Age-related changes in human ciliary muscle and lens: a magnetic resonance imaging study. Invest Ophthalmol Vis Sci 40:1162–1169
33. Weale RA (2000) Why we need reading-glasses before a zimmer-frame. Vision Res 40:2233–2240
34. Wyatt HJ (1993) Application of a simple mechanical model of accommodation to the aging eye. Vision Res 33(5–6):731–738

Graefe's Arch Clin Exp Ophthalmol
DOI 10.1007/s00417-005-0228-8

LETTER TO THE EDITOR

Ronald A. Schachar
Ali Abolmaali
Farhad Kamangar

Comment on the publication "Three-dimensional ultrasound, biomicroscopy environmental and conventional scanning electron microscopy investigations of the human zonula ciliaris for numerical modelling of accommodation" by O. Stachs et al.

Received: 19 October 2005
Accepted: 21 November 2005

R. A. Schachar (✉)
Physics Department,
University of Texas at Arlington,
PO Box 601149, Dallas, TX, USA
e-mail: ron@2ras.com

A. Abolmaali
Civil and Environmental Engineering Department,
University of Texas at Arlington,
Arlington, TX, USA

F. Kamangar
Computer Science Engineering Department,
University of Texas at Arlington,
Arlington, TX, USA

Dear Editor

Stachs et al. constructed three-dimensional images of the architecture of the zonules from two-dimensional UBM images of postmortem human eyes. They compared these images with scanning electron microscopic images of the zonules [20].

The authors used a line between the scleral spur and the base of the ciliary muscle as the basis for a coordinate system to construct the three-dimensional images [20, 21]. Unfortunately, this line is not a sufficient coordinate reference from which to construct a three-dimensional image. The authors did not provide references on the globe or use landmarks sufficient to insure that the three-dimensional UBM images were not affected by perspective distortion. It has been demonstrated that small misalignments of the UBM probe with respect to the eye, which induce as little as a three-pixel shift between compared images, can cause significant perspective distortion [18, 19]. Moreover, since the lens equator is not visible in all images of the UBM, the path of the zonules and the location of their attachment to the lens capsule were inferred by the authors and have not been confirmed by them [20]. Consequently, it is premature for the authors to conclude that the zonular architecture is different from that which has been demonstrated with scanning electron microscopy [5, 22].

Then, using the finite element method (FEM), the authors determined the effect of the position of the lens zonules on the change in central optical power of the lens associated with zonular traction [20]. The authors did not select the most appropriate properties for the model employed in their FEM study, but simply relied on the FEM model performed by Burd et al. [2]. Had they used the correct FEM mesh elements, geometric and material properties in their model, a converged FEM solution would provide a reliable method for analyzing the mechanics of this biological system [1, 11, 13]. Burd et al. have recently re-evaluated the material properties of the lens cortex and nucleus, and acknowledge that the values used in their FEM analysis are inappropriate for modeling the human lens [3].

Burd et al. modeled the lens of a 29y/o in which the cortex was 6 times *harder* than its nucleus [2]. Brillouin light scattering [23], a non-invasive technique, and dynamometric measurements of in vitro *fresh* human lenses [14] and routine clinical observation during in vivo cataract extraction by phacoemulsification demonstrate that the hardness of the nucleus of lenses older than 25 years is either the same or *greater* than its cortex [8].The most appropriate material properties for the lens cortex and nucleus are based on the following:

The mean shear modulus, G, of the young lens is 50 Pa [7] and the bulk modulus, K, of the lens cortex is 2.8 GPa and the lens nucleus is 3.7 GPa [23]. From the relationship between G, K and the elastic modulus, E, the lens Poisson's ratio, v, is [16]:

$$\nu = \frac{3K - 2G}{6K + 2G} \cong 0.49999999$$

From the following relationship [16]:

$$E = \frac{9KG}{3K + G}$$

the elastic modulus of the lens cotex and nucleus is 150 Pa.

In addition, Burd et al. [2] did not consider the fact that the cortex is readily separated from the capsule [15] and should have incorporated contact elements to simulate the capsule-cortex interface. Burd et al. [2] used triangular elements to model the capsule, which are not as reliable as quadrilateral elements [9, 10] and a discontinuous function, consisting of a polynomial, a straight line and a circular end cap, to model the lens profile. It would be more appropriate to use a continuous function to model the lens such as given by Chien et al. [4].

With attention to these needed modifications, the authors should be able to obtain an FEM converged solution of zonular traction, such that the force and lens equatorial displacements required to induce 10 diopters of accommodation, can occur within the physiological force capacity of the ciliary muscle [6, 12, 24] and the space limitations of the equatorial circumlenticular space [17].

References

1. Baldewsing RA, de Korte CL, Schaar JA, Mastik F, van der Steen AF (2004) Finite element modeling and intravascular ultrasound elastography of vulnerable plaques: parameter variation. Ultrasonics 42(1-9):723–729
2. Burd HJ, Judge SJ, Cross JA (2002) Numerical modelling of the accommodating lens. Vision Res 42(18):2235–2251
3. Burd HJ, Wilde GS, Judge SJ (2005) Can reliable values of Young's modulus be deduced from Fisher's (1971) spinning lens measurements? Vision Res DOI 10.1016/j.visres.2005.07.012
4. Chien CH, Huang T, Schachar RA (2005) Analysis of human crystalline lens accommodation. J Biomech DOI 10.1016/j.jbiomech.2005.01.017
5. Farnsworth PN, Burke P (1977) Three-dimensional architecture of the suspensory apparatus of the lens of the Rhesus monkey. Exp Eye Res 25 (6):563–576
6. Fisher RF (1977) The force of contraction of the human ciliary muscle during accommodation. J Physiol (Lond) 270(1):51–74
7. Heys KR, Cram SL, Truscott RJ (2004) Massive increase in the stiffness of the human lens nucleus with age: the basis for age related decline in the amplitude of accommodation? Mol Vis 10: 956–963
8. Kelman C (1976) Phacoemulsification. In: Jaffe N. (ed) Cataract surgery and its complications, 2nd edn. C.V. Mosby Company, St Louis, Missouri, pp 134–152
9. Lau TS, Lo SH (1997) Generation of quadrilateral mesh over analytical curved surface. Finite Elem Anal Des 27:251–272
10. Lee YK, Lee CK (2003) A new indirect anisotropic quadrilateral mesh generation scheme with enhanced local mesh smoothing procedures. Int J Num Meth Eng 58:277–300
11. Lengsfeld M, Kaminsky J, Merz B, Franke RP (1996) Sensitivity of femoral strain pattern analyses to resultant and muscle forces at the hip joint. Med Eng Phys 18(1):70–78
12. Lograno MD, Reibaldi A (1986) Receptor-responses in fresh ciliary muscle. Br J Pharmacol 87(2):379–385
13. Mantell SC, Chanda H, Bechtold JE, Kyle RF (1998) A parametric study of acetabular cup design variables using finite element analysis and statistical design of experiments. J Biomech Eng 120(5):667–675
14. Nordmann J, Mack G Mack G (1974) Nucleus of the human lens: III. Its separation, its hardness. Ophthalm Res 6:216–222
15. Rakic JM, Galand A, Vrensen GF (1997) Separation of fibres from the capsule enhances mitotic activity of human lens epithelium. Exp Eye Res 64(1):67–72
16. Saada AS (1974) Elasticity theory and applications. Pergamon Press, New York, pp 199–204
17. Sakabe I, Oshika T, Lim SJ, Apple DJ (1998) Anterior shift of zonular insertion onto the anterior surface of the human crystalline lens with age. Ophthalmology 105(2):295–299
18. Schachar RA, Kamangar F (2005) Computer image analysis of ultrasound biomicroscopy of primate accommodation. Eye DOI 10.1038/sj.eye.6701838
19. Schachar RA, Kamangar F (2005) Accommodating IOL's require proper evaluation, Letter to the Editor. J Cataract Refract Surg (in press)
20. Stachs O, Martin H, Behrend D, Schmitz KP, Guthoff R (2005) Three-dimensional ultrasound, biomicroscopy environmental and conventional scanning electron microscopy investigations of the human zonula ciliaris for numerical modelling of accommodation Graefe's Arch Clin Exp Ophthalmol DOI 10.1007/s00417–005–0126–0
21. Stachs O, Martin H, Kirchhoff A, Stave J, Terwee T, Guthoff R (2002) Monitoring accommodative ciliary muscle function using three-dimensional ultrasound. Graefe's Arch Clin Exp Ophthalmol 240(11):906–912
22. Streeten BW (1982) Zonular apparatus. In: Jakobiec FA (ed) Ocular anatomy embryology and teratology. Harper and Row, Philadelphia, Pennsylvania, pp 331–353
23. Subbaram MV, Gump JC, Bullimore MA, Sooryakumar R (2002) The elasticity of the human lens. Invest Ophthalmol Vis Sci 43: E-Abstract 468 Abstract
24. Van Alphen GW, Robinette SL, Marci FJ (1962) Drug effects on ciliary muscle and choroids preparations in vitro. Arch Ophthalmol 68(7):111–123

Graefe's Arch Clin Exp Ophthalmol
DOI 10.1007/s00417-005-0229-7

LETTER TO THE EDITOR

Oliver Stachs
Heiner Martin

Reply to comment by R. Schachar et al. regarding our publication "Three-dimensional ultrasound biomicroscopy, environmental and conventional scanning electron microscopy investigations of the human zonula ciliaris for numerical modelling of accommodation"

Received: 18 November 2005
Accepted: 21 November 2005

O. Stachs
Eye Clinic, University of Rostock,
Rostock, Germany

H. Martin
Institute for Biomedical Engineering,
University of Rostock,
Rostock, Germany

O. Stachs (✉)
Universität Rostock,
Medizinische Fakultät, Augenklinik,
Doberaner Str. 140,
18055 Rostock, Germany
e-mail: oliver.stachs@med.uni-rostock.de
Tel.: +49-381-4948566
Fax: +49-381-4948502

Reply: The authors thank R. Schachar and his colleagues for their interest and comments regarding our recent article [11]. The critique can be categorized into two types: data evaluation technique and modeling techniques (material properties, contact conditions and lens geometry). We address each here.

Schachar states that we use a line between sclera spur and the base of the ciliary muscle as a basis for a coordinate system to construct a three-dimensional image. As clearly stated in our paper, we reconstructed the 3D images without using a line between sclera spur and the base of the ciliary muscle as a basis for the coordinate system, but rather used the stacks of the 3D-UBM without additional presumption of a point of origin. These stacks do not have the disadvantage of misalignment of the UBM probe with respect to the eye, and thus avoid the significant perspective distortion described by Schachar [9, 10] using standard B scans. With the UBM microscope used in our recent and earlier [11, 12] study, 3D data sets consisting of stacks of B–scans in parallel planes at a defined distance were obtained. Volumes with a size of 5×5×5 mm and a voxel size of 0.011×0.011× 0.031 mm were reconstructed.

We agree with Schachar et al. that the lens equator is not visible in all images of the UBM. In this context, we indicate that our interest was focused mainly on the location of attachment points on lens and ciliary muscle. In our paper, length measurements of the ciliary processes were not performed.

Schachar stated that it is premature for the authors to conclude that the zonular architecture is different from that which has been demonstrated with scanning electron microscopy [3, 13]. In addition to the two early papers cited by Schachar regarding zonula architecture described by SEM, there are a number of other studies [4, 5, 8, 14] that report that the zonular fibres originate exclusively at the pars plana. In contrast to these findings and Schachar's statements, our study showed that fibres originate not only at the pars plana but also at the lateral wall of the ciliary processes. We further observed that fibres originate at the ciliary ridges consistent with the findings by Davanger [2]. It is possible that the preparation artefacts for scanning electron microscopy (e.g. dehydration) prevent an imaging of some fibre origins as found in our study.

Moreover, Schachar states that the material properties given by Burd et al. [1] that were used in our paper are inappropriate. We are aware of the problem concerning the material properties of lens nucleus and lens cortex as described by Burd et al. These material properties are a subject of current

discussion among researchers in the field. In this context, we have previously carried out a parametric investigation on the pertinent material properties. We showed [6] that the resulting refractive power change depends on the gradient between the lens cortex and lens nucleus material properties. In this paper, it was found that the refractive power change during accommodation decreases when the material properties of the lens cortex and the lens nucleus are varied inversely. Recent investigations by H. Weeber et al. [15] show that the stiffness relation between the lens cortex and the lens nucleus depends on the age. While in young patients the lens nucleus has a lower stiffness than that of the lens cortex, the lens nucleus becomes harder in old lenses. Therefore, the material data of the lens show an age related distribution. In a 29-year-old lens (which was used for our simulation) the lens nucleus might be equal to or softer than the lens cortex.

In their letter, Schachar et al. state that the capsular bag is fully separated from the lens cortex. This may or may not be the case, but in any event the degree of coupling has little influence on the calculated refractive power change of the lens. We have performed investigations on the influence of different contact parameters between the lens capsule and the lens cortex in the past [7]. The variants evaluated include: capsule fully linked to the lens cortex; contact conditions between capsular bag and lens cortex with varied friction coefficient (separation of capsule allowed); contact conditions between capsular bag and lens cortex with varied friction coefficient (separation of capsule forbidden).

These parametric studies showed very little influence of the contact conditions on the refractive power change of the lens.

We agree with Schachar et al. that quadrilateral elements are more appropriate than the triangular elements used by Burd et al. and indeed, quadrilateral elements were used in our paper.

Moreover, Schachar et al. indicate that the lens contour is composed of different parts. We are aware of the fact that the lens contour is only continuous in the first derivative, but we do not think that the lens curvature in the peripheral region has an important influence on the refractive power change in the central region. So we believe that our simplified lens geometry is adequate.

With all the facts considered, our model yields converged solutions, with force and lens power change results somewhat different than that produced by Schachar et al.'s model.

We look forward to further studies published in peer–reviewed scientific journals to eliminate the lack of high-quality geometric and material data to improve the numerical modeling of accommodation and presbyopia.

References

1. Burd HJ, Judge SJ, Cross JA (2002) Numerical modelling of the accommodating lens. Vis Res 42:2235–2251
2. Davanger M (1975) The suspensory apparatus of the lens. The surface of the ciliary body, A scanning electron microscopic study. Acta Ophthalmol 53 (1):19–33
3. Farnsworth PN, Burke P (1977) Three-dimensional architecture of the suspensory apparatus of the lens of the Rhesus monkey. Exp Eye Res 25 (6):563–576
4. Farnsworth PN, Shyne SE (1979) Anterior zonular shifts with age. Exp Eye Res 28:291–297
5. Hogan MJ, Alvarado JA, Wedell JE (1971) Histology of the human eye. Saunders, Philadelphia, pp 272–652
6. Martin H, Stachs O, Guthoff R, Schmitz KP (2003) Biomechanische Modellierung des Akkommodationsprozesses unter Berücksichtigung des Zonulaapparates. Biomed Tech 48 (Suppl 1):358–359
7. Martin H, Terwee T, Guthoff R, Schmitz K-P (2005) Finite element investigations in to polymer refilled lenses. Biomedizinische Technik 50 (Suppl 1):1593–1594
8. Rohen JW (1979) Scanning electron microscopic studies of the zonular apparatus in human and monkey eyes. Invest Ophthalmol Vis Sci 18:133–144
9. Schachar RA, Kamangar F (2005) Accommodating IOL's require proper evaluation. Letter to the Editor. J Cataract Refract Surg (in press)
10. Schachar RA, Kamangar F (2005) Computer image analysis of ultrasound biomicroscopy of primate accommodation. Eye DOI 10.1038/sj.eye.6701838
11. Stachs O, Martin H, Behrend D, Schmitz KP, Guthoff R (2005) Three-dimensional ultrasound, biomicroscopy environmental and conventional scanning electron microscopy investigations of the human zonula ciliaris for numerical modelling of accommodation. Graefe's Arch Clin Exp Ophthalmol DOI 10.1007/s00417-005-0126-0
12. Stachs O, Martin H, Kirchhoff A, Stave J, Terwee T, Guthoff R (2002) Monitoring accommodative ciliary muscle function using three dimensional ultrasound. Graefe's Arch Clin Exp Ophthalmol 240:906–912
13. Streeten BW (1982) Zonular apparatus. In: Jakobiec FA (ed) Ocular anatomy embryology, and teratology. Harper and Row, Philadelphia, Pa., pp 331–353
14. Streeten BW (1994) Anatomy of the zonular apparatus. In Duane TD, Jaeger EA (eds) Biomedical foundations of ophthalmology, vol 1, chapter 14. Harper & Row, New York
15. Weeber HA, Eckert G (2004) Stiffness distribution within the human crystalline lens and its function with age. Invest Ophthalmol Vis Sci 45:1695

Potentially Accommodating Intraocular Lenses—An In Vitro and In Vivo Study Using Three-dimensional High-frequency Ultrasound

Oliver Stachs, PhD; Hanka Schneider, MD; Joachim Stave, PhD; Rudolf Guthoff, MD

ABSTRACT

PURPOSE: To investigate the accommodative performance of new intraocular lenses (IOLs) using the advantages of three-dimensional ultrasound biomicroscopy.

METHODS: An in vitro simulation device was designed to study IOL performance using an artificial capsular bag and a stretching device. The haptic region of the Akkommodative 1CU (HumanOptics AG) and CrystaLens AT-45 (Eyeonics Inc) was visualized in vitro in three dimensions, using an in-house developed three-dimensional ultrasound biomicroscope. The in vitro results were used to describe the in vivo situation in four patients with accommodative implants.

RESULTS: The haptic position and angulation in consideration of the accommodation state was distinguished and analyzed. In the simulation model, a maximal angulation change of 4.5° and 4.3° and a maximal forward shift of 0.33 mm and 0.28 mm was observed for the AT-45 and 1CU, respectively. In vivo, a change in haptic angulation <10° and a maximal forward shift of 0.50 mm was observed for the 1CU. These changes correspond to a theoretical approximate value of 0.50 diopters.

CONCLUSIONS: The in vitro simulation device examined with three-dimensional ultrasound biomicroscopy provided information on the accommodative performance of these potentially accommodative IOL designs. Using three-dimensional ultrasound biomicroscopy, corresponding changes in haptic angulation during pharmacological-induced accommodation were observed. [*J Refract Surg*. 2005;21:37-45.]

An intraocular lens (IOL) is implanted in the capsular bag during cataract surgery. Capsular fibrosis and capsular bag shrinkage result in a hardening of the IOL haptic and optic in the capsule. Despite excellent restoration of visual acuity and biocompatibility, no accommodation is present in pseudophakic eyes, as the IOL optic does not change in shape or position. Pseudophakic accommodation could potentially be achieved by ciliary muscle action if the hard lens cortex and nucleus were replaced by a flexible material. Several authors[1-6] reported refilled lens capsules in animal experiments.

To date, pseudophakic accommodation has only been achieved by multifocal IOLs and by an axial shift of the IOL optic. This shift of the IOL optic occurs when the ciliary muscle contracts and induces a change in haptic configuration. Recently, several attempts using different designs[7-12] have been made to achieve pseudophakic accommodation. The fundamental idea of all approaches to achieve potentially accommodating IOLs is to allow an axial displacement of the IOL optic.

Quantification of the axial IOL movement induced by accommodation in humans has been performed with ultrasound[8,13-15] and by using dual-beam partial coherence interferometry.[16-19] High-frequency ultrasound[20,21] is the only tool available to visualize the IOL haptic geometry hidden behind the iris diaphragm. High-frequency sonographic image analysis becomes difficult if information from only one plane is available. The aim of this study is the evaluation of haptic geometry based on a three-dimensional reconstruction of single section, ultrasound biomicroscopic data sets.

From the Eye Clinic of the University of Rostock, Rostock, Germany.

The authors have no proprietary interest in the development or marketing of this or a competing instrument, drug, or piece of equipment.

Correspondence: Oliver Stachs, PhD, Universität Rostock, Medizinische Fakultät, Augenklinik, Doberaner Str 140, 18055 Rostock, Germany. Tel: 49 381 4948565; Fax: 49 381 4948502; E-mail: oliver.stachs@med.uni-rostock.de

Received: October 6, 2003

Accepted: May 14, 2004

TABLE 1
Intraocular Lens Properties

Model	Special Properties	Overall Size (mm)	Haptic Material	Haptic Design	Optic Diameter (mm)	Optic Material
1CU (HumanOptics)	One piece	9.5	Acrylic	Plate	5.5	Acrylic
AT-45 (Eyeonics Inc)	Multi-part	11.5	Silicone and acrylic	Plate	4.5	Silicone

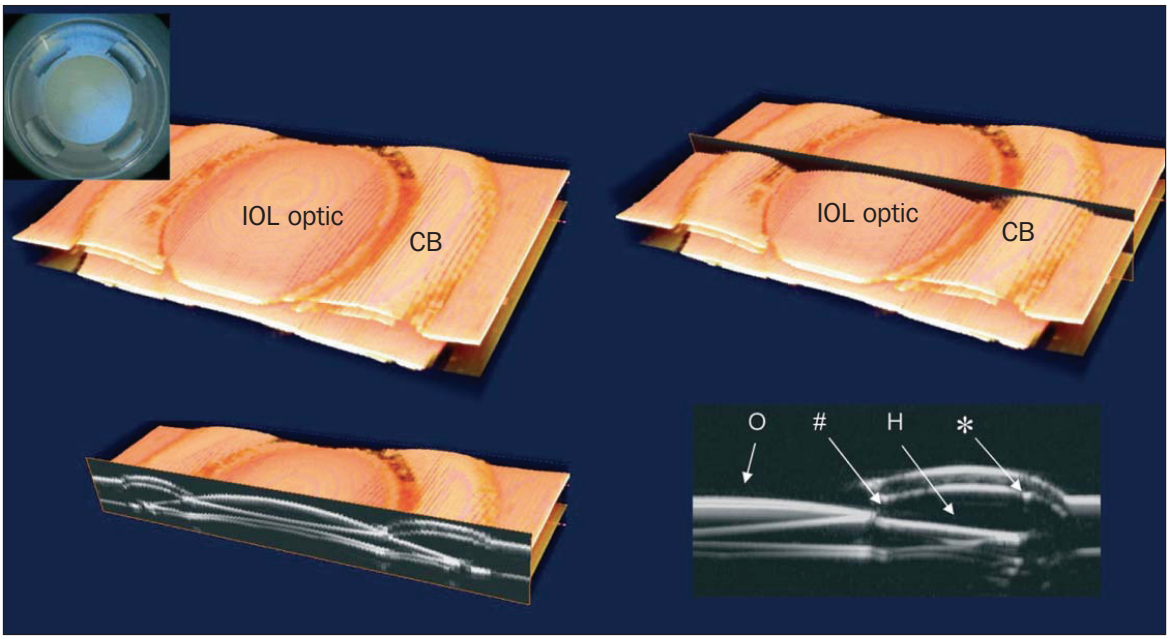

Figure 1. Photograph and three-dimensional ultrasound biomicroscopy image and B-scan of the 1CU in the artificial silicone capsular bag (CB). The optic (O) and haptic (H) are well differentiated. The spot (*) in the equatorial region of the capsular bag is caused by the haptic ridge of the IOL, whereas this point is not always present under different scanning directions. The point (#) acts as the fulcrum and is used as the center of rotation for angulation determination. The echo pattern of the posterior convex side of the haptic is a falsified image due to time-delay effects. Abbreviations: O = optic, # = fulcrum, H = haptic, and * = haptic ridge.

To simulate accommodation, a test chamber using an artificial capsular bag and a stretching device was developed. The haptic regions of the Akkommodative 1CU (HumanOptics AG, Erlangen, Germany) and the CrystaLens AT-45 (Eyeonics Inc, Aliso Viejo, Calif) were scanned in the simulation model during different accommodative (stretched) states. These in vitro results were correlated and used to describe the in vivo condition in four patients with accommodative implants.

MATERIALS AND METHODS

The IOLs studied and their properties are shown in Table 1 and are depicted as insets in Figures 1 and 2. The IOLs were implanted in a silicone capsular bag to allow simulation of the accommodation process. The artificial capsular bag is shown in Figure 3. Its characteristics have been described in detail[22] and the main properties are summarized in Table 2.

An in-house developed three-dimensional ultrasound biomicroscope was used to evaluate IOL placement and haptic configuration in the capsular bag. The principle of the ultrasound biomicroscope has been described in detail.[21] Iezzi et al[23] and Cusumano et al[24] described a technique for three-dimensional ultrasound biomicroscopy, and its application has been demonstrated.[25,26] For this study, three-dimensional

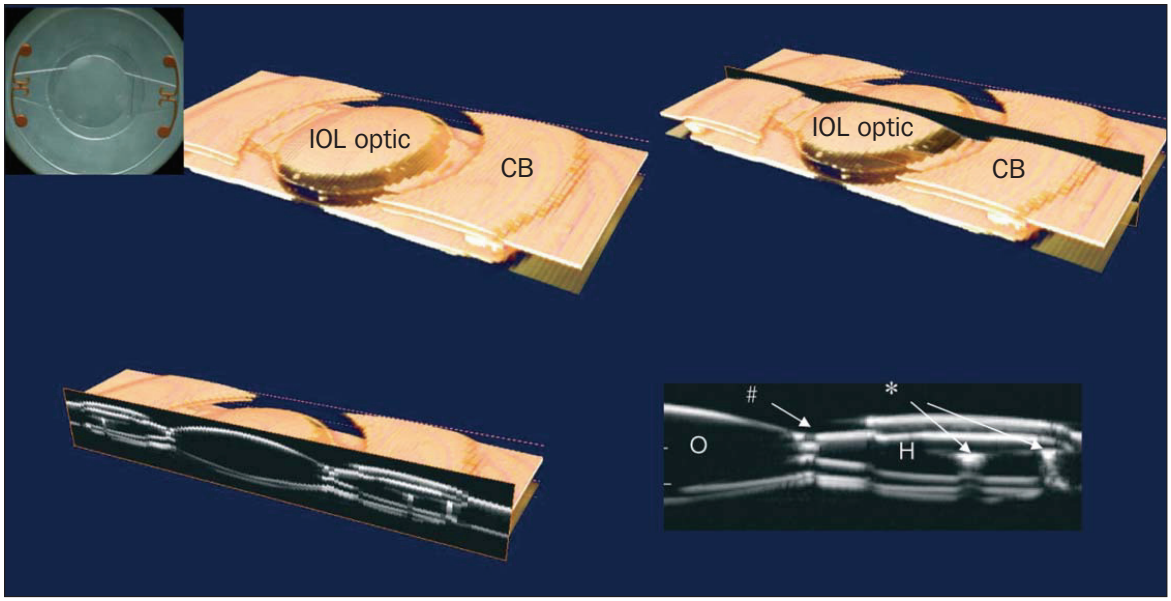

Figure 2. Photograph and three-dimensional ultrasound biomicroscopy image and B-scan of the CrystaLens AT-45 in the artificial silicone capsular bag (CB). The fulcrum is marked (#). The optic (O) and haptic (H) are well differentiated, whereas the echo pattern (*) is caused by the polyimide construction of the AT-45 plate haptic. Abbreviations: O = optic, # = fulcrum, H = haptic, and * = polyimide construction.

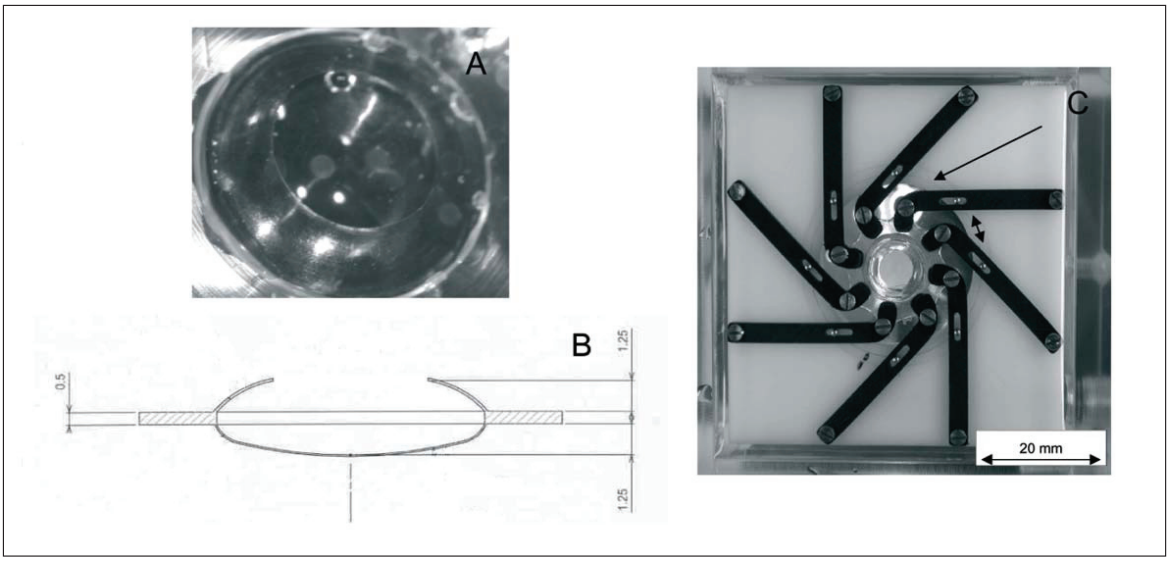

Figure 3. A, B) Artificial capsular bag and **C)** stretching device for accommodation simulation. The rotation of the inner ring with pins (marked in C) shifts the arms and stretches or relaxes the bag to simulate the force effects of the ciliary muscle. The 1CU IOL is implanted.

imaging was accomplished using a standard ultrasound biomicroscope (Model 840; Humphrey Instruments, Carl Zeiss Group, Jena, Germany) extended such that precise movement of the B-scan plane in the z-direction could be obtained. This principle for three-dimensional imaging has been summarized in detail.[27] In this arrangement, three-dimensional data sets consisting of parallel B-scans spaced at defined distances apart could be obtained.

The three-dimensional reconstruction was per-

TABLE 2
Properties of the In Vitro Capsular Bag Model

Material	Nusil (Silicon Technology, France)
Equatorial internal diameter	9.5 mm
Capsular skin thickness	
Posterior	0.06 mm
Anterior	0.1 mm
Ring dimension	15.0 mm
Rhexis diameter	5.5 mm
Young's Modulus	0.25 MPa

formed using VoxelView (Vital Images, Fairfield, Iowa) and Amira (TGS, San Diego, Calif) software. These commercial software packages provide an interactive environment allowing spatial orientation of individual planes, construction of three-dimensional perspectives, segmentation, and determination of distances and surfaces. Building three-dimensional constructs allows outlining of anatomic structures in space and can be used for volume measurements. For evaluation of haptic configurations and axial changes in IOL position, additional software, ImageJ (NIH, Bethesda, Md) and TINA (Raytest, Straubenhardt, Germany), was used.

For analysis of the IOL performance, the artificial capsular bag was mounted in a simulation device (see Fig 3C). The arms of the fixture clamp the bag around its periphery at eight points. Rotation of the inner ring stretches or relaxes the bag. Inner ring rotation is accomplished by a stepping motor driving a worm gear. The amount of stretching correlates with the rotation of the inner ring. The entire arrangement is submerged in water for sonographic imaging. In vitro, no movement artifacts exist, and a high-quality three-dimensional reconstruction can be performed (160 individual B-scans with 440×440 pixel). The three-dimensional volume was used to identify the tangential plane of the IOL respectively haptic, and an oblique reconstruction is possible to perform the biometric measurements. Thus, in vitro, an effect of tilting on the results of the biometric measurements can be excluded. For angulation determination, the center of rotation was placed at the fulcrum (see Figs 1 and 2) and the angle between IOL optic and haptic was measured using the anterior IOL interface. These biometric data were determined in six different extracted B-scan sections taken from six stretching experiments (one IOL implanted in three different bags) followed by mean value determination.

The in vivo measurements were performed following the tenets of the Helsinki agreement. Written informed consent was obtained from all patients after the nature and possible consequences of the study were explained. Three-dimensional ultrasound biomicroscope measurements were performed after pharmacologically induced accommodation (pilocarpine 2%) or disaccommodation (cyclopentolate 1%) on two consecutive days.

The ciliary body regions of four patients were scanned 30 minutes after pharmacological treatment. For the biometric measurements, individual scans were extracted from the scanned three-dimensional volumes because movement artifacts prevent an analysis of oblique reconstructions through the voxel blocks to perform the biometry. Changes in haptic angulation and the IOL shift were analyzed (mean value) using six extracted B-scans. Positive values for ΔACD represent a forward shift of the IOL. For angulation determination, the point of origin was placed at the fulcrum as described above.

RESULTS

The three-dimensional reconstruction and interactive selection of sections across the haptic of the IOLs studied in the artificial capsular bag are shown in Figures 1 and 2. For the 1CU (see Fig 1), the optic (O) and haptic (H) are well differentiated. The spot (*) in the equatorial region of the capsular bag is caused by the haptic ridge of the IOL, whereas this point is not always present under different scanning directions. The point (#) acts as the fulcrum and is used as the center of rotation for angulation determination. The echo pattern of the posterior convex side of the haptic is a falsified image due to time-delay effects. The fulcrum of the AT-45 is also marked (#), of which the three-dimensional reconstruction and image analysis is shown in Figure 2. Optic (O) and haptic (H) are well differentiated, whereas the echo pattern (*) is caused by the polyimide construction of the AT-45 plate haptic. The posterior lens surface could not be imaged.

B-scan series exemplifying the stretching experiments are depicted in Figure 4. The results concerning change in angulation optic haptic and axial shift are summarized in Figure 5. The B-scans of the 1CU IOL show the effect of equatorial stretching/relaxing (max change in r = 0.5 mm). This maximal radius change induces an angulation change of 10.4° and an axial shift around 0.36 mm of the 1CU. For the AT-45, a 9.3° angulation change and a 0.50-mm axial shift were found.

A basic knowledge of echo characteristics was used to describe the in vivo situation in patients with accommodative implants. Figure 6 shows a three-dimensional reconstruction and the image analysis (with design drawing) of the 1CU haptic region. A haptic an-

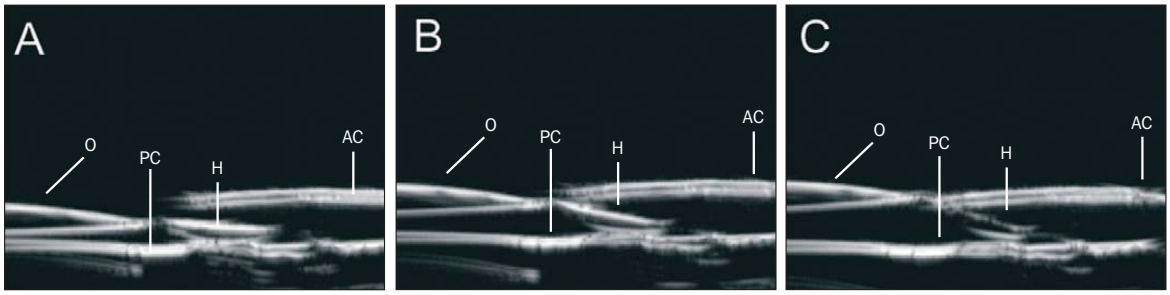

Figure 4. A-C) B-scan series exemplifying the stretching experiment. B-scan of the 1CU IOL showing the effect of equatorial stretching (max change in r = 0.5 mm). This stretching indicates a 10.4° angulation change and a 3.6-mm axial shift. Abbreviations: O = optic, PC = posterior capsule, H = haptic, AC = anterior capsule.

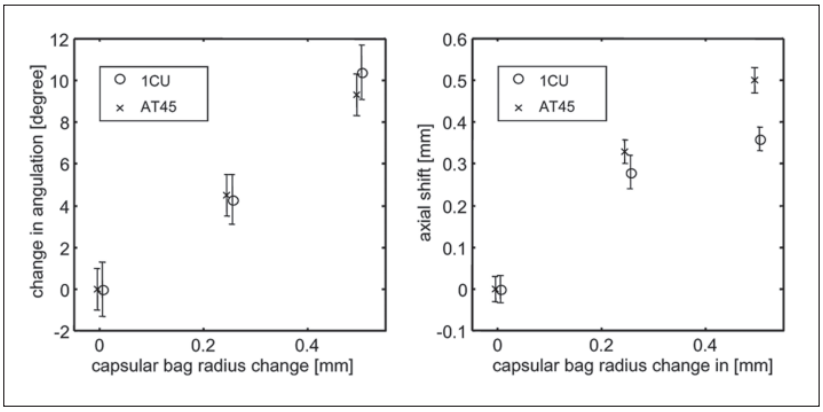

Figure 5. Change in angulation (left) and axial IOL movement (right) by lens type showing the effect of equatorial stretching respectively relaxing (mean value±standard deviation). A change in r of 0.5 mm is a decrease/increase of the equatorial radius of the artificial capsular bag, comparable with a 0.5-mm shift of the ciliary body in lens direction during accommodation.

gulation of 6° compared with the relaxed IOL haptic is observed in this case.

A detailed analysis of accommodative changes in axial lens shift (ΔACD) and haptic angulation was performed for four patients with the implanted 1CU IOL. In Figure 7, the change in angulation shows the effect of cyclopentolate and pilocarpine in a 67-year-old patient 4 months postoperatively. For this patient, in comparison to the relaxed haptic configuration, a 4° angulation was observed using cyclopentolate. Pilocarpine induced an additional 10° angulation.

The results of the four eyes examined are summarized in Figure 8. In disaccommodation, a haptic angulation between 2° and 4° is visible. Pilocarpine induced an additional angulation change <10° for the 1CU. In one case (patient 3), a haptic distortion was found. The haptic was positioned in an angle that results in a position anteriorly to the IOL optic plane and pilocarpine-induced ciliary muscle contraction caused a posterior IOL shift.

DISCUSSION

The biometric analysis of high-frequency sonographic images becomes difficult if the information from only one A-scan section is possible. Regarding the analysis of haptic configurations, undefined tilting effects can falsify biometric measurements. The three-dimensional ultrasound biomicroscopy combined with a powerful volume rendering software provides features such as volume orientation for viewing planes and three-dimensional perspectives. These features include an auxiliary tool for identification and biometric analyzing of the haptic configuration with minimized tilting effects.

The posterior chamber lens 1CU, which was developed based on FEM simulations by Küchle et al,[11] was examined. Theoretically, a contraction of the ciliary muscle, thus a relaxation of the zonules, leads to a relaxation of the capsular bag. The haptics turn and produce an anterior axial shift according to the modified force ratio in the haptic region. Our simulation experiments show a similar effect during capsular bag relaxation. A 0.5-mm change in r was used for maximal relaxation/stretching, which is larger than the in vivo determined shifts of the ciliary muscle center of gravity using three-dimensional ultrasound biomicroscopy[27]

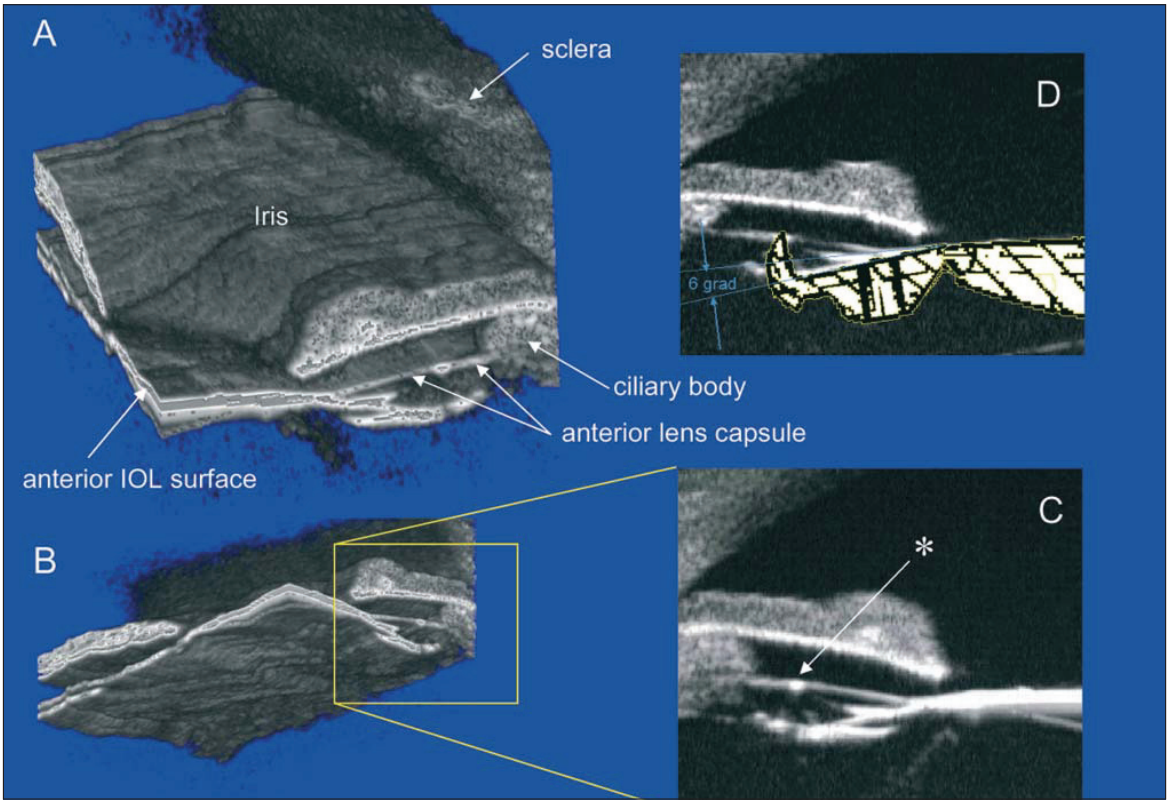

Figure 6. A, B) Three-dimensional reconstruction and **C, D)** image analysis (with design drawing) of the 1CU haptic region in a 75-year-old patient 4 months postoperatively (disaccommodation). A 6° haptic angulation compared with the relaxed IOL condition is observed.

(max 0.26 mm) and magnetic resonance imaging[28] (change in r [mm] = 0.5129−0.00525 × age [y]). With this unphysiological and unexpected amount of relaxation in humans, a 0.36-mm anterior shift was observed for the 1CU caused by a haptic 10.4° angulation change. Using a 50-year lens and the linear regression of Strenk for the ciliary body displacement, a 0.25-mm ciliary body displacement can be assumed. A 0.28-mm anterior IOL shift and an angulation change of 4.3° was observed. For this lens, the theoretically predicted 30° haptic angulation change for 1-mm axial shift could not be achieved. Using Gullstrand's eye model and a 20-diopter (D) IOL placed in the capsular bag, a 1-mm anterior IOL shift causes a change in refraction of approximately 1.90 D in the spectacle plane.[29] A 1-mm shift of a lens in the anterior chamber results in approximately a 1.20 D refraction change. Because the 1CU is placed between the capsular bag and iris plane, a 0.28-mm anterior shift for the 1CU produced a refraction change <0.53 D.

In the in vitro model, a maximal forward shift of 0.50 mm (9.3° haptic angulation change) for the AT-45 lens was observed using the maximal radius change of 0.5 mm. For 0.25-mm radius change as the expected value for the 50-year lens, an axial shift of 0.33 mm with 4.5° angulation change was found. Using Gullstrand's eye model, this shift of 0.33 mm causes a change in refraction <0.63 D. However, the measured shift does not correspond to the theoretical predictions for this lens. The AT-45 IOL was developed to transmit ciliary muscle activity into axial movement of the lens caused by ciliary muscle-induced variations in haptic angulation and vitreous pressure. In our model, equatorial changes can be simulated, but vitreous pressure variations cannot be simulated. Our observed anterior shift of the AT-45 optic therefore can only be caused by the modified geometric ratio in the haptic region, ie, the in vivo potential of this lens could be larger.

Regarding the axial shift, the AT-45 performed 0.14 mm better compared to the 1CU for 0.5-mm radial displacement. This is remarkable, as the changes in angulation for both lenses are similar. From a geometrical

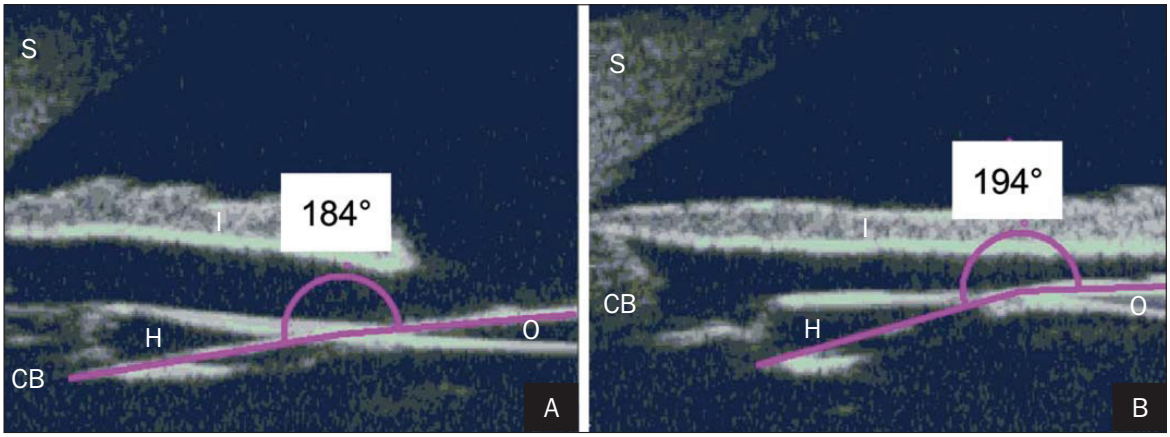

Figure 7. Change in angulation of the 1CU showing the effect of **A)** cyclopentolate and **B)** pilocarpine in a 67-year-old patient 4 months postoperatively. In comparison to the relaxed haptic configuration (180°), a 4° angulation (184°) could be observed using cyclopentolate. Pilocarpine induced an additional 10° angulation (194°). Abbreviations: S = sclera, I = iris, CB = ciliary body, H = haptic, O = optic.

viewpoint, this complex effect is hard to explain and cannot be elucidated completely. A reason could be the different design of the haptic contact point to the capsular bag or a deformation of the IOL optic.

Ultrasonographic patterns of the IOL haptics are used to explain the in vivo situation in patients with the 1CU implant. Changes in angulation and ΔACD by four different individuals show the effect of cyclopentolate and pilocarpine 4 months postoperatively (see Fig 8). In disaccommodation, a haptic angulation between 2° and 4° caused by capsular bag shrinkage and secondary cataract formation is visible. This could mean that a haptic angulation is already present in the disaccommodated state. Also the effect seen in patient 3 is caused by the capsular bag shrinkage (see Fig 8). The IOL haptic is placed anteriorly to the IOL optic plane. In this case, pilocarpine treatment induced a posterior IOL shift (ΔACD = −0.4 mm).

In the cases studied, pilocarpine induced an additional angulation variation between 5° and 10° for the 1CU IOL, which causes a change in anterior chamber depth between 0.2 and 0.5 mm. Using Gullstrand's eye model, this 0.2-mm forward movement results in a refraction change <0.38 D (0.95 D for 0.5 mm of movement), depending on exact IOL position. These found ΔACD values are smaller than the findings of Langenbucher et al.[30] A mean ACD decrease of 0.78 mm (0.49 to 1.26 mm) using the IOL-Master and 0.63 mm (0.34 to 1.12 mm) was found using ultrasound biometry after pilocarpine (6 months postoperatively). Our findings are in agreement with the results of Findl et al.[17,18] Using partial coherence interferometry, Findl et al found a moderate forward movement under pilocarpine with an induced mean accommodative amplitude of 0.50 D. In conclusion, pilocarpine-induced ciliary muscle contraction caused a change in haptic angulation and an anterior shift of the 1CU IOL, which resulted in approximately an estimated accommodative amplitude between 0.40 and 0.95 D.

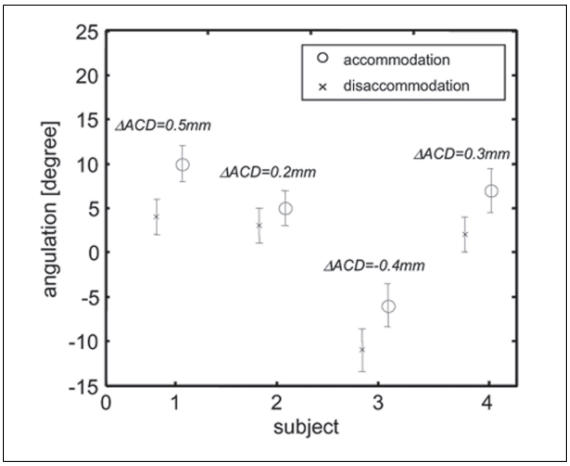

Figure 8. Angulation and anterior chamber depth (ΔACD) by subject (implant 1CU) showing the effect of cyclopentolate and pilocarpine (× = angle of difference to the relaxed haptic configuration, o = change under pilocarpine treatment; mean±standard deviation). Positive values for ΔACD represent a forward shift of the IOL under pilocarpine.

Pilocarpine application is an objective way of stimulating accommodation as it requires no participation from the patient. Topical application of pilocarpine is advised and commonly used to stimulate accommodation.[16-19,31-33] Variability in accommodation amplitudes is partially due to the capability and attendance of vol-

unteers to accommodate to various kinds of stimuli. Using pilocarpine, this subjective component to accommodation is eliminated; however, the role of pilocarpine must be discussed.

Abramson et al[32] measured the accommodation effect in human individuals using A-scan ultrasound. They determined a greater increase in axial lens diameter after pilocarpine application than is possible with stimulus-driven accommodation. Thus, topical application of pilocarpine may produce overstimulation of the ciliary muscle. These early results are consistent with the findings of Find[34] and Köppl et al[35] who used dual-beam partial coherence interferometry. These studies have shown a difference in lens movement between pilocarpine-induced and stimulus-driven ciliary muscle contraction. Pilocarpine acts "physiologically" in young phakics and as a superstimulus in presbyopic phakics and pseudophakes. Therefore, IOL movement and angulation change data may be overestimated when using pilocarpine.

REFERENCES

1. Kessler J. Experiments in refilling the lens. *Arch Ophthalmol*. 1964;71:412-417.
2. Agarwal LP, Narsinhan EC, Mohan M. Experimental lens refilling. *Oriental Archives of Ophthalmology*. 1967;5:205-212.
3. Parel JM, Gelender H, Trefers WF, Norton EW. Phaco-Ersatz: cataract surgery designed to preserve accommodation. *Graefes Arch Clin Exp Ophthalmol*. 1986;224:165-173.
4. Nishi O, Hara T, Hara T, Sakka Y, Hayashi F, Nakamae K, Yamada Y. Refilling the lens with an inflatable endocapsular balloon: surgical procedure in animal eyes. *Graefes Arch Clin Exp Ophthalmol*. 1992;230:47-55.
5. Hettlich HJ, Lucke K, Asiyo-Vogel M, Schulte M, Vogel A. Lens refilling and endocapsular polymerization of an injectable intraocular lens: in vitro and in vivo study of potential risks and benefits. *J Cataract Refract Surg*. 1994;20:115-123.
6. Stachs O, Schneider H, Stave J, Schmitz KP, Terwee T, Guthoff R. The anterior segment in rabbit eyes after lens refilling with injectable silicone polymer. Association for Research in Vision and Ophthalmology Meeting Abstracts. 2003;44:273.
7. Hara T, Hara T, Yasuda A, Yamada Y. Accommodative intraocular lens with spring action, I: design and placement in an excised animal eye. *Ophthalmic Surg*. 1990;21:128-133.
8. Hardman Lea SJ, Rubinstein MP, Snead MP, Haworth SM. Pseudophakic accommodation? A study of the stability of capsular bag supported, one piece, rigid tripod, or soft flexible implants. *Br J Ophthalmol*. 1990;74:22-25.
9. Cumming JS, Kammann J. Experience with an accommodating intraocular lens. *J Cataract Refract Surg*. 1996;22:1001.
10. Legeais JM, Werner L, Werner L, Abenhaim A, Renard G. Pseudoaccommodation: BioComFold versus a foldable silicone intraocular lens. *J Cataract Refract Surg*. 1999;25:262-267.
11. Küchle M, Nguyen NX, Langenbucher A, Gusek-Schneider GC, Seitz B, Hanna KD. Implantation of a new accommodative posterior chamber intraocular lens. *J Refract Surg*. 2002;18:208-216.
12. Sarfarazi FM. Optical and mechanical design for human implantation of the Sarfarazi Elliptical Accommodation intraocular lens [abstract #738]. Proceedings of the American Society of Cataract and Refractive Surgery; April 12-16, 2003; San Francisco, Calif.
13. Nakazawa M, Ohtsuki K. Apparent accommodation pseudophakic eyes after implantation of posterior chamber intraocular lenses: optical analysis. *Invest Ophthalmol Vis Sci*. 1984;25:1458-1460.
14. Ravalico G, Baccara F. Apparent accommodation in pseudophakic eyes. *Acta Ophthalmol*. 1990;68:604-606.
15. Gandolfi SA, Marchini G, Tosi R, Mora P, Pedrotti E, Sartori P, Manzotti F. UBM changes during accommodation in eyes implanted with Crystalens AT 45 and 1CU intraocular lens: a pilot study. *Invest Ophthalmol Vis Sci*. 2003;44:E-Abstract 252.
16. Findl O, Drexler W, Menapace R, Bobr B, Bittermann S, Vass C, Rainer G, Hitzenberger CK, Fercher AF. Accurate determination of effective lens position and lens-capsule distance with 4 intraocular lenses. *J Cataract Refract Surg*. 1998;24:1094-1098.
17. Findl O, Kriechbaum K, Köppl C, Menapace R, Drexler W. Laser interferometric measurements of intraocular lens movement with accommodating IOLs. Proceedings of the American Society of Cataract and Refractive Surgery; April 12-16, 2003; San Francisco, Calif.
18. Findl O, Menapace R, Kriechbaum K, Koeppel C, Drexler W. Laser interferometric measurements of movement of an accommodating intraocular lens. In: Guthoff R, Ludwig K, eds. *Current Aspects in Accommodation II*. Heidelberg, Germany: Kaden; 2003:211-221.
19. Findl O, Kiss B, Petternel V, Menapace R, Georgopoulos M, Rainer G, Drexler W. Intraocular lens movement caused by ciliary muscle contraction. *J Cataract Refract Surg*. 2003;29:669-676.
20. Pavlin CJ, Foster FS. Ultrasound biomicroscopy in glaucoma. *Acta Ophthalmol*. 1992;204:7-9.
21. Pavlin CJ, Foster FS. *Ultrasound Biomicroscopy of the Eye*. Heidelberg, Germany: Springer; 1995.
22. Beck R, Pfeiffer K, Stave J, Guthoff R. A 3-D capsular bag model for describing biomechanical properties of new intraocular lenses [German]. *Ophthalmologe*. 2000;97:546-551.
23. Iezzi R, Rosen RB, Tello C, Liebmann Walsh JB, Ritch R. Personal computer-based 3-dimensional ultrasound biomicroscopy of the anterior segment. *Arch Ophthalmol*. 1996;114:520-524.
24. Cusumano A, Coleman DJ, Silverman RH, Reinstein DZ, Rondeau MJ, Ursea R, Daly SM, Lloyd HO. Three-dimensional ultrasound imaging. Clinical applications. *Ophthalmology*. 1998;105:300-306.
25. Silverman RH, Rondeau MJ, Lizzi FL, Coleman DJ. Three-dimensional high-frequency ultrasonic parameter imaging of anterior segment pathology. *Ophthalmology*. 1995;102:837-843.
26. Silverman RH, Folberg R, Boldt HC, Lloyd HO, Rondeau MJ, Mehaffey MG, Lizzi FL, Coleman DJ. Correlation of ultrasound parameter imaging with microcirculatory pattern in uveal melanoma. *Ultrasound Med Biol*. 1997;23:573-581.
27. Stachs O, Martin H, Kirchhoff A, Stave J, Terwee T, Guthoff R. Monitoring accommodative ciliary muscle function using three-dimensional ultrasound. *Graefes Arch Clin Exp Ophthalmol*. 2002;240:906-912.
28. Strenk SA, Semmlow JL, Strenk LM, Munoz P, Gronlund-Jacob J, DeMarco JK. Age-related changes in human ciliary muscle and lens: a magnetic resonance imaging study. *Invest Ophthalmol Vis Sci*. 1999;40:1162-1169.
29. Holladay JT. Refractive power calculations for intraocular lenses in the phakic eye. *Am J Ophthalmol*. 1993;116:63-66.

30. Langenbucher A, Huber S, Nguyen NX, Seitz B, Gusek-Schneider GC, Kuchle M. Measurement of accommodation after implantation of an accommodating posterior chamber intraocular lens. *J Cataract Refract Surg*. 2003;29:677-685.

31. Kaufman PL. Scleral expansion surgery for presbyopia. *Ophthalmology*. 2001;108:2161-2162.

32. Abramson DH, Franzen LA, Coleman DJ. Pilocarpine in the presbyope. Demonstration of an effect on the anterior chamber and lens thickness. *Arch Ophthalmol*. 1973;89:100-102.

33. Wold JE, Hu A, Chen S, Glasser A. Subjective and objective measurement of human accommodative amplitude. *J Cataract Refract Surg*. 2003;29:1878-1888.

34. Find O. Akkommodative intraocular lens: funktionelle ergebnisse. *Klin Monatsbl Augenheilkd*. 2004;221(Suppl):36.

35. Köppl C, Findl O, Kriechbaum K, Dexler W. Comparison of pilocarpine-induced and stimulus-driven accommodation in phakic eyes. Proceedings of the XXI Congress of the European Society of Cataract and Refractive Surgery; September 6-10, 2003; Munich, Germany.

Stachs Wins Award for Studies of Potentially Accommodating Intraocular Lenses

Oliver Stachs, PhD, has won the 2005 Troutman Award and $5000 prize, funded by the Microsurgical Research Foundation, for an article published in the *Journal of Refractive Surgery*: "Potentially Accommodating Intraocular Lenses—An In Vitro and In Vivo Study Using Three-dimensional High-frequency Ultrasound" by Stachs O, Schneider H, Stave J, and Guthoff R [*J Refract Surg.* 2005;21:37-45]. The winner is selected by a committee of three: Editor-in-Chief of the Journal and the present and previous chairpersons of ISRS/AAO. The selection criteria include originality, relevance, clarity, and scientific rigor. Dr Stachs' article scored highly in each of these categories.

BIOGRAPHICAL SKETCH

Stachs attended the University of Rostock, Germany where he obtained a BSc and a PhD in Physics in 1991 and 1996, respectively. While completing his PhD, Stachs was a Research Assistant in the Department of Physics from 1992 to 1996. After receiving his PhD, he attended the Stanford Synchroton Radiation Laboratory at Stanford University, California as a Research Fellow. He returned to the University of Rostock in 1997 as a Research Associate in the Department of Ophthalmology and currently holds this position.

DESCRIPTION OF RESEARCH FOCUS

Stachs and colleagues' research is based on the optics of the eye—accommodation, presbyopia, and restoring accommodation (ie, accommodative intraocular lenses, lens refilling, etc). This research is conducted using imaging methods such as ultrasonography, three-dimensional high-frequency ultrasound, confocal laser scanning microscopy, and biometry.

SELECTED PUBLICATIONS

1. Meinhardt B, Stachs O, Stave J, Beck R, Guthoff R. Evaluation of biometric methods for measuring the anterior chamber depth in the non-contact mode. *Graefes Arch Clin Exp Ophthalmol.* In press.
2. Stachs O, Schneider H, Beck R, Guthoff RF. Pharmacological induced haptic changes and the accommodative performance in patients with the AT-45 accommodative IOL. *J Refract Surg.* In press.
3. Schneider H, Stachs O, Beck R, Guthoff RF. Clinical investigations regarding implantation of potential accommodative intraocular lenses. *Graefes Arch Clin Exp Ophthalmol.* In press.
4. Stachs O, Martin H, Behrend D, Schmitz KP, Guthoff RF. 3D-ultrasound biomicroscopy and ESEM/SEM investigations of the human zonula ciliaris for numerical modeling of accommodation. *Graefes Arch Clin Exp Ophthalmol.* In press.
5. Stachs O, Martin H, Kirchhoff A, Stave J, Guthoff RF. Monitoring accommodative ciliary muscle function using three-dimensional ultrasound. *Graefes Arch Clin Exp Ophthalmol.* 2002;249:906-912.

OBJECT OF THE TROUTMAN AWARD

The Troutman Award encourages and rewards an outstanding contribution to the literature by a clinician or vision scientist following completion of his or her residency in ophthalmology or doctorate in vision sciences. The awardee must be a member of the ISRS/AAO.

Additional Award Recipients

LIFETIME ACHIEVEMENT AWARD—Daniel S. Durrie, MD, Overland Park, Kansas

Honors an ISRS member who has made significant, internationally recognized, career-long contributions to the advancement of refractive surgery.

BARRAQUER AWARD AND LECTURE—Carmen J. Barraquer, MD, Bogota, Colombia

Honors a senior physician who has made significant contributions in refractive surgery and exemplifies the character and scientific dedication of Jose I. Barraquer, MD—one of the founding fathers of refractive surgery.

LANS DISTINGUISHED AWARD—Paolo Vinciguerra, MD, Milan, Italy

Honors Leedert J. Lans who defined the basics of refractive surgery. The award is given to a young innovative researcher or clinician in refractive surgery.

KRITZINGER MEMORIAL AWARD—Ramon Naranjo Tackman, MD, Mexico City, Mexico

Honors an ISRS member who embodies the clinical, educational, and investigative qualities of Dr. Michiel Kritzinger, whose clinical research advanced the international practice of refractive surgery.

CASEBEER AWARD—Arturo S. Chayet, MD, Tijuana, Mexico

Recognizes outstanding contributions to the research and development of refractive surgery.

FOUNDERS' AWARD—Michael A. Lawless, MD, Chatswood, Australia

Recognizes the vision and spirit of the Society's founders by honoring an ISRS member who has made extraordinary contributions to the advancement of the Society and its mission.

Evidenzbasierte Betrachtungen zu akkommodativen Kunstlinsen

H. Schneider, R. Guthoff

Der Begriff der evidenzbasierten Medizin begegnet uns auch im klinischen Alltag zunehmend. Per definitionem ist die „evidence based medicine" oder „nachweisbasierte Medizin" eine Bewertungsmethodik, die den gewissenhaften, ausdrücklichen und vernünftigen Gebrauch der besten verfügbaren externen Evidenz für medizinische Entscheidungen im Rahmen der Patientenversorgung beinhaltet [21]. Die Betrachtungen sollten die Sicht des Patienten mit seinem individuellen Problem und seinen Erwartungen, des Arztes mit seinen Fähigkeiten und Erfahrungen und die externe Evidenz, also das Wissen aus Studien, sowie die Interessen der Solidargemeinschaft berücksichtigen.

Dies ist sicherlich keine grundsätzlich neue Herangehensweise an eine medizinische Fragestellung. Ausgangspunkt für evidenzbasierte Betrachtungen ist aber unstreitig der Tatbestand, dass es angesichts der rasanten Entwicklung in der Medizin und der daraus resultierenden Fülle an Neuentwicklungen und Veröffentlichungen einer Beurteilung von Wirksamkeit, Nutzen und Anwendbarkeit einer diagnostischen Methode oder einer Therapie bedarf. Evidenzbasierte Beurteilungen sind sicher nicht in jedem Fall einer therapeutischen Entscheidung möglich oder sinnvoll, bei der Beurteilung der Wirksamkeit und der Vorteile so genannter akkommodativer Intraokularlinsen bieten sie sich jedoch vor dem Hintergrund des hohen Standards der heutigen Kataraktchirurgie an.

Die sich zunächst stellende Frage lautet: Ist die Presbyopie behandelbar und welche Methoden stehen zur Verfügung?

Die bisher zum Einsatz gekommenen chirurgischen Verfahren der Presbyopiebehandlung sind entweder von fraglicher Wirksamkeit, wie die so genannten skleraexpandierenden Operationsverfahren [17] oder weisen noch ungelöste Probleme, wie andere versuchte Varianten der Presbyopiebehandlung durch photorefraktive Keratektomie [26], dezentrierte LASIK [2] oder die Implantation kornealer Ringe [13] auf. Mit keiner bisher zum Einsatz gekommenen Therapie kann eine echte Akkommodation erzielt werden. Bestenfalls erlauben multifokale Intraokularlinsen einen besseren unkorrigierten Nahvisus auf Kosten der Kontrastempfindlichkeit [1, 9, 20, 24], so dass diese bisher keinen breiten Einsatz im klinischen Alltag finden. Im vergangenen Jahr wurde auf ophthalmologischen Kongressen über bessere klinische Ergebnisse nach Implantation von neu entwickelten, multifokalen IOL berichtet; möglicherweise gibt es hier eine Neubelebung dieses Konzeptes.

Einen weiteren Lösungsansatz zur Wiederherstellung der Akkommodation im Rahmen der Kataraktchirurgie stellen mechanische Konzepte dar, die auf dem „axial shift"-Prinzip einer Kunstlinsenoptik beruhen. Sie gehen davon aus, dass die erhaltene Funktion des Ziliarmuskels und der Zonulafasern eine Bewegung von Kunstlinsenoptiken mit flexiblen Haptiken im erhaltenen Kapselsack entlang der optischen Achse ermöglichen. Mit der BioComFold 43A (Morcher), der AT-45 Crystalens (Eyonics) und der 1CU (Human Optics) sind derartige so genannte akkommodative Acryl-Kunstlinsen heute kommerziell erhältlich. Voraussetzung für eine Akkommodationsamplitude von 2,9 Dioptrien, welche gleichbedeutend mit einer Lesefähigkeit in 35 cm Abstand ist, wäre nach Holladay eine Vorwärtsbewegung einer Kunstlinse mit einer Brechkraft von 20 dpt. im Auge um 2,2 mm [10]. Hier liegen die Grenzen dieser mechanischen Konzepte, denn diese Verschiebung würde eine Verlagerung des Irisdiaphragmas notwendig machen (Abb. **1**). Bei Kunstlinsenoptiken hoher Brechkraft können jedoch auch kleinere Bewegungen der Optik zu relevanten Brechkraftänderungen im Sinne der Presbyopiebehandlung führen.

Somit sind die theoretischen Grenzen des Axial-shift-Prinzips klar umrissen; welche Aussagen aber lassen bisherige klinische Untersuchungen zur Evidenz der akkommodativen IOL zu?

Eine echte pseudophake Akkommodation ist bedingt durch eine Ziliarmuskelkontraktion.

Pseudoakkommodation dagegen ist das Phänomen der exakten Wahrnehmung von Gegenständen unterschiedlicher Entfernung, ohne Fokusierung durch das Auge. Hierbei spielen Faktoren wie eine enge Pupille oder ein Astigmatismus myopicus simplex eine Rolle. Das Phänomen der Pseudoakkommodation wird sowohl in phaken, pseudophaken als auch in aphaken Augen beobachtet [4, 11, 19, 25].

Um die Axial-shift-Intraokularlinsen bewerten zu können, muss der Akkommodationserfolg objektiv gemessen werden. Voraussetzung ist, dass eine ausreichende Lageänderung der IOL entsprechend der Theorie stattfindet. Möglichkeiten der Quantifizierung der echten, pseudophaken Akkommodation unter Ausschluss pseudoakkommodativer Phänomene bestehen in der Messung der objektiven Refraktionsänderung und der Vorderkammertiefenänderung während der Akkommodation.

Die Human Optics 1CU könnte entsprechend ihrer technischen Daten (Angaben des Herstellers) eine Verschiebung im Auge von max. 1 mm erreichen, was einer Änderung der Brillenkorrektur von 1,3 Dioptrien entspricht. Tatsächlich zeigen eigene Untersuchungen eine mittlere Anteriorverschiebung der 1CU von nur 0,32 mm und maximal von 0,9 mm [22]. Die mit dem Hartinger-

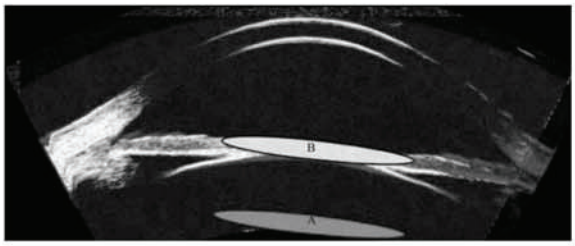

Abb. **1** Schema der notwendigen Lageveränderung von akkommodativen Kunstlinsen im Kapselsack des menschlichen Auges (VHF Ultrasound Arcscan Systems Artemis2, menschliches Auge, 36 Jahre). Für eine Scheitelbrechwertänderung von 2,9 Dioptrien müsste sich eine 20-dpt-Kunstlinse um 2,2 mm nach anterior bewegen. Die Kunstlinse A schematisiert die normale Lage im Kapselsack. Bei einer Verschiebung von 2,2 mm würde sie sich in der Position der Kunstlinse B, also vor der Pupillarebene, befinden.

Koinzidenzrefraktometer gemessenen Akkommodationsamplituden (im Mittel 0,48 Dioptrien) entsprechen nach dem Gullstrand-Modell diesen Werten [22]. In der gleichen Größenordnung liegen die Ergebnisse der untersuchten Patienten mit implantierter AT45-Crystalens mit einer mittleren Vorderkammerabflachung von 0,2 mm und einer mittleren Akkommodationsamplitude von 0,45 dpt (Abb. **2** und **3**). Ultraschallbiomikroskopische Untersuchungen unterstützen diese gemessenen Parameter [23], da bei der Human Optics 1CU eine durchschnittliche Änderung der Haptikanwinkelung von nur 7,5° (max. 10°) unter pilokarpininduzierter Ziliarmuskelkontraktion gemessen wurde. Für die vom Hersteller angegebene maximale Anteriorverschiebung der Optik um ca. 1 mm wäre eine Änderung der Haptikanwinkelung von 30° notwendig. Die AT 45 Crystalens zeigte ebenfalls nur eine unzureichende Änderung der Haptikanwinkelung von durchschnittlich 4,2° (max. 7°) (Abb. **4** und **5**).

Ergebnisse in gleichen Größenordnungen zeigen die Arbeiten von Findl u. Mitarb., welche durchschnittliche Anteriorbewegungen der akkommodativen Intraokularlinsen (Morcher BioComFold, Human Optics 1CU, AT45-Crystalens) mithilfe der Partiellen Kohärenz-Interferometrie ermittelten und die daraus resultierenden Akkommodationsamplituden errechneten. Die AT45 zeigte eine kleine, jedoch nicht signifikante Rückwärtsbewegung, die 1CU eine mediane Anteriorbewegung von 314 µm unter pilokarpininduzierter Ziliarmuskelkontraktion. Die erreichten Akkommodationsamplituden betrugen durchschnittlich weniger als 0,5 dpt. Die Ergebnisse der Patienten mit akkommodativen IOL unterschieden sich nicht von denen der Kontrollgruppen mit herkömmlichen Plattenhaptiklinsen [5–8].

Wie auch in Untersuchungen von Kammann [12] benötigten unsere Patienten nach Implantation einer 1CU oder AT45 alle eine zusätzliche Nahkorrektur im Mittel von 2,7 bzw. 2,75 Dioptrien, mindestens jedoch von 2 Dioptrien. Nach eigenen Erfahrungen zeigen also die so genannten akkommodativen Intraokularlinsen einen nur unbefriedigenden Akkommodationserfolg und keine signifikanten Unterschiede gegenüber Vergleichslinsen mit konventionellem Design.

Küchle und Langenbucher hingegen fanden in Untersuchungen von Patienten mit akkommodativen Intraokularlinsen (Human Optics 1CU) mittlere Akkommodationsamplituden von 0,98 Dioptrien und eine im Vergleich zu einer Kontrollgruppe größere Vorderkammertiefenänderung [14–16]. Diese Ergebnisse können durch eigene Untersuchungen nicht bestätigt werden. Die in den USA für die Zulassung als „akkommodative Kunstlinse" zugrunde gelegten Akkommodationsbreiten sind in europäischen Untersuchungen bisher ebenfalls nicht nachvollziehbar.

Aber auch die von Küchle und Langenbucher ermittelten Akkommodationsamplituden nach Implantation einer Human Optics 1CU können die Lesebrille allenfalls abschwächen, jedoch nicht ersetzen.

Schließlich bleibt die Frage zu beantworten: Wie sind die akkommodativen Intraokularlinsen einzuordnen?

Evidenzbasierte Betrachtungen einer Therapieform fordern nicht zufällig auftretende Effekte, die in kausalem Zusammenhang mit der durchgeführten Intervention stehen. Anforderungen an akkommodative Intraokularlinsen nach dem Axial-shift-Prinzip müssen also lauten:

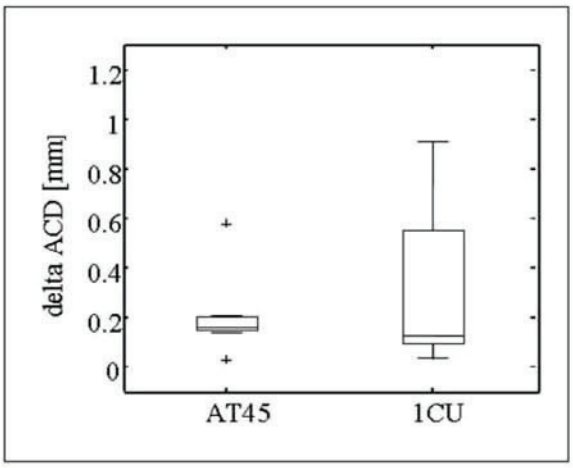

Abb. **2** Median der Vorderkammertiefenänderung nach medikamentöser Ziliarmuskelstimulation, 4 Wochen nach Implantation einer akkommodativen Intraokularlinse (1CU bzw. AT45).

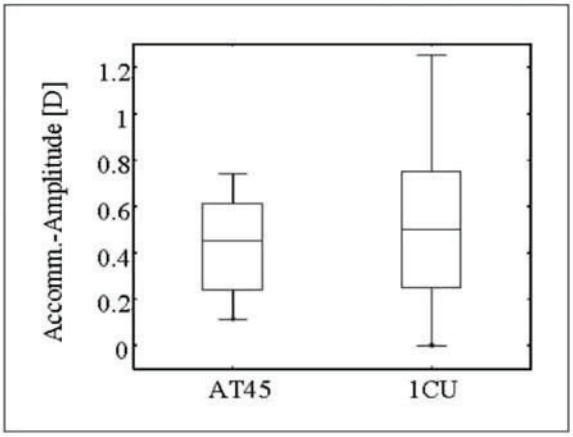

Abb. **3** Median der Akkommodationsamplitude nach medikamentöser Ziliarmuskelstimulation 4 Wochen nach Implantation einer akkommodativen Intraokularlinse (1CU bzw. AT45).

Vorderkammertiefenänderung und Akkommodationserfolg während der Akkommodation müssen objektiv messbar sein und es muss der Vergleich mit etablierten Behandlungsmethoden erfolgen.

Selbst wenn die zum Erreichen des Ziels notwendige Lageveränderung mit den zurzeit verfügbaren Linsentypen noch nicht erreicht werden kann, ist zumindest zu fordern, dass auch bei Einzelfallbetrachtungen die Vorderkammertiefenänderung mit dem Akkommodationserfolg korreliert [3]. Alle weiteren Betrachtungen, die nicht die Linsenverlagerung als Bewertungskriterium nutzen, erlauben keine Aussage über die Evidenz des Axial-Shift-Prinzips.

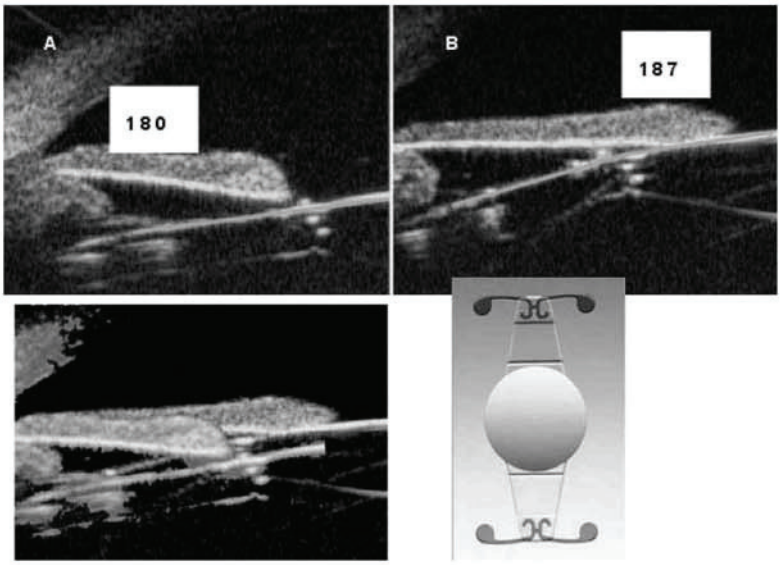

Abb. **4** Bestimmung der Änderung der Haptikanwinkelung (Winkel zwischen IOL-Optik und Haptik) nach medikamentöser Stimulation der Ziliarmuskelkontraktion durch UBM-Untersuchungen am Beispiel der AT 45 Crystalens. Die Änderung der Haptikanwinkelung der 1CU nach Pilocarpin-Gabe (rechts oben) im Vergleich zur Situation unter Cyclopentolat-Beeinflussung (links oben) beträgt in diesem Fall 7°. Unten sind die UBM-Schnitte nach Pilocarpingabe und unter Cyclopentolat übereinander gelegt.

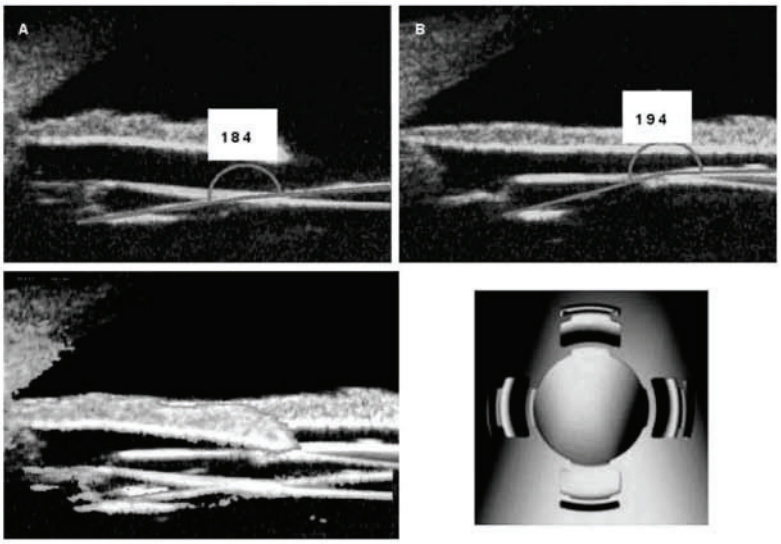

Abb. **5** Bestimmung der Änderung der Haptikanwinkelung (Winkel zwischen IOL-Optik und Haptik) nach medikamentöser Stimulation der Ziliarmuskelkontraktion durch UBM-Untersuchungen am Beispiel der Human optics 1CU. Die Änderung der Haptikanwinkelung der 1CU nach Pilocarpin-Gabe (rechts oben) im Vergleich zur Situation unter Cyclopentolat-Beeinflussung (links oben) beträgt in diesem Fall 10°. Unten sind die UBM-Schnitte nach Pilocarpingabe und unter Cyclopentolat übereinander gelegt.

Unter Berücksichtigung dieser Anforderungen zeigen die so genannten akkommodativen IOL bisher nur einen unzureichenden Akkommodationserfolg und der Beweis der Funktionsfähigkeit des Axial-shift-Prinzips steht noch aus.

Weiterhin stehen die von einigen Arbeitsgruppen und auch in eigenen Untersuchungen beobachteten Komplikationen nach Implantation einiger dieser Linsen bei ungelöstem Nachstarproblem (Haptikabknickungen und Verkippungen der Optik) in keinem Verhältnis zu den nur geringen oder fehlenden Akkommodationserfolgen [18] (Abb. **6**).

Wenn Evidenz einer Therapie bedeutet, dass ein Therapieerfolg nicht zufällig auftritt, sondern in kausalem Zusammenhang zur durchgeführten Intervention steht und außerdem der Patient,

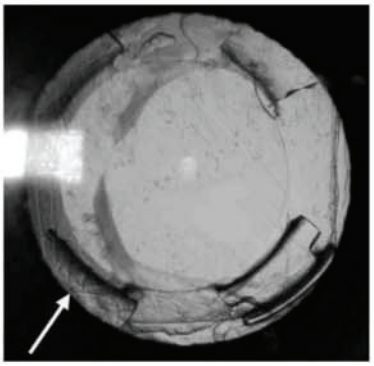

Abb. **6** Spaltlampenfoto 2 Jahre nach Implantation einer akkommodativen IOL (1CU); durch fibrotischen Nachstar bedingte Abknickungen der gekerbten Haptiken nach anterior sichtbar (Pfeil).

das angestrebte Ziel und alternative Behandlungsmöglichkeiten in die Betrachtung einbezogen werden, fehlt bisher die Evidenz der Wirksamkeit des Axial-Shift-Prinzips.

Literatur

[1] Allen ED, Burton RL, Webber SK et al. Comparison of a diffractive and a multifocal intraocular lens. J Cataract Refract Surg 1996; 22: 446 – 451
[2] Bauerberg JM. Centered vs. Inferior off-center ablation to correct hyperopia and presbyopia. J Refract Surg 1999; 15: 66 – 69
[3] Haigis W, Reese S, Jacob C et al. Messung pharmakologisch induzierter Positionsänderungen der Human optics 1CU-Linse. Kongressband DGII, 2004
[4] Elder MJ, Murphy C, Sanderson GF. Apparent accommodation and depth of field in pseudophakia. J Cataract Refract Surg 1996; 22: 615 – 619
[5] Findl O. IOL Movement induced by ciliary muscle function. In: Guthoff R, Ludwig K (eds). „Current Aspects of Human Accommodation"Kaden, 2001
[6] Findl O, Kiss B, Petternel V et al. Intraocular lens movement caused by ciliary muscle contraction. Journal Cataract Refract Surg 2003; 29: 669 – 676
[7] Findl O. Laserferometric measurement of movement of an „accommodative" intraocular lens. In: Guthoff R, Ludwig K (eds). „Current Aspects of Human Accommodation II"Kaden, 2003
[8] Findl O. The Crystalens, Proceedings of the XXII Congress of the ESCRS. Paris, 2004: 115
[9] Gray PJ, Lyall MG. Diffractive multifocal intraocular lens implants for unilateral cataracts in presbyopic patients. Br J Ophthalmol 1992; 76: 336 – 337
[10] Holladay JT. Refractive power calculations for intraocular lenses in the phakic eye. Am J Ophthalmol 1993; 116: 63 – 66
[11] Huber C. Myopic astigmatism; a substitute for accommodation in pseudophakia. Doc Ophthalmol 1981; 52: 123 – 178
[12] Kammann J, Dornbach G. Empirical results regarding accommodative lenses. In: Guthoff R, Ludwig K (eds). „Current Aspects of Human Accommodation" Kaden, 2001
[13] Keates RH, Martines E, Tennen DG et al. Small-diameter corneal inlay in presbyopic or pseudophakic patients. J Cataract Refract Surg 1995; 21: 519 – 521
[14] Küchle M et al. Implantation of a new accommodative posterior chamber intraocular lens. J Refract Surg 2002; May/June 18 (3): 208 – 216
[15] Küchle M et al. Comparison of 6-month results of implantation of the 1CU accommodative intraocular lenses. Ophthalmology 2004; 111: 318 – 324
[16] Langenbucher A, Hubera S, Nguyen NX et al. Measurement of accommodation after implantation of an accommodating posterior chamber intraocular lens. J Cataract Refract Surg 2003; 29: 677 – 685
[17] Mathews S. Scleral expansion surgery does not restore accommodation in human presbyopia. Ophthalmology 1999; 106: 873 – 877
[18] Menapace R. Kapselsackverhalten und Nachstar bei akkommodativen IOLs. Klin Monatsbl Augenheilkd 2004; 221 (Suppl 1): S39
[19] Nakazawa M, Ohtsuki K. Apparent accommodation in pseudophakic eyes after implantation of posterior chamber intraocular lenses. Am J Ophthalmol 1983; 96: 435 – 438
[20] Nowak MR, Jakobi KW. Diffraktive multifocal Intraocular lensn. Diffraktive Multifocal-Intraokularlinsen. Eine prospektive klinische Studie. Klin Monatsbl Augenheilk 1990; 196: 43 – 47
[21] Sackett D, Rosenberg WMC, Muir Gray JA et al. Evidence based medicine: what it is and what it isn't. British Medical Journal 1997; 312: 71 – 72
[22] Schneider H, Stachs O, Göbel K et al. Changes of the accommodative amplitude and the anterior chamber depth after implantation of an accommodative IOL. Graefes Arch Clin Exp Ophthalmol 2005: zur Publikation akzeptiert.
[23] Stachs O, Schneider H, Guthoff RF. Potentially accommodating IOL – an in vitro and in vivo study using 3D high frequence ultrasound. J Refract Surg 2005; 21(1): 37 – 45
[24] Steinert RF, Aker BL, Trentacost DJ et al. A prospective comparative study of the Amo Array zonal-progressive multifokal silicone intraocular lens and monofocal intraocular lens. Ophthalmology 1999; 106: 1243 – 1255
[25] Verzella F, Calossi A. Multifocal effect of against-the-rule myopic astigmatism in pseudophakic eyes. Refract Corneal Surg 1993; 9: 58 – 61
[26] Vinciguerra P, Nizzola GM, Bailo G et al. Excimer laser photorefractive keratectomy for presbyopia: 224-month foolow-up in three eyes. J Refract Surg 1998; 14: 31 – 37

Dr. med. Hanka Schneider

Universitäts-Augenklinik
Deberaner Straße 140
18057 Rostock

Klin Monatsbl Augenheilkd 2004; 221: 357 – 360 · DOI 10.1055/s-2005-858156

Pharmacological-induced Haptic Changes and the Accommodative Performance in Patients With the AT-45 Accommodative IOL

Oliver Stachs, PhD; Hanka Schneider, MD; Ria Beck, MD; Rudolf Guthoff, MD

ABSTRACT

PURPOSE: To investigate the accommodative performance of the AT-45 (eyeonics Inc, Aliso Viejo, Calif) using three-dimensional ultrasound biomicroscopy.

METHODS: The AT-45 haptic region was visualized in vivo 1 month after surgery in four patients using an in-house developed three-dimensional ultrasound biomicroscope. Haptic changes, axial shift, and accommodation amplitude were determined under pharmacologically induced accommodation.

RESULTS: The angulation, depending on the accommodation state, could be distinguished and analyzed. In vivo a mean change in haptic angulation of 3.3±3.3° (range: 0° to 7°) and a mean forward shift of 0.13±0.08 mm (range: 0.05 to 0.2 mm) were observed for the AT-45 using pharmacologically induced accommodation. A mean accommodative amplitude of 0.44±0.24 diopters (D) (range: 0.25 to 0.75 D) was found using a Hartinger coincidence refractometer.

CONCLUSIONS: Minimal angulation changes and axial movements of the AT-45 have been demonstrated using pharmacological stimulation and objective measurement methods. The mechanical performance of the AT-45 in these eyes does not appear to provide the range of accommodation necessary for close work. [*J Refract Surg*. 2006;22:145-150.]

Accommodation is the ability of the eye to project a focused image, positioned at varying distances from near to far, on to the retina. The physiological decrease in accommodation with age (presbyopia) is caused by a decrease in the elasticity of the crystalline lens, an equatorial diameter change of the lens, alterations in the elastic properties of Bruch's membrane, and atrophy of the ciliary muscle.[1] After cataract surgery and because the implanted intraocular lens (IOL) optic can not change its position and/or shape, pseudophakic patients cannot accommodate. However, as a result of a number of factors (eg, pupil size, myopic astigmatism, etc), some patients may have an increased depth of focus, called pseudoaccommodation.

To date, lens-based pseudophakic accommodation has only been achieved by multifocal IOLs and by an axial shift of the IOL optic. This shift of the IOL optic occurs when the ciliary muscle contracts and induces a change in haptic configuration. Recently, several attempts using different designs[2-7] have been made to achieve pseudophakic accommodation. The basic approach to achieve potentially accommodating IOLs is to allow an axial displacement of the IOL optic.

Quantification of axial IOL movements induced by accommodation in humans has been performed with ultrasound[3,8-10] and with the highest resolution by using dual-beam partial coherence interferometry.[11-14] Using coherence interferometry, the measurements show a mean 0.314-mm anterior movement for the 1CU[15] (HumanOptics AG, Erlangen, Germany) and a minimal posterior movement for the AT-45 (eyeonics Inc, Aliso Viejo, Calif).[16-18]

In terms of understanding the principle of so-called accommodative IOLs, high frequency ultrasound[19] is the only tool available to visualize the IOL haptic geometry hidden behind the iris diaphragm. Unfortunately, high frequency so-

From the Eye Clinic of the University of Rostock, Rostock, Germany.

The authors have no proprietary interest in the materials presented herein.

Correspondence: Oliver Stachs, PhD, Universität Rostock, Medizinische Fakultät, Augenklinik, Doberaner Str. 140, 18055 Rostock, Germany. Tel: 49 381 4948565; Fax: 49 381 4948502; E-mail: oliver.stachs@med.uni-rostock.de

Received: August 13, 2004

Accepted: March 30, 2005

nographic image analysis can be difficult if information from only one plane is available. The usefulness of three-dimensional ultrasound biomicroscopy for the evaluation of haptic geometry changes for the 1CU has been demonstrated in vivo and in vitro.[20] For the AT-45 accommodative IOL, only in vitro investigations have been reported previously.[20] This article presents the three-dimensional ultrasound evaluation of pharmacological-induced haptic changes and accommodative response in patients with the AT-45 implant.

PATIENTS AND METHODS

This study was performed following the tenets of the Helsinki agreement. Written informed consent was obtained from all patients after the nature and possible consequences of the study were explained.

The IOL studied (AT-45) and its main properties have been described in detail previously.[20] The patients returned for follow-up at 4 weeks postoperatively.

The objective refractometry was performed using a autorefractometer (Canon RK3; Canon, Tokyo, Japan). Distance visual acuity was determined using a standard Snellen projector system (Optostar IR-2000; Schwind, Kleinostheim, Germany). Near reading vision was determined using Birkhäuser reading charts (Scalae Typographicae Birkhaeuseri, Birkhäuser Verlag, Germany) and an illumination of 70 cd/m^2. After determining best and uncorrected far vision, near vision without additional near/distance correction and with the addition of +1.0, +2.0, +3.0, and +3.5 sphere, was determined. Visual acuity values were expressed in decimal values and logMAR.

An in-house three-dimensional ultrasound biomicroscope (UBM) was used to evaluate IOL placement and haptic configuration in patients with the AT-45 implant. The principles of the UBM[19] and three-dimensional UBM[21-24] have been described in detail elsewhere. For this study, three-dimensional imaging was accomplished using a standard UBM (model 840; Humphrey Instruments, Carl Zeiss, Jena, Germany) extended such that precise movement of the B-scan plane in the z-direction could be obtained. In this arrangement, three-dimensional data sets consisting of parallel B-scans spaced at defined distances could be obtained. The three-dimensional reconstruction was performed using Amira software (TGS, San Diego, Calif). Building three-dimensional constructs allows outlining of anatomical structures in space and can be used for oblique reconstructions. In addition, the software package ImageJ (National Institutes of Health, Bethesda, Md) and MatLab (The MathWorks Inc, Natick, Mass) were used for the evaluation of haptic configurations and axial changes in IOL position.

Three-dimensional UBM measurements were carried out after pharmacologically induced accommodation (two drops of pilocarpine 2% administrated in 5-minute intervals) or disaccommodation (two drops of cyclopentolate 1% administrated in 5-minute intervals) on 2 consecutive days 4 weeks after surgery. The ciliary body regions of four patients were scanned 30 minutes after pharmacological treatment. The three-dimensional volumes were then used to identify the tangential plane of the IOL haptic; an oblique reconstruction is possible to perform the biometric measurements. As in an earlier study of angulation determination,[20] the center of rotation was placed at the fulcrum and the angle between the IOL optic and haptic was measured using the anterior IOL interface. An angle of 157° was used as baseline and set to zero. Positive values in angulation represent an anterior vaulting, and negative values represent a posterior vaulting. Changes in haptic angulation and the IOL shift were analyzed (mean±standard deviation) using five B-scans for each accommodative state and for all patients. Positive values for change in anterior chamber depth represent a forward shift of the IOL. Additionally, the accommodative amplitude was measured objectively using a Hartinger coincidence refractometer when accommodation was stimulated.

RESULTS

The three-dimensional reconstruction and the interactive selection of sections across the haptic as well as a photographic image are shown in Figure 1. In this example, the optic and the haptic can be differentiated. The echo patterns are caused by the polyimide construction of the plate haptic. The posterior lens surface can be imaged, whereas this interface cannot always be seen under different scanning directions. The point # acts as the fulcrum and is used as the center of rotation for angulation determination.

The echo characteristics of the AT-45 were used to describe the in vivo situation in four patients with accommodative implants 4 weeks after surgery. Figure 1 shows the haptic region of a 71-year-old woman after pilocarpine instillation. A haptic angulation of 33° (uncorrected 190°) compared with the relaxed IOL haptic (0°, uncorrected 157°) is seen in this case.

For a descriptive visualization of changes in angulation depending on the accommodation state, corresponding UBM sections were superimposed. Figure 2 demonstrates the situation under cyclopentolate (red) superimposed on a UBM section under pilocarpine stimulation (grey) for patients 1 and 2. Pilocarpine induced an additional angulation change in patient 1 (Fig 2A) and no changes for patient 2 (Fig 2B) compared

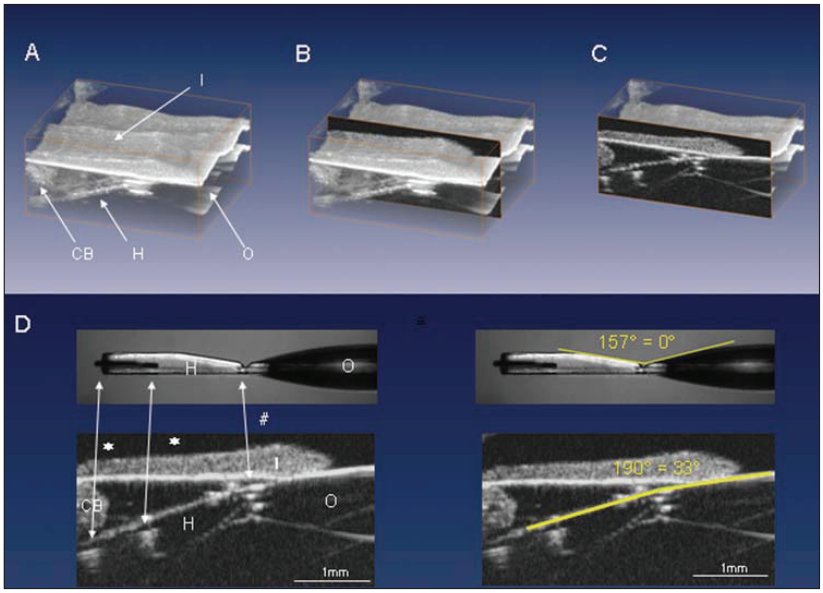

Figure 1. A-C) Three-dimensional reconstruction and **D)** image analysis of the AT-45 haptic region (patient 1: 71-year-old woman, 4 weeks after surgery, pilocarpine-induced accommodation). The fulcrum is marked (#). The optic (O) and haptic (H) are well differentiated, whereas the echo pattern (*) is caused by the polyimide construction of the AT-45 plate haptic. The 157° angle for the relaxed haptic configuration was set to zero for angulation change determination. A haptic angulation of 33° (uncorrected 190°) compared with the relaxed IOL haptic is observed. O = optic, H = haptic, * = polyimide construction, # = fulcrum, I = iris, CB = ciliary body

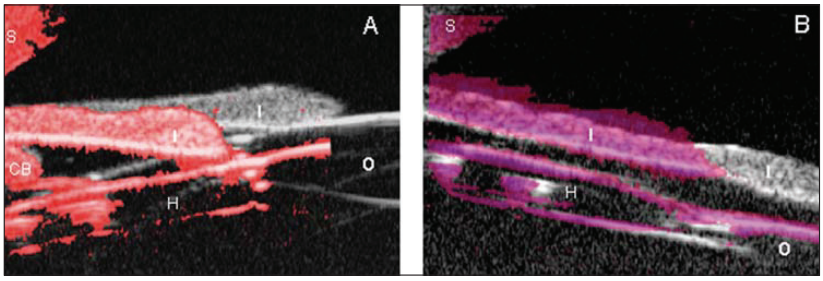

Figure 2. Superimposed UBM sections showing the effect of cyclopentolate and pilocarpine in two patients—**A)** patient 1, 71-year-old woman and **B)** patient 2, 77-year-old woman. The disaccommodated state after cyclopentolate treatment (red) and under pilocarpine stimulation (grey) is shown. S = sclera, I = iris, CB = ciliary body, H = haptic, O = optic

with the configuration after cyclopentolate treatment. The pilocarpine instillation causes a forward shift in patient 1 and no changes in patient 2.

The results of the four eyes are summarized in Figure 3. Under cyclopentolate, a haptic angulation between 10° and 26° was found. A mean change in haptic angulation of 3.3±3.3° (range: 0° to 7°) and a mean forward shift of 0.13 mm (range: 0.06 to 0.2 mm) were observed under pilocarpine treatment. An accommodative amplitude of 0.44±0.24 diopters (D) (range: 0.25 to 0.75 D) was found in the four eyes using a Hartinger coincidence refractometer. Postoperative 4-week follow-up is provided in the Table.

DISCUSSION

To date, high frequency ultrasound is the only tool available to visualize the IOL haptic geometry hidden behind the iris diaphragm. The biometric analysis of these images becomes difficult, if information from only one B-scan section is available. Undefined tilting effects may influence biometric measurements concerning the analysis of haptic configurations. Three-dimensional ultrasound biomicroscopy in combination with volume rendering software is a useful tool for examining lens position and haptic configurations especially for the evaluation of accommodating IOLs. The possibilities of the 1CU and AT-45 for in vitro use have been published previously.[20]

The AT-45 is a single-piece IOL with an overall length of 10.5 mm. The model has a 4.5-mm square edge optic that is joined with a hinge to silicone plate haptics. The optic is made from silicon elastomer, a third-generation silicone with ultraviolet-blocking properties. The lens has flexible hinged plate haptics with two polyimide loop extensions at the end of each plate. These components are well differentiated by high frequency ultrasound (see Fig 1). In theory, the hinged haptics are designed to allow the lens optic to move in an axial direction during accommodation.

Theoretically, the lens was designed to remain in a

TABLE

Postoperative 4-week Follow-up of Four Eyes that Underwent Implantation of an AT-45 IOL

			Far Vision (decimal/logMAR)				Near Vision (decimal/logMAR)					
Patient No.	Age (y)	IOL Power	Preop BSCA	Postop UCVA	Postop BSCVA	Rfx	Postop*	Postop BSCVA in 35 cm	Near Addition (D)	ACD (mm)	ΔACD (mm)	Accommodative Amplitude (D)†
1	71	24	0.5/0.3	0.6/0.22	0.8/0.1	−1	0.2/0.7	0.9/0.05	3.00	4.01	0.20	0.5
2	77	23	0.1/1.0	0.7/0.16	0.8/0.1	0.5	0.3/0.53	0.8/0.1	2.75	4.57	0.06	0.25
3	70	23.5	0.5/0.3	0.7/0.16	1/0	−1	0.2/0.7	1/0	2.75	4.68	0.20	0.25
4	62	23	0.6/0.22	0.8/0.1	1.25/−0.1	−0.5	0.3/0.53	1.25/-0.1	2.25	4.93	0.05	0.75

BSCVA = best spectacle-corrected visual acuity, UCVA = uncorrected visual acuity, Rfx = refraction, ACD = anterior chamber depth, ΔACD = change in anterior chamber depth
**With far distance correction.*
†After drug-induced stimulation.

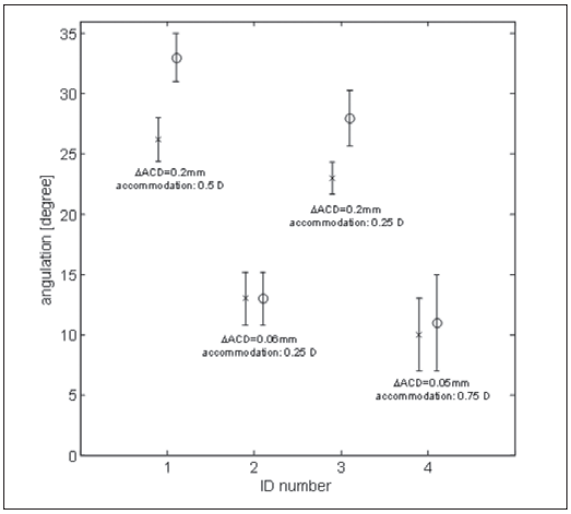

Figure 3. Change in angulation (°) and anterior chamber depth (ACD [mm]) as well as accommodation amplitude (D) in all patients showing the effect of cyclopentolate (cross) and pilocarpine (circle). Positive values for change in anterior chamber depth represent a forward shift of the IOL. Positive values in angulation represent an anterior vaulting.

posteriorly vaulted position to optimize the haptic flexing characteristics. Within the scope of our investigations, we have not found this vaulting posteriorly. We have found the lens relatively centered in the bag in the axial direction (patients 2 and 4) with a distinct vaulting anteriorly (patients 1 and 3). In disaccommodation, a haptic angulation between 10° and 26° is observed (see Fig 3). The strong anterior vaulting seen in patient 1 (see Figs 1 and 2A) may be caused by capsular bag shrinkage or by an undersized capsular bag.

Subjective measurement of accommodation amplitudes is due to the capability and motivation of volunteers to accommodate to various kinds of stimuli.[25] Pilocarpine application is an objective way of stimulating accommodation as it requires no participation from the patient and was used for this study. This is a recommended and commonly used method to stimulate accommodation.[11-14,16,17,26,27] However, the role of pilocarpine should be discussed critically in this context. Abramson et al[27] measured human accommodation and determined a greater increase in axial lens diameter after pilocarpine application than is possible with stimulus-driven accommodation. Thus, topical application of pilocarpine may produce an overstimulation of the ciliary muscle. Findl[17] and Köppl et al[28] found a difference in lens movement between pilocarpine-induced and visual stimulus-driven ciliary muscle contraction: pilocarpine acts "physiologically" in young phakics and as a super stimulus in presbyopic phakics and pseudophakes. Therefore, pilocarpine instillation can be used for a biometrical evaluation of potential accommodative IOLs although the accommodative response may be overestimated with pilocarpine.

For the AT-45, the proposed mechanism is that accommodation restoration occurs through the ciliary muscle activity. The manufacturer has developed the lens to provide good vision at all distances by moving backward and forward along the optical axis of the eye in response to pressure changes in the vitreous and anterior chamber. In the cases studied, pilocarpine induced an angulation change between 0° and 7° (mean 3.3±3.3°) compared with the situation under cyclopentolate. The angulation change causes a change in anterior chamber depth between 0.06 and 0.2 mm (mean 0.13±0.08 mm).

Using Gullstrand's eye model and a 20.0-D IOL placed in the bag, the observed maximal 0.2-mm forward movement results in a refraction change <0.4 D, depending on the exact IOL position.[29] The cases studied showed a maximal accommodation response of mean 0.44±0.24 D (range: 0.25 to 0.75 D) measured by a Hartinger coincidence refractometer. This value is slightly larger than the calculated values using Gullstrand's eye model, possibly caused by individual pseudoaccomodative effects (eg, pupil size, myopic astigmatism, etc).

Pilocarpine-induced ciliary muscle contraction caused a slight change in haptic angulation and an anterior shift of the AT-45 in these four eyes. This slight change in angulation and the anterior shift resulted in an accommodative amplitude between 0.25 and 0.75 D. Therefore, in these four eyes, the AT-45 did not seem to provide the range of accommodation necessary for close work. We expect that capsular fibrosis and capsular bag shrinkage result in a hardening of the haptic and optic in the capsule, resulting in further decrease of the accommodative performance later postoperatively.

Our findings in accommodation amplitude and axial shift are larger than the objective measurements of Findl and Menapace.[16-18] Using partial coherence interferometry, Findl et al[16,17] found a small but significant backwards movement under pilocarpine without an accommodative ability for the AT-45. These results and our objective measurements in these four patients can not explain the published results[30-32] reporting excellent visual acuity with accommodative ability after AT-45 implantation.

REFERENCES

1. Kaufman PL. Accommodation and presbyopia: neuromuscular and biophysical aspects. In: Hart WM Jr, ed. *Adlers Physiology of the Eye: Clinical Application*. 9th ed. St Louis, Mo: Mosby; 1992:391-411.
2. Hara T, Hara T, Yasuda A, Yamada Y. Accommodative intraocular lens with spring action, I: design and placement in an excised animal eye. *Ophthalmic Surg*. 1990;21:128-133.
3. Hardman Lea SJ, Rubinstein MP, Snead MP, Haworth SM. Pseudophakic accommodation? A study of the stability of capsular bag supported, one piece, rigid tripod, or soft flexible implants. *Br J Ophthalmol*. 1990;74:22-25.
4. Cumming JS, Kammann J. Experience with an accommodating IOL. *J Cataract Refract Surg*. 1996;22:1001.
5. Legeais JM, Werner L, Werner L, Abenhaim A, Renard G. Pseudoaccommodation: BioComFold versus a foldable silicone intraocular lens. *J Cataract Refract Surg*. 1999;25:262-267.
6. Küchle M, Nguyen NX, Langenbucher A, Gusek-Schneider GC, Seitz B, Hanna KD. Implantation of a new accommodative posterior chamber intraocular lens. *J Refract Surg*. 2002;18:208-216.
7. Sarfarazi FM. Optical and mechanical design for human implantation of the Sarfarazi Elliptical Accommodation IOL. Proceedings of the American Society of Cataract and Refractive Surgery annual meeting; April 12-16, 2003; San Francisco, Calif. Abstract #738.
8. Nakazawa M, Ohtsuki K. Apparent accommodation pseudophakic eyes after implantation of posterior chamber intraocular lenses: optical analysis. *Invest Ophthalmol Vis Sci*. 1984;25:1458-1460.
9. Ravalico G, Baccara F. Apparent accommodation in pseudophakic eyes. *Acta Ophthalmol*. 1990;68:604-606.
10. Gandolfi SA, Marchini G, Tosi R, Mora P, Pedrotti E, Sartori P, Manzotti F. UBM changes during accommodation in eyes implanted with Crystalens AT45 and 1CU IOL. A pilot study. *Invest Ophthalmol Vis Sci*. 2003;44:E-Abstract 252.
11. Findl O, Drexler W, Menapace R, Bobr B, Bittermann S, Vass C, Rainer G, Hitzenberger CK, Fercher AF. Accurate determination of effective lens position and lens-capsule distance with 4 intraocular lenses. *J Cataract Refract Surg*. 1998;24:1094-1098.
12. Findl O, Kriechbaum K, Köppl C, Menapace R, Drexler W. Laser interferometric measurements of IOL movement with accommodating IOLs. Proceedings of the American Society of Cataract and Refractive Surgery annual meeting; April 12-16, 2003; San Francisco, Calif. Abstract #94.
13. Findl O, Menapace R, Kriechbaum K, Koeppel C, Drexler W. Laser interferometric measurements of movement of an "accommodating" IOL. In: Guthoff R, Ludwig K, eds. *Current Aspects in Accommodation II*. Heidelberg, Germany: Kaden; 2003:211-221.
14. Findl O, Kiss B, Petternel V, Menapace R, Georgopoulos M, Rainer G, Drexler W. Intraocular lens movement caused by ciliary muscle contraction. *J Cataract Refract Surg*. 2003;29:669-676.
15. Findl O, Kriechbaum K, Menapace R, Koeppl C, Sacu S, Wirtitsch M, Buehl W, Drexler W. Laserinterferometric assessment of pilocarpine-induced movement of an accommodating intraocular lens: a randomized trial. *Ophthalmology*. 2004;111:1515-1521.
16. Findl O, Köppel CM, Kriechbaum K, Drexler W. Pilocarpine and stimulus-driven accommodation in phakic and pseudophakic patients with accommodating IOLs. Proceedings of the American Society of Cataract and Refractive Surgery annual meeting; May 1-5, 2004; San Diego, Calif. Abstract #94.
17. Findl O. "Akkommodative" IOL: funktionelle ergebnisse. *Klin Monatsbl Augenheilk*. 2004;221(Suppl):S36.
18. Menapace R. Kapselsackverhalten und nachstar bei akkommodativen IOLs. *Klin Monatsbl Augenheilk*. 2004;221(Suppl):S36.
19. Pavlin CJ, Foster FS. *Ultrasound Biomicroscopy of the Eye*. New York, NY: Springer; 1995.
20. Stachs O, Schneider H, Stave J, Guthoff R. Potentially accommodating intraocular lenses—an in vitro and in vivo study using three-dimensional high-frequency ultrasound. *J Refract Surg*. 2005;21:37-45.
21. Iezzi R, Rosen RB, Tello C, Liebmann J, Walsh JB, Ritch R. Personal computer-based 3-dimensional ultrasound biomicroscopy of the anterior segment. *Arch Ophthalmol*. 1996;114:520-524.
22. Cusumano A, Coleman DJ, Silverman RH, Reinstein DZ, Rondeau MJ, Ursea R, Daly SM. Three dimensional ultrasound imaging. Clinical applications. *Ophthalmology*. 1998;105:300-306.
23. Silverman RH, Rondeau MJ, Lizzi FL, Coleman DJ. Three-dimensional high frequency ultrasonic parameter imaging of anterior segment pathology. *Ophthalmology*. 1995;102:837-843.
24. Stachs O, Martin H, Kirchhoff A, Stave J, Terwee T, Guthoff R. Monitoring accommodative ciliary muscle function using three-dimensional ultrasound. *Graefes Arch Clin Exp Ophthalmol*. 2002;240:906-912.
25. Wold JE, Hu A, Chen S, Glasser A. Subjective and objective measurement of human accommodative amplitude. *J Cataract Refract Surg*. 2003;29:1878-1888.
26. Kaufman PL. Scleral expansion surgery for presbyopia. *Ophthalmology*. 2001;108:2161-2162.

27. Abramson DH, Franzen LA, Coleman DJ. Pilocarpine in the presbyope. Demonstration of an effect on the anterior chamber and lens thickness. *Arch Ophthalmol*. 1973;89:100-102.

28. Köppl C, Findl O, Kriechbaum K, Dexler W. Comparison of pilocarpine-induced and stimulus-driven accommodation in phakic eyes. Proceedings of the XXI Congress of the European Society of Cataract and Refractive Surgeons; September 6-10, 2003; Munich, Germany.

29. Holladay JT. Refractive power calculations for intraocular lenses in the phakic eye. *Am J Ophthalmol*. 1993;116:63-66.

30. Cumming JS, Slade SG, Chayet A; AT-45 Study Group. Clinical evaluation of the model AT-45 silicone accommodating intraocular lens: results of feasibility and the initial phase of a Food and Drug Administration clinical trial. *Ophthalmology*. 2001;108:2005-2009.

31. Dell SJ, Slade SG. FDA Study update. One year results: Crystalens accommodating IOL. Proceedings of the American Society of Cataract and Refractive Surgery annual meeting; May 1-5, 2004; San Diego, Calif. Abstract #689.

32. Colvard DM. Crystalens accommodating IOL in management of the aging hyperopic eye. Proceedings of the American Society of Cataract and Refractive Surgery annual meeting; May 1-5, 2004; San Diego, Calif. Abstract #340.

Performance of the Crystalens

To the Editor:

The small series of four cases presented in the article by Stachs et al[1] as evidence that the Crystalens (eyeonics Inc, Aliso Viejo, Calif) does not move adequately to provide accommodation are atypical. The sweeping conclusions of the article cannot be supported by such a small series, especially when the data conflict with the findings of large, prospective, controlled multicenter studies.

As the developer of the Crystalens, I, with Jochen Kammann, evaluated seven lens designs over 8 years. All designs demonstrated anterior movement by A-scans.[2] As a consultant to eyeonics Inc, I have seen hundreds of eyes implanted with the Crystalens in many parts of the world. Through that experience, it has become clear that successful accommodation with the lens relies on good surgical technique, particularly regarding the creation of an appropriately sized capsulorrhexis. This technique is taught in our surgical training courses, which are a prerequisite for surgeons to implant the lens.

The authors' finding of anterior vaulting of the lens suggests that the eyes suffered from overly large capsulorrhexis. In my clinical experience, I have never seen the lens anteriorly vaulted when properly implanted, with good cortical cleanup and a suitable capsulorrhexis. The Crystalens depends on a posterior vault to function properly; the images in the article that show the optic up against and deforming the posterior iris surface indicate a severe anterior vault. This is a recognized complication, which can occasionally occur and can easily be treated.

To suggest that measurements of eyes with anterior vaults can be used to describe the clinical function of the lens is absurd. Had the authors entitled their article, "Diminished Movement of the Crystalens With Improper Positioning," then the article might make more sense. A Scheimpflug photograph of the Crystalens AT-45 one day postoperative shows the proper position of the lens with a posterior vault (Fig). The posterior vaulting is obvious on slit-lamp examination. This position permits anterior excursion and accommodation. Anterior vaulted lenses, such as those reported by Stachs et al, have no place to go.

The clinical trial that led to the US Food and Drug Administration (FDA) approval of the Crystalens was a prospective, multicenter, controlled study conducted under strict oversight. Results showed that the lens provided approximately 1 diopter more monocular accommodation than a standard lens and significantly outperformed the monofocal intraocular lenses at intermediate and near distances. Subsequent studies have measured Crystalens movement and accommodation using pharmacologically induced accommodation[3,4] (Burrato L, unpublished data), movement with natural accommodation (no medications) (DiChiara, unpublished data), dynamic retinoscopy,[3,4] and wavefront measurements,[5,6] and have all confirmed the FDA study findings. The lens has been implanted in >45,000 eyes and our registry data of >1500 eyes show that the post-approval results are similar to the FDA studies.

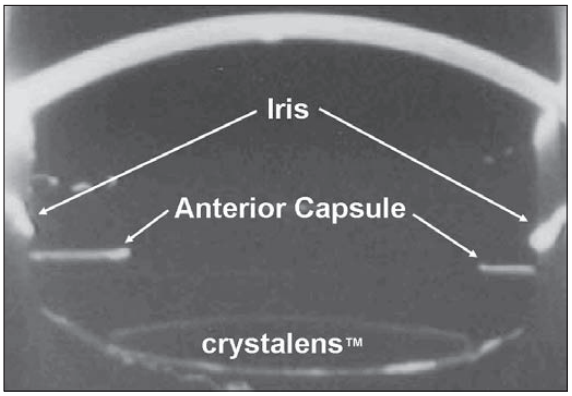

Figure. Scheimpflug photograph of the Crystalens AT-45 (eyeonics Inc, Aliso Viejo, Calif) 1 day postoperative showing the proper position of the lens with a posterior vault.

We believe the Stachs et al article reported abnormal findings in eyes with poorly managed complications. There has been one other article that reported the lens to move backward.[7] This article relied on measurements from "in-house developed" imaging, similar to Stachs et al, and relied on findings in very early cases that probably had unrecognized anterior vaults. Both articles make the mistake of generalizing about overall performance from too few cases, and both papers failed to include representative samples. This is not good science.

Forward displacement of the Crystalens probably accounts for most of the accommodation that it provides. Lens flexing ("accommodative arching") also plays a role,[8] as do the excellent optics inherent in the lens design. The current Crystalens is an early design that will certainly improve over time. It provides an attractive alternative to patients seeking good distance, intermediate, and near acuity without the loss of visual quality that occurs with multifocal lenses.

J. Stuart Cumming, MD, FACS, FRCOphth
Aliso Viejo, California

REFERENCES

1. Stachs O, Schneider H, Beck R, Guthoff R. Pharmacological-induced haptic changes and the accommodative performance in patients with the AT-45 accommodative IOL. *J Refract Surg.* 2006;22:145-150.

2. Cumming JS, Kammann J. Experience with an accommodating IOL. *J Cataract Refract Surg.* 1996;22:1001.
3. Dell SJ. Pilocarpine-induced shift of an accommodating IOL. *J Cataract Refract Surg.* 2005;31:1469-1472.
4. Macsai M, Tanouye D, Padnick-Silver L. Does the accommodating IOL really accommodate? Poster presented at: Association for Research in Vision and Ophthalmology annual meeting; May 1-5, 2005; Ft Lauderdale, Fla.
5. Waltz K. The Crystalens changes its radius of curvature. *Cataract & Refractive Surgery Today.* 2005;66-68.
6. Sloane H. Wavefront analysis of Crystalens patients: amplitude of accommodation. Eyeonics Scientific Advisory Board Meeting; February 25, 2006; Aspen, Colo.
7. Findl O, Kriechbaum K, Koppl C, Menapace R, Drexler W. Laser interferometric measurements of IOL movement with accommodating IOLs. Proceedings of the American Society of Cataract and Refractive Surgery annual meeting; April 12-16, 2003; San Francisco, Calif. Abstract #94.

Reply:

We thank Dr Cumming for his comments; however, his concerns seem more hypothetical than factual.

Cumming states that the findings of our four cases are atypical. As clearly stated in our article, the biomechanical performance (optic shift) of the Crystalens (eyeonics Inc, Aliso Viejo, Calif) in the eyes studied does not appear to provide the range of accommodation necessary for close work. This is not a generalization and not in conflict with the findings of the large, prospective, controlled multicenter studies using subjective methods for determination of the accommodation range named, but not cited, by Cumming in his letter. In this context, we discuss the difference between true accommodation and pseudoaccommodation. A forward shift of the Crystalens under accommodation is supposedly mediated by an increase in vitreous pressure as a result of a mass redistribution under ciliary muscle contraction as postulated by Coleman.[2] This lens is reported,[3] and affirmed in Cumming's letter, to result in excellent uncorrected distance and near visual acuity. However, psychophysical assessment for proof of true pseudophakic accommodation by optic shift of an accommodating intraocular lens (IOL) is problematic because it is dependent mainly on depth of focus or pseudoaccommodation. The latter are in turn influenced by numerous factors such as pupil size, astigmatism, and multifocality. The basic need for an objective method that assesses IOL shift or haptic angulation during ciliary muscle contraction is obvious. Several methods exist to measure accommodation objectively,[4] which include stimulating accommodation with trial lenses or pilocarpine and measuring the accommodative response with an objective optometer (Hartinger coincidence refractometer), partial coherence interferometry (AC-Master; Zeiss Meditec, Jena Germany), and high frequency ultrasound.

Cumming states that the findings in our study are abnormal findings in eyes with poorly managed complications. A justification of this assumption is not named. All surgeries were performed by a surgeon with long-term experience in implanting a large variety of IOL styles. The decision to provide the patients with a capsulorrhexis that ensures a small overlap between the anterior capsule and the IOL optic rim was based on proven knowledge that allowing a capsule bend to form at the sharp posterior optic edge will reduce regeneratory posterior capsule opacification. Analogous to our findings Koeppl et al[5] found eyes that showed a pronounced posterior vaulting of the IOL with a gap between the capsulorrhexis and the anterior IOL surface and other eyes showed contact between the anterior capsule and the IOL surface, including cases of partial button hole. Obviously, the reason for this variability in IOL position found in our study[1] and Koeppl et al[5] may be the variability in capsular bag diameter or inter-patient differences in capsular bag shrinkage and fibrosis. These effects are supported by the clinical findings of Jardim et al,[6] with an asymmetric vault of the Crystalens, and by Cazal et al.[7] Cazal et al reported a complication (increased astigmatism, decreased visual acuity) after AT45 implantation caused by tilting. Intraocular lens repositioning was unsuccessful because of fibrosis of the haptics and the IOL was replaced with a monofocal acrylic sulcus-fixated IOL.

Cumming cites a letter he coauthored with Kammann that all Crystalens designs show anterior optic movement.[8] But Kammann[9] also noted that he did not achieve the good results (Nieden 4 or better) found in the US Food and Drug Administration (FDA) study. Cumming criticizes a second study,[10] which used partial coherence interferometry. These results were published in the peer-reviewed literature[5] and show an objectively measured backward movement of the Crystalens during accommodation. The method used, partial coherence interferometry, is not an imaging method as stated by Cumming but a high precision method for anterior segment biometry[11,12] incorporated in a commercially available device (AC-Master). The authors have done nothing more than measure the position of the IOL optic in different accommodative states. The same principle was used in our recent articles[1,15] to check the postulated angulation of the IOL haptics by high frequency ultrasound (UBM 840, Zeiss-Humphrey). To identify the position as accurately as possible, a previously evaluated[13-18] method for three-dimensional scanning was used.

In conclusion, we agree with Cumming that the Crystalens is an early design. It certainly needs im-

provement over time. We disagree with his comment about bad science. Cumming cites presentations and unpublished data and no peer-reviewed literature to substantiate his criticism. The acceptance of scientific ideas should be based on a process of publication and peer review. Cumming ends with expressing his feelings that this lens provides an attractive alternative to patients compared with multifocal lenses, who also are seeking good near visual acuity. This is remarkable, because the FDA mentions that the lens[19] is intended for near vision without spectacles, but has approved the lens for labeling of having an accommodation amplitude of approximately 1.0 diopter. And that is definitively not enough for good near visual acuity.

We agree with the comment by Findl and Menapace in their response[20] to the letter by Dell regarding their article about the pilocarpine-induced shift of the Crystalens[5]: "Development of a novel IOL should be done in a step-by-step manner, however, and with accumulation of real evidence derived from randomized controlled trails, which the company have yet to publish." Additionally, objective measurement methods should be used to separate accommodation from pseudoaccommodation.

Sir Karl Popper (1902-1994): "Some genuinely testable theories, when found to be false, are still upheld by their admirers—for example by introducing ad hoc some auxiliary assumption, or by reinterpreting the theory ad hoc in such a way that it escapes refutation. Such a procedure is always possible, but it rescues the theory from refutation only at the price of destroying, or at least lowering, its scientific status."[21]

Oliver Stachs, PhD
Rudolf Guthoff, MD
Rostock, Germany

REFERENCES

1. Stachs O, Schneider H, Beck R, Guthoff R. Pharmacological-induced haptic changes and the accommodative performance in patients with the AT-45 accommodative IOL. *J Refract Surg*. 2006;22:145-150.
2. Coleman DJ. On the hydraulic suspension theory of accommodation. *Trans Am Ophthalmol Soc*. 1986;84:846-868.
3. Cumming JS, Slade SG, Chayet A, AT-45 Study Group. Clinical evaluation of the model AT-45 silicone accommodating intraocular lens: results of feasibility and the initial phase of a Food and Drug Administration clinical trial. *Ophthalmology*. 2001;108:2005-2009.
4. Wold JE, Hu A, Chen S, Glasser A. Subjective and objective measurement of human accommodative amplitude. *J Cataract Refract Surg*. 2003;29:1878-1888.
5. Koeppl C, Findl O, Menapace R, Kriechbaum K, Wirtitsch M, Buehl W, Sacu S, Drexler W. Pilocarpine-induced shift of an accommodating intraocular lens: AT-45 Crystalens. *J Cataract Refract Surg*. 2005;31:1290-12997.
6. Jardim D, Soloway B, Starr C. Asymmetric vault of an accommodating intraocular lens. *J Cataract Refract Surg*. 2006;32:347-350.
7. Cazal J, Lavin-Dapena C, Marin J, Verges C. Accommodative intraocular lens tilting. *Am J Ophthalmol*. 2005;140:341-344.
8. Cumming JS, Kammann J. Experience with an accommodating IOL. *J Cataract Refract Surg*. 1996;22:1001.
9. Kammann J, Dornbach G. Empirical results regarding accommodative lenses. In: Guthoff R, Ludwig K, eds. *Current Aspects in Accommodation*. Heidelberg, Germany: Kaden Verlag; 2001:163-170.
10. Findl O, Kriechbaum K, Koppl C, Menapace R, Drexler W. Laser interferometric measurements of IOL movement with accommodating IOLs. Proceedings of the American Society of Cataract and Refractive Surgery annual meeting; April 12-16, 2003; San Francisco, Calif. Abstract #94.
11. Drexler W, Baumgartner A, Findl O, Hitzenberger CK, Sattmann H, Fercher AF. Submicrometer precision biometry of the anterior segment of the human eye. *Invest Ophthalmol Vis Sci*. 1997;38:1304-1313.
12. Hitzenberger CK. Optical measurement of the axial eye length by laser Doppler interferometry. *Invest Ophthalmol Vis Sci*. 1991;32:616-624.
13. Stachs O, Martin H, Behrend D, Schmitz KP, Guthoff R. Three-dimensional ultrasound biomicroscopy, environmental and conventional scanning electron microscopy investigations of the human zonula ciliaris for numerical modelling of accommodation. *Graefes Arch Clin Exp Ophthalmol*. 2006;244:836-844.
14. Schneider H, Stachs O, Gobel K, Guthoff R. Changes of the accommodative amplitude and the anterior chamber depth after implantation of an accommodative intraocular lens. *Graefes Arch Clin Exp Ophthalmol*. 2006;244:322-329.
15. Stachs O, Schneider H, Stave J, Guthoff R. Potentially accommodating intraocular lenses—an in vitro and in vivo study using three-dimensional high-frequency ultrasound. *J Refract Surg*. 2005;21:37-45.
16. Stachs O, Schneider H, Stave J, Beck R, Guthoff RF. Three-dimensional ultrasound biomicroscopic examinations for haptic differentiation of potentially accommodative intraocular lenses [German]. *Ophthalmologe*. 2005;102:265-271.
17. Stachs O, Martin H, Kirchhoff A, Stave J, Terwee T, Guthoff R. Monitoring accommodative ciliary muscle function using three-dimensional ultrasound. *Graefes Arch Clin Exp Ophthalmol*. 2002;240:906-912.
18. Kirchhoff A, Stachs O, Guthoff R. Three-dimensional ultrasound findings of the posterior iris region. *Graefes Arch Clin Exp Ophthalmol*. 2001;239:968-971.
19. Food and Drug Administration. Center for Devices and Radiological Health. Premarket Approval Database. http://www.accessdata.fda.gov/scripts/cdrh/cfdocs/cfPMA/PMA.cfm?ID=6374. Accessed November 2003.
20. Findl O, Menapace R. Pilocarpine-induced shift of an accommodating IOL. *J Cataract Refract Surg*. 2005;31:1472-1475.
21. Popper KR. *Conjectures and Refutations: The Growth of Scientific Knowledge*. New York, NY: Routledge, Taylor & Francis; 1963.

Graefe's Arch Clin Exp Ophthalmol
(2006) 244: 322–329

CLINICAL INVESTIGATION

DOI 10.1007/s00417-004-1052-2

Hanka Schneider
Oliver Stachs
Katja Göbel
Rudolf Guthoff

Changes of the accommodative amplitude and the anterior chamber depth after implantation of an accommodative intraocular lens

Received: 2 March 2004
Revised: 30 August 2004
Accepted: 19 September 2004
Published online: 17 August 2005

H. Schneider (✉) · O. Stachs ·
K. Göbel · R. Guthoff
Department of Ophthalmology,
Rostock University,
Doberaner Strasse 140,
18055 Rostock, Germany
e-mail: hanka.schneider@med.
uni-rostock.de
Tel.: +49-381-4948501
Fax: +49-381-4948502

Abstract *Background:* Modern cataract surgery is interested in recovery of the accommodative power. This investigation aimed at determining pseudophakic accommodation in subjects implanted with the accommodative Human Optics 1 CU intraocular lens after drug-induced ciliary muscle stimulation by measuring the objective refraction and the changes in anterior chamber depth in comparison with a PMMA intraocular lens with rigid haptics. *Methods:* The studied sample involved 30 eyes of 30 patients undergoing cataract surgery due to age-related cataract. Patients were between 50 and 77 years of age (67.71±8.0). No randomization was performed. The 1 CU accommodative intraocular lens and the PMMA intraocular lens were implanted in 15 eyes of patients with an expected visual acuity of at least 0.7. Objective refraction under pilocarpine-stimulated ciliary muscle contraction was determined with a Hartinger coincidence refractometer. The anterior chamber depth was measured with Jäger's Haag–Streit slit-lamp attachment. The accommodative amplitude and the anterior chamber flattening were calculated from the measured values. *Results:* Twelve weeks after surgery the average accommodative amplitude in eyes with a 1 CU intraocular lens calculated from the refractive change under drug-induced stimulation was 0.48± 0.36 D (with a maximum of 1.25 D). The measured change of anterior chamber depth under drug-induced stimulation was 0.3±0.32 mm (at a maximum of 0.9 mm). In the reference group with PMMA lenses, the mean accommodative amplitude derived from the refractive changes under drug-induced stimulation was 0.34±0.27 D (at a maximum of 0.85 D). The measured change in anterior chamber depth under drug-induced stimulation was 0.18±0.09 mm (at a maximum of 0.31 mm). No statistically significant differences were found between the two groups of lenses concerning change in anterior chamber depth and accommodative amplitude. *Conclusions:* This investigations indicate a mean anterior 1 CU shift of only 0.32 mm and a maximum of 0.9 mm. The accommodative amplitudes measured with the Hartinger coincidence refractometer (mean value 0.47 D) correspond to these values. Similar conclusions may be drawn from existing investigative results of the reference group, which are on the same order of magnitude as those of the 1 CU group. Objective accommodation measurements are needed to evaluate commercially available accommodative intraocular lenses in a scientifically satisfactory manner. Objectively measurable parameters include changes of the anterior chamber depth as well as refraction, as determined for instance by coincidence refractometry and streak retinoscopy. Future studies should also consider the IOL properties, astigmatism, and pupillary diameter. This is the only way to identify pseudoaccommodation and a decisive factor for further development of accommodative artificial lenses.

Introduction

In recent years, modern cataract surgery has seen considerable improvement and change. For a long time presbyopia was considered to be an age-related, inevitable decline, but now research is interested in recovery of the accommodative power in conjunction with cataract surgery.

The term "accommodation" pertains to the eye's ability to adjust to an object at any given distance, projecting this object onto the retina where it creates a focused image. The refractive setting of the optical system of the eye is adjusted either by removing the projection plane further from the focal plane, or by changing the focal distance of the imaging system. Thus, on the one hand, the distance between the retina and the lens may change during accommodation. On the other hand, the focal distance may change with the radii of curvature or the refractive indices of the structures involved in imaging. In comparison, pseudoaccommodation is the phenomenon of exact perception of objects at varying distances without ocular focusing. Factors such as narrow pupils or simple myopic astigmatism play a role in this context. The phenomenon of pseudoaccommodation is observed in phakic, pseudophakic, and aphakic eyes [5, 14, 24, 38].

True pseudophakic accommodation is caused by ciliary muscle contraction.

The only currently available method of attaining pseudophakic accommodation involves effecting refractive changes by moving the optical system of the artificial lens along the optical axis, which is made possible by flexible haptics. Examples of accommodation mechanisms based on lens shifting are found among animals [9]. According to Gullstrand's eye model, a 1-mm shift of the artificial lens optics corresponds to a vertex refractive change of approximately 1.3 D [13]. So-called accommodative intraocular lenses are now commercially available from three manufacturers.

True pseudophakic accommodation (excluding pseudoaccommodative phenomena) may be quantified by measuring objective refractive changes as well as changes in anterior chamber depth during accommodation. Ciliary muscle contraction may be effected by near stimulation or by administering appropriate drugs.

This investigation aimed at determining pseudophakic accommodation in subjects implanted with the accommodative Human Optics 1 CU intraocular lens after drug-induced ciliary muscle stimulation by measuring the objective refraction and the changes in anterior chamber depth in comparison with a PMMA intraocular lens with rigid haptics.

Patients and method

The 1 CU study group

The studied sample involved 15 eyes of 15 patients undergoing surgery between May and September 2002 at Rostock University Eye Clinic due to age-related cataract. Patients were between 50 and 77 years of age (67.7±8.0). No randomization was performed. The 1 CU accommodative intraocular lens was implanted only in the eyes of patients with an expected visual acuity of at least 0.7 (retinometer vision). The refractive power of the implanted lenses was between +18.0 D and +24.0 D.

Patients more than 50 years of age and those with vision-impairing retinal or corneal diseases, optic neuropathies, preceding perforating injuries or intraocular surgery, chronic or relapsing uveitis, biomicroscopically detectable zonular defects were excluded, as were those who complied inadequately with subsequent check-ups.

After creation of a 5.0-mm capsulorrhexis and phakoemulsification of the lens via the corneoscleral tunnel, the accommodative artificial lens (Human Optics 1 CU) was implanted into the capsular bag. The corneoscleral incision size was 3 mm.

The reference group

The reference group included 15 eyes of 15 patients undergoing surgery between March and October 2002 at Rostock University Eye Clinic due to age-related cataract. Patients were aged between 64 and 89 years (78.1±7.3).

In this case, the inclusion and exclusion criteria were the same as those for the 1 CU group. The patients in the reference group, after phakoemulsification of the lens via a corneoscleral tunnel, received a PMMA intraocular lens (Bausch & Lomb 75 ST6) that was implanted into the capsular bag. The corneoscleral incision size was 6 mm. The refractive power of the implanted lenses was between +16.0 D and +26.0 D.

Postoperative investigations

The patients of the 1 CU group returned for check-ups at 6 and 12 weeks postoperatively, while the reference group was reexamined only once, 12 weeks after surgery.

At first, the objective refractometry was performed using an autorefractometer (Canon RK3). Distance visual acuity was determined using a standard Snellen projector system (Schwind Optostar IR-2000, Germany). Near reading vision was determined using Birkhäuser reading charts (Scalae Typographicae Birkhaeuseri, Birkhäuser Verlag) and an illumination of 70 Cd/m^2. After determination of the best-corrected and the uncorrected far vision, near vision was determined without additional near correction and with addition of +1.0, +2.0, +3.0, and +3.5 sph respectively. Visual acuity was expressed in decimal values and logMAR units. A slit-lamp examination was performed. Subsequently, two drops of cyclopentolate 1% were administered, one 5 min after the other. Thirty minutes later, objective refraction and anterior chamber depth were measured. On

the next day each patient received two drops of pilocarpine 2%, again at a 5-min interval. Approximately 30 min later, both the objective refraction and the anterior chamber depth were determined once more. The measurements obtained after pilocarpine administration were supposed to reveal a pupillary diameter between 2.0 and 2.5 mm. However, none of the patients attained this pupillary diameter during the 30-min waiting time. The waiting time was extended to a maximum of 45 min if after 30 min the pupil was still wider than 2.5 mm.

Objective refraction was determined with a Hartinger coincidence refractometer, which is based on Scheiner's principle of the coincidence of certain patterns of lines on the retina; the primary issue, therefore, is not the focusing on a test mark, but merely this coincidence of a pattern of lines. At a pupillary diameter of >2 mm, measurements performed with a Hartinger coincidence refractometer could be obtained in a measuring range between +15.5 and −28.5 D. In each case, three of the measuring results were averaged to yield a mean value.

The anterior chamber depth was measured with Jäger's Haag–Streit slit-lamp attachment. In this case, doubling of the image is effected by shifting two glass plates in a plane-parallel configuration, so that equal parts protrude from above and from below into the path of the rays. The image-splitting eyepiece uses a prism effect to guide one half of these individual images into the upper half of the field of vision and the rest into the lower half. The measuring points lying in the optical split field are then brought into coincidence. A better depth of field of the slit image is attained by using a slit diaphragm, which makes it possible to select a wider slit illumination. The corneal epithelium and the anterior surface of the lens were designated as measuring points. Another slit-lamp attachment was used to measure the corneal thickness, which was then subtracted from the measured value. In each case, three measurements were obtained and averaged to yield a mean value. The accommodative amplitude and the anterior chamber flattening were calculated from the measured values.

Statistical analysis of the results was performed using MatLab 6.5 (The MatWorks, USA). Data are presented as mean±standard deviation. Differences between data were determined by the Wilcoxon rank sum test and p values less than 0.05 were considered statistically significant.

Results

In all cases, both the accommodative and the PMMA intraocular lenses were implanted into the capsular bags

Table 1 Results 6 weeks after implantation of an accommodative IOL (Human Optics 1 CU). *VF preOP* preoperative, best corrected far vision; *VF post sc* uncorrected postoperative far vision; *VF post cc* best-corrected postoperative far vision; *Refraction* spherical equivalent of the optimum postoperative distance correction in diopters; *VN post sc* postoperative near vision with distance correction; *VN post cc* best-corrected near vision in 35 cm; *Near addition* optimum near addition in diopters; *Accommodative amplitude* accommodative amplitude after drug-induced stimulation in diopters; *ACD change* change of the anterior chamber depth; *MW* mean value; *SD* standard deviation

	Age (years)	VF preOP (dec/logMAR)	VF post sc (dec/logMAR)	VF post cc (dec/logMAR)	Refraction	VNpost sc (dec/logMAR)	VNpost cc (dec/logMAR)	Near addition	Accommodative amplitude	ACD change
1	74	0.4/0.4	0.8/0.1	1.25/−0,1	−1	0.4/0.4	1.25/−0,1	2.5	0.75	0.56
2	71	0.2/0.7	0.5/0.3	1/0	0.5	0.2/0.7	1/0	3	0.5	0.1
3	58	0.5/0.3	0.9/0.05	1/0	−0.5	0.3/0.53	1/0	3	0.5	0.13
4	72	0.3/0.53	0.8/0.1	0.8/0.1	0	0.1/1.0	0.7/0.16	3.5	0	0.03
5	66	0.5/0,3	0.8/0.1	1/0	−0.75	0.3/0.53	1/0	3	0.25	0.2
6	75	0.4/0.4	0.4/0.4	0.8/0.1	−0.5	0.2/0.7	1/0	3	0.5	0.05
7	69	0.5/0.3	1/0	1/0	−0.5	0.2/0.7	0.8/0.1	3.5	0	0.08
8	55	0.7/0.16	1/0	1.25/−0,1	−0.25	0.3/0.53	0.8/0.1	3.5	1	0.9
9	66	0.6/0.22	0.8/0.1	0.9/0.05	−0.25	0.2/0.7	1/0	3	0.25	0.05
10	66	0.6/0.22	0.8/0.1	1.25/−0,1	−0.5	0.4/0.4	1.6/−0.2	2	0.25	0.12
11	71	0.7/0.16	0.7/0.16	0.9/0.05	−0.75	0.5/0.3	1/0	2	0.75	0.9
12	72	0.5/0.3	0.9/0.05	0.9/0.05	−1	0.4/0.4	1/0	2	1.25	0.7
13	72	0.4/0.4	0.7/0.16	1.25/−0,1	−0.75	0.3/0.53	1/0	3	0.25	0.1
14	77	0.4/0.3	0.9/0.05	1.25/−0,1	−0.5	0.4/0.4	1.25/−0.1	2	0.75	0.5
15	76	0.3/0.53	0.9/0.05	1/0	−0.5	0.3/0.53	1/0	3	0.25	0.1
MW	69.3	0.48/0.35	0.79/0.11	1.04/−0.01	−0.48	0.3/0.56	1.02/0	2.8	0.48	0.30
SD	6.28	0.15/0.15	0.17/0.10	0.17/0.07	0.38	0.11/0.17	0.19/0.01	0.56	0.36	0.32

without any complications. Recovery, too, was normal for all patients. Eccentricities or deformations, especially in the accommodative intraocular lenses, were not observed. At 12 weeks postoperatively, one patient in the 1 CU group and two patients in the reference group revealed a minor regenerative secondary cataract without objectifiable vision impairment (patient 5 in the 1 CU group and patients 4 and 7 in the reference group).

The Human Optics 1 CU group

After 6 weeks, the best-corrected far vision was −0.01 logMAR (1.04±0.17 in decimal values) at a remaining refraction of −1.0 to +0.5 D (−0.48±0.38). Near vision without additional near correction was 0.56 logMAR (0.3± 0.11 in decimal values); the value with optimum near correction was 0 logMAR (1.02±0.19 in decimal values). An average near correction of +2.8±0.56 D was obtained subjectively.

The average accommodative amplitude calculated from the refractive change under drug-induced stimulation was 0.48±0.36 D (with a maximum of 1.25 D). The measured change of anterior chamber depth under drug-induced stimulation was 0.3±0.32 mm (at a maximum of 0.9 mm).

The values 12 weeks postoperatively largely corresponded with those of the 6-week check-up. The parameters of the individual patients are shown in Tables 1 and 2.

The reference group

In the reference group, the best-corrected far visual acuity 12 weeks postoperatively was also 0.01 logMAR (0.99± 0.15 in decimal values) at a remaining refraction of −0.75 to +0.75 D (−0.12±0.49). Near vision without additional near correction was 0.44 logMAR (0.39±0.12 in decimal values); while with optimum near correction it was 0.03 logMAR (0.95±0.15 in decimal values). Subjectively, an average near correction of +2.67±0.56 D was obtained.

The mean accommodative amplitude derived from the refractive changes under drug-induced stimulation was 0.34±0.27 D (at a maximum of 0.85 D). The measured change of anterior chamber depth under drug-induced stimulation was 0.18±0.09 mm (at a maximum of 0.31 mm).

The parameters of the individual patients are listed in Table 3. Using Wilcoxon rank sum test the medians in refraction power of the two IOL groups are not significantly different (p=0.83). No statistically significant differences have been found between the 1-CU and the control group concerning the change in anterior chamber depth (p=0.07) and accommodative amplitude (p=0.17) under pharmacological stimulation. There has not been found any correlation between the refraction power of the used 1 CU IOLs and their accommodative effect, based on the of a linear correlation (R^2=0.005, linear model).

Table 2 Results 12 weeks after implantation of an accommodative IOL (Human Optics 1 CU). For explanation of abbreviations see Table 1

	Age (years)	VF preOP (dec/logMAR)	VF post sc (dec/logMAR)	VF post cc (dec/logMAR)	Refraction	VN post sc (dec/logMAR)	VN post cc (dec/logMAR)	Near addition	Accommodative amplitude	ACD change
1	74	0.4/0.4	0.8/0.1	1.25/−0.1	−1	0.4/0.4	1.25/−0.1	2.5	0.75	0.7
2	71	0.2/0.7	0.5/0.3	0.9/0.05	0.5	0.2/0.7	0.9/0.05	3	0.75	0.4
3	58	0.5/0.3	0.9/0.05	1/0	−0.5	0.3/0.53	1/0	3	0.5	0.13
4	72	0.3/0.53	0.9/0.05	1/0	0	0.1/1.0	1/0	3.5	0	0.03
5	66	0.5/0.3	1.25/−0.1	1.25/−0.1	−0.75	0.3/0.53	1.25/−0.1	3	0.5	0.2
6	75	0.4/0.4	0.5/0.3	0.7/0.16	−0.5	0.2/0.7	0.7/0.16	3	0.38	0.1
7	69	0.5/0.3	1/0	1/0	−0.5	0.2/0.7	0.8/0.1	3.5	0	0.08
8	55	0.7/0.16	1/0	1.25/−0.1	−0.25	0.3/0.53	0.8/0.1	2.5	0.75	0.7
9	66	0.6/0.22	0.8/0.1	0.9/0.05	−0.25	0.2/0.7	0.9/0.05	3	0.5	0.25
10	66	0.6/0.22	0.8/0.1	1.25/−0.1	−0.5	0.4/0.4	1.6/−0.2	2	0.25	0.12
11	71	0.7/0.16	0.7/0.16	0.9/0.05	−0.75	0.5/0.3	1/0	2	0.75	0.7
12	72	0.5/0.3	0.9/0.05	0.9/0.05	−1	0.4/0.4	1/0	2	1	0.7
13	72	0.4/0.4	0.6/0.22	1.25/−0.1	−0.75	0.3/0.53	1/0	3	0.25	0.1
14	77	0.6/0.22	0.9/0.05	1.25/−0.1	−0.5	0.4/0.4	1.25/−0.1	2	0.75	0.55
15	76	0.3/0.53	0.9/0.05	1/0	−0.5	0.3/0.53	1/0	3	0.25	0.1
MW	69.3	0.48/0.35	0.83/0.1	1.05/−0.02	−0.48	0.3/0.56	1.02/−0.04	2.73	0.47	0.32
SD	6.28	0.15/0.15	0.2/0.11	0.18/0.08	0.38	0.11/0.18	0.21/0.08	0.53	0.30	0.27

Table 3 Results at 12 weeks after implantation of a PMMA posterior chamber lens (Bausch & Lomb 75 ST 6). For explanation of abbreviations see Table 1

	Age (years)	VF preOP Dec/logMAR	VF post sc dec/logMAR	VF post cc dec/logMAR	Refraction	VN post sc dec/logMAR	VN post cc dec/logMAR	Near addition	Accommodative amplitude	ACD change
1	84	0.2/0.7	0.7/0.16	0.9/0.05	−0.5	0.6/0.22	0.9/0.05	2	0.85	0.31
2	73	0.5/0.3	0.9/0.05	1.25/−0.1	0.5	0.4/0.4	1.25/−0.1	2.5	0.5	0.28
3	87	0.5/0.3	0.8/0.1	0.8/0.1	0	0.2/0.7	0.8/0.1	3	0.25	0.15
4	87	0.6/0.22	0.7/0.16	1/0	−0.75	0.3/0.53	1/0	3	0.25	0.3
5	64	0.4/0.4	1.25/−0.1	1.25/−0.1	0	0.4/0.4	1.25/−0.1	3	0	0.1
6	74	0.3/0.53	0.8/0.1	1/0	−0.5	0.5/0.3	1/0	2.5	0.25	0.1
7	67	0.4/0.4	1/0	1/0	0	0.5/0.3	1/0	2.5	0.2	0.11
8	77	0.7/0.16	0.7/0.16	1/0	0.5	0.3/0.53	0.9/0.05	3	0	0.06
9	83	0.5/0.3	0.8/0.1	0.9/0.05	−0.5	0.4/0.4	0.8/0.1	2.5	0.5	0.2
10	75	0.3/0.53	1/0	1.25/−0.1	0.25	0.5/0.3	1/0	2.5	0.5	0.23
11	77	0.6/0.22	0.7/0.16	0.9/0.05	−0.75	0.4/0.4	0.9/0.05	2.5	0.5	0.2
12	83	0.5/0.3	0.6/0.22	0.8/0.1	0.75	0.2/0.7	0.8/0.1	3	0.25	0.15
13	78	0.6/0.22	0.8/0.1	1/0	−0.75	0.5/0.3	0.8/0.1	2	0.85	0.3
14	74	0.3/0.53	1/0	1/0	0	0.4/0.4	1/0	3	0	0.06
15	89	0.2/0.7	0.8/0.1	0.8/0.1	0	0.2/0.7	0.8/0.1	3	0.25	0.13
MW	78.13	0.44/0.39	0.84/0.09	0.99/0.01	−0.12	0.39/0.44	0.95/0.03	2.67	0.34	0.18
SD	7.34	0.15/0.17	0.17/0.08	0.15/0.06	0.49	0.12/0.16	0.15/0.07	0.35	0.27	0.09

Discussion

Currently available surgical techniques of presbyopia treatment are either of questionable value, as are the so-called sclera-expanding surgical techniques [4, 23], or they are still facing unsolved problems, like other attempts at presbyopia treatment by photorefractive keratectomy [39], eccentric LASIK [3], or implantation of corneal rings [16]. None of these approaches has been able to attain actual accommodation; at best, multifocal intraocular lenses [1, 10, 27, 36] allow improved uncorrected near vision to the detriment of contrast vision [36], which limits their broad use in daily clinical practice even in the elderly.

All attempts at developing accommodative artificial lenses rely on the fact that the ciliary muscle, even at advanced age, is still able to contract. This was confirmed by various studies involving impedance cyclography [37] and ultrasound biomicroscopy [2, 33–35]. Thus, presbyopia should be expected to largely result from increasing loss of lens elasticity due to sclerogenesis [40]. This suggests that it ought to be useful to utilize the remaining contractive power of the ciliary muscle even in human beings of advanced age.

The ideal accommodative artificial lens should completely fill the capsular bag and exhibit the same optical and biomechanical properties as those of natural lenses in young eyes. This concept of microsurgical recovery of the accommodative power involves removal of the lens substance through a narrow opening and refilling of the capsular bag with flexible materials, the so-called phakoersatz. For several years, various groups have made renewed attempts to develop such an artificial lens [11, 17, 25, 26, 29, 31]. Flexible silicone polymers and hydrogels are being tested as potentially suitable materials for capsular bag filling. Surgical techniques are being optimized in animal experiments, and investigations regarding the biocompatibility of the used materials are being performed. The concept of injectable lenses appears to be the most promising option in terms of recovery of the accommodative power in conjunction with cataract surgery. Even though initial surgical results involving primate eyes yielded promising results, with accommodative amplitudes of up to 8 D [11, 26], this method has, as yet, been limited to animal experiments.

Other efforts are relying on mechanical concepts based on the assumption that the continued functional ability of the ciliary muscle and of the zonular fibers allows movement of artificial lenses with flexible haptics along the optical axis inside the intact capsular bag. Such acrylic artificial lenses are commercially available today; the list includes the BioComFold 43A (Morcher), the AT-45 Crystalens (C&C Vision) and the 1 CU (Human Optics). According to Holladay, an accommodative amplitude of 2.9 D, which is equivalent to reading ability at a distance of

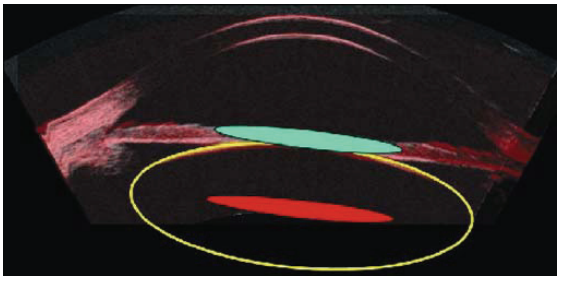

Fig. 1 Diagram showing the inevitable positional change of accommodative artificial lenses inside the capsular bag of the human eye (VHF Ultrasound Arcscan Systems Artemis 2; human eye, 36 years of age). To attain a refractive power change of 2.9 D, a 20-D artificial lens would have to undergo a 2.2-mm anterior shift. The *red* artificial lens schematically indicates the normal position inside the capsular bag. At a shift of 2.2 mm, it would assume the position of the *green* artificial lens, ending up in front of the pupillary plane.

35 cm, would necessitate a forward displacement of 2.2 mm inside the eye of an artificial lens with a refractive power of 20 D [13]. This indicates the limits of such mechanical concepts of presbyopia, since such a shift would cause a displacement of the iris diaphragm—which, in turn, would considerably impair the control of physiological processes in the anterior portion of the eye (Fig. 1).

The Human Optics 1 CU investigated in this study, according to the technical data supplied by the manufacturer, may shift up to 1 mm inside the eye, corresponding to an eyeglass correction change of 1.3 D (Fig. 2). In fact, the investigations discussed in this context indicate a mean anterior 1 CU shift of only 0.32 mm and a maximum of 0.9 mm. The accommodative amplitudes measured with the Hartinger coincidence refractometer (mean value 0.47 D) correspond to these values. Findl et al. arrived at the same results when investigating the mean anterior displacement of accommodative intraocular lenses (Morcher BioComFold and Human Optics 1 CU) by partial coherence interferometry. Based on these results they calculated the resulting accommodative amplitudes. The maximum accommodative amplitude attained by the two patient populations was 1 D (mean value 0.5 D). Thus, these results were very similar to those shown by reference groups implanted with conventional intraocular lenses [6–8]. Similar conclusions may be drawn from the results in the reference group, which are at least on the same order of magnitude as those of the 1 CU group. The variable forward shift of capsular bag-supported PMMA lenses and foldable lenses after pilocarpine administration has been confirmed by other authors [21].

Kammann, too, who investigated patients with accommodative intraocular lenses (C&C Vision AT 45), found unsatisfactory results, since all patients required additional correction for near tasks [15]. Our own investigations confirmed that all patients, after being implanted with a 1 CU intraocular lens, required additional near correction of 2.8 D on average, with a minimum of 2 D.

Küchle et al. [19] and Langenbucher et al. [20], when examining patients with accommodative intraocular lenses (Human Optics 1 CU), found mean accommodative amplitudes of 1.2 D and a greater change in anterior chamber depth than in the reference group. Küchle et al. and Langenbucher et al. measured the anterior chamber depth with an IOL Master, which, however, precludes measurement of pseudophakic eyes [18]. In conjunction with the present investigations, a Haag–Streit slit-lamp attachment according to Jäger was used to perform anterior chamber depth measurements. Compared to automated measurements with an IOL Master, this has the advantage that the position of the anterior lens surface under optical control, despite differences in reflectivity of the artificial lens, may be precisely determined in relation to the natural lens. However, even the accommodative amplitudes attained after implantation of a Human Optics 1 CU, as determined by Küchle et al. and Langenbucher et al., can only reduce but not eliminate the dependency on eyeglasses.

Objective accommodation measurements are needed to evaluate commercially available accommodative intraocular lenses in a scientifically satisfactory manner. Available methods, especially for measuring near vision, tend to depend on subjective patient information and a variety of influences that are difficult to objectify, such as the type of eyeglass correction, illumination, distance, and the type of reading test. Objectively measurable parameters include

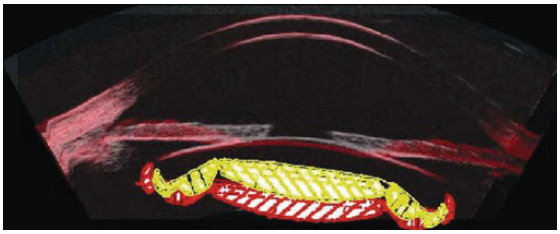

Fig. 2 An accommodative intraocular lens (Human Optics 1 CU according to Hanna) and a schematic representation of its positional change inside the capsular bag (*red* lens). In view of the technical conditions, this lens might possibly undergo a maximum shift of 1 mm at 30° haptic angulation (*yellow* lens). This corresponds to a vertex refractive change of 1.3 D.

changes of the anterior chamber depth (which, however, should be obtained by suitable methods, such as those published by Findl et al. [6–8]) as well as objective measurements of refraction, for instance by coincidence refractometry according to Scheiner's principle (Hartinger coincidence refractometer), and streak retinoscopy. Future studies regarding accommodative lenses should also consider the IOL properties, astigmatism, and pupillary diameter. This is the only way to identify pseudoaccommodation. Although possibly of secondary importance to the patient, it is a decisive factor for further development of accommodative artificial lenses.

References

1. Allen ED, Burton RL, Webber SK, Haaskjold E, Sandvig K, Jyrkkio H, Leite E, Nystrom A, Wollensak J (1996) Comparison of a diffractive and a multifocal intraocular lens. J Cataract Refract Surg 22:446–451
2. Bacskulin A, Martin H, Kundt G, Terwee T, Guthoff R (2000) Analysis of the dynamics of the ciliary muscle during accommodation. Ophthalmologe 97:855–859
3. Bauerberg JM (1999) Centered vs. inferior off-center ablation to correct hyperopia and presbyopia. J Refract Surg 15:66–69
4. Drexler W, Findl O, Schmetterer L, Hitzenberger CK, Fercher AF (1998) Eye elongation during accommodation in humans: differences between emmetropes and myopes. Invest Ophthalmol Vis Sci 39:2140–2147
5. Elder MJ, Murphy C, Sanderson GF (1996) Apparent accommodation and depth of field in pseudophakia. J Cataract Refract Surg 22:615–619
6. Findl O, Kiss B, Petternel V, Menapace R, Georgopoulos M, Rainer G, Drexler W (2003) Intraocular lens movement caused by ciliary muscle contraction. J Cataract Refract Surg 29:669–676
7. Findl O (2001) IOL movement induced by ciliary muscle function. In: Guthoff R, Ludwig K (eds) Current aspects of human accommodation. Kaden, Heidelberg
8. Findl O (2003) Laserferometric measurement of movement of an "accommodative" intraocular lens. In: Guthoff R, Ludwig K (eds) Current aspects of human accommodation II. Kaden, Heidelberg
9. Glasser A (2003) How other species accommodate. In: Guthoff R, Ludwig K (eds) Current aspects of human accommodation II. Kaden, Heidelberg
10. Gray PJ, Lyall MG (1992) Diffractive multifocal intraocular lens implants for unilateral cataracts in presbyopic patients. Br J Ophthalmol 76:336–337
11. Haefliger E, Parel JM (1994) Accommodation of an endocapsular silicone lens (Phaco-Ersatz) in the aging rhesus monkey. J Refract Corneal Surg 10:550–555
12. Hardman Lea SJ, Rubinstein MP, Snead MP, Haworth AM (1990) Pseudophakic accommodation? A study of the stability of capsular bag supported, one piece, rigid tripod, or soft flexible implants. Br J Ophthalmol 74:22–25
13. Holladay JT (1993) Refractive power calculations for intraocular lenses in the phakic eye. Am J Ophthalmol 116:63–66
14. Huber C (1981) Myopic astigmatism; a substitute for accommodation in pseudophakia. Doc Ophthalmol 52:123–178
15. Kammann J, Dornbach G (2001) Empirical results regarding accommodative lenses. In: Guthoff R, Ludwig K (eds) Current aspects of human accommodation. Kaden, Heidelberg
16. Keates RH, Martines E, Tennen DG, Reich C (1995) Small-diameter corneal inlay in presbyopic or pseudophakic patients. J Cataract Refract Surg 21:519–521
17. Koopmans SA, Terwee T, Barkhof J, Haitjema H, Kooijman AC (2003) Polymer refilling of presbyopic human lenses in vitro restores the ability to undergo accommodative changes. Invest Ophthalmol Vis Sci 44:250–257
18. Kriechbaum K, Findl O, Kiss B, Sacu S, Petternel V, Drexler W (2003) Comparison of anterior chamber depth measurement methods in phakic and pseudophakic eyes. J Cataract Refract Surg (Jan), 29(1):89–94
19. Küchle M et al (2002) Implantation of a new accommodative posterior chamber intraocular lens. J Refract Surg (May/June)
20. Langenbucher A, Hubera S, Nguyen NX, Seitz B, Gusek-Schneider GC, Küchle M (2003) Measurement of accommodation after implantation of an accommodating posterior chamber intraocular lens. J Cataract Refract Surg 29:677–685
21. Lesiewska-Junk H, Kaluzny J (2000) Intraocular lens movement and accommodation in eyes of young patients. J Cataract Refract Surg 26:562–565
22. Martin H, Schmidt W, Schmitz KP, Schneider H, Guthoff R, Terwee T (2003) The material properties of the isolated human capsular bag. In: Guthoff R, Ludwig K (eds) Current aspects of human accommodation II. Kaden, Heidelberg
23. Mathews S (1999) Scleral expansion surgery does not restore accommodation in human presbyopia. Ophthalmology 106:873–877
24. Nakazawa M, Ohtsuki K (1983) Apparent accommodation in pseudophakic eyes after implantation of posterior chamber intraocular lenses. Am J Ophthalmol 96:435–438
25. Nishi O, Nakai Y, Yamada Y, Mizumoto Y (1993) Amplitudes of accommodation of primate lenses refilled with two types of inflatable endocapsular balloons. Arch Ophthalmol 111:1677–1684
26. Nishi O, Nishi K (1998) Accommodative amplitude after lens refilling with injectable silicone by sealing the capsule with a plug in primates. Arch Ophthalmol 116:1358–1361
27. Nowak MR, Jakobi KW (1990) Diffraktive multifocale Intraocularlinsen. Eine prospektive klinische Studie. Klin Monatsbl Augenheilkd 196:43–47
28. Packer M, Fine H, Hoffman S (2002) Restoring accommodation in the pseudophacic patient. Eye World (May)
29. Parel JM, Gelender H, Treffers WF, Norton EWD (1986) Phako-Ersatz: cataract surgery designed to preserve accommodation. Graefes Arch Clin Exp Ophthalmol 224:165–173
30. Preußner PR, Wahl J, Gerl R, Kreiner C, Serester A (2001) Accommodatives Linsenimplantat. Ophthalmologe 98:97–102

31. Schneider H, Stave J, Terwee T, Guthoff R (2003) Intraoperative refraction control in lens refilling. In: Guthoff R, Ludwig K (eds) Current aspects of human accommodation II. Kaden, Heidelberg
32. Stachs O, Beck R, Stave J, Guthoff R (2002) 3D Ultraschallbiomikroskopische Untersuchungen zu Positionierung von Intraokularlinsen im in vitro capsular bagmodel, Jahrestagung der DOG 2002. Ophthalmologe 99:183
33. Stachs O, Kirchhoff A, Martin H, Hornych K, Stave J, Guthoff R (2001) Die Charakterisierung der Ziliarmuskelfunktion während der Akkommodation unter Nutzung der dreidimensionalen Ultraschallbiomikroskopie. Ophthalmologe 98:170
34. Stachs O, Martin H, Kirchhoff A, Stave J, Terwee T, Guthoff R (2002) Monitoring accommodative ciliary muscle function using three-dimensional ultrasound. Graefes Arch Clin Exp Ophthalmol 240:906–912
35. Stachs O (2003) Monitoring the human ciliary muscle function during accommodation. In: Guthoff R, Ludwig K (eds) Current aspects of human accommodation II. Kaden, Heidelberg, pp 105–118
36. Steinert RF, Aker BL, Trentacost DJ, Smith PJ, Tarantino N (1999) A prospective comparative study of the Amo Array zonal-progressive multifocal silicone intraocular lens and monofocal intraocular lens. Ophthalmology 106:1243–1255
37. Swegmark G (1969) Studies with impedance cyclography on human ocular accommodation at different ages. Acta Ophthalmol 47:1186–1206
38. Verzella F, Calossi A (1993) Multifocal effect of against-the-rule myopic astigmatism in pseudophakic eyes. Refractive Corneal Surgery 9:58–61
39. Vinciguerra P, Nizzola GM, Bailo G, Nizzola F, Ascari A, Epstein D (1998) Excimer laser photorefractive keratectomy for presbyopia: 224-month follow-up in three eyes. J Refract Surg 14:31–37
40. Weale RA (2000) Why we need reading-glasses before a zimmer-frame. Vision Res 40:2233–2240
41. Weeber H, Martin H (2001) Finite elements simulation of accommodation. In: Guthoff R, Ludwig K (eds) Current aspects of human accommodation. Kaden, Heidelberg, pp 135–144

Graefe's Arch Clin Exp Ophthalmol
(2006) 244: 559–564

CLINICAL INVESTIGATION

DOI 10.1007/s00417-005-0103-7

B. Meinhardt
O. Stachs
J. Stave
R. Beck
R. Guthoff

Evaluation of biometric methods for measuring the anterior chamber depth in the non-contact mode

Received: 24 March 2005
Revised: 13 July 2005
Accepted: 18 July 2005
Published online: 15 September 2005

Presented at the 102nd Conference of the German Ophthalmological Society (DOG)

None of the authors has a financial or proprietary interest in any material or method mentioned.

B. Meinhardt · O. Stachs · J. Stave · R. Beck · R. Guthoff
Eye Clinic of the University of Rostock,
Rostock, Germany

O. Stachs (✉)
Faculty of Medicine, Eye Clinic,
University of Rostock,
Doberaner Strasse 140,
18055 Rostock, Germany
e-mail: oliver.stachs@med.uni-rostock.de
Tel.: +49-381-4948566
Fax: +49-381-4948502

Abstract *Purpose:* High-resolution biometry of the anterior ocular segment is now becoming more and more important against a background of refractive surgery and the evaluation of potentially accommodative lens replacement materials. The aim of this study was a systematic investigation of the currently available non-contact methods for measuring the anterior chamber depth (ACD). *Methods:* The ACDs of 50 phakic eyes of 27 patients aged between 19 and 59 years were measured with the IOL-Master (Zeiss), the AC-Master (Zeiss), the Pentacam (Oculus) and slit-lamp pachymetry by Jaeger (Haag-Streit). *Results:* The median anterior chamber depth in the investigated eyes was 3.63 mm for the IOL-Master (minimum 2.88 mm, maximum 4.22 mm), 3.802 mm for the AC-Master (2.816 mm–4.373 mm), 3.915 mm for the Pentacam (minimum 2.994 mm, maximum 4.614 mm) and 3.75 mm for Jaeger (2.887 mm–4.29 mm). With a probability of error of α=0.05 there were no significant differences concerning the ACD between the methods of Jaeger and AC-Master, Jaeger and IOL-Master, or Pentacam and AC-Master (Wilcoxon and Wilcox). The intra-individual variability was ±5.4 μm for AC-Master, ±12.7 μm for Pentacam, ±24.5 μm for IOL-Master and ±41.2 μm for Jaeger. The maximum method-dependent difference in ACD determination was 285 μm. *Conclusions:* All the methods allow non-contact biometry, but the results might differ due to measuring principles inherent to the system, experience of the examiner and compliance of the patient. Partial coherence interferometry with the AC-Master offers the advantage of measurement exactly along the optical axis with the highest reproducibility and patient compliance.

Keywords Biometry · Anterior chamber depth

Introduction

The exact measurement of the anterior chamber depth is of major importance for determining the actual position of the lens. This is of particular interest in conjunction with the assessment of accommodation-induced configuration changes of the phakic eye [18] and with potentially accommodative intraocular lenses based on the axial shift principle. Various intraocular lenses (IOLs) of this type have been developed in the past few years. The accommodative ability of these lenses has been evaluated in numerous studies via measurement of the anterior chamber depth [1, 8–11]. Different methods, such as, for example, the IOL-Master [14], Orbscan [11], AC- Master and ultrasound [11], were used for this purpose. Owing to this fact alone, different documented results are obtained on comparison of these studies [12, 16].

In the past few years ultrasound has played a decisive role in the biometry of the anterior segment in everyday clinical practice [15]. Currently, non-contact biometry is

possible, for example, with the slit-lamp pachymeter by Jaeger, Orbscan, Pentacam, IOL-Master and AC-Master. With regard to the comparability of these methods with each other, the questions arises as to what optical interfaces the various methods detect and what corrective factors specific to the instrument and method concerned are utilized by the manufacturer.

This study will evaluate the comparability of different non-contact methods for the analysis of the anterior chamber depth in the phakic eye. It will incorporate not only established instruments such as the IOL-Master and the slit-lamp pachymeter by Jaeger, but also such new developments as the Pentacam and AC-Master.

Material and method

In this prospective study the anterior chamber depth of 50 phakic eyes of 27 patients aged between 19 and 59 years was determined. All measurements were conducted by one examiner.

The anterior chamber depth was defined as the distance between the front surface of the cornea and the front surface of the lens. The methods or instruments used incorporated biometry by means a photographic imaging method—IOL-Master (Zeiss, Germany), partially coherent interferometry—AC-Master (Zeiss, Germany), Scheimpflug imaging—Pentacam (Oculus, Germany) and optical pachymetry—the slit-lamp pachymeter by Jaeger (Haag-Streit, Swiss).

IOL-master

It should be pointed out that the IOL-Master (Carl Zeiss Meditec, Germany; software version 3.01.0294) does not use partially coherent interferometry for measuring the anterior chamber depth (ACD). The principle used to measure the ACD is based on an "optical section" through the anterior chamber by means of a slit illumination system with subsequent image evaluation. The right eye is illuminated from the right, the left eye from the left. The measurement is performed by image evaluation, with illumination at an angle of 30° relative to the optical axis. The anterior chamber depth standard in biometry is measured which, anatomically, is the anterior chamber depth plus corneal thickness. During the examination, the patient fixes the eyes on a yellow light source inside the IOL-Master. The measurement is performed along the visual axis.

AC-master

In addition, a prototype of the AC-Master from Carl Zeiss Meditec AG, Germany (software version 1.11.0096) was used. The measuring principle is based on a further development of partially coherent interferometry. Here, a short-coherence infrared laser beam is emitted by a luminescent diode and separated into two partial rays with different optical path lengths using a Michelson interferometer [2, 7]. These partial rays are reflected onto different intraocular structures. An interference signal occurs and is recorded if the path difference between the partial rays is smaller than the coherence length. This instrument allows measurement not only of the anterior chamber depth but also of the corneal and lens thicknesses, exactly along the optical axis [5, 6]. For this purpose, the four Purkinje images resulting from reflection at the interfaces of the cornea and lens must be superimposed within the measurement. During the examination the patient fixes the eyes on a target inside the AC-Master, which is movable and hence allows the superimposition of the four Purkinje images.

Scheimpflug Prinzip

The anterior chamber depth was also determined with the Pentacam (Oculus, Germany; software version 1.09), which is modelled on the Scheimpflug principle. During the measurement and recording of a sectional image, a CCD camera rotates and provides section planes from the three spatial planes. The measured data obtained are used to calculate a 3D model, from which the anterior chamber depth can be computed. Here, the anterior chamber depth is defined as the distance between the back surface of the cornea and the front surface of the lens. To obtain a comparison with the measured data received with the other instruments, we added the respective Pentacam corneal thicknesses to the Pentacam anterior chamber depths. During the measurement the patient's eyes are fixed on a blue light source [light-emitting diode (LED) 475 nm] within the centre of rotation of the CCD camera.

Slit lamp with Jaeger attachment

For anterior chamber depth measurement on the slit lamp (as devised by Jaeger, Haag-Streit, Switzerland), the measuring attachment II was used. This consists essentially of two plane-parallel glass plates through which the ray path passes in equal portions. The upper plate rotates around the swivel axis when the scale segment is swung horizontally. Image doubling results, with the images being displaced relative to each other so that the epithelium of the lower image and the lens front surface of the upper image coincide. For better visualization of the interfaces, a drop of fluorescein is administered. The patient looks into the light of the slit lamp passing though the slit diaphragm. Corrective values from the appropriate tables were taken into account.

In all instruments used, at least three successive measurements were performed per eye, and the resultant mean

Table 1 Statistical analysis of the anterior chamber depth of 50 phakic eyes (values in millimetres)

Instruments	Median	Mean	Standard deviation	Minimum	Maximum
Jaeger	3.75	3.712	0.319	2.887	4.29
IOL-Master	3.63	3.64	0.324	2.88	4.22
AC-Master	3.802	3.779	0.339	2.816	4.373
Pentacam	3.915	3.909	0.366	2.994	4.614

value then examined. To evaluate the precision of the instruments, we determined the standard deviation for ten successive measurements conducted by one examiner on one phakic eye.

Different measuring data were assessed by the Wilcoxon matched-pairs signed-rank test. The selected significance level was 0.05, with the result that *P* values smaller than 0.05 are seen as statistically significant. The statistical analysis was performed with the aid of MatLab 6.5 software (The MathWorks). The results are shown as median, minimum and maximum. The Bland–Altman plot [3, 4] was used to reveal a relationship between the differences and the averages, to look for any systematic bias and to identify possible ouliers (Table 1).

Results

In the phakic eyes examined the median of the anterior chamber depth (Fig. 1) measured with the IOL-Master was 3.63 mm (minimum 2.88 mm, maximum 4.22 mm) and 3.802 mm (2.816 mm−4.373 mm) when measured with the AC-Master. The difference between the medians of the IOL-Master and AC-Master was −0.172 mm. This proved to be statistically significant (*P*=0.0319).

The highest ACD values (median 3.915 mm; minimum 2.994 mm; maximum 4.614 mm) were obtained with the Pentacam. The median of the ACD measurement with the slit lamp pachymeter by Jaeger lay at 3.75 mm (2.887 mm–4.29 mm). The difference between the medians of the Pentacam instrument and the slit lamp amounted to 0.165 mm and proved to be significant (*P*=0.0063).

No significant difference was found between the AC-Master and Pentacam (*P*=0.0739; Δmedian=−0.113 mm). The difference between the ACD medians of the IOL-Master and slit lamp was −0.12 mm and was not statistically significant (*P*=0.2243). With a value of −0.285 mm, the largest method-dependent difference was established between the medians of the IOL-Master and Pentacam. This proved to be statistically significant (*P*=3.4201 e–004). The smallest median difference lay at 0.052 mm (AC-Master versus slit lamp) and was not statistically significant (*P*=0.2646). The Bland–Altman plots for all combined data sets (Fig. 2) demonstrate the mean and the limits of agreement.

In order to evaluate the precision of the four methods, we conducted ten measurements with each instrument. These were performed by one examiner on one phakic eye. As a quality criterion for precision, the standard deviations (SD) are shown (Fig. 3). The smallest deviation from the mean value (3.977 mm) was found in the ACD measurement using the AC-Master (SD ±5.4 μm). The standard deviation of the IOL-Master amounted to ±24.5 μm (mean 3.913 mm), and that of the Pentacam ±12.7 μm (mean 4.1717 mm). The Jaeger-type slit-lamp pachymeter displayed the lowest precision (SD ±41.2 μm; mean 3.865 mm). The clearly different reproducibility of the individual in-

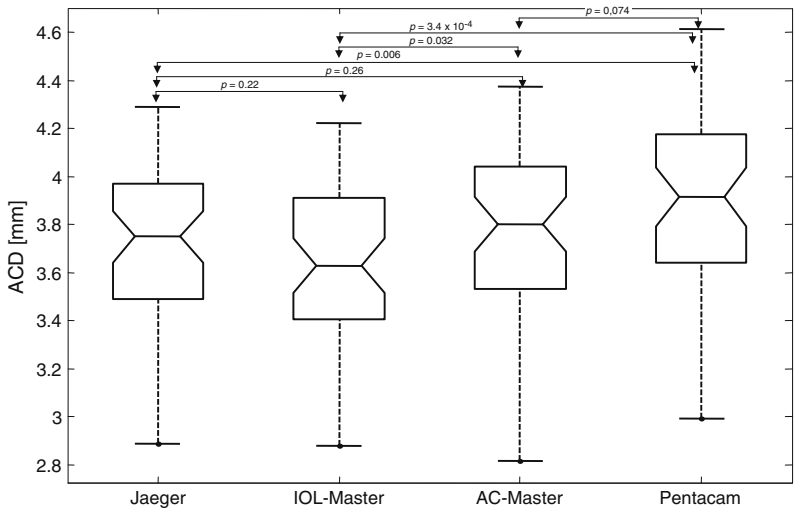

Fig. 1 Box plots of the anterior chamber depth measurement on 50 phakic eyes with the slit-lamp pachymeter by Jaeger, IOL-Master, AC-Master and Pentacam. Presented are medians, 25% and 75% quartiles, as well as minimum and maximum values

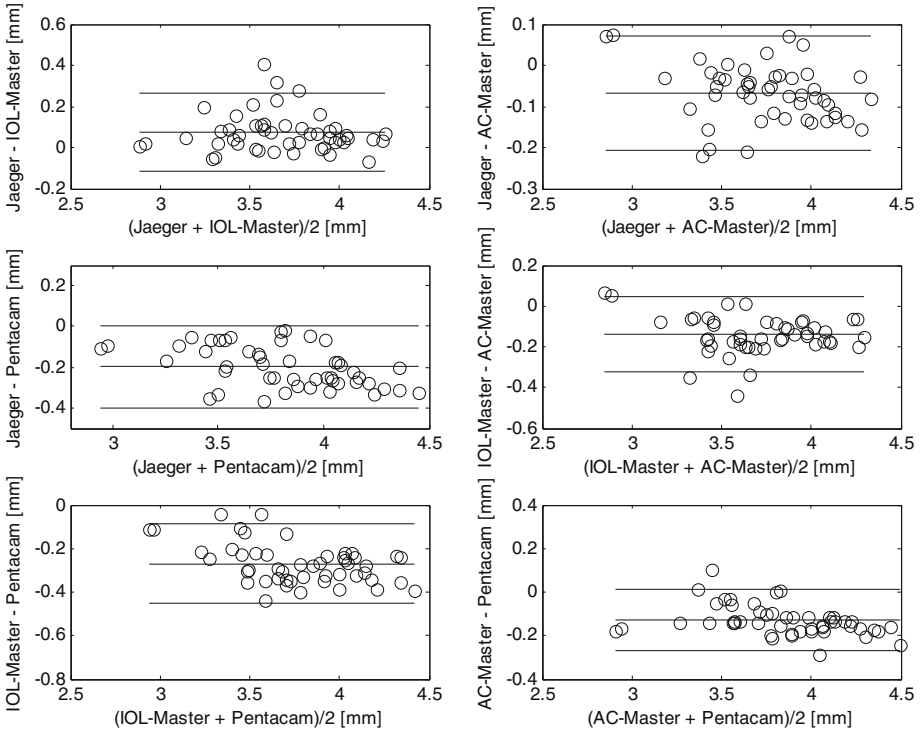

Fig. 2 Bland–Altman plots of the investigated data. *The solid line* is the mean difference, and *the dashed lines* are the limits of agreement

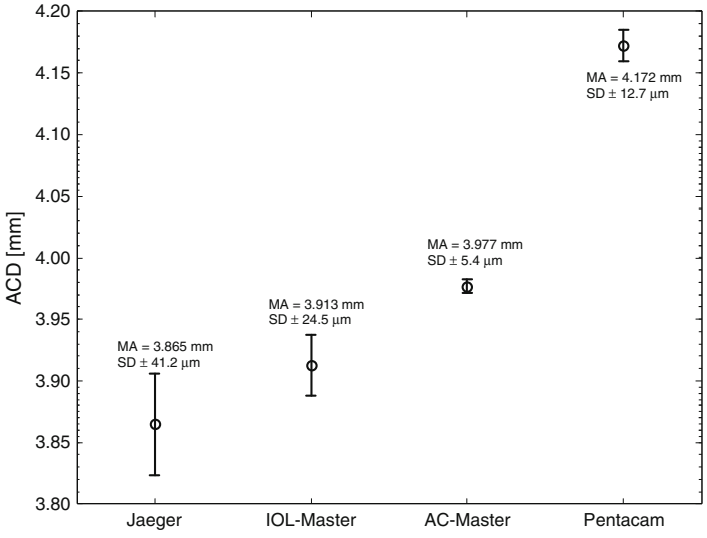

Fig. 3 Illustration of the reproducibility of the anterior chamber depth with the slit-lamp pachymeter by Jaeger, the IOL-Master, the AC-Master and the Pentacam (ten successive measurements on one phakic eye). The mean *MA (o)* and the standard deviation *SD (I)* are shown

strument designs as well as the median and mean values found are summarized in Fig. 3.

Discussion

All the methods used permit non-contact biometry on phakic eyes. Systematic differences between the four methods examined were seen regarding the medians determined for the anterior chamber depths (Fig. 1). The Bland–Altman plots for the combined data (Fig. 2) demonstrate the systematic differences between the four methods. There are no proportional or magnitude-dependent errors. Pentacam generally measured the highest values, IOL-Master the lowest, with the slit-lamp pachymeter by Jaeger and the AC-Master occupying roughly a middle position between these two instruments with regard to the ACD values obtained. The different physical measuring principles used, and, hence, also instrument-specific corrective factors, must be taken into account as a possible cause of those systematic differences. Anterior chamber depth measurement with the IOL-Master is adapted to the measurements with immersion ultrasound by the use of corrective factors. In this context it should be noted that the IOL-Master does not use partial coherence interferometry but a photographic technique for measuring the ACD. In the AC-Master, which uses partial coherence interferometry, the known refractive indices or velocities of light of the ocular media for the relevant measuring wavelength are utilized. Here, adaptation to immersion ultrasound is also possible. Measurements with the slit-lamp pachymeter by Jaeger are influenced by the corneal radius.

In the future, what optical interfaces the various methods detect must be examined. One approach here is the use of confocal, in vivo microscopy with the HRT II (Heidelberg Engineering) in conjunction with the Rostock cornea module. It must be assumed, however, that the cause of the different median and mean values should primarily be sought in the different conversions of the original data. The basic problem always lies in the knowledge of the velocity of light and sound in the respective ocular media as well as their frequency distribution in the population. With the use of partial coherence interferometry optical paths are measured, which are converted into geometrical path lengths via the refractive index. By contrast, ultrasound measures the transit time in the medium, and the geometric path is calculated via the sound velocity.

The dependence of the results obtained by the examiner were not examined within the framework of this study. Further investigations would be necessary for this purpose. However, some studies already show that optical measuring techniques like that of the IOL-Master are examiner-independent to the greatest possible extent [17]. With the use of the slit-lamp pachymeter by Jaeger, on the other hand, a certain subjective factor cannot be ruled out. The type of measuring axis can also lead to a difference. In the AC-Master, the measurement is performed along the optical axis, while the visual axis is used in the other methods. In all instruments used, different targets were fixed at infinity. It could, nevertheless, be possible to conclude different states of accommodation and, hence, different anterior chamber depths. In further study, accommodation should be additionally deactivated pharmacologically if possible, or the non-participating eye should be fixed on a constant target [13].

On the subject of reproducibility, it can be said that IOL-Master, Pentacam and, above all, AC-Master are very precise instruments for measuring the anterior chamber depth. Measurements with the AC-Master display by far the smallest standard deviation and are therefore highly reproducible. As an analog optical measuring method, the slit-lamp pachymeter by Jaeger exhibits the lowest reproducibility.

Our investigations show relatively large systematic deviations in the median of the anterior chamber depths determined. Appropriate consideration must be given to these when anterior chamber measurements performed with different methods are compared.

Anterior chamber dept measurements with the IOL-Master and Pentacam require a relatively short learning curve and relatively little time to perform. The slit-lamp pachymeter by Jaeger displays the lowest reproducibility and needs a certain degree of practice. In the AC-Master a relatively high level of experience in the handling of the instrument and a high degree of patient compliance are required. The benefit of this method is its high measure of precision and measurement along the optical axis.

References

1. Auffarth GU, Martin M, Fuchs HA, Rabsilber TM, Becker KA, Schmack I (2002) Validity of anterior chamber depth measurements for the evaluation of accommodation after implantation of an accommodative Humanoptics 1CU intraocular lens. Ophthalmologe 99:815–819 (in German)
2. Augustin AJ (2001) Augenheilkunde, 2nd edn, Springer, p 1062
3. Bland JM, Altman DG (1986) Statistical method for assessing agreement between two methods of clinical measurement. Lancet 1:307–310
4. Bland JM, Altman DG (1999) Measuring agreement in method comparison studies. Stat Methods Med Res 8:135–160
5. Drexler W, Baumgartner A, Findl O, Hitzenberger CK, Sattmann H, Fercher AF (1997) Submicrometer precision biometry of the anterior segment of the human eye. Invest Ophthalmol Vis Sci 38:1304–1313

6. Drexler W, Baumgartner A, Findl O, Hitzenberger CK, Fercher AF (1997) Biometric investigation of changes in the anterior eye segment during accommodation. Vision Res 37:2789–2800
7. Fercher AF, Mengedoht K, Werner W (1988) Eye-length measurement by interferometry with partially coherent light. Opt Lett 13:186–188
8. Findl O, Drexler W, Menapace R, Hitzenberger CK, Fercher AF (1998) High precision biometry of pseudophakic eyes using partial coherence interferometry. J Cataract Refract Surg 24:1087–1093
9. Findl O, Drexler W, Menapace R, Bobr B, Bittermann S, Vass C, Rainer G, Hitzenberger CK, Fercher AF (1998) Accurate determination of effective lens position and lens–capsular distance with 4 intraocular lenses. J Cataract Refract Surg 24:1094–1098
10. Findl O, Kriechbaum K, Menapace R, Koeppl C, Sacu S, Wirtitsch M, Buehl W, Drexler W (2004) Laser interferometric assessment of pilocarpine-induced movement of an accommodating intraocular lens: a randomized trial. Ophthalmology 111:1515–1521
11. Koranyi G, Lydahl E, Norrby S, Taube M (2002) Anterior chamber depth measurement: A-scan versus optical methods. J Cataract Refract Surg 28:243–247
12. Kriechbaum K, Findl O, Kiss B, Sacu S, Petternel V, Drexler W (2003) Comparison of anterior chamber depth measurement methods in phakic and pseudophakic eyes. J Cataract Surg 29:89–94
13. Lam AK, Chan R, Pang PC (2001) The repeatability and accuracy of axial length and anterior chamber depth measurements from the IOLMaster. Ophthalmic Physiol Opt. 21:477–483
14. Langenbucher A, Huber S, Nguyen NX, Seitz B, Gusek-Schneider GC, Küchle M (2003) Measurement of accommodation after implantation of an accommodating posterior chamber intraocular lens. J Cataract Refract Surg 29:677–685
15. Leaming DV (2001) Practice styles and preferences of ASCRS members—2000 survey. J Cataract Refract Surg 27:948–955
16. Vetrugno M, Cardascia N, Cardia L (2000) Anterior chamber depth measured by two methods in myopic and hyperopic phakic IOL implant. Br J Ophthalmol 84:1113–1116
17. Vogel A, Dick HB, Krummenauer F (2001) Reproducibility of optical biometry using partial coherence interferometry; intraobserver and interobserver reliability. J Cataract Refract Surg 27:1961–1968
18. Vilupuru AS, Glasser A (2003) Dynamic accommodative changes in rhesus monkey eyes assessed with A-scan ultrasound biometry. Optom Vis Sci 80:383–394

International Ophthalomology, submitted 1

Evaluation of Biometric Methods for Measuring the Corneal Thickness in Comparison to Confocal Laser Scanning Microscopic Investigations

Meinhardt B., Stachs O., Zhivov A. and Guthoff R.F.

Department of Ophthalmology, University of Rostock, Germany

oliver.stachs@med.uni-rostock.de

Purpose: The exact determination of corneal thickness (CT) is an important component in preoperative diagnostics prior to refractive surgery and for intraocular pressure determination. For this reason a systematic investigation of the currently available methods for measuring the corneal thickness was undertaken.

Methods: In a prospective comparative study the central CT of 50 phakic eyes of 27 patients (age range 19 to 59 years) was measured with Scheimpflug Imaging (Pentacam, Oculus), Dual-beam partial coherence interferometry (AC-Master, Zeiss), slit-lamp pachymetry by Jaeger (Haag-Streit) and with optical slit scanning (Orbscan II, Orbtek). In addition, AC-Master measurements were directly compared to in vivo confocal laser scanning microscopy (CLSM, Heidelberg Engineering). In all cases, at least three successive measurements were performed on each eye, and a mean value was calculated. To evaluate the precision of the instruments, the standard deviation was determined for ten successive measurements which were conducted by one examiner on one phakic eye. The Bland-Altman plot was used to reveal a relationship between the differences and averages.

Results: The median CT values were 550µm (Pentacam), 522µm (AC-Master), 500µm (Jaeger) and 536µm (Orbscan II). The precision was ± 6.1µm (Pentacam), ±1.7µm (AC-Master), ±14µm (Jaeger), ±8.9µm (Orbscan II) and ±6.0µm (CLSM). The maximum method-dependent difference in CT determination was 50µm. The median CT's measured with the non-contact methods differed significantly ($\alpha = 0.05$, Wilcoxon and Wilcox). No significant difference was found between AC-Master (median 546µm) and CLSM (median 560µm).

Conclusions: All used methods allow a determination of CT, but the results might differ due to measuring principles inherent to the system, experience of the examiner and compliance of the patient. Jaeger and CLSM are less suited for clinical use, but CLSM is an excellent method to visualise corneal cell layers with high acuity. The AC-Master requires a relatively high level of experience in the use of the instrument and a high degree of patient compliance. Nevertheless, the AC-Master produces extremely precise measurements of the CT at the anatomic or optical axis.

Introduction

The exact determination of corneal thickness (CT) currently gains great importance in the area of refractive surgery. Precise CT-values should be measured preoperatively to disqualify risk patients and to avoid, as possible, complications such as ectasia [24]. Postoperative CT-determination allows a certain evaluation of the conducted LASIK (*Laser in situ Keratomileusis*). Within such postoperatively conducted studies interesting insights were won about the interrelation between the corneal thickness and the eye's intraocular pressure (IOP) [18]. In various studies the IOP decreased between 0.46 – 0.71 mmHg per 10µm CT reduction [6, 7]. The interrelation between CT and IOP also plays an important role in the medical diagnosis and care of glaucoma patients [26]. In addition, the evaluation of CT allows certain predication about the undisturbed function of the cornea. In the clinical routine ultrasound is usually used to measure the thickness of the cornea, although several studies have shown the advantages of newer methods [2, 10]. This study evaluates the comparability of newer techniques for the analysis of CT on the phakic eye. Consequently, new developments like AC-Master and CLSM, as well as Orbscan II, Pentacam and slit-lamp pachymetry by Jaeger, were included in this study.

Material and Method

In this study we measured the central corneal thickness on 50 phakic eyes of 27 test persons (age range between 19 and 59) using the Pentacam, the Orbscan II, the slit-lamp pachymetry by Jaeger and the AC-Master. For the purpose of finding out how the confocal microscopy integrates into the comparison of methods for the determination of corneal thickness, we added a direct comparison between AC-Master and CLSM. For this the central CT on 10 phakic eyes was determined with both methods.

Measuring principles of used instruments: AC-Master (Carl Zeiss Meditec AG, Germany), (AC-Master, Version 1.11.0096)

The measuring principle of the AC-Master by Carl Zeiss Meditec Inc. is based on the advancement of the partial coherence interferometry (PCI). Here an infrared laser beam of short coherence is emanated by a luminescence diode and separated into two split beams of different optical path lengths via a Michelson – interferometer [1, 12]. These split beams are reflected on different intraocular structures. An interference signal appears and is detected when the path difference between the split beams is smaller than the coherence length. This instrument allows the determination of corneal thickness, but also of the anterior chamber depth and lens thickness, exactly along the optical axis [9, 10]. For this the four Purkinje-pictures which result from the reflection on the interface of the cornea and lens must be put on top of each other within the measurement. The test person fixates on a target (cross or dot) within the AC-Master during the examination. This target is relocatable and thus enables the overlapping of the four Purkinje-pictures. In addition, the instrument has a pachymetry mode in which the central and peripheral corneal thickness can be determined.

Pentacam (Scheimpflug-Principle, Oculus, Germany), (PentCam 1.09)

Furthermore, the CT was determined with the Pentacam which is based on the Scheimpflug-principle. During the measurement and shooting of a section diagram, a CCD camera rotates and provides section planes from the three space planes. A 3D map is generated from the measured data, and with it the corneal thickness, among others, can be calculated [19]. During the measurement the test person fixates on a blue illuminant (LED, 475nm) in the camera's rotation centre.

Slit-lamp Pachymetry by Jaeger (Haag-Streit, Switzerland)

The measuring adaptor used on the slit lamp (by Jaeger) for the determination of the CT. It basically consists of two coplanar lantern slides through which the course of beam passes in equal shares. The top slide spins around the axis of rotation during the deviation of the scale segment. It comes to picture duplication whereas the pictures are displaced to each other in such a way that the epithelium of the bottom picture meets the endothelium of the top picture [13]. For better illustration the epithelium was slightly dyed with fluorescein. The test person looked into the light coming through the aperture of the slit lamp. Correction values from respective tables were taken into account.

Orbscan II (Orbtek Inc., Salt Lake City, Bausch & Lomb)

Orbscan II combines the advantages of Placido-derived and slit-scanning derived topography [5]. This technique takes a series of split beam images (40 slit-scan and 3 placido images) by means of two scanning slit lamps, which project beams in a 45 degree angle to the right or left of the instrument's axis. Orbscan II acquires over 9000 data points in 1.5 seconds. It produces a 3D map of the curvature, of the front and back surfaces of the cornea, and it measures the corneal thickness. During the examination a system also measures the eye movement. The patient fixates on a blinking red light, during the examination [3].

Confocal laser scanning microscopy (HRTII + RCM, Heidelberg Engineering GmbH, Germany)

The technique developed by Webb [26] (scanning laser ophthalmoscope) was further developed and expanded with the use of the commercially available instrument Heidelberg Retina Tomograph II (HRT II), (Heidelberg Engineering GmbH, Germany) [28]. The HRT II combined with an anterior segment adapter (Rostock Cornea Module) [22, 24] provides the opportunity to visualise corneal cell layers with high acuity [23]. Thus the distance between superficial epithelial cells and endothelial ones can be investigated. The front lens is coupled to the cornea via a polymethylmethacrylate (PMMA) cup with interposition of transparent gel (Vidisic ^{TM}, Mann Pharma Germany) for *in vivo* imaging. During the measurement the test person fixates a light source with the uninvolved eye. During the measurement a camera helps control whether the laser beam points onto the correct spot of the cornea.

With each instrument at least three successive measurements were performed on each eye, and the resulting mean value was calculated. All measurements were performed by one examiner. In order to evaluate the precision of the instruments, the standard deviation of 10 successive measurements on a phakic eye was determined by one examiner. The different measurement data were evaluated by means of the Wilcoxon-matched-pairs-signed-rank-test. The significance level was set to 0.05, which means that p-values smaller than 0.05 are statistically significant. The Bland-Altman plot was used to reveal a relationship between the differences and averages. With this analysis systematic or proportional biases and possible outlier can be illustrated. The differences between two methods are plotted against the averages of two methods [4]. The statistical analysis was performed with the help of the software MatLab 6.5 (The MathWorks, Inc.).

Results

The median of the corneal thickness (CT) of the 50 investigated phakic eyes was 536µm (minimum = 438µm – maximum = 621µm) with Orbscan II and 522µm (450µm – 592µm) using the AC-Master (Table 1). The difference of 14µm between the median of Orbscan II and AC-Master was the smallest median-difference within this study. With the Pentacam the highest CT-values were measured (median = 550µm; minimum = 473µm;

maximum = 653µm) (Figure 1). The median of the corneal thickness using slit-lamp pachymetry by Jaeger was 500µm (440µm – 547µm). The difference between the median measured by the instruments Pentacam and slit lamp were 50µm, the biggest method-dependent difference. In this study, the statistically difference between all used non-contact-methods from each other was significant. ($\alpha = 0.05$, Wilcoxon).

	mean	median	maximum	minimum	precision
Jaeger	498	500	547	440	±14
Pentacam	557	550	653	473	±6.1
AC-Master	527	522	592	450	±1.7
Orbscan II	542	536	621	438	±8.9

Table 1: Overview of the investigated statistical parameter [µm]

The Bland-Altman analysis demonstrates that slit-lamp pachymetry by Jaeger measured the smallest corneal thickness compared to the three other methods (Figure 2). The deviation between Jaeger and the other methods rose in thicker corneas. The Bland-Altman analysis demonstrates that the deviation between Pentacam and AC-Master tended to rise in thicker corneas. The deviation between Orbscan II and Pentacam tended to remain constant. As in the other cases, the deviation between Orbscan II and AC-Master rose in thicker corneas too.

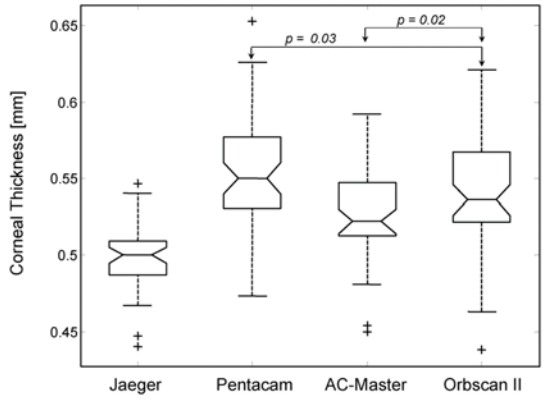

Fig. 1 The boxplots of CT measurements with slit-lamp pachymetry by Jaeger, Orbscan II, Pentacam and AC-Master illustrate median, 25% and 75% quantile, minimum and maximum.

In the direct comparison between Confocal Laser Scanning Microscopy and AC-Master there was no significant difference (Wilcoxon). The median values of the central corneal thickness for CLSM was 560µm (range 537µm - 589µm; mean: 563.6µm) and 546µm for the AC-Master (range 524µm- 576µm; mean: 552.4µm). In the Bland-Altman analysis the mean difference between both methods was 10 µm (figure 3). This mean difference between the AC-Master and CLSM tended to be constant in thick and thin corneas.

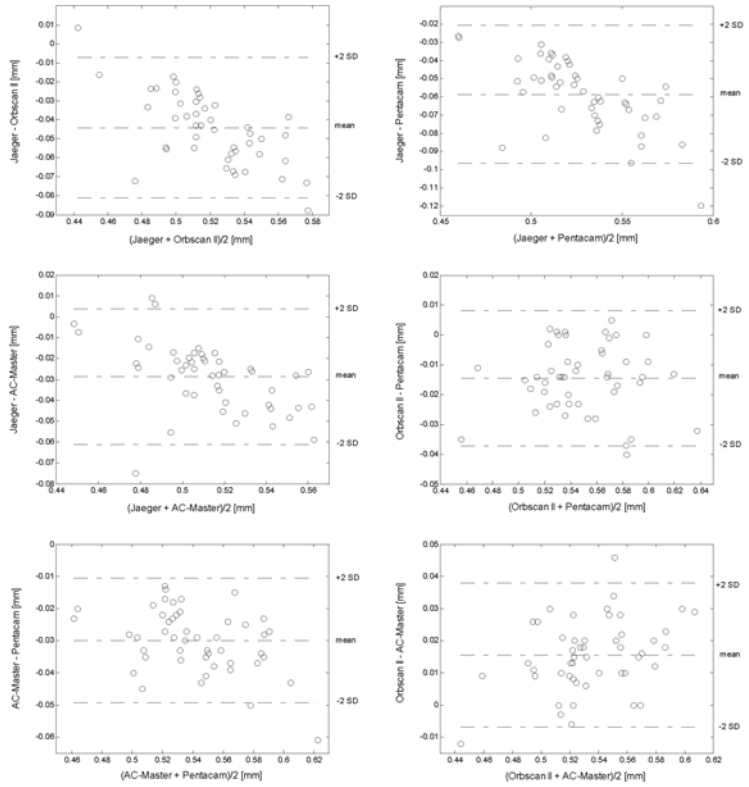

Fig. 2 Bland-Altman plots demonstrating means and differences of measurements with slit-lamp pachymetry by Jaeger, Orbscan II, Pentacam and AC-Master. The mean ±tw o standard deviations (SD) are illustrated as dotted lines.

To evaluate the precision of the five methods, 10 measurements were done with each instrument. All measurements were performed by one examiner on one phakic eye. During the determination of precision of CLSM another reference eye was used and therefore, the data are not directly comparable with the other four methods. The quality factor for the precision is the standard deviation (std) as shown in Figure 4. The smallest deviation from the mean value (515µm) was determined during the CT-measurement using the AC-Master (std = ±1.7µm). The standard deviation of Orbscan II was ±8.9µm (mean value = 524.4µm), of Pentacam ± 6.1µm (mean value = 537.5µm) and the one of CLSM ±6.0µm (mean value = 569.4µm). The slit-lamp pachymeter by Jaeger proved to be at the last rank of precision among tested instruments (std = ±14µm; mean value = 485µm).

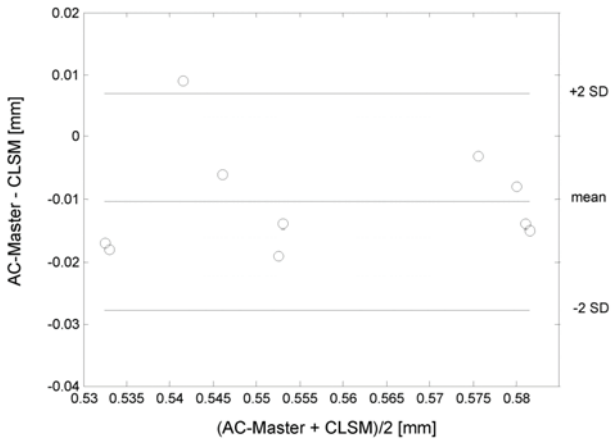

Fig. 3 Bland-Altman plot illustrates the mean difference between AC-Master and CLSM. The mean ±two standard deviations (SD) are pictured as dotted lines.

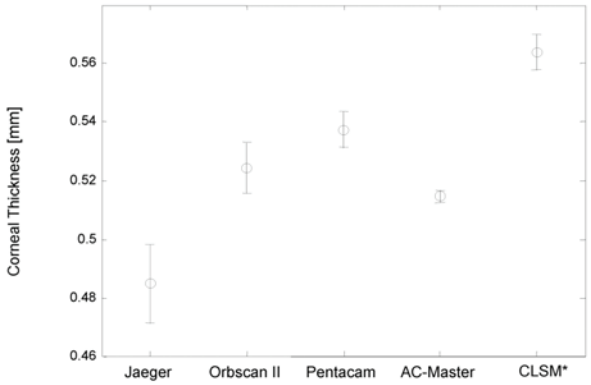

Fig. 4 To demonstrate the precision, means (o) and standard deviations (I) are pictured. The precision was investigated by one examiner on one phakic eye. (* another reference eye, i.e. that the mean is not directly comparable)

Discussion

The investigated methods permit a determination of corneal thickness, but the methods Pentacam, Orbscan II, Jaeger und AC-Master differ significantly from each other. Only between the AC-Master and CLSM there tends to be no difference. The results might differ due to measuring principles inherent to the system, experience of the examiner and compliance of the patient. At this point it is difficult to say which method comes closest to the actual corneal thickness value. Pentacam generally measured the largest corneal thickness values and the slit-lamp pachymeter the smallest. The instruments Orbscan II and AC-Master took a centre position with regard to the determined CT-values. Because the difference between slit-lamp pachymetry by Jaeger and the other methods (Orbscan II, AC-Master and Pentacam) increased with increasing corneal thickness, we must assume proportional error.

When comparing the pairs AC-Master - Pentacam and Orbscan II - AC-Master these biases tend to exist as well. In the Bland-Altman analysis of Orbscan II and Pentacam a systematic error tends to be apparent.

The comparison between the CLSM and AC-Master resulted in a mean-difference of 10µm, which tended to be insignificant (n = 10). With the help of the Bland-Altman-plot of both methods a systematic error can be assumed. A study with larger falling numbers is planned to prove these results.

Regarding the repeatability, one can say that Orbscan II, Pentacam, CLSM and especially the AC-Master are very precise instruments for measuring the corneal thickness. According to Marsich et al., Orbscan II is more repeatable than ultrasound [15]. In this study, as well as in Drexler et al., the partial coherence interferometry (PCI ~AC-Master) is the most precise method of all [10]. Also in the comparison between PCI, ultrasound and Orbscan system by Rainer et al. the PCI is the method with the least intraobserver or interobserver variability [21]. The slit-lamp pachymeter by Jaeger as analogue optical measurement procedure has the least repeatability.

The advantages of the non-contact methods are that there is no need for anaesthesia and no risk of corneal infection. Unlike with contact methods, an influence on the tear film or the cornea respectively, does not occur.

In the clinical routine the precise measurement of corneal thickness plays an important role especially with regard to refractive surgery and treatment of glaucoma. In refractive surgery CT measurement is important to disqualify patients with thin corneas to minimize the risk of ectasia and to evaluate the outcome of laser refractive surgeries [14, 25]. When treating glaucoma the central corneal thickness (CCT) must be considered, because intraocular pressure measurements are dependent on the CCT. Thin corneas produced underestimations of the intraocular pressure, whereas thick corneas produced overestimations [27]. In the Dresden table of correction values these relationships taken into accounted. For 25µm deviation per 550µm the IOD is corrected by ±1 mmHg [8].

Jaeger and CLSM are less suited for clinical use, but CLSM is an excellent method to visualise corneal cell layers with high acuity. Slit-lamp pachymetry by Jaeger allows only a rough estimation of the corneal thickness due to scale gradations. Orbscan II and Pentacam are very convenient techniques for the patient. Only one measurement is necessary to evaluate the central CT, the thinnest part of the cornea, and some values in the periphery. Those are presented as a profile map of the cornea. The AC-Master requires a relatively high level of experience in the use of the instrument and a high degree of patient compliance. Nevertheless, the AC-Master produces extremely precise measurements of the CT at the anatomic or optical axis. No significant difference was found in the thickness determination between AC-Master and CLSM.

References

1. Augustin A.J. Augenheilkunde, 2. Edition, Springer
2. Barkana Y, Gerber Y, Elbaz U, Schwartz S, et al. Central corneal thickness measurement with the Pentacam Scheimpflug system, optical low-coherence reflectometry pachymeter, and ultrasound pachymetry. J Cataract Surg. 2005 Sep ;31(9):1729-35.
3. Bausch &Lomb, www.bausch.com
4. Bland JM, Altman DG. Measuring agreement in method comparison studies. Stat Methods Med Res. 1999 Jun;8(2):135-60.
5. Cairns G, Collins A, McGhee CN. A corneal model for slit-scanning elevation topography. Ophthalmic Physiol Opt. 2003 May;23(3):193-204.

6. Cennamo G, Rosa N, La Rana A, et al. Non-contact tonometry in patients that underwent photorefractive keratoectomy.Ophthalmologica 1997;211:341-343
7. Chatterje A, Shah S, Bessant DAR, et al. Reduction in intraocular pressure after excimer laser photorefractive keratectomy. Correlation with pre-treatment myopia. Ophthalmology 1997;104:355-359
8. Dresdner Korrekturtabelle, http://augen.uniklinikum-dresden.de
9. Drexler W, Baumgartner A, Findl O, et al. Biometric investigation of changes in the anterior eye segment during accommodation. Vision Res. 1997;37:2789-2800
10. Drexler W, Baumgartner A, Findl O, Hitzenberger CK, Sattmann H, Fercher AF. Submicrometer precision biometry of the anterior segment of the human eye. Invest Ophthalmol Vis Sci. 1997 Jun;38(7):1304-13.
11. Eckard A, Stave J. Guthoff R (2006) In vivo Investigations of the corneal epithelium with a confocal laser scanning microscope. Cornea, 25(2):127-31.
12. Fercher AF, Mengedoht K, Werner W. Eye-length measurement by interferometry with partially coherent light. Opt Lett. 1988;13:186-188
13. Haag-Streit Herstellerinformationen, Tiefenmessung an der Spaltlampe 900®
14. Kawana K, Tokunaga T, Miyata K, Okamoto F, Kiuchi T and Oshika T. Comparison of corneal thickness measurements using Orbscan II, non-contact specular microscopy, and ultrasonic pachymetry in eyes after laser in situ keratomileusis. Br J Ophthalmol. 2004 Apr;88(4):466-8.
15. Marsich MW, Bullimore MA. The rereatability of corneal thickness measures. Cornea 2000; 19:792-5
16. Masters BR, Bohnke M. Three-dimensional confocal microscopy of the human cornea in vivo. Ophthalmic Res 33(3):125-35 (2001)
17. Masters BR, Farmer MA. Three-dimensional confocal microscopy and visualization of the in situ cornea. Comput Med Imaging Graph. 17(3):211-9 (1993)
18. www.onjoph.com/Onjoph/AdM0001/Goldma nn%2520ApplanationKorrekturbody.htm
19. Oculus, www.oculus.de
20. Petroll WM, Cavanagh HD, Jester JV. Clinical confocal microscopy. Curr Opin Ophthalmol 9:59-65. (1998)
21. Rainer G, Findl O, Petternel V, Kiss B, Drexler W, Skorpik C, Georgopoulos M, Schmetterer L. Central corneal thickness measurements with partial coherence interferometry, ultrasound, and the Orbscan system. Ophthalmology. 2004 May;111(5):875-9
22. Stachs O, Zhivov A, Kraak R, Stave J, Guthoff R. In vivo three-dimensional confocal laser scanning microscopy of the epithelial nerve structure in the human cornea. Graefes Arch Clin Exp Ophthalmol. 2006 Aug 29; PMID: 16941142
23. Zhivov A, Stachs O, Kraak R, Stave J, Guthoff RF. In vivo confocal microscopy of the ocular surface. Ocul Surf. 2006 Apr;4(2):81-93.
24. Stave J, Zinser G, Grummer G, Guthoff RF [Modified Heidelberg Retinal Tomograph HRT. Initial results of in vivo presentation of corneal structures] Ophthalmologe. 2002 Apr;99(4):276-80.
25. Vinciguerra P, Camesasca FI. Prevention of corneal ectasia in laser in situ keratomileusis. J Refract Surg. 2001 Mar-Apr;17(2 Suppl):S187-9.
26. Webb R H, Hughes G W and Delori FC. Confocal scanning laser ophthalmoscope Appl. Opt. 26:1492–9 (1987)
27. Whitacre MM, Stein RA, Hassanein K. The effect of corneal thickness on applanation tonometry. Am J Ophthalmol. 1993 May 15;115(5):592-6.
28. Zinser G, Harbarth U, Schröder H. Formation and analysis of three-dimensional data with the Laser Tomographic Scanner (LTS). Nasemann JE, Burk ROW (eds) Scanning Laser Ophthalmoscopy and Tomography, Quintessenz Verlag, München, pp 243-252, 1990

Invest Ophthalmol Vis Sci., submitted 1

An ex vivo model for drug-induced secondary cataract prevention

Experimental results with Disulfiram, Methotrexate and Actinomycin D

Katrin Sternberg[1,*], Thom Terwee[2], Oliver Stachs[3], Hanka Schneider[3], Rudolf Guthoff[3], Sven Kramer[1], Marian Löbler[1], Gerhard Hennighausen[4], Detlef Behrend[1], Klaus-Peter Schmitz[1]

University of Rostock, 18057 Rostock, Germany, [1]Institute for Biomedical Engineering, [3]Department of Ophthalmology, [4]Institute for Experimental Pharmacology,

[2]AMO Groningen BV, Van Swietenlaan 5, 9728 NX Groningen, Netherlands

Purpose: Secondary cataract formation may occur after lens replacement due to proliferation and transformation of lens epithelial cells. A clinical approach to prevent secondary cataract by inhibition or removal of lens epithelial cells involves the intraocular application of pharmacological agents. The goal of our study was to develop an ex vivo model that can be utilized to test for the effectiveness of pharmacological agents for the ablation of lens epithelial cells from the basal membrane.

Methods: Cultured human capsular rhexis specimens from standard cataract surgery were used for these experiments. For the evaluation of the cell inhibitory and detaching potential of drugs the culture medium was replaced by different drug solutions. The specimens were incubated with these solutions for 5 minutes. The model drugs Disulfiram, Methotrexate and Actinomycin D were dissolved in pure water or were embedded in the hyaluronic acid in a drug concentration of 10µmol/l. After drug treatment the total number of residual cells on the surfaces of capsular rhexis specimens was assessed by use of microscopic methods. The residual viable and dead lens epithelial cells were differentiated by use of the Live-dead assay. Quantification of the lens epithelial cells was facilitated by staining with Hoechst-dye.

Results: An ex vivo model was established which allows for the differentiation of drug action on lens epithelial cell ablation from the basal membrane. To estimate the effectiveness of drugs it was necessary to determine the cell numbers of untreated capsular rhexis specimens. The Live-dead assay on untreated capsular rhexis specimens has shown 1361 +/- 482 viable cells/mm2. The treatment with Disulfiram, Methotrexate or Actinomycin D reduced the number of viable cells on capsular rhexis specimens drastically, because it ranges between 0.44 +/- 0.53 % (6.0 +/- 7.3 cells/mm^2) for Disulfiram, 0.27 +/-0.50 % (3.7 +/- 6.9 cells/mm^2) for Methotrexate and 0.07 +/- 0.19 % (0.1 +/- 0.27 cells/mm^2) for Actinomycin D. Of the three tested drugs Actinomycin D was slightly more potent in cell ablation than Disulfiram and Methotrexate.

Conclusions: The screening of drugs in the described ex vivo model can help to reduce the number of preclinical studies for secondary cataract prevention. Furthermore, a safe drug application can be achieved by using hyaluronic acid as a hydrophilic polymeric carrier.

Introduction

The most frequent complication of cataract-intraocular lens surgery is the posterior capsule opacification (PCO, also called secondary cataract or after cataract). A variety of studies has led to a better understanding of the pathogenesis of PCO caused by postoperative proliferation, migration, and transdifferentiation of lens epithelial cells (LECs) left on the anterior capsule and the equatorial region of the capsular bag at the time of cataract surgery [1,2]. There are recent attempts to restore accommodation with various complex implant designs for intra capsular bag placement (e.g. 1CU (Human Optics), Crystalens (Eyeonics), Synchrony (Visiogen)). They all relay on stable capsular bag biomechanics. This can only be maintained when there is no proliferation of remaining lens epithelial cells on the inner surface of the capsular bag. A permanent and successful restoration of accommodation will be possible when we find ways to fully prevent migration and fibrosis of lens epithelial cells [46].

PCO has been observed since extracapsular cataract surgery started and was noticed by Sir Harold Ridley after his first intraocular lens (IOL) implantations [3,4]. Today PCO is still the most frequent complication after extracapsular cataract surgery. A meta-analysis, published in 1998 [5], showed that the PCO rates after extracapsular cataract surgery combined with intraocular lens implantation increased from 11.8 % after one year to 20.7 % after three years to 28.4 % after five years [5]. Furthermore PCO is a major problem in paediatric cataract surgery with an incidence approaching 100 % [6,7].

Development of modern cataract surgery causing minimal trauma has lead to a gradual decrease in the incidence of PCO. At present, with modern techniques and IOLs the expected rate of PCO and the subsequent Nd:YAG laser posterior capsulotomy rate has dropped to below 10% [8,9]. To further reduce PCO the surgical performance has been improved by hydrodissection enhanced cortical cleanup [10] and the in-the-bag (capsular) fixation [11,12]. In addition the IOL has been improved by enhancing its biocompatibility [13], improving the maximal IOL optic-posterior capsule contact [14] and exploiting the barrier effect of the IOL optic by sharp optic edge designs [15-17].

Another approach to prevent PCO involves the intraocular application of pharmacological agents [18,19]. For the 1980s, numerous investigators like Hartmann et al. [20,21] examined in cell culture studies the potential of pharmacological substances in order to successfully prevent LECs from proliferating and migrating. Pharmacologic agents that have been investigated include cytostatic drugs, such as 5-Fluorouracil [22,23], Daunomycin [20], Colchicine, Doxorubicin [24], Mitomycin C [22,25], Methotrexate [26]), anti-inflammatory substances, such as Dexamethasone [27] and Diclofenac [27,28], calcium-channel blockers, such as Mibefradil [29], and immunological agents, such as Cyclosporine A [30]. In addition adhesion inhibitors [31] and osmotic effective solutions [23] were tested. In several studies different drug delivery systems [32-35] were investigated in order to provide a longer and more effective impact on LECs. To avoid toxic side effects an irrigation device may allow for the isolated safe delivery of pharmacologic agents into the sealed capsule following cataract surgery [23,36,37].

The goal of the current study was to develop an ex vivo model by utilizing human capsular rhexis specimens obtained during standard cataract surgery that can be tested for the ablation of LECs from the basal membrane. Since capsular rhexis specimens contain a LEC layer on its natural substrate, the basal membrane, an effective cell ablation method established in the ex vivo model should also be effective in vivo.

To test the suitability of the model to differentiate drug effects on LECs of the capsular bag three pharmacological compounds known for their antiproliferative activity, Disulfiram, Methotrexate and Actinomycin D were tested for their effect on LEC ablation. Disulfiram, chemically tetraethylthiuramdisulfide (TETD), and its primary metabolite diethyldithiocarbamate are known to have in vitro antiproliferative effects on tumor cells [38], and inhibit several enzymes and cell proteins by formation of a metal complex or by reaction

with functional sulfhydryl-groups. In addition it has been shown that a topical ocular drug delivery system containing TETD has anticataract effects in vivo on selenite-treated rats [39].

Methotrexate (MTX) is an antimetabolite drug used in treatment of cancer and autoimmune diseases. It acts by inhibiting the metabolism of folic acid. Based on research efforts in cancer chemotherapy, Hansen and co-workers [26] have found that a conjugate of MTX with an antibody specific for basement membrane collagen in the lens capsule is an effective inhibitor of LEC outgrowth in cell culture.

Actinomycin is any of a class of polypeptide antibiotics isolated from soil bacteria of the genus Streptomyces. As chemotherapeutic drug Actinomycin D (AM) intercalates into DNA, thereby interfering with the action of enzymes engaged in replication and transcription. Therefore it could be also an effective inhibitor of LEC viability [45].

All these drugs interfere with vital cellular processes and might cause cell ablation from the basal membrane by reducing cell viability.

Material and Method

Materials

Disulfiram (tetraethylthiuramdisulfide, TETD, M = 296 g/mol), Methotrexate (MTX, M = 454.4 g/mol) and Actinomycin D (AM, M = 1255.4 g/mol) were obtained from Sigma-Aldrich Chemie GmbH (Taufkirchen, Germany). Stock solutions of 1 x 10^{-1} mol/l (M) TETD or AM in ethanol and of 1 x 10^{-1} M MTX in dimethylsulfoxide were prepared, which were further diluted with pure water to 10 µM TETD, MTX or AM (corresponding to a non-toxic concentration of the organic solvent of 0.01 %, [28]). Pure water was obtained by purification with an ion exchange resin (Typ Ultra clear UV plus, SG-Wasseraufbereitung und Regenerierstation GmbH Hamburg-Barsbüttel, Germany). Ethanol and dimethylsulfoxide were received in analytical grade purity from VWR International GmbH (Darmstadt, Germany). The substance hyaluronic acid sodium salt (HA) was supplied by Advanced Medical Optics Uppsala AB (Uppsala, Sweden). HA was dissolved in pure water or in the 10 µM drug solutions (10 µM drug/HA) to yield a concentration of 1 % (w/w).

Capsular rhexis specimens obtained during standard cataract surgery were immediately placed into reaction tubes containing Dulbecco's modified Eagle medium (DMEM, Applichem, Darmstadt, Germany). The specimens were approximately circular with a diameter of about 4 mm. Informed consent was obtained from all patients. Procedures utilizing human capsular rhexis specimens followed the tenets of the Declaration of Helsinki (Cardiovascular Research 1997;35:2-4), and the protocol was approved by the Ethics Committee of the Medical School, University of Rostock.

Capsular rhexis specimens were cultured in DMEM supplemented with 10 % fetal calf serum (FCS, Biochrom, Berlin, Germany), 50 µg/ml Gentamycin (Sigma, Steinheim, Germany) and 2,5 µg/ml Amphotericin B (PAA Laboratories, Cölbe, Germany). Phosphate buffered saline (PBS) (PAA Laboratories) was used for rinsing of the specimens.

Classification and culture of capsular rhexis specimens

Within two hours of removal the capsular rhexis specimens were placed into 12-well plates with one milliliter of culture medium (see Materials). The initial state of the specimens was assessed by light microscopy (see Microscopy). All specimens were classified according to the density of LECs on the capsular bag: 0 - no cells observed, 1 – less than 33 % of the specimen covered by LECs, 2 – 33 % to 66 % of the specimen surface covered by LECs, 3 – 66 % to 100 % of the specimen surface covered by LECs. Only specimens of category 3 (more than two thirds of the specimen is covered with LECs) were used immediately for the ex vivo tests.

Microscopy

Light microscopic evaluation was carried out using a Nikon ECLIPSE TE300 microscope equipped with a Nikon Epi-Fluoresence and Hoffman contrast modulation module. Digital

acquisition of the images was done using a color video camera (Sony Progressiv 3CCD DXC 9100P) in conjunction with Software Image Archive Version 4.10.

In addition the capsular rhexis surface was examined with an environmental scanning electron microscope (Philips XL 30 ESEM with Philips Electron Optics, Eindhoven, The Netherlands) operating in the SEM mode. For SEM the specimens were freeze dried and sputtered with gold. The morphology of an untreated capsular rhexis specimen is seen exemplarily in Figure 1.

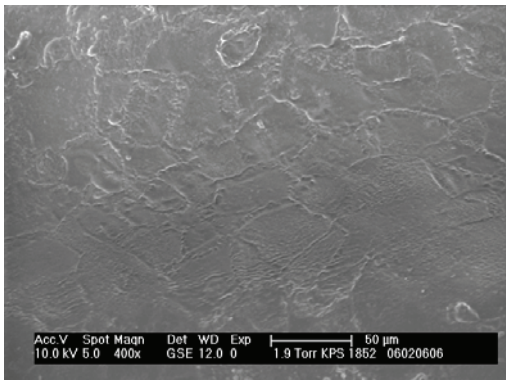

Fig. 1: Scanning electron microscopy (SEM) of an untreated capsular rhexis specimen (initial state with category 3), bar: 50 µm.

Drug treatment of the rhexis specimens

For treatment of capsular rhexis specimens the culture medium was replaced by drug solution and specimens were incubated for 5 minutes at room temperature. Capsular rhexis specimens were incubated in 1) 10 µM TETD/pure water, 2) 10 µM MTX/pure water, 3) 10 µM AM/pure water, 4) 10 µM TETD/HA, 5) 10 µM MTX/HA, 6) 10 µM AM/HA, and 7) HA. After the 5 minutes incubation the drug solution was removed and the specimens were rinsed twice with PBS. Subsequently the specimens were stained with the Live-dead assay and with Hoechst 33342 (see Staining methods).

For the treatment of the capsular rhexis specimen with the viscous HA solutions a self-developed two-partite test chamber was used. Within the lower half of the chamber a glass micrometer scale is inserted onto which the capsular rhexis specimen is placed within a drop of PBS, cells facing up. The upper half of the chamber carries a gauze to hold the specimen in place and to allow for the application of HA solutions and rinsing of the specimen before staining (Fig. 2A-B).

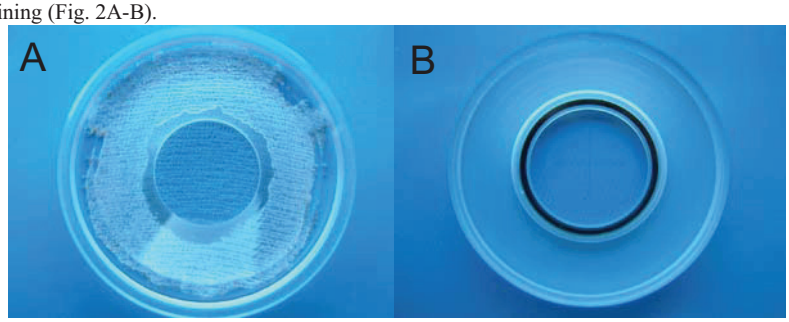

Fig. 2: Upper half (A) and ower half (B) of the test chamber.

Staining methods

The LEC viability was determined with the Live-dead assay (Molecular Probes, Leiden, Netherlands) [40]. This assay differentiates vital from dead cells. Non-fluorescent Calcein AM permeates the plasma membrane and is metabolized by intracellular esterases to yield green fluorescent Calcein. EthD-1 cannot pass the membrane of vital cells and only binds to the DNA of dead cells yielding red fluorescent nuclei.

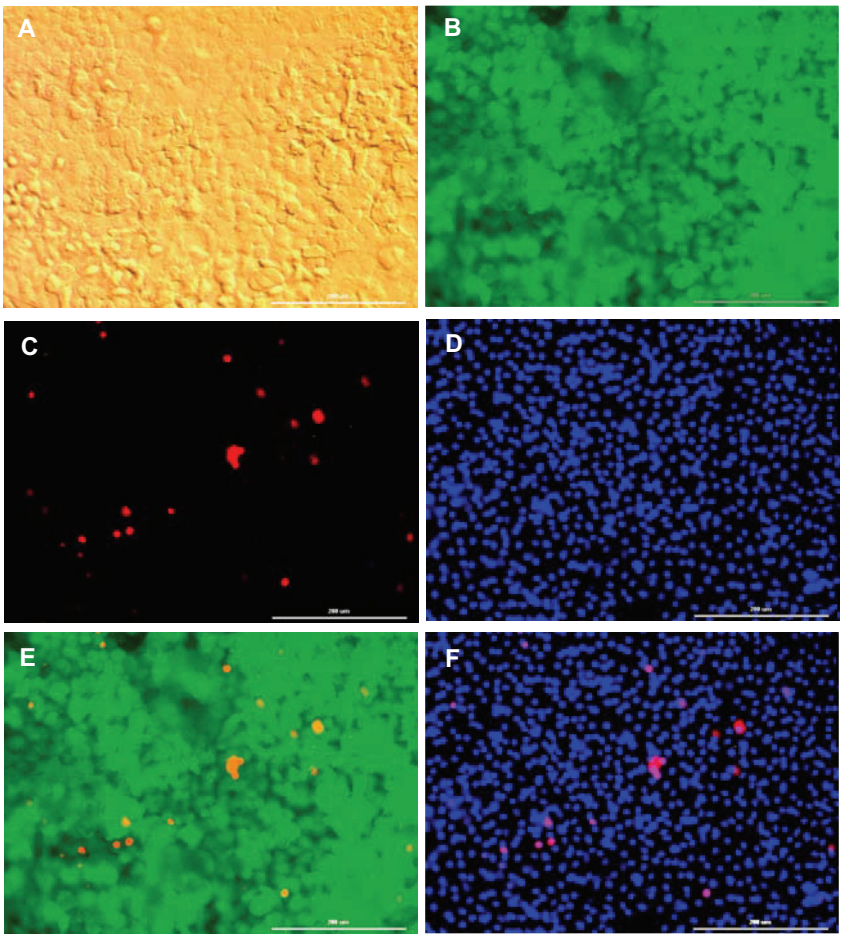

Fig. 3: A - bright field, B-F - fluorescence microscopy, of an untreated capsular rhexis specimen (initial state with category 3), bar: 200 µm. A – bright field; B – Calcein staining (green: viable LECs); C – EthD-1 staining (red: cell nuclei of dead LECs); D – Hoechst 33342 staining (blue: cell nuclei of all LECs); E – superimposed images of the Calcein/EthD-1 staining; F – superimposed images of Hoechst 33342/EthD-1 staining

For easier quantification of cells nuclear DNA was stained with Hoechst 33342 (Fluka, Taufkirchen, Germany) [41]. This dye specifically binds to DNA and stains the nuclei of vital and dead cells. The labeled nuclei fluoresce bright blue. After three washes with PBS the

rhexis specimens were incubated in 500 µl of Calcein AM and EthD-1 incubated for 40 minutes at room temperature and then rinsed three times with PBS.

Subsequently the specimens were incubated for 2 minutes at room temperature in 500 µl of 10 µg/ml Hoechst 33342. Then the reagent was replaced by a drop of PBS and cover-slips were placed over the specimens for microscopic examination. Bright field (Fig. 3A) and fluorescence photomicrographs (Figs. 3B-F) were taken.

Quantitative evaluation

In addition to the strictly qualitative description obtained from light microscopic evaluation, a quantitative assessment (cell count) was performed on the samples in their initial state and after drug treatment. Cell counting was done by superimposing the images of the Calcein/EthD-1 (Fig. 3E) and the Hoechst 33342/EthD-1 staining (Fig. 3F). All nuclei (blue) and nuclei of dead cells (red) were counted for each field of view. All cell numbers are expressed as cells/mm^2.

Statistical analysis

Data were analyzed using Microsoft Excel calculation software. Mean values and standard errors were calculated from 10 individual capsular rhexis specimens. To test whether observed differences between drug treatments were statistically significant a Student t test with $p < 0.05$ was applied to the data.

Results

For the evaluation of the capsular rhexis specimen quality the initial state of the specimens was characterized and classified (cell density categories 0-3). Only specimens with a cell density of at least 66 % (category 3) were chosen for the experiments.

To estimate the success of the drug treatment it was necessary to determine the cell numbers of untreated capsular rhexis specimens. The Live-dead assay on untreated capsular rhexis specimens has shown mostly viable cells with occasional dead cells (Fig. 4). The number of viable cells ranges between 840 and 2542 (1361 +/- 482) LECs/mm2. The photographs of Figure 3 (3B, C and F) show a typical Live-dead assay of an untreated capsular rhexis specimen.

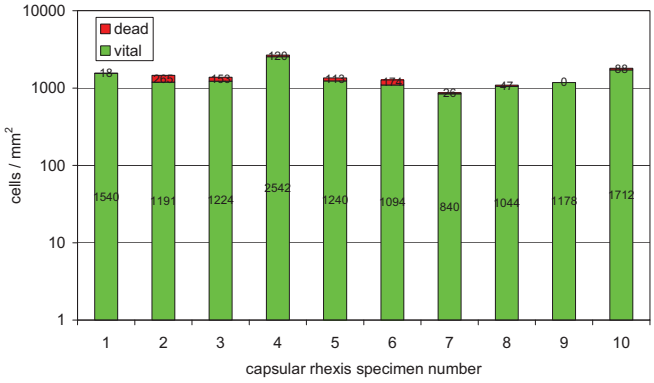

Fig. 4: Results from cell viability assessments of 10 untreated capsular rhexis specimens as logarithmic diagram (each bar represents one specimen).

To evaluate the cell inhibitory and detaching potential of drugs in the ex vivo model the pharmacological agents TETD, MTX and AM were tested in a first experimental series as

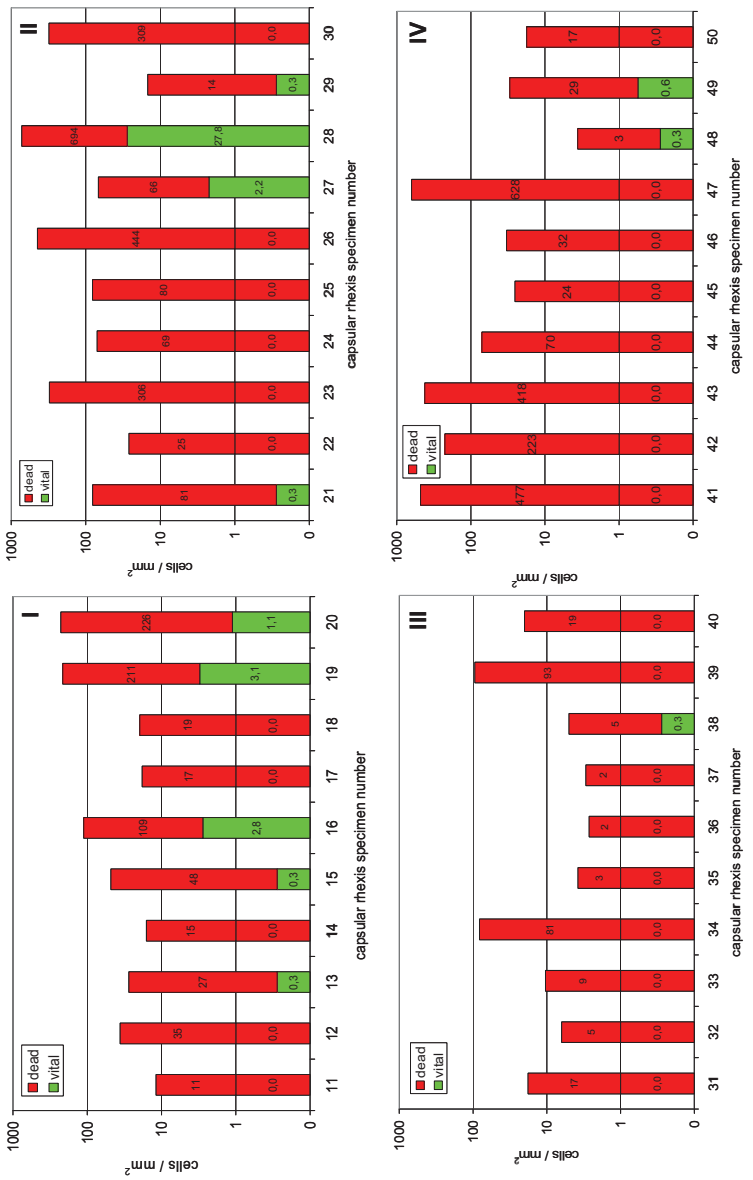

Fig. 5: Results from cell viability assessments of capsular rhexis specimens (each bar represents one specimen) incubated with 10 µM drug/pure water for 5 minutes as logarithmic diagram. (I: TETD/pure water; II: MTX/pure water; III: AM/pure water; IV: pure water)

aqueous solutions. The temporal window of 5 minutes for drug treatment was chosen to match clinical requirements. The quantitative data for 10 capsular rhexis specimens expressed as number of residual viable (green) and dead (red) LECs after the different drug treatments are shown in the logarithmic diagrams (Fig. 5). The exemplary photographs (Fig. 6) reflect the Live-dead assays of treated capsular rhexis specimens from each group with the most viable cells (qualitative data).

In comparison to the initial state (Fig. 4) the treatments with 10 µM TETD, MTX and AM reduce the number of viable LECs by ablation drastically (Fig. 5). Immediately after the TETD treatment some viable LECs (up to 3.1 cells/mm²) could still be seen on the capsular rhexis specimens (Fig. 5I).

AM dissolved in pure water is more effective in ablation of LECs than TETD. After treatment with AM only in one case 0.3 cells/mm^2 were observed (Fig. 5III). In all other experiments no viable cells were detected (Fig. 6III). In contrast, the treatment with MTX was less effective than with AM, because in one case a high number of viable LECs (28 LECs/mm^2) was found after incubation with aqueous MTX. This aspect indicates the limits of variation of the biological donor material.

To determine the pure water-induced cellular damage and ablation by hypotonic shock pure water was examined as reference (Fig. 5IV). The high impact in terms of cell death and cell ablation by the use of pure water was similar to the effects observed with AM dissolved in pure water. The treatments with TETD and MTX were less effective than the treatment with pure water.

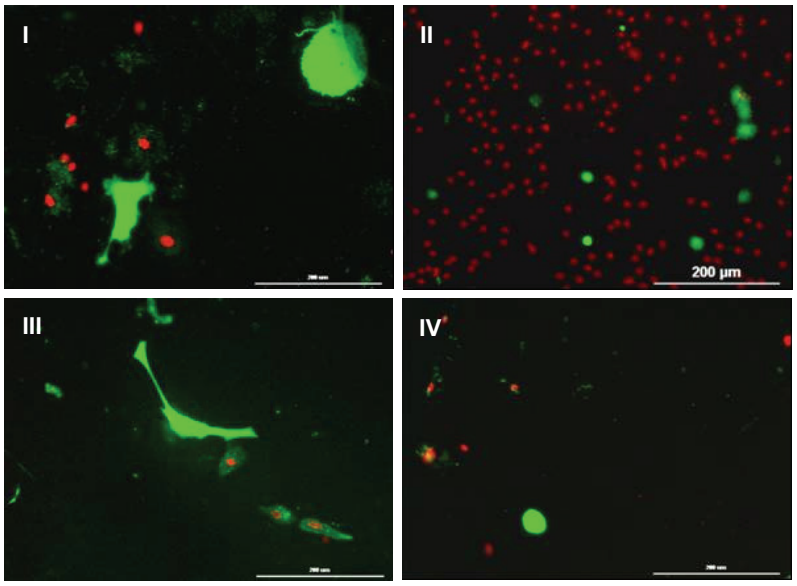

Fig. 6: Fluorescence microscopy (superimposed images of the Calcein/EthD-1 staining) of capsular rhexis specimens incubated with 10 µM drug/pure water for 5 minutes, bar: 200 µm. (I: TETD/pure water (specimen number: 19); II: MTX/pure water (specimen number: 28); III: AM/pure water (specimen number: 38); IV: pure water (specimen number: 49))

For a safe drug application 10 µM TETD, MTX and AM were embedded in 1 % hyaluronic acid sodium salt (HA) as viscoelastic, hydrophilic drug carrier and their actions were studied in a second experimental series. As reference the drug-free HA dissolved in pure water was tested. From our experiments with the drug-free HA (Fig. 7IV) it became evident

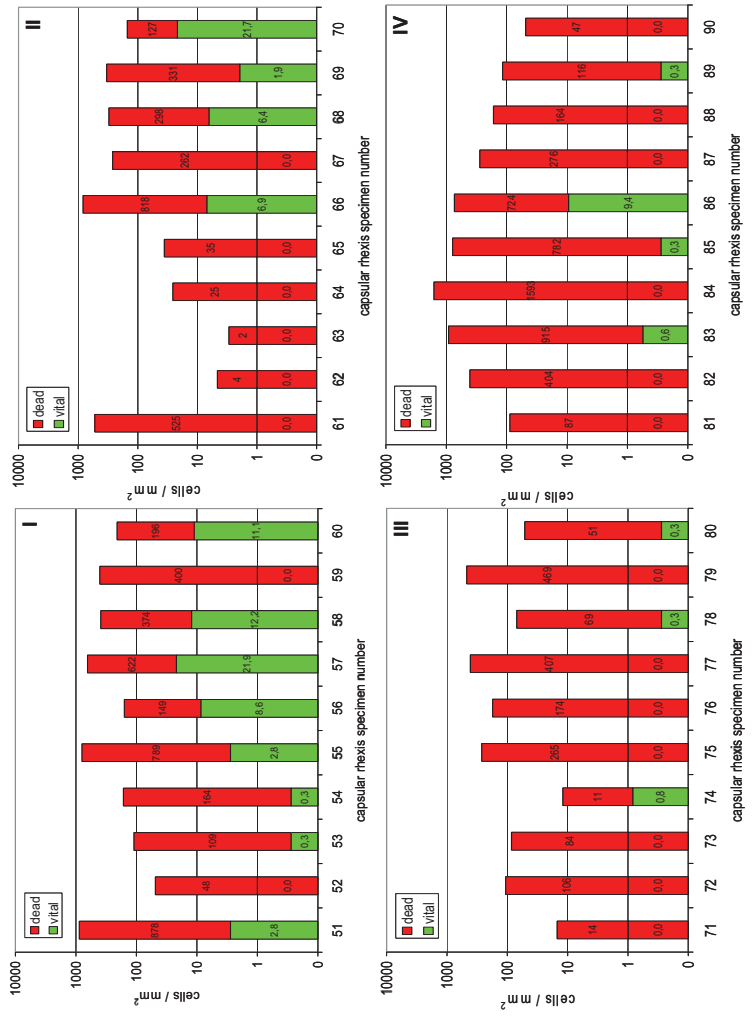

Fig. 7: Results from cell viability assessments of capsular rhexis specimens (each bar represents one specimen) incubated with 10 µM drug/HA for 5 minutes as logarithmic diagram. (I: TETD/HA; II: MTX/HA; III: AM/HA; IV: pure HA)

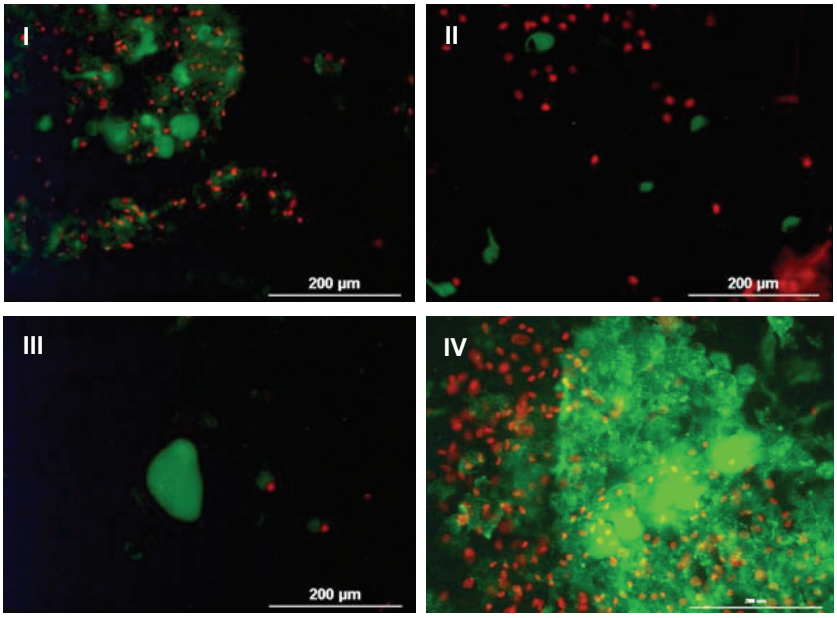

Fig. 8: Fluorescence microscopy (superimposed images of the Calcein/EthD-1 staining) of capsular rhexis specimens incubated with 10 µM drug/HA for 5 minutes, bar: 200 µm. (I: TETD/HA (specimen number: 47); II: MTX/HA (specimen number: 60); III: AM/HA (specimen number: 64); IV: pure HA (capsular bag specimen number: 76))

that HA decreases the number of viable cells considerably, but in comparison to pure water treatment (Fig. 5IV) more LECs stick to the basal membrane of the specimen. In our studies with the drug-loaded HA we have observed that TETD is less effective in HA regarding to LEC ablation, because we have found more viable LECs (up to 21.9 cells/mm^2, Fig. 7I) than in pure HA (up to 9.4 cells/mm^2, Fig. 7IV). Figure 8I demonstrates the existence of viable cells on the surface of capsular rhexis specimens after incubation with TETD/HA.

AM is more effective in HA than TETD, as it causes an important reduction of viable LECs (up to 0.8 cells/mm^2, Fig. 7III). Furthermore by addition of AM into the HA matrix an increase in cell ablation in comparison to the drug-free HA matrix was achieved.

Similar to the obtained results with MTX dissolved in pure water (Fig. 5II) MTX applied in HA was less effective than AM, because a high number of viable LECs (up to 21.7 LECs/mm^2) was found after MTX treatment (Fig. 7II). In addition the treatment with MTX embedded in HA showed a lower effectiveness in cell ablation than the treatment with the drug-free HA.

AM has shown a more potent inhibitory effect than TETD, because a statistically significant difference ($p < 0.05$, Student t test) regarding the number of viable LECs was obtained between the group of capsular rhexis specimens treated with AM/HA when compared with the group treated with TETD/HA (Table 1). However, the differences between MTX and TETD or MTX and AM embedded in HA were not significant ($p < 0.05$, Student t test). In addition no statistically significant differences between TETD, MTX and AM applied in pure water were observed ($p < 0.05$, Student t test).

Table 1: Viable LECs (cells/mm^2, %) after different drug treatments (mean value +/- standard deviation) and statistical comparisons (s. = significant, n. s. no significant) using Student t test with $p < 0.05$.

Drug	Drug treatment	Viable LECs (cells/mm^2)	Viable LECs (%)
TETD	pure water*	0.8 +/- 1.2	0.06 +/- 0.09
TETD	HA**	6.0 +/- 7.3	0.44 +/- 0.53
MTX	pure water*	3.1 +/- 8.7	0.23 +/- 0.64
MTX	HA**	3.7 +/- 6.9	0.27 +/- 0.50
AM	pure water*	0.03 +/- 0.09	0.02 +/- 0.06
AM	HA**	0.1 +/- 0.27	0.07 +/- 0.19

*) drug dissolved in pure water; differences between TETD-MTX n. s., TETD-AM s., MTX-AM n. s.
**) drug embedded in HA; differences between TETD-MTX n. s., TETD-AM n. s., MTX-AM n. s.

In comparison to the number of viable cells in the initial state (1361 +/- 482 cells/mm^2) the tested drugs TETD, MTX and AM reduced the number of viable LECs on the capsular rhexis specimens by more than 99 % (Table 1).

Discussion

Different pharmacological concepts have shown an inhibition of LEC growth and PCO formation [18,19]. As pre-requisite for this success the biological effectiveness of drugs regarding the inhibition of LECs was examined in different in vitro [20,21,24,26,28,29,45] and in vivo animal models, such as in rats [39], rabbits [23,30,42] and monkeys [43]. Furthermore different methods for drug application were tested [25,32,33,35,44, 46]. Irrespective of the drug application the effective local drug concentration must have been adequate to reduce the LEC viability to result in a long-term decrease in PCO. Additionally, the agent-induced LEC ablation plays an important role for the prevention of PCO.

For the evaluation of those pharmacological concepts and with the goal to reduce the number of later preclinical studies the effectiveness of active compounds has to be tested and optimized with experimental models. Therefore we have developed an ex vivo model that utilizes human capsular rhexis specimens obtained from routine cataract surgery. This experimental model allows for the differentiation of the number (quantitative data) and viability (qualitative data) of LECs on the surface of the capsular rhexis specimens.

In relation to PCO prevention by using pharmacological concepts this model was then utilized to test the effects of drugs on LEC viability and on LEC ablation from the basal membrane.

In our studies the non-dissociated model drugs TETD, MTX and AM were diluted with pure water in order to determine the action on LECs. However, while pure water is very efficient in vitro in cytolysis and cell ablation, it is insufficient in vivo, because the PCO appears few weeks postoperatively [23,42,44]. In contrast, antiproliferative drugs, such as 5-fluorouracil [23], were effective in preventing PCO in the same time frame. Thus it appears that a combination of pure water with a pharmacological agent could lead to sustained results in vivo.

Distilled or pure water might cause damage to other ocular cells and tissues. Therefore for a safe drug application in vivo the used model drugs were also embedded in HA as a hydrophilic polymeric drug carrier. We have calculated that the 1 % HA solution contains 25 mM sodium ions whereas in isotonic (0.9 %) sodium chloride solution 154 mM sodium ions are present. Thus the HA solution includes only sixth part sodium ions and could therefore induce cellular damage and ablation. This assumption was confirmed with our ex vivo results (see Results).

Our data show that the established ex vivo model is suitable to examine the drug-induced inhibition of LECs on the surface of the human capsular rhexis specimens. The advantage of our studies in comparison to conventional cell culture studies is that we can also observe the ablation of LECs from their natural substratum, the basal membrane. In summary, of the three tested drugs Actinomycin D was slightly more potent in cell ablation than Disulfiram and

Methotrexate. Furthermore a safe drug application can be achieved by using hyaluronic acid as a hydrophilic polymeric carrier.

The ex vivo model is an option to differentiate the LEC viability and LEC ablation on the human capsular bag after drug treatment. However, further studies regarding the re-proliferation potential of the residual viable LECs after the 5-minutes drug treatment are necessary to determine whether agents, such as AM, could be efficient in long-term PCO preventing in vivo.

Acknowledgements

The authors would like to thank Martina Nerger, Babette Hummel, Andrea Rohde and Carmen Hohmann for expert technical assistance. The authors are furthermore grateful to Prof. Axel Haubold and Prof. Theo van Kooten for helpful notes and suggestions. The work was financially supported by the AMO Groningen BV, Netherlands.

References

1. Apple DJ. Influence of intraocular lens material and design on postoperative intracapsular cellular reactivity. Trans Am Ophthalmol Soc 2000; 98: 257-83.
2. Werner L, Apple DJ, Pandey SK. Postoperative proliferation of anterior and equatorial lens epithelial cells: A comparison between various foldable IOL designs. In: Buratto L, Osher R, Masket S, editors, Cataract Surgery in Complicated Cases. Thorofare, NJ, Slack Inc., 2000; pp 399-417.
3. Ridley H. Long-term results of acrylic lens surgery. Proc R Soc Med 1970; 63: 309-310
4. Ridley H. The origin and objectives of intraocular lenticular implants. Trans Am Acad Ophthalmol Otolaryngol 1976; 81: 65-6.
5. Schaumberg DA, Dana MR, Christen WG, Glynn RJ. A systematic overview of the incidence of posterior capsule opacification. Ophthalmology. 1998;105: 1213-21.
6. Pandey SK, Ram J, Werner L, Brar GS, Jain AK, Gupta A, Apple DJ. Visual results and postoperative complications of capsular bag and ciliary sulcus fixation of posterior chamber intraocular lenses in children with traumatic cataracts. J Cataract Refract Surg. 1999; 25: 1576-84.
7. Pandey SK, Wilson ME, Trivedi RH, Izak AM, Macky TA, Werner L, Apple DJ. Pediatric cataract surgery and intraocular lens implantation: current techniques, complications and management. Int Ophthalmol Clin 2001; 41: 175-96.
8. [Apple DJ, Peng Q, Visessook N, Werner L, Pandey SK, Escobar-Gomez M, Ram J, Auffarth GU. Eradication of posterior capsule opacification: documentation of a marked decrease in Nd:YAG laser posterior capsulotomy rates noted in an analysis of 5416 pseudophakic human eyes obtained postmortem. Ophthalmology. 2001; 108: 505-18.
9. Cheng JW, Wei RL, Cai JP, Xi GL, Zhu H, Li Y, Ma XY. Efficacy of different intraocular lens materials and optic edge designs in preventing posterior capsular opacification: a meta-analysis. Am J Ophthalmol. 2007;143(3):428-36.
10. Fine IH. Cortical cleaving hydrodissection. J Cataract Refract Surg. 1992; 18: 508-12.
11. Ram J, Apple DJ, Peng Q, Visessook N, Auffarth GU, Schoderbek RJ Jr, Ready EL. Update on fixation of rigid and foldable posterior chamber intraocular lenses. Part I: Elimination of fixation-induced decentration to achieve precise optical correction and visual rehabilitation, Part II: Choosing the correct haptic fixation and intraocular lens design to help eradicate posterior capsule opacification. Ophthalmology. 1999; 106: 883-90, 891-900.
12. Apple DJ, Reidy JJ, Googe JM, Mamalis N, Novak LC, Loftfield K, Olson RJ. A comparison of ciliary sulcus and capsular bag fixation of posterior chamber intraocular lenses. J Am Intraocul Implant Soc 1985; 11:44-63.
13. Apple DJ. Intraocular lens biocompatibility (editorial). J Cataract Refract Surg 1992; 18: 217-18.
14. Linnola RJ, Werner L, Pandey SK, Escobar-Gomez M, Znoiko SL, Apple DJ. Adhesion of fibronectin, vitronectin, laminin, and collagen type IV to intraocular lens materials in pseudophakic human autopsy eyes. Part 1: histological sections. Part 2: explanted intraocular lenses. J Cataract Refract Surg. 2000; 26(12): 1792-806, 1807-18.
15. Nishi O, Nishi K, Akura J, Nagata T. Effect of round-edged acrylic intraocular lenses on preventing posterior capsule opacification. J Cataract Refract Surg. 2001; 27: 608-13.
16. Auffarth GU, Golescu A, Becker KA, Volcker HE. Quantification of posterior capsule opacification with round and sharp edge intraocular lenses. Ophthalmology. 2003; 110: 772-80.
17. Kruger AJ, Schauersberger J, Abela C, Schild G, Amon M. Two year results: sharp versus rounded optic edges on silicone lenses. J Cataract Refract Surg. 2000; 26: 566-70.
18. Auffarth GU, Rabsilber TM, Reuland AJ. New methods for the prevention of posterior capsule opacification. Ophthalmologe. 2005 Jun; 102: 579-86.

19. Rabsilber TM, Auffarth GU. Pharmacological means to prevent secondary cataract. Klin Monatsbl Augenheilkd. 2006 Jul;223(7):559-67.
20. Weller M, Wiedemann P, Fischbach R, Hartmann C, Heimann K. Evaluation of daunomycin toxicity on lens epithelium in vitro. Int Ophthalmol. 1988;12(2):127-30.
21. Rieck PW, Kriegsch J, Jaeckel C, Hartmann C. Effect of suramin on proliferation and migration of lens epithelial cells in vitro. Ophthalmologe. 2004;101(1):73-9.
22. Ismail MM, Alio JL, Ruiz Moreno JM. Prevention of secondary cataract by antimitotic drugs: experimental study. Ophthalmic Res. 1996;28(1):64-9.
23. Abdelwahab MT, Kugelberg M, Kugelberg U, Zetterstrom C. After-cataract evaluation after using balanced salt solution, distilled deionized water, and 5-fluorouracil with a sealed-capsule irrigation device in the eyes of 4-week-old rabbits. J Cataract Refract Surg. 2006;32:1955-60.
24. McDonnell PJ, Krause W, Glaser BM. In vitro inhibition of lens epithelial cell proliferation and migration. Ophthalmic Surg. 1988; 19: 25-30.
25. Shin DH, Kim YY, Ren J, Weatherwax AL, Pearlman RB, Kim C, Glover KB, Muenk SB. Decrease of capsular opacification with adjunctive mitomycin C in combined glaucoma and cataract surgery. Ophthalmology. 1998; 105: 1222-6.
26. Hansen TJ, Tyndall R, Soll DB. Methotrexate-anticollagen conjugate inhibits in vitro lens cell outgrowth. Invest Ophthalmol Vis Sci. 1987; 28: 1206-9.
27. Symonds JG, Lovicu FJ, Chamberlain CG. Differing effects of dexamethasone and diclofenac on posterior capsule opacification-like changes in a rat lens explant model. Exp Eye Res. 2006;83:771-82.
28. Cortina P, Gomez-Lechon MJ, Navea A, Menezo JL, Terencio MC, Diaz-Llopis M. Diclofenac sodium and disulfiram A inhibit human lens epithelial cell proliferation in culture. Graefes Arch Clin Exp Ophthalmol. 1997; 235: 180-5.
29. Beck R, Nebe B, Guthoff R, Rychly J. Inhibition of lens epithelial cell adhesion by the calcium antagonist Mibefradil correlates with impaired integrin distribution and organization of the cytoskeleton. Graefes Arch Clin Exp Ophthalmol. 2001; 239: 452-8.
30. Stamer L, Bohnke M, Vogelberg K, Arndt R. Tissue levels of locally applied cyclosporin A in the rabbit eye, Fortschr Ophthalmol. 1989; 86: 540-2.
31. Nishi O, Nishi K, Mano C, Ichihara M, Honda T, Saitoh I. Inhibition of migrating lens epithelial cells by blocking the adhesion molecule integrin: a preliminary report. J Cataract Refract Surg. 1997;23:860-5.
32. Kleinmann G, Apple DJ, Chew J, Hunter B, Stevens S, Larson S, Mamalis N, Olson RJ. Hydrophilic acrylic intraocular lens as a drug-delivery system for fourth-generation fluoroquinolones. J Cataract Refract Surg. 2006;32:1717-21.
33. Siqueira RC, Filho ER, Fialho SL, Lucena LR, Filho AM, Haddad A, Jorge R, Scott IU, Cunha Ada S. Pharmacokinetic and toxicity investigations of a new intraocular lens with a dexamethasone drug delivery system: a pilot study. Ophthalmologica. 2006;220: 338-42.
34. Kim HC, Hartner S, Behe M, Behr TM, Hampp NA. Two-photon absorption-controlled multidose drug release: a novel approach for secondary cataract treatment. J Biomed Opt. 2006;11:34024.
35. Tetz MR, Ries MW, Lucas C, Stricker H, Volcker HE. Inhibition of posterior capsule opacification by an intraocular-lens-bound sustained drug delivery system: an experimental animal study and literature review. J Cataract Refract Surg. 1996; 22: 1070-8.
36. Maloof AJ, Pandey SK, Neilson G, Milverton EJ. Selective death of lens epithelial cells using demineralized water and Triton X-100 with PerfectCapsule sealed capsule irrigation: a histological study in rabbit eyes. Arch Ophthalmol. 2005;123(10):1378-84.
37. Maloof A, Neilson G, Milverton EJ, Pandey SK. Selective and specific targeting of lens epithelial cells during cataract surgery using sealed- capsule irrigation. J Cataract Refract Surg. 2003; 29: 1566-8.
38. Mashiba H, Matsunaga K, Inhibition of Meth-A tumor cell proliferation in combined use of disulfiram with catalase. Toxicol Lett 61 (1992) 75-80.
39. Wang S, Li D, Ito Y, Nabekura T, Wang S, Zhang J, Wu C, Bioavailability and anticataract effects of a topical ocular drug delivery system containing disulfiram and hydroxypropyl-beta-cyclodextrin on selenite-treated rats. Curr Eye Res (29) 2004 51-58.
40. Papadopoulos NG, Dedoussis GV, Spanakos G, Gritzapis AD, Baxevanis CN, Papamichail M: An improved fluorescence assay for the determination of lymphocyte-mediated cytotoxicity using flow cytometry. J Immunol Methods. 177 (1994) 101-11.
41. Lalande ME, Ling V, Miller RG. Hoechst 33342 dye uptake as a probe of membrane permeability changes in mammalian cells. Proc Natl Acad Sci USA. 78 (1981) 363-7.
42. Fernandez V, Fragoso MA, Billotte C, Lamar P, Orozco MA, Dubovy S, Willcox M, Parel JM. Efficacy of various drugs in the prevention of posterior capsule opacification: experimental study of rabbit eyes. J Cataract Refract Surg. 2004; 30: 2598-605.
43. Ishibashi T, Araki H, Sugai S, Tawara A, Ohnishi Y, Inomata H. Anterior capsule opacification in monkey eyes with posterior chamber intraocular lenses. Arch Ophthalmol. 1993; 111: 1685-90.
44. Rabsilber TM, Limberger IJ, Reuland AJ, Holzer MP, Auffarth GU. Long-term results of sealed capsule irrigation using distilled water to prevent posterior capsule opacification: a prospective clinical randomised trial. Br J Ophthalmol. 2007 Jan 3;
45. van Kooten TG, Koopmans S, Terwee T, Norrby S, Hooymans JM, Busscher HJ. Development of an accommodating intra-ocular lens--in vitro prevention of re-growth of pig and rabbit lens capsule epithelial cells. Biomaterials. 2006 Nov;27(32):5554-60.

46. Koopmans SA, Terwee T, Glasser A, Wendt M, Vilupuru AS, van Kooten TG, Norrby S, Haitjema HJ, Kooijman AC. Accommodative lens refilling in rhesus monkeys. Invest Ophthalmol Vis Sci. 2006 Jul;47(7):2976-84.

45 Intraocular Behavior of Accommodative Intraocular Lenses

OStachs (Germany)

SUMMARY

The fundamental idea of some approaches to achieve potentially accommodating intraocular lenses is to allow an axial displacement of the IOL optic. The currently commercial available accommodative implants are designed to convey ciliary muscle activity via the haptic into an optic shift of the optic. The aim of this contribution is the evaluation of haptic geometry based on a three-dimensional reconstruction of single section, ultrasound biomicroscopic data sets. To simulate accommodation, a test chamber using an artificial capsular bag and a stretching device was developed. The haptic regions of the Accommodative 1CU and the CrystaLens AT-45 were scanned in the simulation model during different accommodative (stretched) states. These in vitro results were correlated and used to describe the in vivo condition in patients with these implants in different accommodative states.

INTRODUCTION

Accommodation is the ability of the eye to project a focused image, positioned at varying distances from near to far, on to the retina. The physiological decrease in accommodation with age (presbyopia) is caused by a decrease in the elasticity of the crystalline lens, an equatorial diameter change of the lens, alterations in the elastic properties of Bruch's membrane, and atrophy of the ciliary muscle.[17] After cataract surgery and because the implanted intraocular lens optic cannot change its position and/or shape, pseudophakic patients cannot accommodate. However, as a result of a number of factors (e.g., pupil size, myopic astigmatism, etc.), some patients may have an increased depth of focus, called pseudoaccommodation. To date, lens-based pseudophakic accommodation has only been achieved by multifocal IOLs and by an axial shift of the IOL optic. Other surgical techniques like lens refilling with an inflatable endocapsular ballon or flexible gel are in early experimental stages. Additionally varying outcomes have been reported: scleral expansion surgery, zonal refractive keratectomy and decentred LASIK.

The shift of the IOL optic occurs when the ciliary muscle contracts and induces a change in haptic configuration. Recently, several attempts using different designs[3, 13, 14, 19, 21, 26] [Hara 1990, Hardman 1990, Cumming 1996, Legeais 1999, Küchle 2002, Sarfarazi 2003] have been made to achieve pseudophakic accommodation. The basic approach to achieve potentially accommodating IOLs is to allow an axial displacement of the IOL optic. Quantification of axial IOL movements induced by accommodation in humans has been performed with ultrasound[12, 14, 22, 24]

and with the highest resolution by using dual-beam partial coherence interferometry.[5, 6, 7, 8, 10] In terms of understanding the principle of so-called accommodative IOLs, high frequency ultrasound[23] is the only tool available to visualize the IOL haptic geometry hidden behind the iris diaphragm. Unfortunately, high frequency sonographic image analysis can be difficult if information from only one plane is available. This contribution is based mainly on two publications in Journal of Refractive Surgery[29, 31] and presents the three-dimensional ultrasound evaluation of pharmacological-induced haptic changes and accommodative response in patients with the AT-45 and 1CU implant.

Three-dimensional Ultrasound Biomicroscopy

It has long been appreciated that three-dimensional (3D) ultrasonic images can be produced from an ordered series of scan planes. This technique was first applied to the anterior segment of the eye by Iezzi,[15] et al and required considerable effort and ingenuity with regard to apparatus. Iezzi et al. used a scanning control arm for a continuous z-movement and stored the data on videotape for subsequent digitalization. Silverman,[27] characterized the ciliary body including the state of the ciliary processes of rabbits and normal human subjects using 3D high-resolution ultrasound. There the scanning system consists of two orthogonal linear stages with a computer-controlled stepping motor.

In author's laboratory a simple and low-cost extension of the commercial Ultrasound Biomicroscope Model 840 (Humphrey Instruments, Carl Zeiss Group) into a userfriendly 3D- ultrasonic imaging system was developed. Here 3D data sets consist of B-scan stacks of in-parallel planes with a defined distance between them. Patients were scanned with the ultrasound probe coupled to the eye with Methocel (Ciba Vision) and a normal saline water bath. The examiner positioned the transducer in the center of the ocular segment of interest using standard B-mode. For 3D imaging the computer-controlled scanning system moved the transducer perpendicular (z-direction) to the B-scan plane (xy-plane) over the area being scanned. For this motion an additional miniature skid was mounted on the original linear motor of the UBM scanning device where the ultrasound transducer is attached. Because of its weight it is not possible to attach also the drive of this skid. Therefore the skid is powered from an external stepping motor via a Bowden wire. The video signal of the ultrasound unit is digitized using a frame-grabber board (HaSoTec, Germany) synchronized with the z-motion control system. That means during image capturing the zmovement is stopped and the image plane is exactly perpendicular to the z-axis. 10 s acquisition time with a scanning range of 2.5 mm was used for all subjects, which is thought to be the maximum considering patient and examiner movements. Thus, all 3D scans have the same sampling density. The original UBM raw data (256 scan lines x 1024 samples per line, 256- level grayscale) pictured on the UBM display with 880 × 440 pixels were converted into 440 × 440 pixels (256-level gray scale) during capturing by the frame grabber. No degradation of the image quality is observable and the influence of the conversion is negligible compared with the movement artefacts and contour finding. The motion control and data acquisition system is connected with an SGI workstation via a local area network for 3D reconstruction using AMIRA (TGS, San Diego, CA, USA). This commercial volume rendering software package provides an interactive environment allowing features such as volume orientation for viewing planes and 3D perspectives, segmentation and determination of distances and surfaces. The feature of model building allows outlining of anatomic structures in space and can be used for volume measurements.

An example for 3D imaging is given in Figure 45.1 showing the anterior segment with ciliary body.

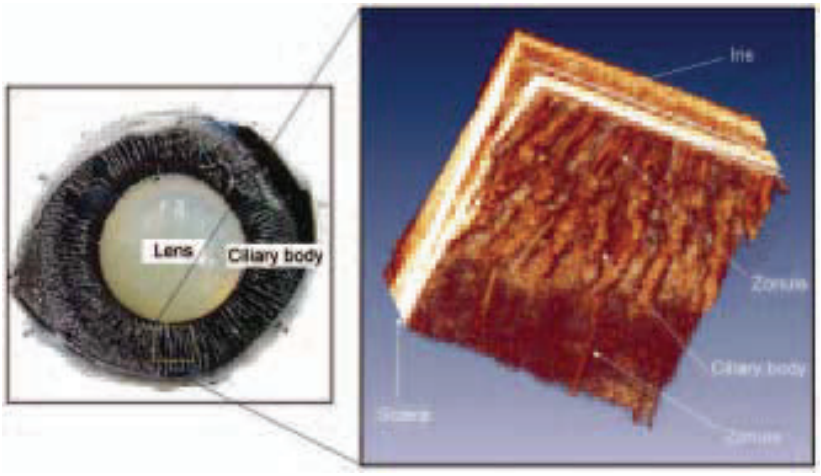

Fig. 45.1: 3D Reconstruction of the human ciliary body (anterior segment viewed from behind)

There are some publications about ex vitro and in vivo applications of these instruments.[16,28,29,30,31] The investigations are mainly focused on accommodation studies and the evaluation of so-called accommodative lenses.

Streching Device for in vitro Experiments

To simulate accommodation, a test chamber using an artificial capsular bag and a stretching device was developed.[29] For analysis of the IOL performance, the artificial capsular bag was mounted in a simulation device. The arms of the fixture clamp the bag around its periphery at eight points. Rotation of the inner ring stretches or relaxes the bag (Figs 45.2A to C). Inner ring rotation is accomplished by a stepping motor driving a worm gear. The amount of stretching correlates with the rotation of the inner ring. The entire arrangement is submerged in water for sonographic imaging. The haptic regions of the Accommodative 1CU and the CrystaLens AT-45 were scanned in the simulation model during different accommodative (stretched) states (Figs 45.3A to C). These in vitro results were correlated and used to describe the in vivo condition in patients with accommodative implants.

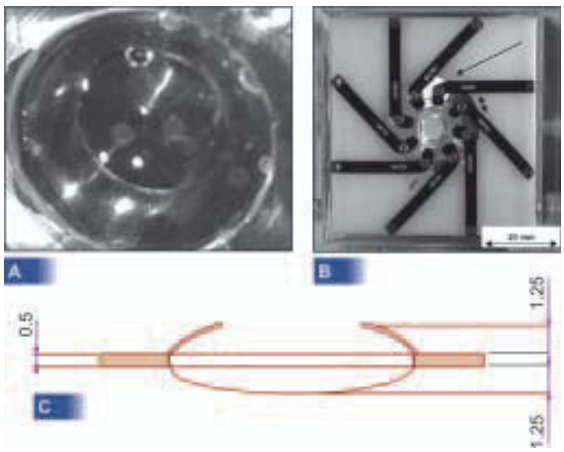

Fig. 45.2A to C: **A** and **C.** Artificial capsular bag, and **B.** stretching device for accommodation simulation. The rotation of the inner ring with pins (marked in **B**) shifts the arms and stretches or relaxes the bag to simulate the force effects of the ciliary muscle. The 1CU IOL is implanted[29]

In vitro Findings: Accommodative 1 CU

The posterior chamber lens 1CU was examined. Theoretically, a contraction of the ciliary muscle, thus a relaxation of the zonules, leads to a relaxation of the capsular bag. The haptics turn and produce an anterior axial shift according to the modified force

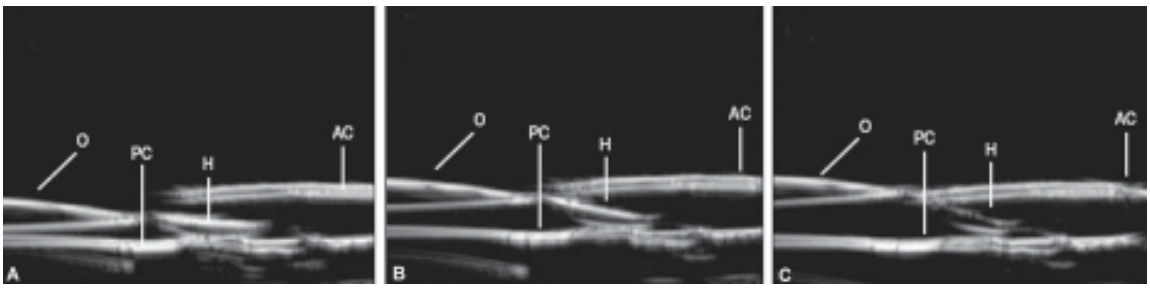

Figs 45.3A to C: B-scan series exemplifying the stretching experiment (impact 1 CU)
Abbreviations: O = optic, PC = posterior capsule, H = haptic, AC = anterior capsule[29]

ratio in the haptic region. Our simulation experiments show a similar effect during capsular bag relaxation. A 0.5-mm change in r was used for maximal relaxation/stretching. With this unphysiological and unexpected amount of relaxation in humans, a 0.36-mm anterior shift was observed for the 1CU caused by a haptic 10.4° angulation change. Using a 50-year lens and the linear regression of Strenk for the ciliary body displacement, a 0.25 mm ciliary body displacement can be assumed. A 0.28 mm anterior IOL shift and an angulation change of 4.3° was observed. For this lens, the theoretically predicted 30° haptic angulation change for 1-mm axial shift could not be achieved.

In vitro Findings: CrystaLens AT-45

The three-dimensional reconstruction and the interactiveselection of sections across the haptic as well as a photographic image are shown in Figure 45.6. In this example, the optic and the haptic can be differentiated. The echo patterns are caused by the polyimide construction of the plate haptic. The posterior lens surface can be imaged, whereas this interface cannot always beseen under different

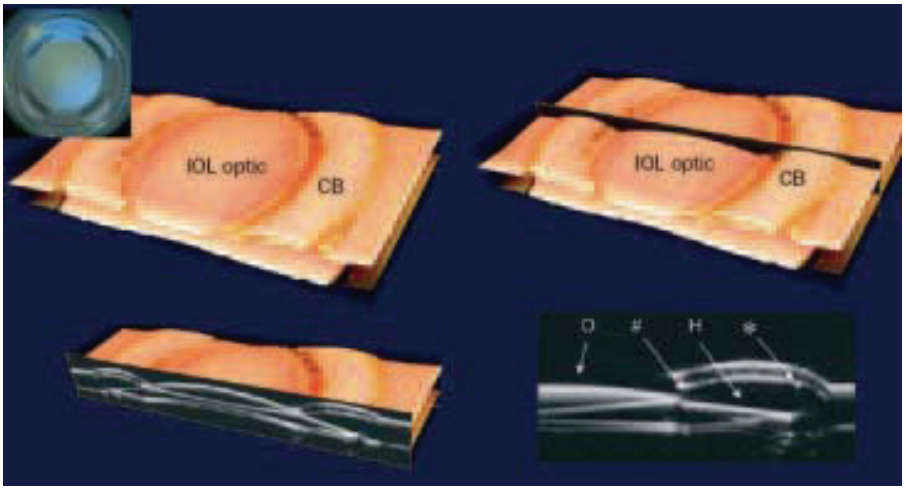

Fig. 45.4: Photograph and three-dimensional ultrasound biomicroscopy image and B-scan of the 1CU in the artificial silicone capsular bag (CB).
Abbreviations: O = optic, # = fulcrum, H = haptic, and * = haptic ridge[29]

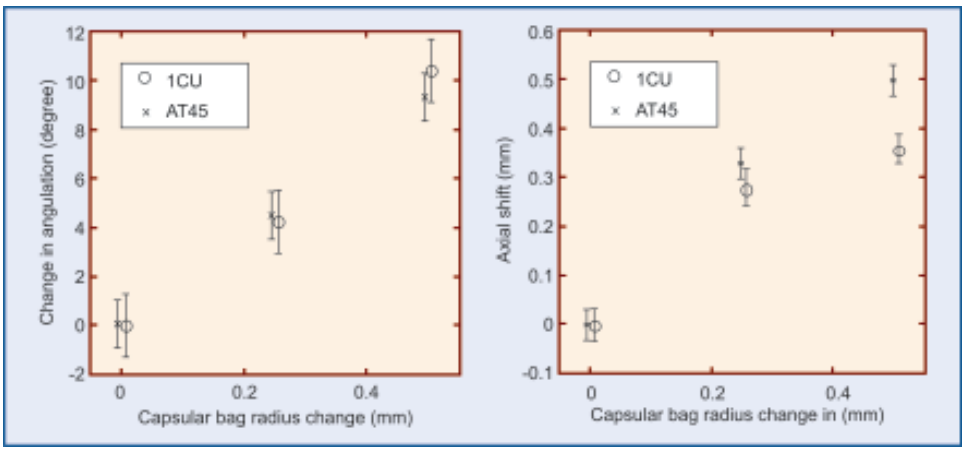

Fig. 45.5: Change in angulation (left) and axial IOL movement (right) by lens type showing the effect of equatorial stretching respectively relaxing[29]

scanning directions. The point # acts as the fulcrum and is used as the center of rotation for angulation determination. In the in vitro model, a maximal forward shift of 0.50 mm (9.3° haptic angulation change) for the AT-45 lens was observed using the maximal radius change of 0.5 mm. For 0.25-mm radius change as the expected value for the 50-year lens, an axial shift of 0.33 mm with 4.5° angulation change was found. In our model, equatorial changes can be simulated, but vitreous pressure variations cannot be simulated. Regarding the axial shift, the AT-45 performed 0.14 mm better compared to the 1CU for 0.5-mm radial displacement.

In vivo Investigations

Patients returned for follow-up between 4 and 12 weeks postoperatively depending on study.[29, 31] The objective refractometry was performed using a

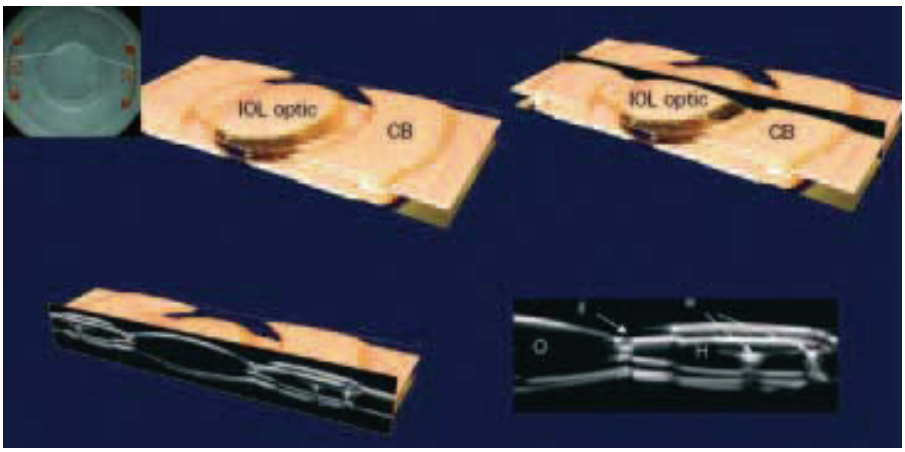

Fig. 45.6: Photograph and three-dimensional ultrasound biomicroscopy image and B-scan of the CrystaLens AT-45 in the artificial silicone capsular bag (CB). Abbreviations: O = optic, # = fulcrum, H = haptic, and * = polyimide construction[29]

autorefractometer (Canon RK3). Distance visual acuity was determined using a standard Snellen projector system (Optostar IR-2000; Schwind, Kleinostheim, Germany). Near reading vision was determined using Birkhäuser reading charts (Scalae Typographicae Birkhaeuseri, Birkhäuser Verlag) and an illumination of 70 cd/m^2. After determining best and uncorrected far vision, near vision without additional near/distance correction and with the addition of +1.0, +2.0, +3.0, and +3.5 sphere, was determined. Visual acuity values were expressed in decimal values and logMAR. Details can be seen in [Stachs 2005, Stachs 2006]. An in-house three-dimensional ultrasound biomicroscope (UBM) was used to evaluate IOL placement and haptic configuration in patients with the AT-45 implant. The principles of the UBM and three-dimensional UBM have been described in detail elsewhere. The three-dimensional reconstruction was performed using Amira software (TGS, San Diego, Calif). Building three-dimensional constructs allows outlining of anatomical structures in space and can be used for oblique reconstructions. In addition, the software package ImageJ (National Institutes of Health, Bethesda, Md) and MatLab (The MathWorks Inc.) were used for the evaluation of haptic configurations and axial changes in IOL position.

Three-dimensional UBM measurements were carried out after pharmacologically induced accommodation (two drops of pilocarpine 2 percent administrated in 5-minute intervals) or disaccommodation (two drops of cyclopentolate 1% administrated in 5-minute intervals) on 2 consecutive days 4 weeks after surgery. The ciliary body regions of four patients were scanned 30 minutes after pharmacological treatment. The three dimensional volumes were then used to identify the tangential plane of the IOL haptic; an oblique reconstruction is possible to perform the biometric measurements. The center of rotation was placed at the fulcrum and the angle between the IOL optic and haptic was measured using the anterior IOL interface. Positive values in angulation represent an anterior vaulting, and negative values represent a posterior vaulting. Changes in haptic angulation and the IOL shift were analyzed (mean and standard deviation) using five B-scans for each accommodative state and for all patients. Positive values for change in anterior chamber depth represent a forward shift of the IOL.

Accommodation Stimulus

Pilocarpine application is an objective way of stimulating accommodation as it requires no participation from the patient. Topical application of pilocarpine is advised and commonly used to stimulate accommodation. Variability in accommodation amplitudes is partially due to the capability and attendance of volunteers to accommodate to various kinds of stimuli. Using pilocarpine, this subjective component to accommodation is eliminated; however, the role of pilocarpine must be discussed. Abramson et al. measured the accommodation effect in human individuals using A-scan ultrasound. They determined a greater increase in axial lens diameter after pilocarpine application than is possible with stimulus-driven accommodation. Thus, topical application of pilocarpine may produce overstimulation of the ciliary muscle. These early results are consistent with the findings of Findl[10, 11, 18] and Köppl [Köppl 2003] who used dual-beam partial coherence interferometry. These studies have shown a difference in lens movement between pilocarpine-induced and stimulus-driven ciliary muscle contraction. Pilocarpine acts "physiologically" in young phakics and as a superstimulus in presbyopic phakics and pseudophakes. Therefore, IOL movement and angulation change data may be overestimated when using pilocarpine.

In Vivo findings: Accommodative 1CU

Figure 45.7 shows a three-dimensional reconstruction and the image analysis of a 1 CU haptic region. Changes in angulation and ΔACD by four different

individuals show the effect of cyclopentolate and pilocarpine 4 months postoperatively (Fig. 45.8). In disaccommodation, a haptic angulation between 2° and 4° caused by capsular bag shrinkage and secondary cataract formation is visible. This could mean that a haptic angulation is already present in the disaccommodated state. In the cases studied, pilocarpine induced an additional angulation variation between 5° and 10° for the 1CU IOL, which causes a change in anterior chamber depth between 0.2 and 0.5 mm. Using Gullstrand's eye model, this 0.2 mm forward movement results in a refraction change <0.38 D (0.95 D for 0.5 mm of movement), depending on exact IOL position. These findings are in agreement with the results of Findl et al.[6, 10, 16] Using partial coherence interferometry, et al. Findl found a moderate forward movement under pilocarpine with induced mean accommodative amplitude of 0.50 D. These mechanical performance of the does not appear to provide the range of accommodation necessary for close work.

In vivo Findings: CrystaLens AT-45

The echo characteristics of the AT-45 seen in Figure 6 were used to describe the in vivo situation in four patients with accommodative implants 4 weeks after surgery. Figure 45.9 shows the haptic region of a 71-year-old woman after pilocarpine instillation. A haptic angulation of 33° (uncorrected 190°) compared with the relaxed IOL haptic (0°, uncorrected 157°) is seen in this case. For a descriptive visualization of changes in angulation depending on the accom-

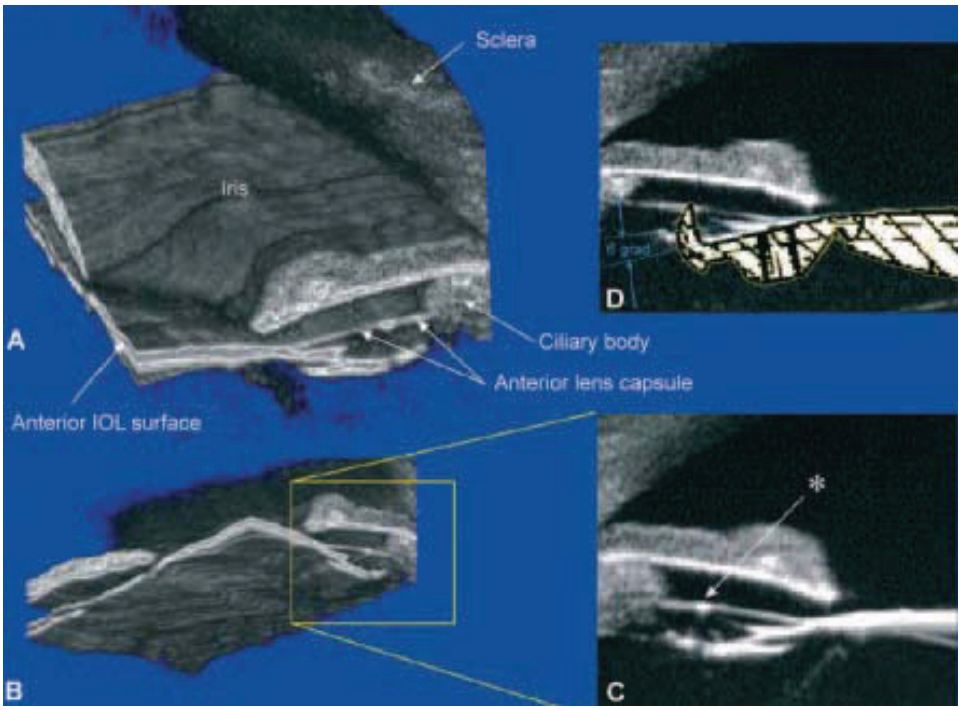

Figs 45.7A to D: **A** and **B.** Three-dimensional reconstruction; and **C** and **D** image analysis (with design drawing) of the 1CU haptic region in a 75-year-old patient 4 months postoperatively (disaccommodation). A 6° haptic angulation compared with the relaxed IOL condition is observed[29]

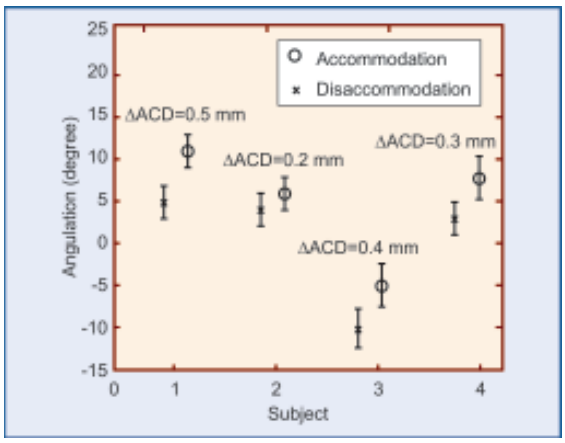

Fig. 45.8: Angulation and anterior chamber depth (Δ ACD) by subject (implant 1CU) showing the effect of cyclopentolate and pilocarpine (Δ = angle of difference to the relaxed haptic configuration, o = change under pilocarpine treatment; mean ± standard deviation). Positive values for ΔACD represent a forward shift of the IOL under pilocarpine[29]

modation state, corresponding UBM sections were superimposed. Figure 45.10 demonstrates the situation under cyclopentolate (red) superimposed on a UBM section under pilocarpine stimulation (gray) for two patients. Pilocarpine induced an additional angulation change in patient 1 (Fig 45.2A) and no changes for patient 2 (Fig 45.2B) compared with the configuration after cyclopentolate treatment. The pilocarpine instillation causes a forward shift in patient 1 and no changes in patient 2. The results of the four eyes are summarized in Figure 45.11. Under cyclopentolate, a haptic angulation between 10° and 26° was found. A mean change in haptic angulation of 3.3 ± 3.3° (range: 0° to 7°) and a mean forward shift of 0.13 mm (range: 0.06 to 0.2 mm) were observed under pilocarpine treatment. An accommodative amplitude of 0.44 ± 0.24 diopters (D) (range: 0.25 to 0.75 D) was found in the four eyes using a Hartinger coincidence refractometer.

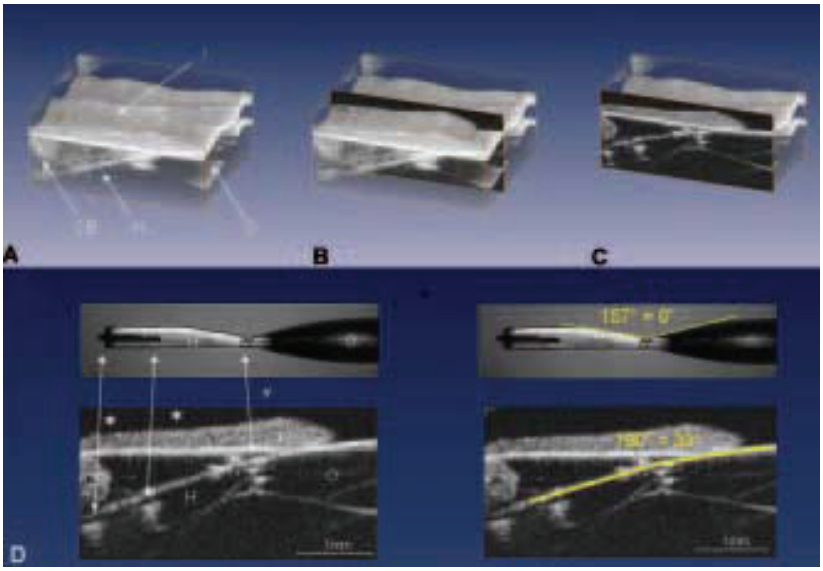

Fig. 45.9A to D: Three-dimensional reconstruction and **D** image analysis of the AT-45 haptic region (patient 1: 71-year-old woman, 4 weeks after surgery, pilocarpineinduced accommodation). The fulcrum is marked (#). The optic (O) and haptic (H) are well differentiated, whereas the echo pattern (*) is caused by the polyimide construction of the AT-45 plate haptic. The 157° angle for the relaxed haptic configuration was set to zero for angulation change determination. A haptic angulation of 33° (uncorrected 190°) compared with the relaxed IOL haptic is observed. O = optic, H = haptic, * = polyimide construction, # = fulcrum, I = iris, CB = ciliary body[31]

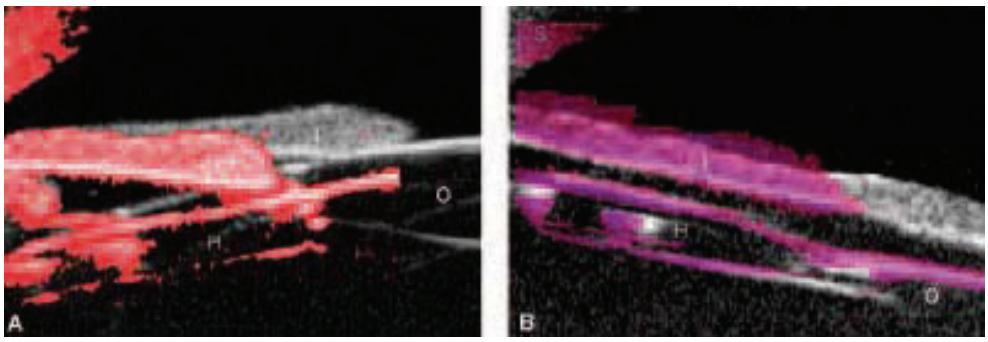

Figs 45.10A and B: Superimposed UBM sections showing the effect of cyclopentolate and pilocarpine in two patients—**A.** patient 1, 71-year-old woman and **B.** patient 2, 77- year-old woman. The disaccommodated state after cyclopentolate treatment (red) and under pilocarpine stimulation (gray) is shown. S = sclera, I = iris, CB = ciliary body, H = haptic, O = optic[31]

For the AT-45, the proposed mechanism is that accommodation restoration occurs through the ciliary muscle activity. The manufacturer has developed the lens to provide good vision at all distances by moving backward and forward along the optical axis of the eye in response to pressure changes in the vitreous and anterior chamber. In the cases studied, pilocarpine induced an angulation change between 0° and 7° (mean 3.3 ± 3.3°) compared with the situation under cyclopentolate. The angulation change causes a change in anterior chamber depth between 0.06 and 0.2 mm (mean 0.13 ± 0.08 mm). Using Gullstrand's eye model and a 20.0-Dpt IOL placed in the bag, the observed maximal 0.2-mm forward movement results in a refraction change 0.4 D, depending on the exact IOL position. The cases studied showed a maximal accommodation response of mean 0.44 ± 0.24 D (range: 0.25 to 0.75 D) measured by a Hartinger coincidence refractometer. This value is slightly larger than the calculated values using Gullstrand's eye model, possibly caused by individual pseudo-accommodative effects (e.g., pupil size, myopic astigmatism, etc.).

Pilocarpine-induced ciliary muscle contraction caused a slight change in haptic angulation and an anterior shift of the AT-45 in these four eyes. This slight change in angulation and the anterior shift

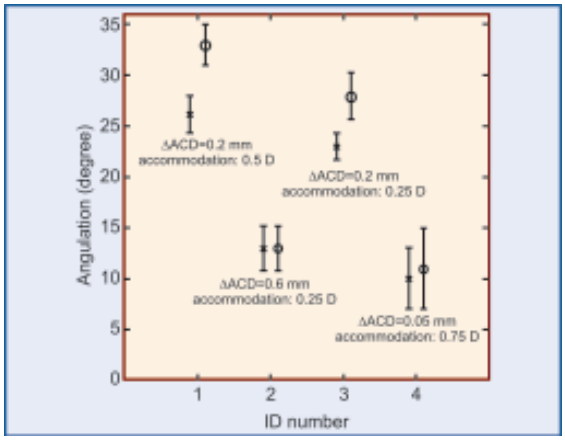

Fig. 45.11: Change in angulation (°) and anterior chamber depth (ACD) [mm]) as well as accommodation amplitude (D) in at –45 patients showing the effect of cyclopentolate (cross) and pilocarpine (circle). Positive values for change in anterior chamber depth represent a forward shift of the IOL. Positive values in angulation represent an anterior vaulting[31]

resulted in an accommodative amplitude between 0.25 and 0.75 D. Therefore, in these four eyes, the AT-45 did not seem to provide the range of accommodation necessary for close work. We expect that capsular fibrosis and capsular bag shrinkage result in a hardening of the haptic and optic in the capsule, resulting in further decrease of the accommodative performance later postoperatively.

CONCLUSION

One of the challenging tasks of the cataract surgery is the conservation or restoring of the accommodative performance in pseudophakic patients. Various attempts have been made so solve the problem of presbyopia. One example is the development of so-called accommodative IOL's. The in vitro simulation device examined with three-dimensional ultrasound biomicroscopy provided information on the accommodative performance of these potentially accommodative IOL designs. Using three-dimensional ultrasound biomicroscopy, corresponding changes in haptic angulation during pharmacological induced accommodation were observed. Pilocarpine-induced ciliary muscle contraction caused a change in haptic angulation and an anterior shift of the investigated IOL's, which resulted in approximately an estimated accommodative amplitude between 0.40 and 0.95 D (1CU) as well as 0.25 and 0.75 (AT45) The mechanical performance of the investigated IOL's in vitro and in the eyes studied does not appear to provide the range of accommodation necessary for close work.

FURTHER READING

1. Abramson DH, Franzen LA, Coleman DJ. Pilocarpine in the presbyope. Demonstration of an effect on the anterior chamber and lens thickness. Arch Ophthalmol 1973;89:100-102.
2. Coleman D, Silverman R, Daly S. Advances in ophthalmic ultrasound. Radiol Clin North Am 1998;36:p.1073-82.
3. Cumming JS, Kammann J. Experience with an accommodating IOL. J Cataract Refract Surg 1996;22:1001.
4. Cusumano A, Coleman D, Silverman R, Reinstein D, Rondeau M, Ursea B, Daly S. Three dimensional ultrasound imaging – clinical applications. Ophthalmology 1998; 105:p.300-306.
5. Findl O, Drexler W, Menapace R, Bobr B, Bittermann S, Vass C, Rainer G, Hitzenberger CK, Fercher AF. Accurate determination of effective lens position and lens-capsule distance with 4 intraocular lenses. J Cataract Refract Surg 1998;24:1094-98.
6. Findl O, Kriechbaum K, Köppl C, Menapace R, Drexler W. Laser interferometric measurements of IOL movement with accommodating IOLs. Proceedings of the American Society of Cataract and Refractive Surgery annual meeting; 2003 April 12-16, San Francisco, Calif. Abstract #94.
7. Findl O, Kiss B, Petternel V, Menapace R, Georgopoulos M, Rainer G, Drexler W. Intraocular lens movement caused by ciliary muscle contraction ; Journal Cataract Refract Surg 2003;29,669-76.
8. Findl O, Menapace R, Kriechbaum K, Koeppel C, Drexler W. Laser interferometric measurements of movement of an "accommodating" IOL. In: Guthoff R, Ludwig K (Eds): Current Aspects in Accommodation II. Heidelberg, Germany: Kaden 2003;211-21.
9. Findl O, Kiss B, Petternel V, Menapace R, Georgopoulos M, Rainer G, Drexler W. Intraocular lens movement caused by ciliary muscle contraction. J Cataract Refract Surg. 2003;29:669-76.
10. Findl O, et al. Laserinterferometric assessment of pilocarpine-induced movement of an accommodating intraocular lens: a randomized trial. Ophthalmology. 2004a Aug;111(8):1515-21.
11. Findl O. Accommodative intraocular lens: funktionelle Ergebnisse. Klin Monatsbl Augenheilkd. 2004b;221 (Suppl):36.
12. Gandolfi SA, Marchini G, Tosi R, Mora P, Pedrotti E, Sartori P, Manzotti F. UBM changes during accommodation in eyes implanted with Crystalens AT45 and 1CU IOL. A pilot study. Invest Ophthalmol Vis Sci 2003;44:E- abstract 252.
13. Hara T, Hara T, Yasuda A, Yamada Y. Accommodative intraocular lens with spring action, I: design and placement in an excised animal eye. Ophthalmic Surg 1990;21:128-133.
14. Hardman Lea SJ, Rubinstein MP, Snead MP, Haworth SM. Pseudophakic accommodation? A study of the stability of capsular bag supported, one piece, rigid tripod, or soft fl exible implants. Br J Ophthalmol 1990;74:22-25.
15. Iezzi R, Rosen R, Tello C, Liebmann J, Walsh F, Ritch R, Personal computer-based 3-dimensional ultrasound biomicroscopy of the anterior segment. Arch Ophthalmol 1996;114:520-24.
16. Kirchhoff A, Stachs O, Guthoff R. Three-dimensional ultrasound findings of the posterior iris region. Graefes Archive for Clinical and Experimental Ophthalmology 2001 December;239(12):968-71.
17. Kaufman PL. Accommodation and presbyopia: neuromuscular and biophysical aspects. In: Hart WM Jr, ed. Adlers Physiology of the Eye: Clinical Application. 9th ed. St Louis, Mo: Mosby; 1992:391-411.
18. Köppl C, Findl O, Kriechbaum K, Dexler W. Comparison of pilocarpine-induced and stimulus-driven accommodation in phakic eyes. Proceedings of the XXI Congress of the European Society of Cataract and Refractive Surgery; September 6-10, 2003; Munich, Germany
19. Küchle M, Nguyen NX, Langenbucher A, Gusek-Schneider GC, Seitz B, Hanna KD. Implantation of a new accommodative posterior chamber intraocular lens. J Refract Surg 2002;18:208-216.

20. Langenbucher A, Huber S, Nguyen NX, Seitz B, Gusek-Schneider GC, Kuchle M. Measurement of accommodation after implantation of an accommodating posterior chamber intraocular lens. J Cataract Refract Surg. 2003;29:677-685.
21. Legeais JM, Werner L, Werner L, Abenhaim A, Renard G. Pseudoaccommodation: BioComFold versus a foldable silicone intraocular lens. J Cataract Refract Surg. 1999;25:262-267.
22. Nakazawa M, Ohtsuki K. Apparent accommodation pseudophakic eyes after implantation of posterior chamber intraocular lenses: optical analysis. Invest Ophthalmol Vis Sci. 1984;25:1458-1460.
23. Pavlin CJ, Foster FS. Ultrasound Biomicroscopy of the Eye. New York, NY: Springer; 1995.
24. Ravalico G, Baccara F. Apparent accommodation in pseudophakic eyes. Acta Ophthalmol. 1990;68:604-606.
25. Reinstein D, Raevsky T, Coleman D. Improved system for ultrasonic imaging and biometry. J Ultrasound Med, 1997;16:p.117-24.
26. Sarfarazi FM. Optical and mechanical design for human implantation of the Sarfarazi Elliptical Accommodation IOL. Proceedings of the American Society of Cataract and Refractive Surgery annual meeting; April 12-16, 2003;San Francisco, Calif. Abstract #738.
27. Silverman R, Lizzi F, Ursea B, Rondeau M, Eldeen N, Kaliscz A, Lloyd H, Coleman D. High-resolution ultrsonic imaging and characterization of the ciliary body. Invest Ophthalmol Vis Sci 2001;42:p.885-94.
28. Stachs O, Martin H, Kirchhoff A, Stave J, Terwee T, Guthoff R. Monitoring accommodative ciliary muscle function using three-dimensional ultrasound. Graefes Arch Clin Exp Ophthalmol 2002;240:906-12.
29. Stachs O, Schneider H, Stave J, Guthoff R. Potentially accommodating intraocular lenses—an in vitro and in vivo study using three-dimensional high-frequency ultrasound. J Refract Surg. 2005 Jan-Feb;21(1):37-45.
30. Stachs O, Martin H, Behrend D, Schmitz KP, Guthoff R. Three dimensional ultrasound biomicroscopy, environmental and conventional scanning electron microscopy investigations of the human zonula ciliaris for numerical modelling of accommodation. Graefe's Arch Clin Exp Ophthalmol, 2006;244(7):836-44.
31. Stachs O, Schneider H, Beck R, Guthoff R. Pharmacological-induced haptic changes and the accommodative performance in patients with the AT-45 accommodative IOL. J Refract Surg 2006 Feb;22(2):145-50.

Chapter 8

Ultrasonography within the Framework of Ophthalmologic Differential Diagnosis

Rudolf F. Guthoff, MD
Oliver Stachs, PhD

Introduction

"Measure whatever can be measured, and what cannot be measured, make measurable"

Galileo Galilei

"What cannot be made measurable …?"

Herbert Pietschmann

The pioneer work in the area of ophthalmic echography was already performed before 1960. This work fertilized other areas of ultrasound use. Nevertheless, ophthalmology was neglected for a long time when new machines were developed. A highly developed diagnostic tool evolved which was mainly based on the A-mode. Ossoinig, in particular, described this under the general concept of "standardized echography". Since the last 20 years ophthalmologic machines have been available which use digital processing, thereby producing temporal and spatial high-resolution echograms[1]. This easily interpretable method of presentation facilitates learning the first steps of making an ultrasound diagnosis.

This chapter attempts to delineate the possibilities of ultrasonography in our specialty, while putting the cross-section display at the centre of our considerations. By comparing the ultrasound display with histopathologic sections, we try to demonstrate the limits of ultrasound diagnosis. Computerized B-scan guided ultrasound Doppler equipment has been introduced into the ophthalmology, and has opened up remarkable new perspectives. Examples of colour-coded Doppler examinations are given for the differential diagnosis of intraocular tumours and the differentiation of ocular and orbital vascular diseases. In this way we attempt to determine the position of ultrasound diagnosis in the clinical decision-making process, thereby facilitating the learning process for the neophyte.

This short chapter does not attempt to replace standard text books of ophthalmic ultrasound [2-8]. It updates clinically most relevant facts to introduce and stimulate also non-specialists in ophthalmic ultrasound as it is the firm conviction of the authors that ultrasonography should be considered as an everydays tool of every ophthalmologist whenever optic examination techniques do not lead to clear decisions.

Ophthalmic Ultrasonography - Past, Present and Future

Toward the end of the 19th century it was found that acoustic energy also existed outside of the limits perceived by the human ear. This was a scientifically fruitful time during which radio waves, radioactivity and Roentgen rays were discovered. However, only a few scientists concerned themselves with ultrasound. In 1793 the Italian scholar Spallanzani discovered that bats could fly in a completely darkened surrounding[9]. If the animal's heads were covered by hoods, they could not avoid obstacles when flying, even when the hoods were transparent. Spallanzani

modified these experiments in order to prove that type of hearing helps the animals in orientation. Rather than using hoods, he placed wax spherules into animal's auditory canals; this also eliminated their faculty of orientation. He postulated: "The uncanny faculty of bats to orient themselves when flying in darkness is connected with hearing."

Spallanzanis contemporaries thought the concept that bats could "see with their ears" was absurd. Scientists ridiculed the so-called Spallanzani bat problem. Finally, in 1940 Griffin and Galambos proved the connection [10]. Bats and some water mammals have the capability to emit ultrasound impulses and then recognize and evaluate their echoes; this actually represents the principle of clinical ultrasound diagnosis.

It took a long time before the discovery of ultrasound energy was applied purposefully. The brothers Curie described in 1880 the piezo-electric effect. They discovered that by mechanically pressing on a tourmaline crystal, a difference in electric potential is created between opposing surfaces. On the other hand, an electric current will deform the shape of the crystal.

During World War I, the French physicist, Paul Langevin, used an underwater orientation device which, on the basis of the piezo-electric effect, was capable of emitting and receiving ultrasound waves under water. His device became the principle for the sonar system which was important during World War II.

The invention of the so-called "reflectoscope" by Firestone (1942) was the most significant advance for ultrasound diagnosis. This instrument is used for testing different kinds of material without damaging the material itself. With a similar device, Ludwig (1949) succeeded in detecting gallstones in patients. The first publication on ophthalmologic ultrasound diagnosis appeared in 1956 and was published by G. H. Mundt and W. F. Hughes[11]. They succeeded in localizing intraocular tumours with a certain degree of reliability. In 1958 Baum demonstrated the B-scan [12]. The A- and B-scan formats became, and remain, the bases of ophthalmic biometric applications and diagnostic imaging, respectively.

The A-scan is displayed in the form of a plot of echo amplitude along a single line of sight. By measuring the time interval between emission of the acoustic pulse and echo return, the range to the tissue structure generating the echo can be determined. In 1957 Oksala and Lehtinen published a series of fundamental papers on the ophthalmic A-mode diagnostic method[13-16]. This method was further developed, especially in Europe[1, 17-19], and was complemented by the diagnosis of orbital processes and by biometry [20]. The ability to measure axial length (the distance from the cornea to the retina) facilitated a revolution in cataract surgery in the 1970s. By the mid-1970s, ultrasound technology had made the determination of axial length possible in a clinical setting. This, in combination with corneal curvature measurement (keratometry), allowed the development of IOLpowering formulae, several of which were proposed at that time. Currently, optical interferometry provides an alternative to ultrasound for the measurement of axial length. Optical techniques, while very accurate, cannot be used in circumstances where opacities such as dense cataract are present.

The B-scan is a two-dimensional (2-D) cross-section image formed by mechanically sweeping the direction axis of the transducer over an angle of, typically, 50–60º. G. Baum and J. Greenwood introduced their two-dimensional B-mode to ophthalmology[2]. They stated that their apparatus simulates a slit lamp, except that a pulsed ultrasound beam is substituted for the light beam. It projected light-modulated points on a screen, thereby obtaining acoustic tissue sections. They succeeded already in recognizing retinal detachment, hemorrhages and even orbital pathologic changes. This technique required a complicated water bath coupling between the eye and the transducer. Bronson (1972) developed a hand-held contact B-mode transducer [21]. This led to rapid dissemination of echographic diagnostic methods in ophthalmology. The realtime nature of the examination facilitates evaluation of retinal detachment and vitreous membranes, as well as the capability of visualising the pulsation of vessels in tumours.

In the early 1990s, ultrasound systems operating at 35–50MHz became available and were used to image the anterior segment of the eye, consisting of the cornea, iris, anterior chamber, ciliary body and lens. Owing to the fact that attainable axial resolution is inversely related to frequency, these systems provided a four- or five-fold improvement in resolution relative to the 10MHz scanners that were used until then. When 1990 Pavlin, Sherar and Foster published their first paper on "Subsurface ultrasound microscopic imaging of the intact eye"[22] ophthalmic ultrasound

has regained the cutting edge of ultrasound technology which, in terms of high resolution ultrasound imaging is still unsurpassed. The first commercial instrument manufactured by Zeiss-Humphrey was an outgrowth of the work of Pavlin and Foster and was widely applied for studies of pathologies affecting the anterior segment, such as glaucoma, tumours and cysts of the iris and ciliary body, hypotony, hyphaema and trauma.

The authors' laboratory developed a prototype scanning system for 3D imaging based on the Zeiss-Humphrey instrument. These systems generating high-resolution images, allowed the acquisition of scans in a series of ordered planes, from which 3-D images could be constructed [23, 24] (Figure 1).

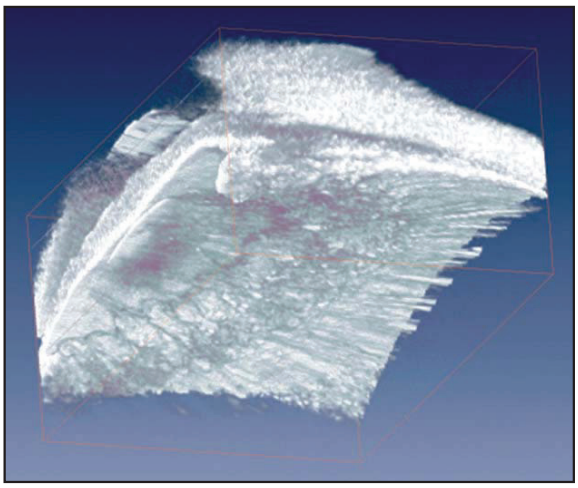

Figure 1: *3D high-frequency image of the anterior segment with ciliary body and zonula ciliaris.*

Refractive surgery presently is benefiting from developments based on the work of Coleman, Silverman and Reinstein where high frequency ultrasound arc scanning allows anterior segment imaging without any anamorphic distortion [25-28]. They developed an arcshaped scan geometry, allowing them to maintain constant range and normal incidence to the corneal surface. This technology is called Artemis-2, manufactured by Ultralink LLC. In addition to providing quantitative analysis of the cornea, the Artemis-2 allows visualisation of the entire anterior segment in one scan, and is therefore useful for measurements of angle-to-angle and sulcus-to-sulcus dimensions (crucial for the proper sizing of phakic lens implants) introduced for refractive correction. An example of the anterior lens shape in accommodation and disaccommodation is shown in Figure 2.

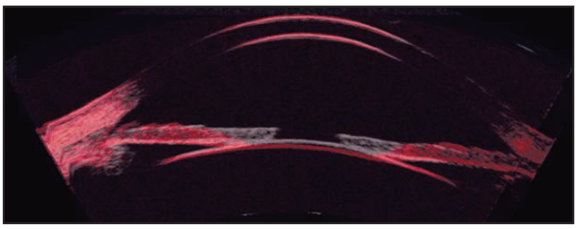

Figure 2: *Cross-section of the anterior lens in accommodation (grey) and disaccommodation (red); (Artemis-2, Ultralink).*

Examination Techniques

Recommendations for a Rational Sequence of Examinations

The Examination Procedure

The echographic examination of the eye and the orbit can be performed in a facile way if the patient lies flat or sits in an examining chair that can be tilted backwards. Infants and children are best examined in their mother's arms.

The high frequency of the ultrasound cannot be transmitted through air; therefore, a gel-like contact substance, e.g. 2% methylcellulose solution, has to be applied to the transducer or to the patient's skin. Sterility should not be a problem if commercially available gels are used. The transducer is cleaned by wiping with a disinfectant, whereby the number of microorganisms can be kept low. If sterile conditions have to be maintained (e.g. when examining during a surgical intervention), a sterile plastic finger cot or surgical glove can be pulled over the transducer. In order to reduce impedance differences between the membranes, it is necessary to apply a drop of the methylcellulose solution on the transducer to guarantee direct coupling. In the area of the exit window of the ultrasound, the plastic finger cot should be in direct contact with the transducer cover.

Examining through the closed lid does not appreciably weaken the sound energy. This allows a wide radius of rotation when turning the transducer. In order to facilitate quantitated gaze movements, the nonexamined eye should be only partly covered.

Direct contact of the transducer with the globe is only necessary for special A-mode techniques. In this way the less well-defined sound attenuation by the lids can be avoided when using quantitative examination techniques. One problem for biometric measurements of the axial length is the coupling pressure, which necessarily leads to a minimal deformation of the globe [29].

Principles of Obtaining the Optimal Ultrasonogram

During the entire examination, we should pay attention so that:

1. The examination structure is in the middle of the scanned sector; and

2. Acoustic interfaces are at a right angle to the propagation direction of the ultrasound.

These postulates can be fulfilled by corresponding changes in the patient's gaze and by the appropriate movements of the transducer (kinetic echography). It is absolutely necessary to follow these rules if we want to quantify signal intensities (quantitative echography).

Spontaneous Motions as a Diagnostic Sign

Already after a few examinations, the echographic neophyte will realize that diagnosis can only be made during the examination procedure. He will be impressed by the extent of intraocular movements, e.g. of floating vitreous opacities (Figure 3). The type of aftermovements of the vitreous induced by changes in the patient's gaze also provides valuable information. Some pathologic processes will produce echographically demonstrable movements which are extremely important for the diagnosis. Among these are arteriovenous fistules of the orbit or the effect of blood flow within highly vascularized melanomas. It is also important to examine all normal anatomical structures from different directions so that we get a clear picture of the extent of a pathologic process.

Identical examination parameters are difficult to reproduce during an examination – and even more so during a follow-up examination. We have discussed the importance of calibrating and standardizing the instrument. The variables induced by the examiner represent an uncertainty factor which cannot be quantified. The ultrasound reflected by the tissues is influenced by the angle under which the transducer is applied, by the location of the scanning plane, by the position of the globe and, not least of all, the pressure with which the transducer is applied.

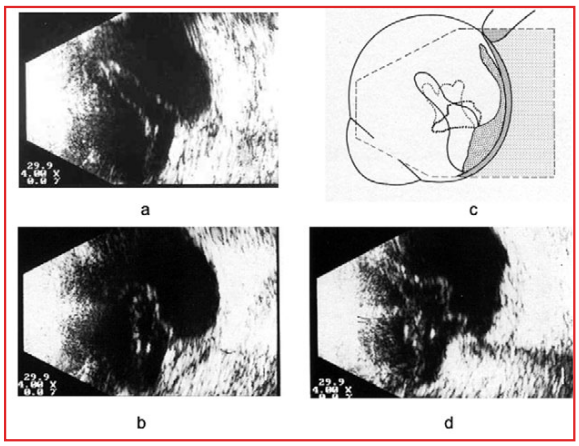

Figure 3: *(**a-d**) Aftermovements of a vitreous membrane adherent to the area of the exoplant.*

The "Critical Moment" Decides

In X-rays and in magnetic resonance imaging we project the soft tissues onto skeletal structures which are imaged simultaneously. This allows an unequivocal topographic orientation. Echographic techniques imaging soft tissue only, however, need "landmarks" for the orientation. Such landmarks are the entrance of the optic nerve into the globe (Figure 4) or the insertions of the extraocular muscles (Figure 5). Amplification control plays an important role in gaining orientation in the area to be examined. Absorption of ultrasound energy in the tissue depends upon the specific sound running time. It is therefore impossible to display with equal quality in acoustic cross section structures lying at different distances from the transducer.

In the B-mode echogram, quality of imaging is identical with creating "a pretty image" in which the crucial structures can be well recognized. It is therefore not only necessary to shift our attention to various structures, but also to adjust amplification so that we always obtain an optimal setting of the apparatus.

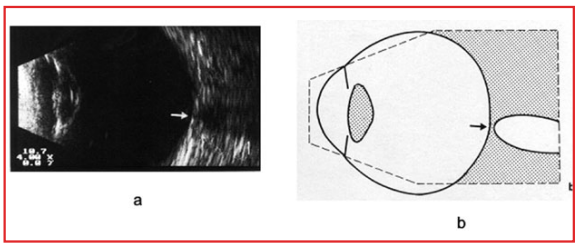

Figure 4: a) Cross sectional echogram through a normal globe; the arrow marks the entrance of the optic nerve. b) Schematic drawing.

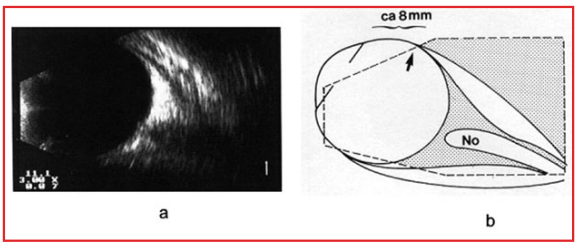

Figure 5: a) Image of the globe and the orbit. The insertions of the recti muscles (arrow) projected onto the ocular coats provide some orientation. Distance of muscle insertion to limbus is about 8mm; NO = optic nerve. b) Schematic drawing.

No examination should be terminated before all echographically visible structures, from the ciliary body to the orbital soft tissues, have been evaluated. Anybody who is well versed in the method will take no more than a few minutes for this type of screening.

The Three-Dimensional Image

The introduction of rapid scanning contact B-mode devices with high resolution power has made the results of our examinations much more vivid. However, constructing a three-dimensional image from individual acoustic sections may occasionally represent difficulties (Figure 6). Bronson (1976) refers in this connection to the surprising cross sectional images which can be obtained when examining a wine bottle (Figure 7)[21].

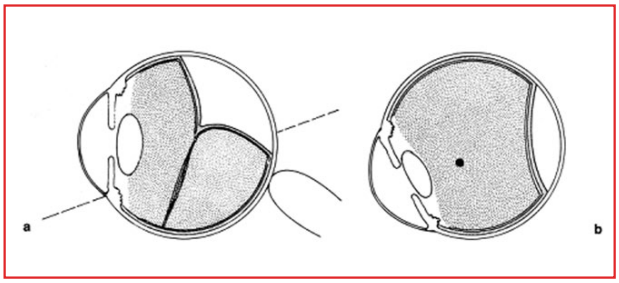

Figure 6: (a, b) Schematic drawing of traction detachment in two planes at 90° to each other. Only examination from different directions enables us to differentiate strands and membranes.

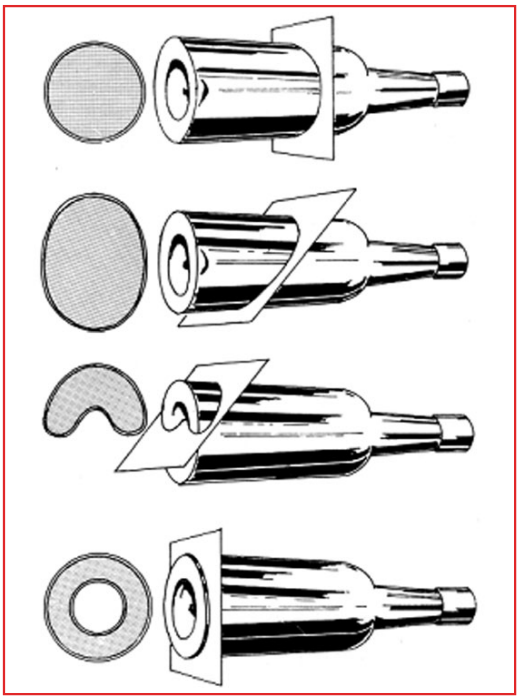

Figure 7: Bronson has pointed out the surprising sectional images which we obtain when examining a wine bottle echographically.

The currently available instruments suggest a course of examination which, independent of the problem at hand, consists of four steps (Figures 8-11).

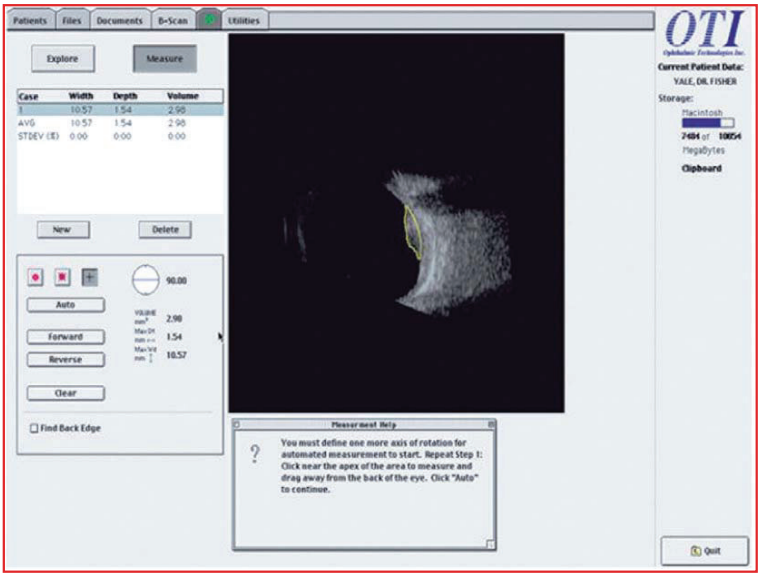

Figure 8: *3D contour determination using a scan unit of OTI (Ophthalmic Instruments, Inc.).*

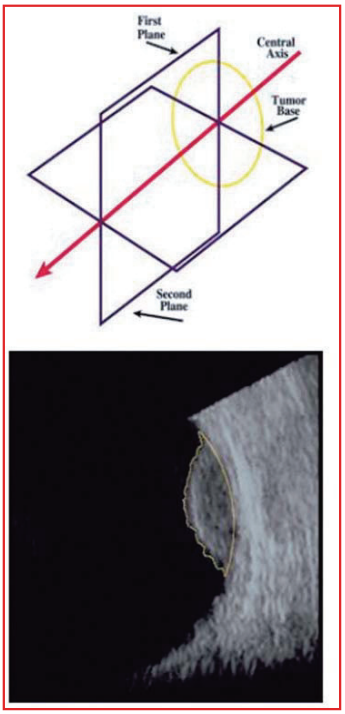

Figure 9: *Example for the automated contour finding procedure of space-occupying lesions (OTI, Ophthalmic Instruments, Inc.)*

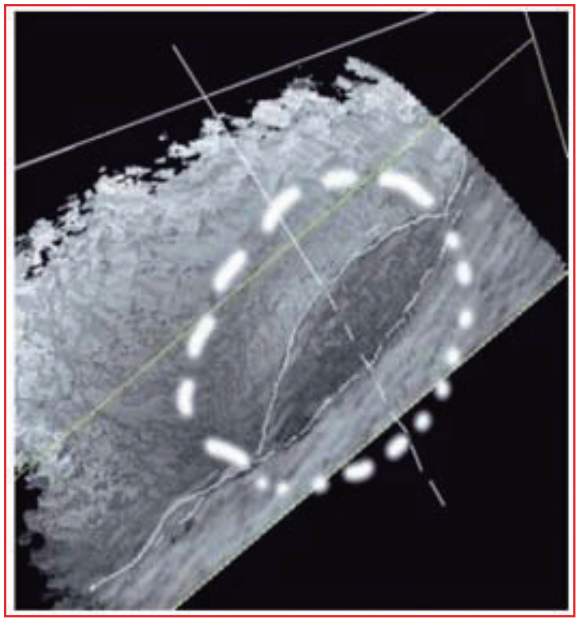

Figure 10: *Example for 3D rendering of the posterior segment with marked areas of interest and outlined space-occupying lesions (OTI, Ophthalmic Instruments, Inc.).*

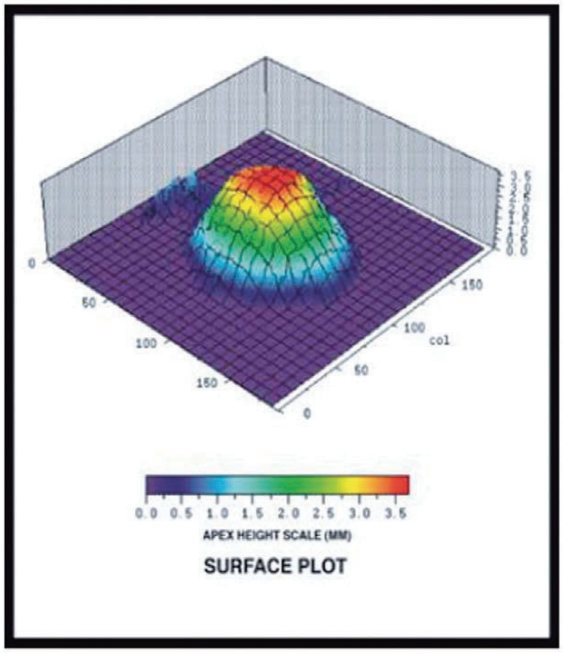

Figure 11: Surface plot for volume determination of space-occupying lesions (OTI, Ophthalmic Instruments, Inc.)

1. Finding the known anatomical landmarks with the help of contact B-scan technique;
2. Determining the location of pathologic findings with special consideration of the motility of pathologic structures;
3. Giving a detailed description of the pathologic findings on the basis of its reflection properties considering quantitative echography (comparison with standards) and estimating the sound attenuation;
4. Including all available clinical information for final evaluation.

Figures 8-10 show examples for automated contour finding procedure, 3D rendering and volume determination.

The Integration of B-Mode Doppler Instruments (Duplex Scanner)

The routine A- and B-mode techniques have matured; the possibilities and limitations of these methods are known. Only during the last years have we been able to use the Doppler effect of frequency shifts to evaluate and measure movements within a tissue and flow conditions within vessels. These frequency shifts can be observed in tissue volumes of less than 10mm; they therefore represent additional information about the circulation in small tissue areas. So far there is no instrument available which is designed specifically for use in ophthalmology. On the basis of interesting results in cardiology and pediatrics [30], it seems worthwhile to use similar instruments in ophthalmology [31, 32]. With this examination method small tissue areas can be investigated in cross sectional echograms and tested for a frequency shift. By colour coding a large ultrasonic cross section, all areas in which a frequency shift occurs can be made conspicuous by a specific colour. The first results were reported and summarized in 1989 [32].

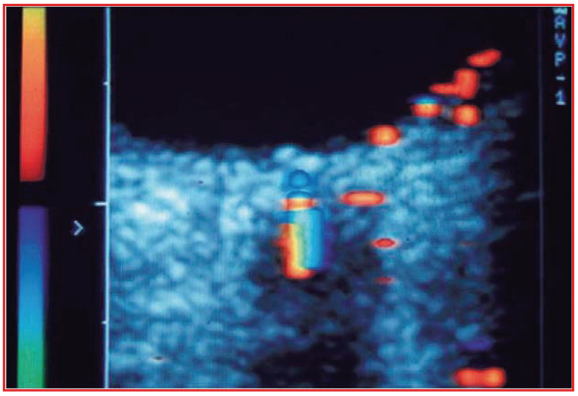

Figure 12: Cross sectional ultrasonogram through the posterior pole of the eye, color-coded signals from central retinal artery (red) and central retinal vein (blue) are displayed inside the distal optic nerve.

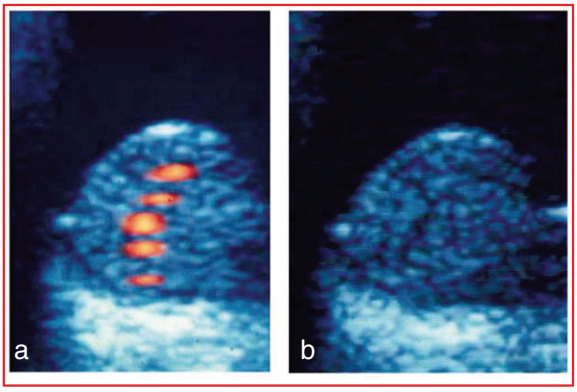

*Figure 13: **a**) Using highest sensitivity of the amplifier and decreasing the wall filter setting, we can differentiate between a structure of red color coding (vessels with the flow toward the transducer) and a circumscribed area close to the peak of the melanoma in which the blood flows away from the transducer (blue). This type of sonography may give us new clues as to planning and controlling the treatment of intraocular tumours. **b**) Color-coded Doppler signal analysis shouws that this area is the origin of frequency shifts toward the transducer.*

Ultrasound Biomicroscopy

Ultrasound biomicroscopy is a recent technique to visualize the anterior segment with the help of high frequency ultrasound[3]. Pavlin and Foster developed this technique at the Princess Margaret Hospital at Toronto, Canada in 1989. They developed three probes - 50, 80 & 100 Mhz for clinical trials [33, 34]. 80 & 100 MHz probes were used to see the cornea and the anterior chamber as the depth of penetration is only 2 mm. They reached to a conclusion that a 50 MHz is an ideal compromise between depth and resolution to visualize the entire anterior segment. They published the first papers on UBM in 1990 [22]. The first commercially available machine was developed by Zeiss in 1991. These machines were available with 30 and 50 MHz probes.

The transducer used mainly in UBM's has a frequency of 50 MHz. The radiofrequency of 50 MHz is produced by a piezoelectric crystal[35]. This radiofrequency penetrates the body tissue and is reflected back to the transducer. Normal B-scan transducer has oil filled covering with a membrane over the piezoelectric crystals. The penetration of the 50 MHz UBM transducer is poor, hence the transducer has an open crystal and there is no membrane covering the crystal. In UBM's the movements of the transducer have to be subtle to scan appropriate areas in the anterior segment. To enable this subtle movement there is a special motion control device for the transducer. The transducer is mounted on a skit for a linear scan fixed on a large handle.

The most important limitation of UBM is depth. UBM cannot visualize structures deeper more that 4 mm from the surface. The other limitation is that UBM cannot be performed in presence of an open corneal or scleral wound.

UBM is done with the patient in the supine position and the eye is open. Since the piezoelectric crystal of the transducer is open it should not come in direct contact with the eye to prevent injury to the cornea. There is a special cup which fits in between the eyelids, keeping them open. The eye cup is filled with saline or sterile methylcellulose. The crystal of the transducer is placed in saline approximately 1- 2 mm from the eye surface. Images produced by UBM have a resolution of 30-40 microns hence they are seen similar to those seen on a low power microscope [36] (Figure 14).

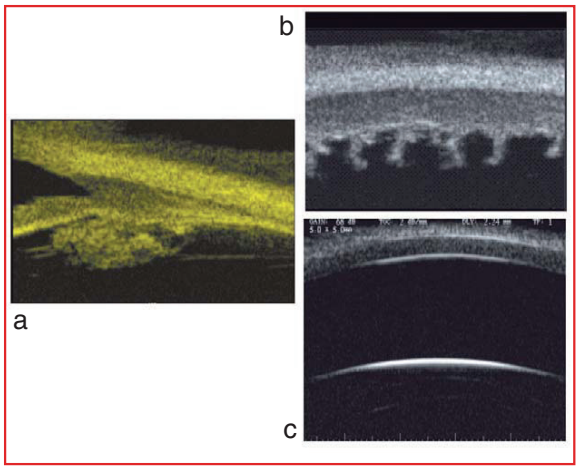

Figure 14: UBM images of the anterior segment, A – ciliary body area, B – ciliary processes, C – anterior chamber with sclera and lens.

The cornea is the first structure seen on ultrasound biomicroscopy. The anterior chamber is seen as an echo-poor area between the cornea and the iris. The anterior chamber depth can be measured from the posterior surface of the cornea to the anterior lens pole. The posterior lens pole can not be imaged.

The iris is seen as a flat uniform echogenic area. The iris and ciliary body converge in the iris recess and insert into the scleral spur. The area under the peripheral iris and above the ciliary processes is defined as the ciliary sulcus. The angle can be studied in a cross section by orienting the probe in a radial fashion at the limbus. The scleral spur is the most important landmark in the angle on UBM. The exact quantification of the angle measurement and structures around the iris.

The ciliary body can be clearly defined by UBM from the ciliary processes to the pars plana. The ciliary processes vary in appearances and configuration. The axial view of the ciliary processes is seen when taking a section of the angle. The individual processes are better seen in a transverse section through the ciliary processes. The posterior ciliary body tapers off towards the pars plana. The anterior zonular surface can be consistently imaged by UBM. The zonules are seen as a medium reflective line extending from the ciliary processes to the lens surface. The posterior chamber is defined as the space between the anterior vitreous face and the posterior surface of the iris. Indications for UBM:

- Glaucoma
- Uveitis
- Trauma
- Tumours
- Scleritis

Recently some other instruments are on the market e.g. P60 UBM (Paradigm Medical Industries Inc.) and VuMax UBM 35/50 (Sonomed Inc.) using the sector scan technique (Figure 15). Anterior and posterior lens pole can be imaged with booth instruments. Although none of the instruments achieve the spatial resolution of the Zeiss-Humphrey unit.

3D Ultrasound Biomicroscopy

It has long been appreciated that three-dimensional (3D) ultrasonic images can be produced from an ordered series of scan planes. This technique was first applied to the anterior segment of the eye by Iezzi et al. [37] and required considerable effort and ingenuity with regard to apparatus [27, 38, 39]. Iezzi et al. used a scanning control arm for a continuous z-movement and stored the data on videotape for subsequent digitalization. Silverman et al. [28] characterized the ciliary body including the state of the ciliary processes of rabbits and normal human subjects using 3D high-resolution ultrasound. There the scanning system consist of two orthogonal linear stages with a computer-controlled stepping motor.

In author's laboratory a simple and low-cost extension of the commercial Ultrasound Biomicroscope Model 840 (Humphrey Instruments, Carl Zeiss Group) into a userfriendly 3D- ultrasonic imaging system was developed. Here 3D data sets consist of B-scan stacks of in-parallel planes with a defined distance between them. Patients were scanned with the ultrasound probe coupled to the eye with Methocel (Ciba Vision) and a normal saline water bath. The examiner positioned the transducer in the center of the ocular segment of interest using standard B-mode.

For 3D imaging the computer-controlled scanning system moved the transducer perpendicular (z-direction) to the B-scan plane (xy-plane) over the area being scanned. For this motion an additional miniature skid was mounted on the original linear motor of the UBM scanning device where the ultrasound transducer is attached (Figure 15). Because of its weight it is not possible to attach also the drive of this skid. Therefore the skid is powered from an external stepping motor via a Bowden wire.

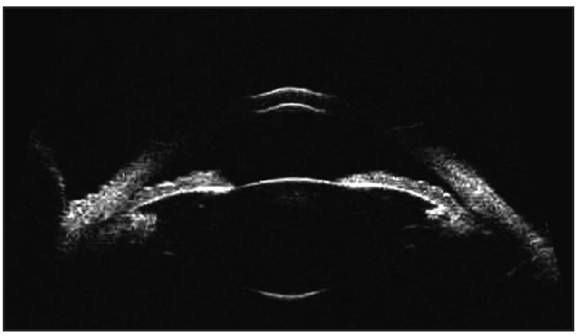

Figure 15: *The anterior segment using the VuMAX UBM 35/50, Sonomed, Inc.*

The video signal of the ultrasound unit is digitized using a frame-grabber board (HaSoTec, Germany) synchronized with the z-motion control system. That means during image capturing the z-movement is stopped and the image plane is exactly perpendicular to the z-axis. 10 s acquisition time with a scanning range of 2.5 mm was used for all subjects, which is thought to be the maximum considering patient and examiner movements. Thus, all 3D scans have the same sampling density. The original UBM raw data (256 scan lines x 1024 samples per line, 256-level grayscale) pictured on the UBM display with 880x440 pixels were converted into 440x440 pixels (256-level gray scale) during capturing by the frame grabber. No degradation of the image quality is observable and the influence of the conversion is negligible compared with the movement artefacts and contour finding. The motion control and data acquisition system is connected with an SGI workstation via a local area network for 3D reconstruction using AMIRA (TGS, San Diego, CA, USA). This commercial volume rendering software package provides an interactive environment allowing features such as volume orientation for viewing planes and 3D perspectives, segmentation and determination of distances and surfaces. The feature of model building allows outlining of anatomic structures in space and can be used for volume measurements.

An example for 3D imaging is given in Figure 16 showing the anterior segment with ciliary body. There are some publications about ex vitro and in vivo applications of these instruments[23, 24, 40-43]. The investigations are mainly focused on accommodation studies and the evaluation of so-called accommodative lenses.

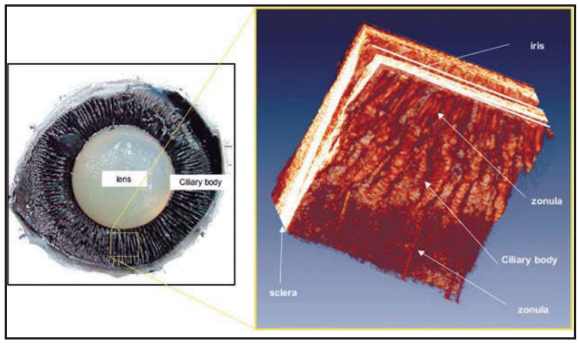

Figure 16: *3D Reconstruction of the human ciliary body (anterior segment viewed from behind).*

Practical Approaches based on Ultrasonography

We shall attempt in this chapter to represent a brief discussion on the role of echography within routine clinical practice. We shall only exceptionally mention those disease entities for which echography is not of diagnostic help.

The Red Eye

The conjunctival vessels can easily be examined with biomicroscope because they lie superficially in the tissue, and the conjunctive is only slightly pigmented. The degree of blood flow is regulated by arteriovenous anastomoses, which can be influenced by locally synthesized inflammatory mediators[44]. This clinically produces the picture of a circumscribed hyperemia in which all vessels, which are otherwise transciently open, will be filled with blood. This produces an intensive red discoloration which may be confined to the bulbar conjuncitva or may involve the entire conjunctival sac. On the other hand, passive hyperemia, as it is caused by a cavernous sinus fistule, will dilate the vascular network, in which, after a prolonged course, the blood vessels become rarified (Figure 17).

Frequently, the clinical picture or history alone will not suffice for a differentiation between the active hyperemia produced by inflammatory mediators from a purely mechanical orbital congestion.

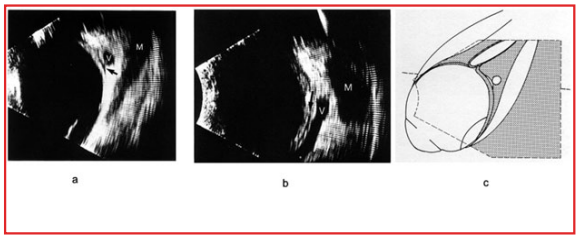

Figure 17: *Spontaneous arteriovenous fistula of the cavernous sinus in a 83-year old woman. Increasing unilateral dilatation of the episcleral veins for the preceding four weeks. Progressive non-specific decreased ocular motility. a) Horizontal cross sectional echogram through the nasal part of the orbit. b) Frontal cross sectional echogram. The overload on the venous vascular system has not only dilated the vein, but has also led to a circumscribed edema in Tenon's space, a widening of the recti muscles (here of the medial rectus), and a peripheral choroidal detachment. c) Schematic drawing.*

Echography can give us important clues concerning the differential diagnosis[45]. In Table 1 the final diagnosis of 93 patients are listed. Their main sign was a dilatation of the conjunctival and episcleral vessels, and echography was useful in establishing the correct diagnosis.

A spontaneous carotid cavernous sinus fistule will most often lead to a circular dilatation of the episcleral vessels. In patients with orbital pseudotumor, a sectorial vascular dilatation usually points toward an involvement of extraocular muscles. If all other etiologic factors can be excluded, these patients with unilateral increased intraocular pressure may suffer from an idiopathic dilatation of the episcleral veins[46-48]. A massive circular vascular dilatation is the principal sign of a brawny scleritis. The differential diagnosis is especially important here because the intraocular elevation can clinically and echographically not be differentiated from a choroidal melanoma[49,50]. Unfortunately, neither A- nor B-mode echography provides reliable differential diagnostic points, so that this disease, even today, may occasionally lead to an unnecessary enucleation because a melanoma had been suspected. A pseudotumor of the anterior orbit may lead to less conspicuous and partly sectorial vascular dilatations. In myositis a few or individual extraocular muscles are affected and the conjunctival hyperemia if present is sectorially limited to the area of their insertions. Table 2 compares diagnoses and typical echographic findings for the main sign "red eye".

Table 1
Diseases with dilatation of the episcleral vessels (n = 93)

Spontaneous cavernous sinus fistula	26
Traumatic cavernous sinus fistula	9
Orbital pseudotumor ± involvement of extraocular muscles	21
Episcleritis	5
Brawny scleritis	3
Graves' orbitopathy	5
Aseptic thrombosis of orbital veins	4
Idiopathic dilatation of episcleral veins	5
Conjunctival nevus	2
Ciliary body melanoma	3
Metastatic bronchial carcinoma to the ciliary body	1
Tolosa-Hunt syndrome	2
Osler disease	1
Sturge-Weber syndrome	4
Arteriovenous anomaly of the orbit	1

Table 2: The red eye. Echographic findings.

Sectorial Vascular Dilatation	
Diagnosis	Echographic Finding
Ciliary body melanoma	Evident tumor
Metastatic tumor to the ciliary body	Evident tumor
Scleritis	Widening of sclera and of Tenon's space
Episcleritis	Widening of Tenon's space
Myositis	Widening of the muscle, also at the insertion. Low acoustic reflectivity otihe muscle belly
Circular Vascular Dilatation	
Diagnosis	Echographic Finding
Uveitis	Vitreous opacities
Secondary glaucoma due to intraocular tumor	Evident tumor
Orbital pseudotumor	Widening of various orbital structures with low acoustic reflectivity
Orbital cellulitis	Widening of various orbital structures with low acoustic reflectivity, ± detachment of periosteum, sound propagation into perinasal sinuses
Thrombosis of orbital veins	The ophthalmic vein or its branches can be echo graphically demonstrated, not compressible, not pulsating
Spontaneous cavernous sinus fistula (Red eye shunt syndrome) traumatic cavernous sinus fistula	Ophthalmic vein or its branches demonstrable, on pressure pulsation, muscles widened
Graves' orbitopathy	Widening of muscles, high acoustic reflectivity of muscle belly
Idiopathic dilatation at episcleral veins	No pathologic findings

Episcleral vascular dilatations which present diagnostic difficulties are mainly (in a ration 1:3) due to congestion. Figure 18 summarizes the etiologic possibilities of congestive hyperemia; the numbers behind the diagnosis refer to the location of the lesion as discussed in the subsequent paragraph.

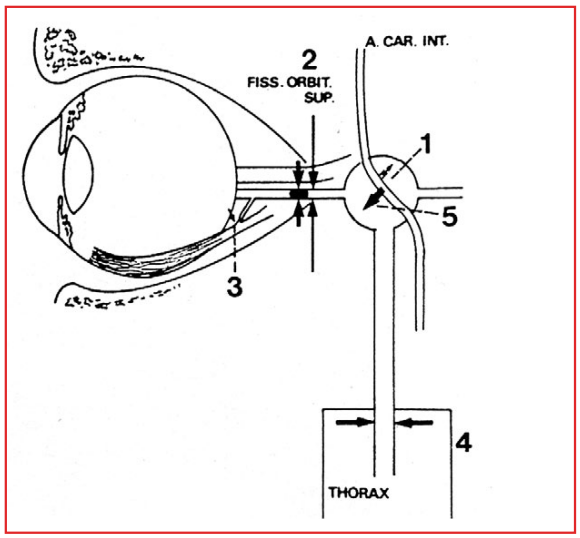

Figure 18: *Possible causes of stasis hyperemia (explanation in the text)*

Most numerous are spontaneous cavernous sinus fistules (1), which can only exceptionally be diagnosed before their first radiologic or echographic examination. An obstacle for outflow may lie in the superior orbital fissure (2) and will usually be produced by a tumour or pseudotumor. According to the reports published so far, the impedance for outflow in idiopathic episcleral venous stasis lies in the extraocular muscles (3). From a theoretical point of view and also according to the published literature, a thoracic stasis, as it exists in the superior vena cava syndrome, may cause similar signs and symptoms (4). Conspicuous arteriovenous shunts, as we seen them in traumatic cavernous sinus fistules (5), can usually be diagnosed by history and the clinical picture (Figure 19). Mixtures between active and passive hyperemia may develop, especially in patients with inflammatory orbital pseudotumor.

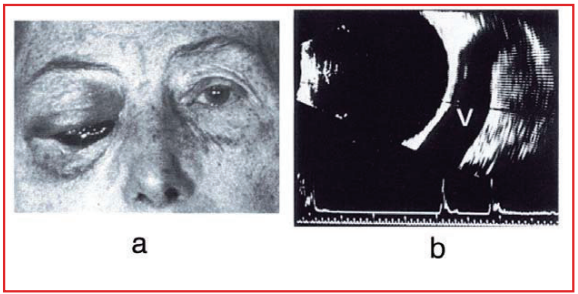

Figure 19: *Clinical picture and echographic findings in a case of traumatic cavernous sinus fistula. a) Marked chemosis after acute deterioration of a traumatic fistula which had been present for years; the picture shows the patient after numerous attempts to close the fistula by embolization. b) Widening of the ophthalmic vein to about 8 mm (V); upon pressure there is a collapse of the vessel synchronously with the pulse.*

Blurred Disk Margins – Elevation of the Optic Nerve head

We frequently cannot decide with certainty whether a disk with blurred margins and slight elevation represents a pathologic condition or not. If unequivocal pathologic findings are lacking, it is up to the examiner to decide how far the diagnostic procedures should be carried. It may be necessary to obtain neurologic consultations and to perform neuroradiologic investigations, including an MRI. On the other hand, after weighing the cost-benefit ratio and the risk of some side effects, the investigator may rely on his clinical acumen and decide that the condition only represents a variant of the norm.

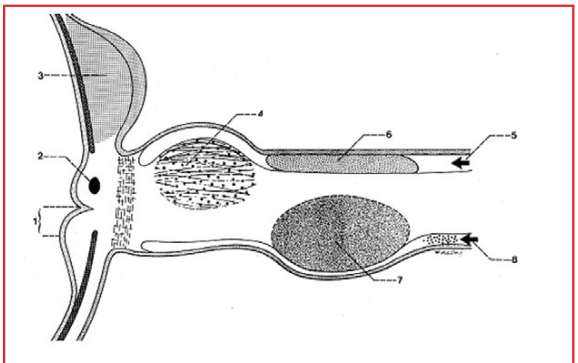

Figure 20: *Blurred disk margins – elevated optic nerve head. Differential diagnostic contributions of echography (explanations: see table 3).*

Echographic examinations make it possible to support the clinical impression to a certain extent and to delineate somewhat the diagnosis of blurred disk margins. Figure 20 in association with Table 3 facilitate in a schematic form the correlation between clinical and echographic findings. Examples are given in Figures 21, 22, 23 and 24.

Table 3
Blurred disk margins – elevated optic nerve head. Echographic contributions to the differential diagnosis (numbers behind the diagnosis refer to the location of lesion in figure 20.

Diagnosis	Echographic Finding
Pseudopapilledema in hyperopia (1)	Short axial length, widened ocular wall
Disc drusen (2)	Structures of high acoustic reflectivity in the area of the optic nerve head (independent from the degree of calcification)
Ocular hypotony	Widening of ocular coats, occasionally with choroidal detachment
Posterior scleritis (3)	Widening of ocular coats, Tenon's space demonstrable
Optic neuritis (4)	Widening of dural diameter (always found in diskedema, present in 70% of eyes with retrobulbar neuritis)
Optic disk edema (5)	Widening of dural diameter
- Due to increased intracranial pressure	
- Due to compression of the orbital part of the optic nerve	
Optic nerve tumors	
- Meningioma (6)	Widening of dural diameter (opticociliary shunt vessels)
- Glioma (7)	Widening of dural diameter, occasionally spindle-shaped thickening of optic nerve
- Metastatic carcinoma (8)	Widening of dural diameter
Blurred disk margins without echographically demonstrable changes	
- Congenital disk anomalies	
- Central vein occlusion	
- Anterior polemic optic neuropathy	

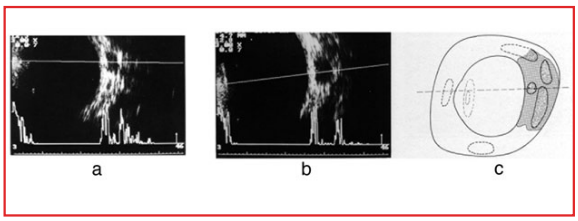

Figure 21: a,b) *Comparison of the A- and B-echograms of the orbits in a patient with acute retrobulbar neuritis. The dural diameter of the involved optic nerve is 4,7mm. On the uninvolved side the diameter is 2,8mm on the available cross section. Upon temporal examination with maximal abduction of the globe, the ultrasound encounters the optic nerve nearly vertically.* ***c)*** *Schematic drawing.*

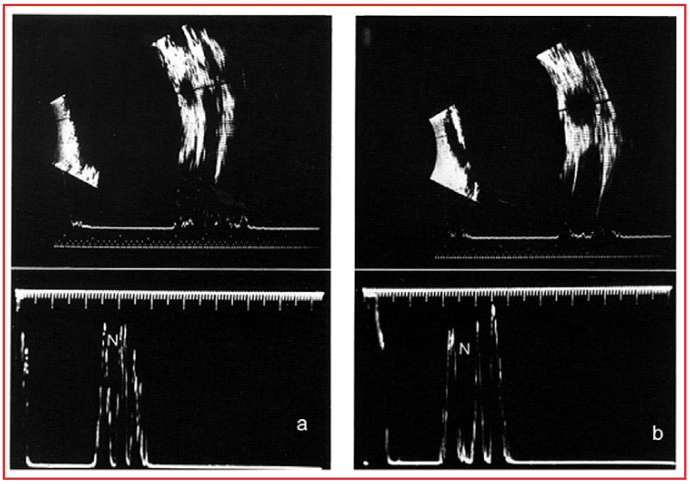

Figure 22: *Marked widening of the subarachnoidal space in chronic papilledema. If the optic nerve head has become atrophic, a dilated dural diameter represents an important proof that the intracranial pressure is still elevated. a) Normal dural diameter (5,0µs corresponds to 4,0mm). b) Markedly dilated dural diameter (7,0µs corresponds to 5,6mm).*

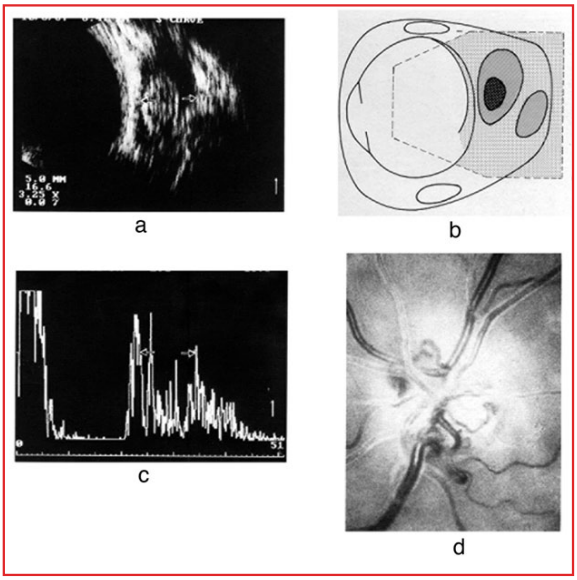

Figure 23: a-d*) Meningioma of the optic nerve sheath. Echographically, the dural diameter is widened to about 10mm, both on A- and B-echography (arrows). The optic nerve is surrounded by a tumor envelope which shouws low acoustic reflectivity. Cilioretinal shunt vessels on the optic nerve head associated with an echographically increased dural diameter can be regarded as pathognomonic for a meningioma of the optic nerve sheaths.*

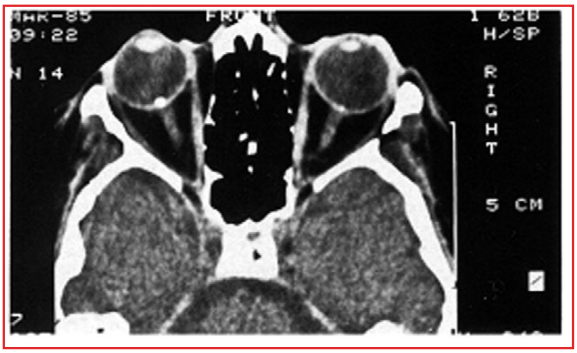

Figure 24: *CT scan of a patient with bilateral drusen of the optic nerve. On the left, the drusen lie in the cross section; on the right, they are barely visible because they are only partly encompassed.*

Choroidal Folds

In the older literature choroidal folds were always interpreted as a sign of an orbital space-occupying lesion[51, 52]. They are typically horizontal folds and rarely extend beyond the equator. Fluorescein angiography allows an exact differentiation between retinal and choroidal folds [53, 54]. Newell was the first to express some critical comments on the above interpretation [55]. Reports appeared in the literature describing intraocular diseases or scleritis, producing a comparable ophthalmoscopic picture [56-58]. Our own examinations [59] show that during a longterm follow up, the pathologic ophthalmoscopic findings may disappear and the associated refractive errors may return to normal values. Verbeek [60] summarized, on the basis of literature review complemented by his own findings, the importance of echography for the differential diagnosis. Analyzing 167 patients, he found an ocular cause in 46 of them; in 26, an orbital lesion, and in 17, an atypical papilledema was diagnosed. No definite diagnosis could be established in 11 patients (Tables 4-6; Figure 25).

Table 4
Choroidal folds. Orbital causes (after Verbeek)

Diagnosis	Number of Patients
Graves orbitopathy	11
Sinusitis	5
Mucocele	2
Hemangioma	6
Orbital pseudotumor	5
Various orbital tumors	8
Unexplained	6
Total	43

Table 5
Choroidal folds. Ocular causes

Diagnosis	Number of Patients
Hyperopic Eye	17
Macular degeneration	12
Ocular hypotony	12
Posterior scleritis	9
Buckling operation	9
Trauma	6
Intraocular tumor	3
Miscellaneous	10
Total	78

Table 6: Choroidal folds. Echographic findings.

Diagnosis	Echographic Finding
Myositis, Graves' orbitopathy (1)	Thickened extraocular muscles
Periorbital space occupying lesion (2)	Change in the relief otthe orbital wall, sound propagation into perinasal sinuses
Orbital neoplasma(3)	Directly evident (it maybe difficult to demonstrate a small cavernous hemangioma because of its high acoustic reflectivity)
Inflammatory orbital pseudotumor (4)	Widening of normal orbital structures, low acoustic reflectivity, Tenon's space may be demonstrable
Disk edema (5)	Widened dural diameter of the optic nerve
Axial hyperopia (6)	Axis length below 22 mm, ocular coats concentrically thickened
Ocular hypotony (7)	Ocular coats concentrically thickened
Macular degeneraron	Thickening of the ocular coats in the area of the macula, high acoustic reflectivity
Scleritis (8)	Circumscribed widening of the ocular coats, Tenon's space demonstrable

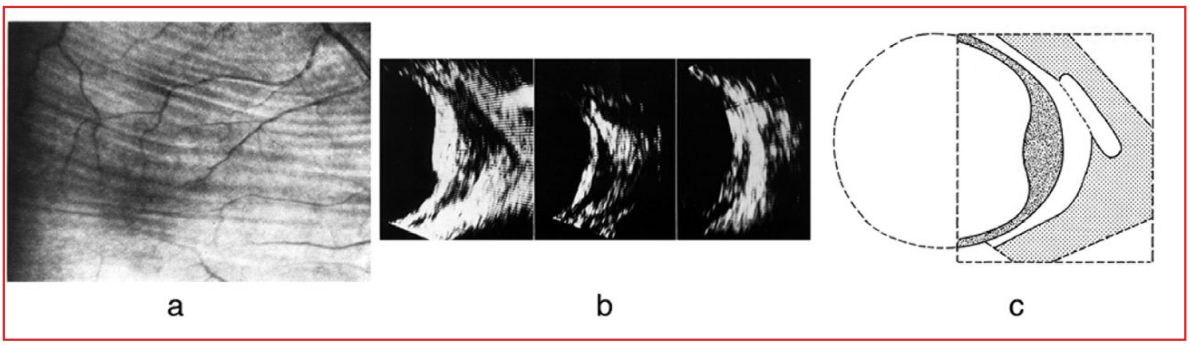

Figure 25: 34-years old patient with pain induced by ocular movements, hyperopic shift (3 dpt) and reduction of visual acuity (0,4). a) Fundusphotography. Marked retinal/choroidal folds at the posterior pole. b) B-scan ultrasound: massive thickening of ocular coats, widening of Tenons' space and fluid accumulation around the superior oblique muscle. c) Schematic drawing: clinical findings improved after systemics steroid treatments. Despite full clinical regression infiltration of Tenons' space remained visible by ultrasound for several weeks. There is no recurrency for at least five years.

Leukokoria

Whenever we diagnose leukokoria, a retinoblastoma has to be excluded. Figure 26 and table 7 illustrate and list the differential diagnostic help given by echography. Examples are given in Figures 27-30.

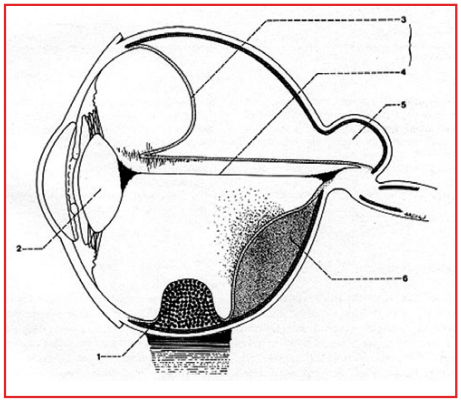

Figure 26: Leukokoria – echographic contributions to the differential diagnosis (explanation: see table 7).

Table 7
Leukokoria. Echographic findings helpful for differential diagnosis (numbers behind the diagnosis refer to the location of the lesion in figure 26)

The Axial Length Normal for Patient's Age	
Diagnosis	Echographic Finding
Retinoblastoma (1)	Widening of the ocular coats, extremely high acoustic reflectivity, shadowing effect, atypical findings posible
Congenital cataract (2)	Increased reflectivity from the posterior lens surface, vitreous space empty, ocular coats normal.
Shortened Axial Length	
Diagnosis	Echographic Finding
Retinopathy of prematurity (3)	In stages IV and V, beginning or complete traction detachment (normal echographic findings in stages I-III)
Persistent hyperplastic primary vitreous (PHPV) (4)	Dense strand of tissue between optic nerve head and posterior lens pole; formes frustes may occur (posterior or anterior PHPV)
Retinal anomalies	Membranes in the vitreous, atypical detachment, which in part appears solid (no typical echogram)
Fundus coloboma (5)	Directly demonstrable protrusion of ocular coats, sometimes with orbital cyst (microphthalmus with cyst)
Coats' disease (6)	Floating crystals in the vitreous and subretinal space (fast flickering spikes on A-mode)

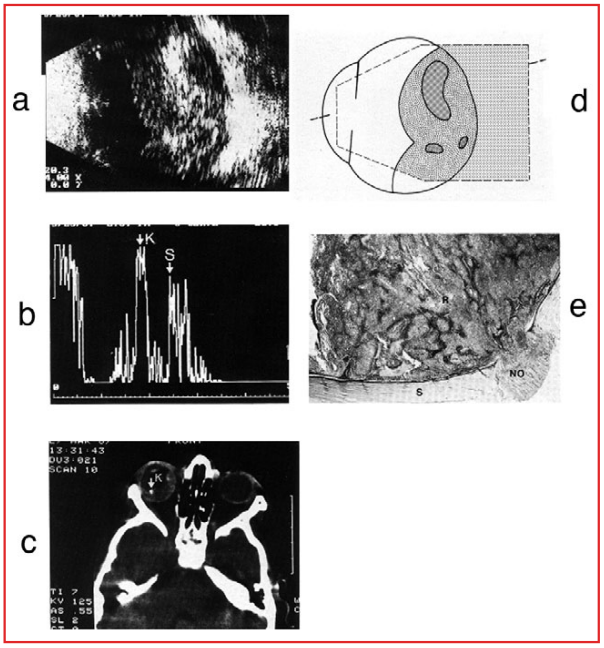

Figure 27: *Extensive retinoblastoma. a) In cross sectional echographic images the tumor is characterized by areas of high acoustic reflectivity alternating with areas of low reflectivity. b) The difference in reflection can be quantified on A-mode echography: calcified parts of the tumor (K) have markedly higher amplitudes than the sclery (S). c) in a CT scan the calcified parts of the tumor can be identified with greater certainty than in a plain X-ray picture. d) Schematic drawing. e) Already under loupe magnification the heterogenous structure of the tumor with calcium deposits can be recognized. These structures explain the nearly pathognomonic echogram. Tumor invasion on the anterior optic nerve can be echographically demonstrated only exceptionally by widening on the dural diameter (NO = optic nerve, R = retinoblastoma).*

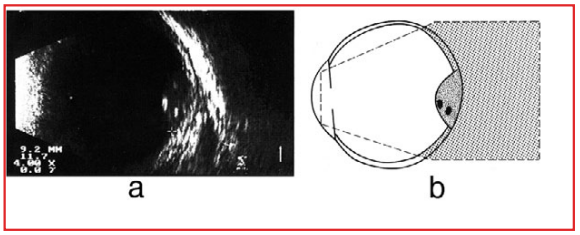

Figure 28: *a) Small retinoblastoma (elevation 3mm) with circumscribed calcium deposits. Even small tumors may show calcium deposits due to rapid tumor growth. These deposits are especially well demonstrable in linear amplification. b) Schematic drawing.*

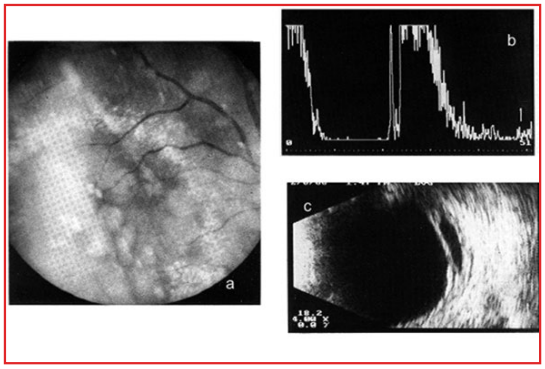

Figure 29: *Circumscribed, strongly reflecting retinal detachment in Coats' disease. a) Clinical photo. b, c) The strongly reflecting membrane in association with floating opacities in the subretinal space corroborates the diagnosis.*

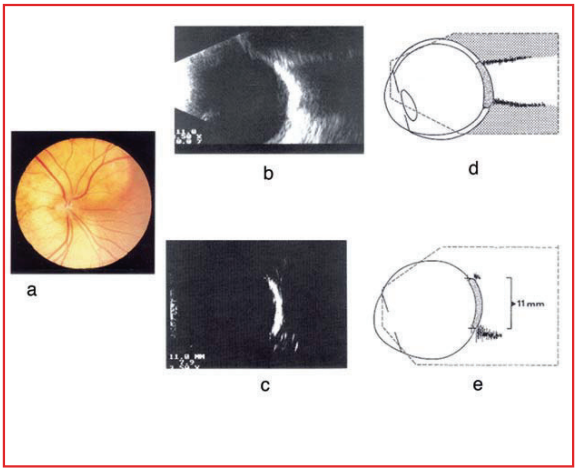

Figure 30: *Choroidal osteoma. a) Right fundus of a 9-year-old girl. Vision at the time the photo was taken 0,8. A yellow-brown, space-occupying lesion covers the posterior pole of the globe. Ophthalmoscopically, it is hardly elevated. It surrounds the optic nerve head like a pair of pincers. b)Cross sectional echogram of the choroidal osteoma shown in a: in this echogram the lesion is characterized by total reflection of the ultrasound, and shadow formation. An Elevation cannot be unequivocally documented. c) Schematic drawing d) With reduced amplification it is possible to image the ossification as an isolated signal. The horizontal diameter is 11,0mm. e) Schematic drawing.*

Vitreous Hemorrhage

An acute vitreous hemorrhage will nearly always lead the patient to the ophthalmologist. As discussed, echography is the method of choice to evaluste the situation and to estimate the prognosis. Entoptic functional tests can complement the echographic findings. Figures 31 and Table 8 summarize the most important differential diagnoses . Examples are given in Figures 32-35.

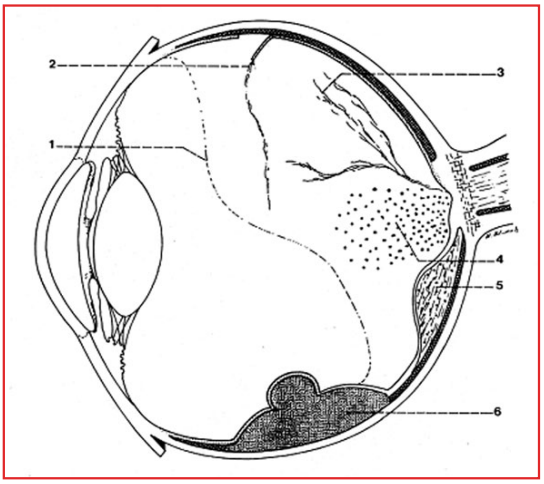

Figure 31: *Vitreous hemorrhage – echographic contributions to determine the pathogenisis (explanation: see table 8)*

Table 8: Vitreous hemorrhage. Echographic findings helpful for establishing the etiology (numbers behind the diagnostic refer to the location of the lesion in figure 31).

Diagnosis	Echographic Finding
Symptomatic posterior vitreous detachment (1)	Thickened detached posterior hyaloid membrane, occasionally beginning retinal detachment
Recently formed retinal break with torn vessel (2)	Blood-covered vitreous strands converge toward the retinal break; occasionally a high floating operculum may be detected
Proliferative retinopathy (3)	Strands or membranes extending from the optic newshead or the posterior pole, high acoustic reflectivity
Terson syndrome (vitreous hemorrhage after subarachnoidal bleeding) (4)	Vitreous opacities in front of the optic nerve head or behind the detached vitreous
Disciform macular degeneration (5)	Widening of the ocular coats in the macular area, high acoustic reflectivity, vitreous strands extending fromthe macula
Choroidal melanoma (6)	Biconvex thickening of the ocular wall, low acoustic reflectivity, sometimes washroom-shaped. Accompanying retinal detachment distant from the tumor

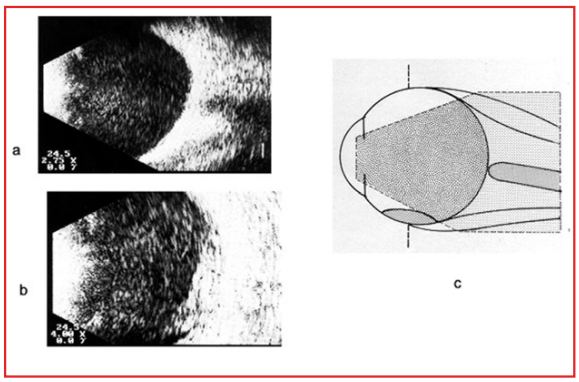

Figure 32: *a, b) Conspicuous bleeding into a synergetic vitreous. A static picture may give the impression of a solid lesion. After a few hours the opacities usually accumulate in the lower aspect of the vitreous cavity. c) Schematic drawing.*

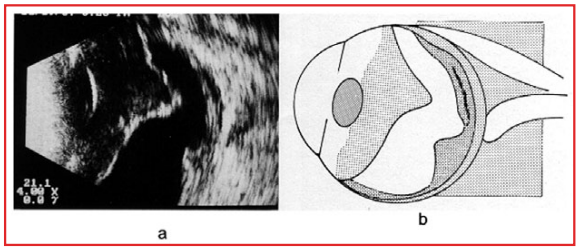

Figure 33: *a) Extensive bleeding from a disciform macular degeneration the presence of which was known. The bleeding disseminates onto the ocular coats and the formed vitreous. The retrovitreal space is already clear because of its high fluid exchange. b) Schematic drawing.*

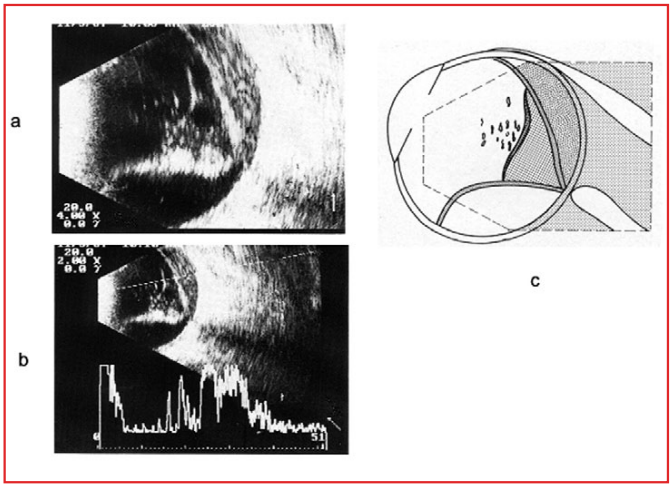

Figure 34: a, b) Long-standing retinal detachment with floating opacities in the subretianl space. The densifications in the vitreous space indicate a tendency for shrinkage. c) Schematic drawing.

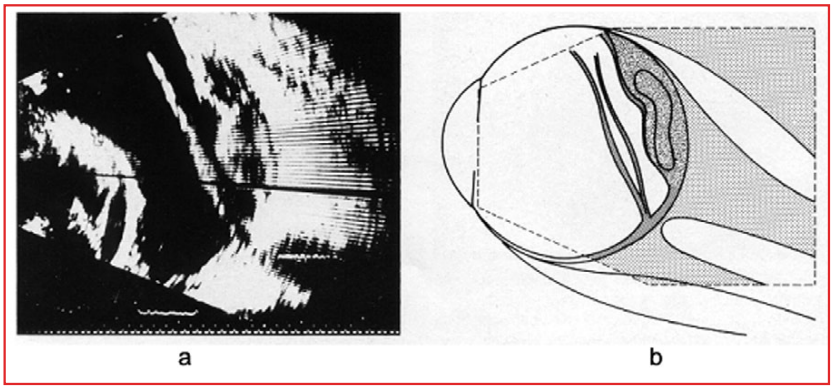

Figure 35: a) Total retinal detachment in an eye with extensive disciform macular degeneration. Beneath the completely collapsed retinal leaves, heterogenous, partly strongly reflecting thickened ocular coats can be observed. b) Schematic drawing.

Examination before a Vitrectomy

Still in the 1980-years echography was the decisive examination to determine the indications for vitreous surgery. Further developments of surgical methods, especially the advances in illumination technique, prove that the surgeon may not need a detailed knowledge of the conditions within the vitreous body. A few findings which can only be obtained echographically are still important to estimate prognosis and risks of an operation. Figure 36 and Table 9 list some of the possible echographic information and the subsequent conclusions as far as the operative plan is concerned. Examples are given in Figures 37-40.

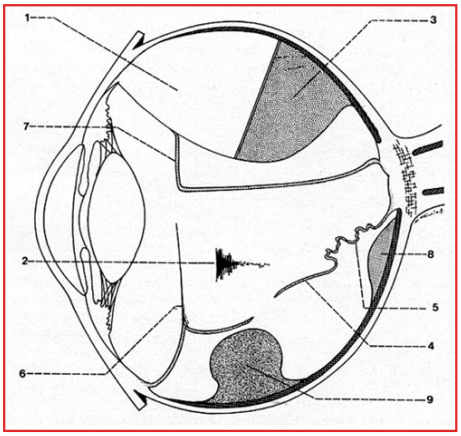

Figure 36: Examination before a vitrectomy – echographic contributions to the planning of the operation (explanation: see table 9).

Table 9
Examination before a vitrectomy. Echographic findings helpful for planning the operation (numbers behind the questions refer to the location of the lesion in figure 36.

Questions on the Echographic Examination	Consequences for Planning the Operation
Choroidal detachment including the pars plana? (1)	Avoiding this area when inserting the ports
Post-traumatic vitreous hemorrhage, retina attached?	If retina detached, strong indication for vitrectomy
Intraocular foreign body demonstrable? Location in regard to ocular coats (2)	Choice of surgical approach: magnet extraction possible?
Estimating the Prognosis	
Choroidal detachment caused by blood (3)	Extremely poor prognosis; perhaps even abandon the operation
Free-floating retinal detachment (4)	Reattachment probable, can be achieved without tamponade from the inside
Rigid retinal detachment? Thickened retina? (5)	Removal of preretinal membranes necessary
Vitreous strands with traction effect demonstrable? (6)	Cutting the strands
Retinal parts behind the lens? (7)	Special care indicated when entering the vitreous space
Thickened ocular coats in the macula (disciform degeneration?) (8)	Poor prognosis for central vision
Indications of a secondary, e. g., solid, retinal detachment? (9)	Additional diagnostic examinations; enucleation may be necessary
Attached retina with minimal remaining vision?	Reconsider indication for operation; prognosis for vision extremely poor

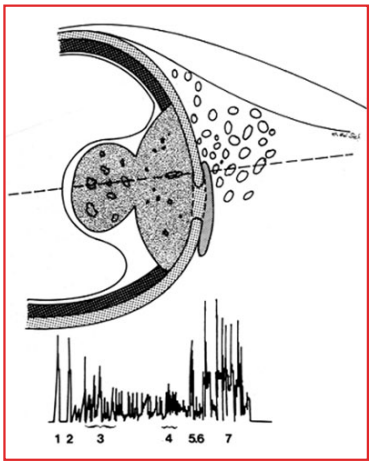

Figure 37: *Schematic presentation of A- and B-mode echographic criteria for the choroidal melanoma. 1- Stongly reflecting retinal surface. 2- Spike with similar amplitude from the tumor surface. 3-6 – Signals from inside the tumor which can be used to characterize the type of neoplastic tissue. 3 – Strong reflectivity produced by the dilated vessels in the part of the tumor lying in front of Bruch's membrane. 4 – Flickering spikes on A-mode, produced by blood flow. 5 –Scleral spike. 6 – Extraocular tumor growth with reflectivity. 7 – Orbital fat showing high reflectivity.*

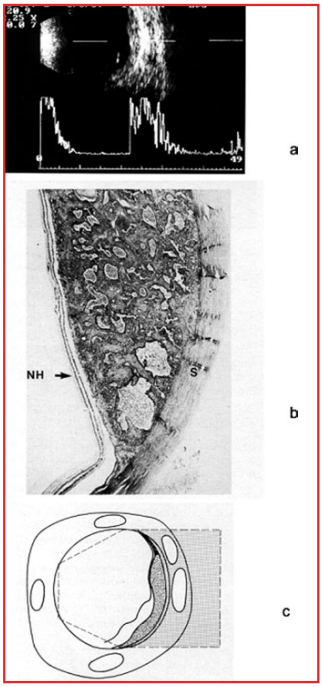

Figure 38: *Extensive choroidal metastatic tumor in the lower nasal quadrant. a) On the echogram the choroids is widened to about 2,5mm; the retina is partly detached by an exudates. The tissue inside the metastatic tumor shows high acoustic reflectivity. b) Histologic section of a metastatic adenocarcinoma in the choroids. The gland-like structure provides good acoustic interface.c)Schematic drawing.*

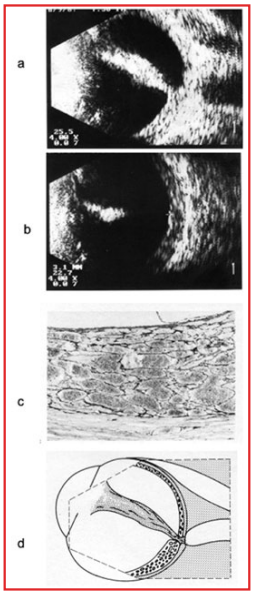

Figure 39: *Extensive choroidal hemangioma in Sturge-Weber syndrome (additional finding: total retinal detachment). a) Cross sectional echogram through the area of the optic nerve head. In the lower quadrant the ocular coats are markedly thickend. (In spite of the associated retinal detachment, the intraocular pressure was 50mmHg by applanation). b) With reduced sensitivity, the scleral surface can be delineated in spite of the high acoustic reflectivity within the tumor (distance of measuring marks 3.1mm). c) Histologic section through the tumor illustrated in a and b: The septa of the cavities are thin and lined with endothelium. They produce strong reflectivity within the lesion. d) Schematic drawing.*

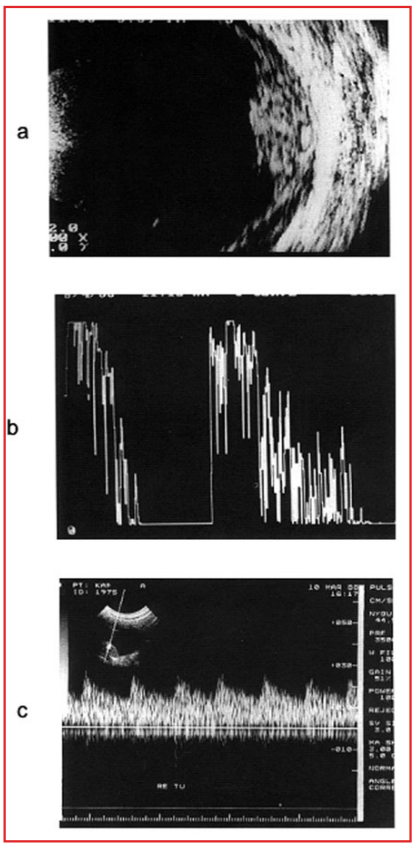

Figure 40: a) Cross sectional echogram of a circumscribed choroidal hemangioma in a 12 year old boy. The tumor has an elevation of 4 mm. b) In an A-mode echogram with S-shaped amplification the cross sectional picture corroborates the high reflectivity of the tumor. c) On Doppler sonography (Duplex scanner ATL MARK 8), we see blood circulating within the tumor, synchronous with the pulse. The illustrated velocity profile speaks for a relatively low resistance by the blood vessels

Exophthalmus

Before CT and MRI was introduced, echography was the only diagnostic method which enabled us to examine soft tissue pathology in the orbit. Ossoinig and Till, in particular, contributed to the value of echography for the preoperative differential diagnosis of orbital lesions[18]. However, it seems dubious whether it is reasonable to delineate – as some authors have attempt to do – 80 different pathologic processes involving the orbit by echographic findings. When a malignant space-occupying lesion is suspected, a histologic examination will be necessary in all doubtful cases in order to ascertain a correct diagnosis. Speculations about the benign or malignant nature of a lesion on the basis of echographic findings are of little help.

We attempt here to present a classification which enables the examiner to use the echographic diagnosis as a filter to separate thoses disease processes in which the echographic examination can ascertain the diagnosis from pathologic processes in which other diagnostic examinations, usually by other medical specialists, will be necessary. Figure 41 and Table 10 correlate the most frequent causes of exophthalmus with the echographic findings (the numbers behind the diagnoses indicate the location of the lesion as shown in Figure 41). Patients with pseudoexophthalmus may be diagnosed by measuring the refractive error of the affected eye, but they can be definitely recognized echographically.

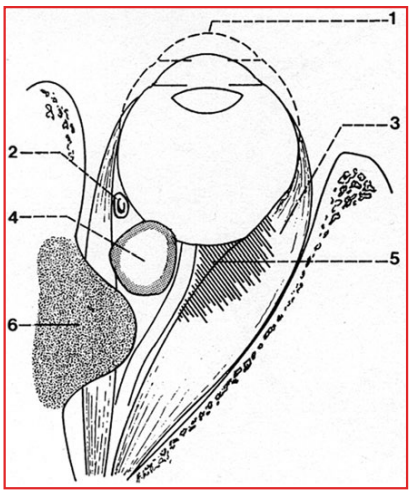

Figure 41: Exophthalmus – echographic contributions to differential diagnosis (explanation: see table 10).

Table 10: Exophthalmus. Echographic findings helpful for differential diagnosis.

Diagnosis	Echographic Findings
Pseudoexophthalmus (1)	Myopic globe, flat orbit
Vascular exophthalmus (2)	Branches of the ophthalmic vein demonstrable
• Spontaneous or traumatic cavernous sinus fistula	Venous branches pulsate on pressure
• Thrombosis of orbital veins	Noncompressible venous branches demonstrable
Myogenic exophthalmus (3)	Widening of the recti muscles (differential diagnosis: Graves' orbitopathy, myositis, lymphoma, metastatic carcinoma, carotid-cavernous sinus fistules)
Neoplasms (4)	Space-occupying lesion separated from orbital fat, varying acoustic reflectivity
Inflammatory infiltration (5)	Widening of pre-existing orbital structures, homogeneous acoustic properties. Tenon's space demonstrable
Exophthalmus caused by space occupying lesion extending from the surroundings (6)	Changes in the contour of the orbital walls, detachment of periosteum, sound propagation into the perinasal sinuses

The various types of vascular exophthalmus can be echographically differentiated up to a certain degree. In our experience, the entity of "red eye shuntsyndrome", the spontaneous dura cavernous sinus fistule, has so far been diagnosed too sparingly. The diagnosis can be regarded as certain if we find a combination of a slightly elevated intraocular pressure, a red eye and veins that pulsate on pressure. The condition occurs mainly in older patients and has, with few exception, a good prognosis with a good chance of spontaneous healing [61]. In the individual patient we have to consider whether angiography would not constitute an unjustifiably high risk.

The differential diagnostic conditions of a myogenic exophthalmus are listed in Table 10. The clinical picture including laboratory work-up, will usually allow a definite diagnosis. A CT scan or MRI is often unnecessary.

Cysts, especially those associated with microphthalmus, are usually congenital and need no further diagnostic test or treatment if they cause no signs or symptoms. Dermoids do not always appear echographically as true cysts because the varying components have different acoustic reflectivities. In case of doubt, a CT scan will help to characterize and diagnose these space-occupying lesions because of their fat content.

Echography alone will not suffice if there is an involvement of periorbital structures. In these cases, we need other methods to image soft tissues for diagnostic purposes in order to evaluate the pathologic process affecting adjacent structures. The treatment is often provided by nonophthalmologists.

The inflammatory exophthalmus usually presents a differential diagnostic problem. We first have to exclude a propagation of the inflammation from the perinasal sinuses by using other diagnostic procedures. It then has to be decided individually whether a working diagnosis of orbital pseudotumor is justified and whether such a diagnosis can be ascertained by a trial run of systemic treatment with corticosteroids. In case of doubt, a histologic clarification will be necessary.

A CT scan is indispensable when an orbital neoplasm needing as surgical intervention is suspected. With the exception of the cavernous hemangioma,

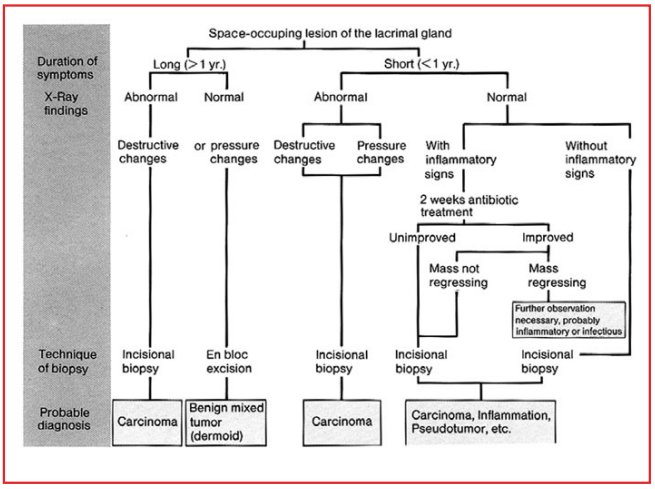

Figure 42: *Space-occupying lesions of the lacrimal gland (from Spalton and Wright in: Spalton, DJ, Hitchings RA, Hunter PA. Atlas der Augenkrankheiten; Thieme Verlag, Stuttgart 1999).*

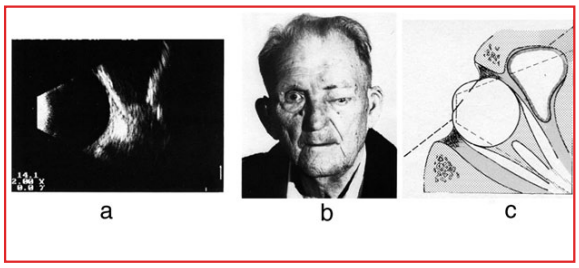

Figure 43: *a-c) Mucocele of the frontal sinus in a 72-year-old man, eight years after an impression fracture of the frontal bone. Echographically, this condition is characterized by a smooth protrusion of the orbital roof with sound propagation into the frontal sinus, which is filled with secretion. Frequently, we can obtain a slight deformation of the tumor by pressing on it with the transducer.*

which, due to its internal structure, provides a nearly pathognomonic echogram, the ultrasonic differential diagnosis remains speculative.

Space-occupying lesions of the lacrimal fossa need, independent from the echographic findings, a therapeutic approach which is mainly guided by clinical and radiological parameters. Wright (1984) has published a schematic orientation for this purpose (Figures 42-46).

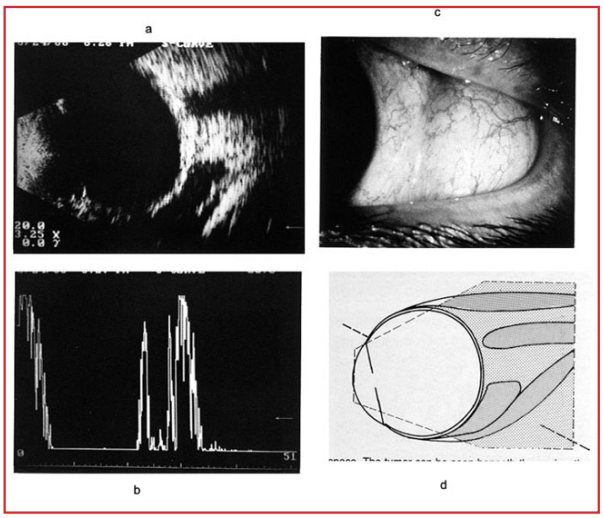

Figure 44: a-d) Lymphoma of the orbit, involving Tenons's space. The tumor can be seen beneath the conjunctiva extending into the muscle cone.

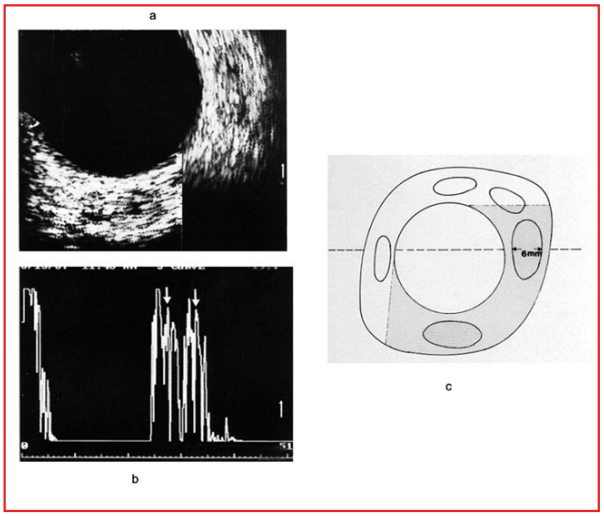

Figure 45: a, b) Pronounced Graves' orbitopathy with symptoms for the preceding 12 months. The muscle can be delineated from the orbital fat only with difficulty; the muscle thickness is about 6,0mm (medial rectus) and 7,8mm (inferior rectus). c) Schematic drawing

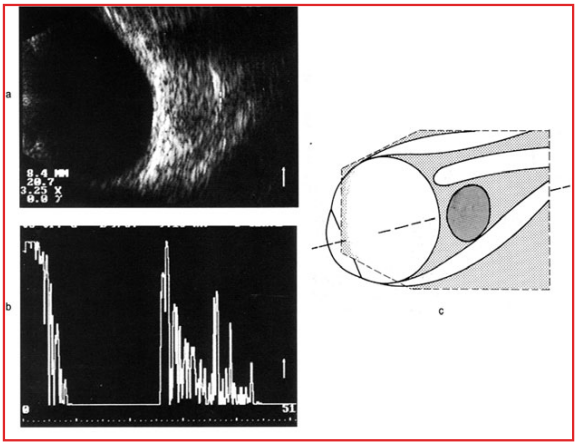

Figure 46: Small cavernous hemangioma in the muscle cone. a) A suitable gray scale with logarithmic representation delineates the tumor clearly from the surroundings also on B-mode. b) The diagnosis is corroborated by the characteristic sound attenuation with linearly decreasing internal echoes when the S-mode amplification is used for A-mode. c) Schematic drawing.

Deficits in Ocular Motility

Deficits in ocular motility can be analyzed by diagnostic methods revealing the soft tissue of the orbit whenever the cause of the deficit lies in the orbit itself. Neurogenic lesions cannot be imaged echographically. In our experience, echographic examinations are only of limited help when evaluating posttraumatic motility deficits. We are, however, capable of differentiating between lesions within and outside of the muscle[62]. Figure 47 and Table 11 list the most frequent echographically demonstrable etiologic factors.

If an enlarged muscle has been found, we have to decide whether loss of effective contraction or loss of stretchability is the cause of reduced activity of the involved muscle. If only one muscle is affected, the answer to the question is simple. In doubtful cases, we have to consider the concept of common visual axes between the two eyes. Whenever one muscle cannot be normally stretched, contraction of the antagonist will press on the globe and therefore increase the intraocular pressure, depending on the direction of gaze. Table 12 lists the correlation between possible muscle widening and the expected ocular motility deficits. Unequivocal statements can only be made

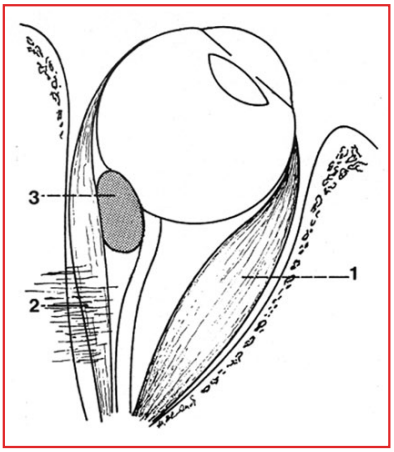

Table 11
Orbital causes of decreased ocular motility. Echographic findings helpful for the differential diagnosis (numbers behind the diagnosis refer to the location of the lesion in figure 47).

Diagnosis	Echographic Findings
Widened extraocular muscle (1)	Myositis: Low acoustic reflectivity of muscle belly; insertion also widened Graves' orbitopathy: Muscle belly with strong acoustic reflectivity; in protracted course muscle can barely be differentiated from orbital fat Metastatic carcinoma Lymphoma Cavernous sinus fistula
Extension of a pathologic process (2)	Purulent sinusitis, tumor invasion
Expanding orbital process (3)	E.g., hemangioma, neurinoma

Figure 47: *Orbital causes of disturbed ocular motility – echographic contributions to the differential diagnosis (explanation: see table 11).*

about "Graves orbitopathy: whenever there is a motility deficit in the disease, we always find a loss of stretchability of the involved muscle. In late stages the contraction capability of the muscle is further decreased by the atrophy of normal muscle fibres which are replaced by connective or adipose tissue. In the literature idiopathic myositis is nearly exclusively associated with decreased contractility[63]. According to our examinations[64], this narrow correlation does not exist. In more than 50% of such patients there is primarily a loss of stretchability of the affected muscles. If the area of the cavernous sinus is also involved (Tolosa-Hunt syndrome), we primarily find neurogenic deficits. Metastatic tumors to the muscles may produce both kinds of motility deficits. In our experience a loss of stretchability is more frequently seen[64].

In cases of bacterial infection the contractility of the muscle will be decreased, even if the muscle itself is only slightly enlarged.

Circulatory disorders, e.g. cavernous sinus fistules or thrombosis of the orbital veins, will usually produce a mixed picture with reduced contractility and stretchability.

Expanding space-occupying lesions may have a mechanical effect on ocular motility without directly invading the muscle. This applies especially to intraocular lesions. In these cases the intraocular pressure will nearly always increase in certain directions of gaze. If this sign is absent, we should consider a neurogenic component of the decreased motility.

Table 12
Widened extraocular muscles. Correlation between etiology and expected motility defect.

Diagnosis	Motility Defect	
	Decreased Stretchability	Decreased Contractility
Graves' orbitopathy	+	(+) in late stages
Idiopathic myositis	+	(+)
Metastatic carcinoma	+	(+)
Lymphomatous infiltration	(+)	+
Muscle involvement in orbital cellulitis	(+)	+
Muscle edema in circulatory disorders	(+)	(+)

Anterior Segment Space Occupying Lesions

The ultrasound biomicroscopy is able to detect anterior segment space occupying lesions. Examples for application are anterior segment tumors (iris tumors, ciliary body tumors, cysts, peripheral choroidal tumors and lymphoma) as well as trauma. Pavlin and Foster[3] have discussed this in detail. Figures 48 and 49 show two examples using the conventional two-dimensional technique as well as Figures 50-52 using 3D ultrasound biomicroscopy [41].

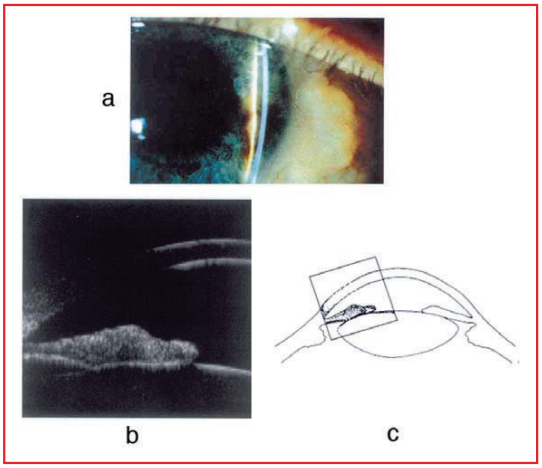

Figure 48: *a) Slit lamp photography. b) UBM: Solid space-occupying lesion in midperipheral iris respecting integrity of the iris pigment epithelial layer. c) Schematic drawing.*

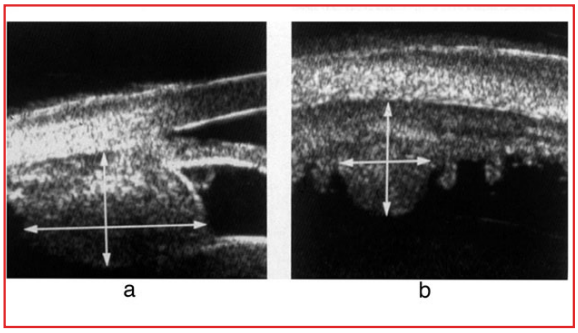

Figure 49: *Measurement of iris neoplasia. a) UBM, radial section (tumor diameter 2,6mm, tumor thickness 1,9mm). b) UBM, meridional section (tumor diameter 2,6mm, tumor thickness 1,9mm).*

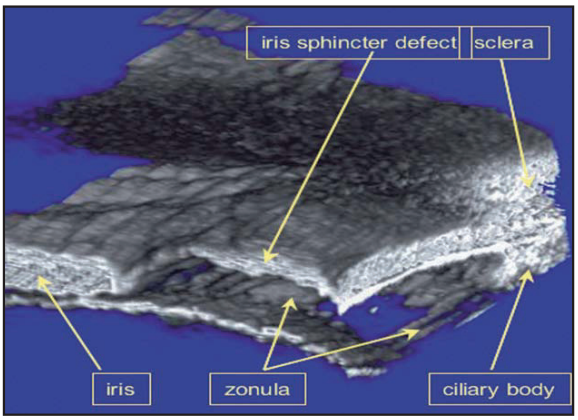

Figure 50: *3D-reconstructed volume of the iris sphincter defect, zonulolysis and prolaps of the vitreous body after contusion bulbi after 3D UBM.*

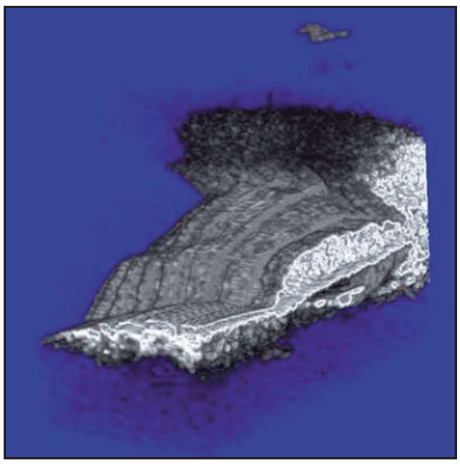

Figure 51: 3D-reconstructed volume of the iris naevus in 3D UBM

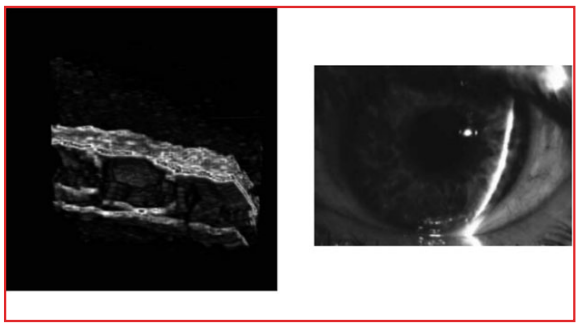

Figure 52: A view into the volume of cysts of the iris and ciliary body in 3D UBM and the clinical picture.

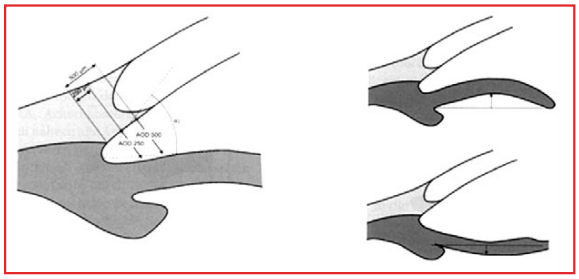

Figure 53: Measuring lines after Pavlin (left) to characterize iris convexity/concavity following a suggestion of Potash (right).

Chamber Angle Abnormalities of Questionable Origin

Ultrasound biomicroscopy can be used to image various structural chamber angle abnormalities of the anterior segment. The method is usually able to determine the mechanism of elevated intraocular pressure (angle closure versus open angle) showing the relationship between the peripheral iris and the trabecular meshwork. Strong correlation between gonioscopic and UBM findings of angle configuration has been established. In addition, imaging of the anterior segment structures is possible even in eyes with several corneal edema that precludes gonioscopic assessment of the angle. In open-angle glaucoma, UBM can be used to measure the anterior chamber angle in degrees, to assess the configuration of the peripheral

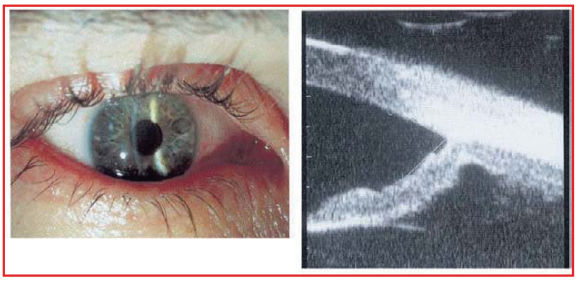

Figure 54: Pigmentary dispersion syndrome.

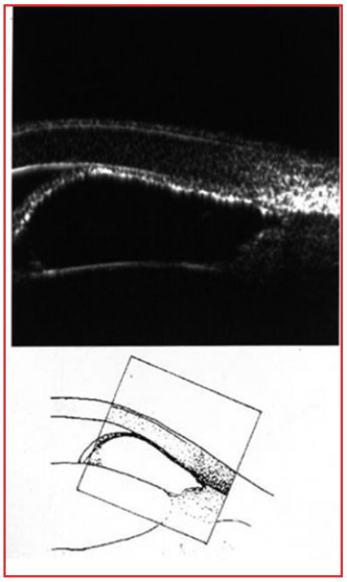

Figure 55: Secondary pupil block.

iris, and to evaluate the trabecular meshwork. The angle configuration can be graded (Figure 53) and compared with gonioscopic findings.

In certain patients with open-angle glaucoma, UBM can provide additional diagnostic information. For example, in pigment dispersion syndrome UBM typically reveals posterior bowing of the peripheral iris (Figure 54). In plateau iris syndrome UBM usually reveals abnormally steep anterior angulation of the peripheral iris, insertion of the iris from the anterior ciliary body, and retroiridic projection of the ciliary processes. In eyes with peripheral anterior synechiae, UBM can reveal the extent of iridocorneal adhesion even if by opaque and hazy cornea. In eyes with a narrow angle (Figure 55), UBM shows the extent of angle closure, reveals the depth of the anterior and posterior chambers, and identifies pathologic processes pushing the lens and iris forward UBM is been able to differentiate between primary angle closure i.e., cases of angle closure without additional pathology responsible for the anterior lens-iris displacement and secondary angle closure due to processes such as lens swelling and dislocation, massive hemorrhagic retinal detachment pushing the lens and iris anteriorly and multiple neuroepithelial cysts of the iridociliary sulcus.

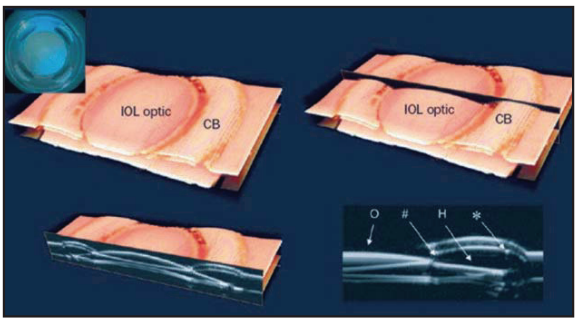

Figure 56: *Photograph and three-dimensional ultrasound biomicroscopy image and B-scan of the 1CU in the artificial silicone capsular bag (CB). Abbreviations: O = optic, # = fulcrum, H = haptic, and * = haptic ridge.*

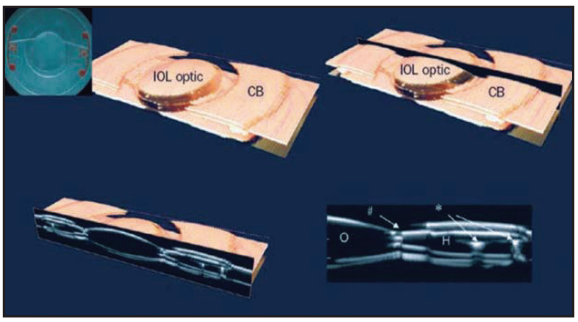

Figure 57: *Photograph and three-dimensional ultrasound biomicroscopy image and B-scan of the CrystaLens AT-45 in the artificial silicone capsular bag (CB). Abbreviations: O = optic, # = fulcrum, H = haptic, and * = polyimide construction.*

Accommodative Artificial Intraocular Lenses – Contributions of Ultrasonography

The fundamental idea of some approaches to achieve potentially accommodating IOLs is to allow an axial displacement of the IOL optic. In author's laboratory the haptic regions of the Akkommodative 1CU and the CrystaLens AT-45 were scanned in the simulation model during different accommodative states. These in vitro results were correlated and used to describe the in vivo condition in four patients with accommodative implants.

The biometric analysis of high-frequency sonographic images becomes difficult if the information from only one A-scan section is possible. Regarding the analysis of haptic configurations, undefined tilting effects can falsify biometric measurements. The three-dimensional ultrasound biomicroscopy[24] combined with a powerful volume rendering software provides features such as volume orientation for viewing planes and three-dimensional perspectives. These features include an auxiliary tool for identification and biometric analyzing of the haptic configuration with minimized tilting effects (Figures 56 and 57).

Streching Device

For analysis of the IOL performance, an artificial capsular bag was mounted in a simulation device The arms of the fixture clamp the bag around its periphery at eight points. Rotation of the inner ring stretches or relaxes the bag. Inner ring rotation is accomplished by a stepping motor driving a worm gear. The amount of stretching correlates with the rotation of the inner ring. The entire arrangement is submerged in water for sonographic imaging.

In Vitro results: 1CU

The posterior chamber lens 1CU was examined. Theoretically, a contraction of the ciliary muscle, thus a relaxation of the zonules, leads to a relaxation of the capsular bag. The haptics turn and produce an anterior axial shift according to the modified force ratio in the haptic region. Our simulation experiments show a similar effect during capsular bag relaxation. A 0.5-mm change in r was used for maximal relaxation/stretching. With this unphysiological and unexpected amount of relaxation in humans, a 0.36-mm anterior shift was observed for the 1CU caused by a haptic 10.4° angulation change. Using a 50-year lens and the linear regression of Strenk for the ciliary body displacement, a 0.25-mm ciliary body displacement can be assumed. A 0.28-mm anterior IOL shift and an angulation change of 4.3° was observed. For this lens, the theoretically predicted 30° haptic angulation change for 1-mm axial shift could not be achieved (Figures 58 and 59).

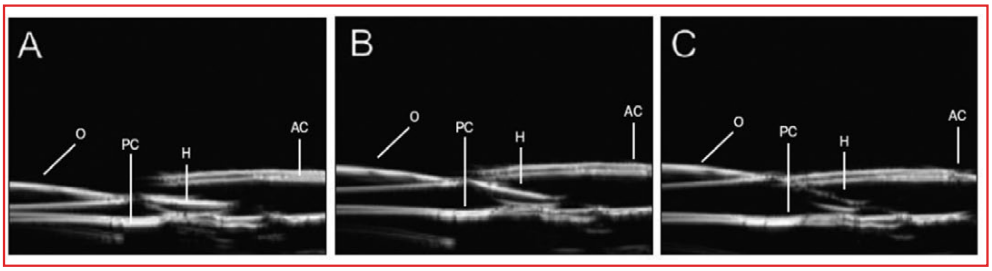

Figure 58: *A-C) B-scan series exemplifying the stretching experiment.*
Abbreviations: O = optic, PC = posterior capsule, H = haptic, AC = anterior capsule.

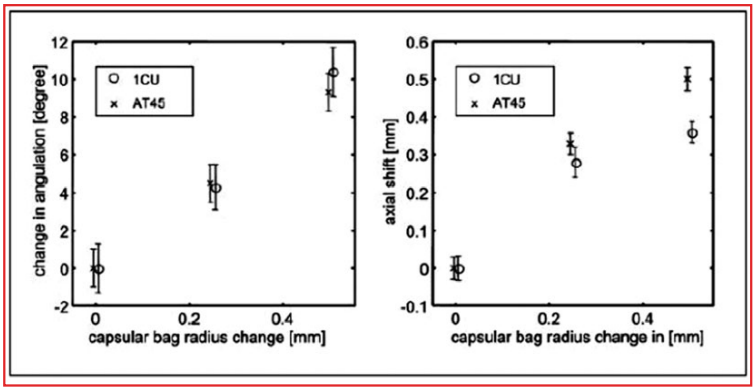

Figure 59: *Change in angulation (left) and axial IOL movement (right) by lens type showing the effect of equatorial stretching respectively relaxing.*

In Vitro results: AT-45

In the in vitro model, a maximal forward shift of 0.50 mm (9.3° haptic angulation change) for the AT-45 lens was observed using the maximal radius change of 0.5 mm. For 0.25-mm radius change as the expected value for the 50-year lens, an axial shift of 0.33 mm with 4.5° angulation change was found. In our model, equatorial changes can be simulated, but vitreous pressure variations cannot be simulated. Regarding the axial shift, the AT-45 performed 0.14 mm better compared to the 1CU for 0.5-mm radial displacement.

In Vivo situation: 1CU

Figure 60 shows a three-dimensional reconstruction and the image analysis of the 1CU haptic region. Changes in angulation and ΔACD by four different individuals show the effect of cyclopentolate and pilocarpine 4 months postoperatively. In disaccommodation, a haptic angulation between 2° and 4° caused by capsular bag shrinkage and secondary cataract formation is visible. This could mean that a haptic angulation is already present in the disaccommodated state. In the cases studied, pilocarpine induced an additional angulation variation between 5° and 10° for the 1CU IOL, which causes a change in anterior chamber depth between 0.2 and 0.5 mm. Using Gullstrand's eye model, this 0.2-mm forward movement results in a refraction change <0.38 D (0.95 D for 0.5 mm of movement), depending on exact IOL position. These found ΔACD values are smaller than the findings of Langenbucher et al. [65]. A mean ACD decrease of 0.78 mm (0.49 to 1.26 mm) using the IOL-Master and 0.63 mm (0.34 to 1.12 mm) was found using ultrasound biometry after pilocarpine (6 months postoperatively). Our findings are in agreement with the results of Findl et al. [66, 67]. Using partial coherence interferometry, Findl et al found a moderate forward movement under pilocarpine with an induced mean accommodative amplitude of 0.50 D.

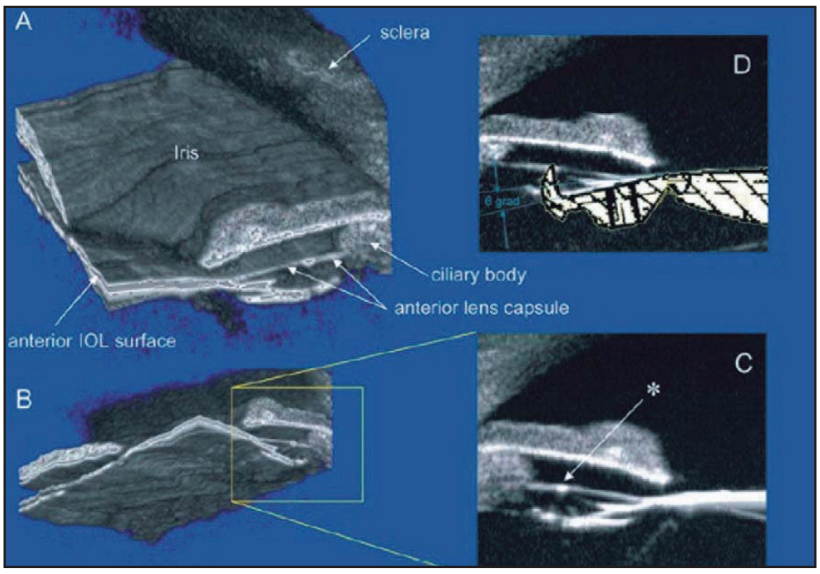

Figure 60: *Three-dimensional reconstruction and C, D) image analysis (with design drawing) of the 1CU haptic region in a 75-year-old patient 4 months postoperatively (disaccommodation). A 6° haptic angulation compared with the relaxed IOL condition is observed.*

In Vivo situation: AT45

The angulation depending on the of the accommodation state could be distinguished and analysed (Figure 61). In-vivo, a mean change in haptic angulation 3.3 ± 3.3° (range 0° to 7°) and a mean forward shift of 0.13 ± 0.08 mm (range 0.05 to 0.2 mm) was observed for the AT-45 using pharmacologically induced accommodation. An accommodative amplitude of mean 0.44 ± 0.24 diopters (range 0.25 to 0.75 D) was found using a Hartinger coinicidence refractomter. Conclusions: Minimal angulation changes and axial movements of the AT-45 have been demonstrated using pharmacological stimulation and objective measurement methods. The mechanical performance of the AT-45 in the eyes studied does not appear to be sufficient to provide the range of accommodation necessary for close work.

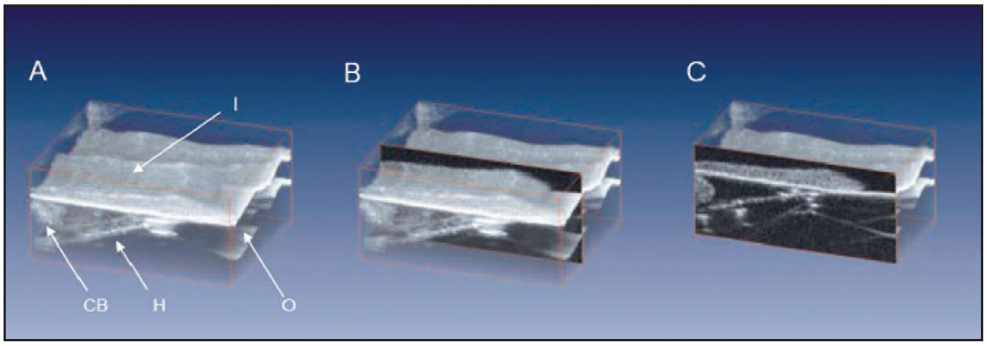

Figure 61: *3D reconstruction (A - C) of the AT-45 haptic region, (71 year old female, 4 weeks after surgery) The optic (O) and haptic (H) are well differentiated. Abbreviations: O – optic, H – haptic, I = iris, CB = ciliary body.*

Axial Shift Principle - Conclusion

Three-dimensional ultrasound biomicroscopy provided information on the accommodative performance of these potentially accommodative IOL designs. Using three-dimensional ultrasound biomicroscopy, corresponding changes in haptic angulation during pharmacological induced accommodation were observed. Pilocarpine-induced ciliary muscle contraction caused a change in haptic angulation and an anterior shift, which resulted in approximately an estimated accommodative amplitude smaller than 1 D. The mechanical performance of the investigated lenses in the eyes studied does not appear to be sufficient to provide the range of accommodation necessary for close work.

Literature

1. Ossoinig, K., Standardized echography: basic principles, clinical applications and results. Int Ophthalmol Clin, 1979. 19 (4): p. 127.
2. Baum, G.,Greenwood, J., Ultrasound in ophthalmology. Am J Ophthalmol, 1960. 49(Feb): p. 249-61.
3. Pavlin, C.,Foster, F., Ultrasound Biomicroscopy of the Eye. 1995, New York: Springer.
4. Berges, O.,Torrent, M., Echographie de l'oeil et de l'orbite. 1986, paris: Vigot.
5. Guthoff, R., Ultrasound in Ophthalmologic Diagnosis - A Practical Guide. 1991, Stuttgart: Thieme Verlag.
6. Guthoff, R., Pauleikhoff, D., Hingst, V., Bildgebende Diagnostik in der Augenheilkunde. 1999, Stuttgart: Enke Verlag.
7. Spalton, D., Hitchings, R., Hunter, P., Atlas der Augenkrankheiten. 1999, Stuttgart: Thieme Verlag.
8. Coleman, D., Lizzi, S., Jack, R., Ultrasonography of the eye and orbit. 1977, Philadelphia: Lea and Febiger.
9. Spallanzani, I., Opere, V. Fabroni, Editor. 1825.
10. Griffin, D., Audible and ultrasonic sounds of bats. Experienta, 1951. 7(12): p. 448-453.
11. Mundt, G.,Hughes, W., Ultrasonics in ocular diagnosis. Am J Ophthalmol, 1956. 41: p. 488.
12. Baum, G.,Greenwood, J., The application of ultrasonic locating techniques to ophthalmology, part 1. Am J Ophthalmol, 1958. 46: p. 319.
13. Oksala, A.,Lehtinen, A., Diagnostic of detachment of the retina by means of ultrasound. Acta Ophthalmol, 1957. 35(5): p. 461-467.
14. Oksala, A.,Lehtinen, A., Diagnostic value of ultrasonics in ophthalmology. Ophthalmologica, 1957. 134(6): p. 387-395.
15. Oksala, A.,Lehtinen, A., Diagnostic of rupture of the sclera by means of ultrasound. Acta Ophthalmol, 1958. 36(1): p. 37-42.
16. Oksala, A.,Lehtinen, A., Measurement of the velocity of sound in some parts of the eye. Acta Ophthalmol, 1958. 36(4): p. 633-639.
17. Buschmann, W.,Haigis, W., Influence of equipment parameters on results in ophthalmic ultrasonography. Doc Ophthalmol Proc Ser, 1981. 29: p. 487.
18. Ossoinig, K.,Till, P., 10 years' study on clinical echography in orbital disease. Bibl Ophthalmol, 1975. 83: p. 200.
19. Ossoinig, K., Kaefring, S., McNutt, L., Weinstock, S., Echographic measurement of the optic nerve. Ultrasound in Medicine, ed. R. Brown. 1977, New York: Plenum Press.
20. Gernet, H., Ultrasonic biometry of the eye. Klin Monatsbl Augenheilkd, 1967. 151(6): p. 853-871.
21. Bronson, N., RFisher, Y., Pickering, N., Trayner, E., Ophthalmic contact B-scan ultrasonography. 1976, Westport, CT: Intercontinental.
22. Pavlin, C., Sherar, M., Foster, F., Subsurface ultrasound microscopic imaging of the intact eye. Ophthalmology, 1990. 97: p. 244.
23. Stachs, O., Martin, H., Behrend, D., Schmitz, K.P., Guthoff, R., Three-dimensional ultrasound biomicroscopy, environmental and conventional scanning electron microscopy investigations of the human zonula ciliaris for numerical modelling of accommodation. Graefe's Arch Clin Exp Ophthalmol, 2005. Oct 5: p. epub ahead of print.
24. Stachs, O., Martin, H., Kirchhoff, A., Stave, J., Terwee, T., Guthoff, R., Monitoring accommodative ciliary muscle function using three-dimensional ultrasound. Graefe's Arch Clin Exp Ophthalmol, 2002. 240: p. 906-912.
25. Coleman, D., Woods, S., Rondeau, M., Silverman, R., Ophthalmic ultrasonography. Radiol Clin North Am, 1992. 30: p. 1105.
26. Silverman, R., Rondeau, M., Lizzi, S., Coleman, D., Three-dimensional high-frequency ultrasonic parameter imaging of anterior segment pathology. Ophthalmology, 1995. 102: p. 837-843.

27. Reinstein, D., Raevsky, T., Coleman, D., Improved system for ultrasonic imaging and biometry. J Ultrasound Med, 1997. 16: p. 117-124.
28. Silverman, R., Lizzi, F., Ursea, B., Rondeau, M., Eldeen, N., Kaliscz, A., Lloyd, H., Coleman, D., High-resolution ultrsonic imaging and characterization of the ciliary body. Invest Ophthalmol Vis Sci, 2001. 42: p. 885-894.
29. Guthoff, R., Techniques in ocular biometry: influences of intraocular pressure and probe contact pressure, in Proceedings , SIDUO XI., G. Cennamo, Editor. 1988, Kluwer: Dordrecht.
30. Winkler, P.,Helmke, K., Duplex-scanning of the deep venous drainage in the evaluation of the bolld flow velocity of the cerebral vascular system in infants. Pediatr Radiol, 1989. 19(2): p. 79-90.
31. Berger, R., Guthoff, R., Helmke, K., Winkler, B., Dräger, J., Dopplersonographische Befunde der Arteria und Vena centralis retineae. Fortschr Ophthalmol, 1988: p. 85.
32. Guthoff, R., Berger, R., Helmke, K., Winkler, B., Dopplersonographische Befunde bei intraokulären Tumoren. Fortschr Ophthalmol, 1989. 86: p. 239.
33. Sherar, M., Starkowski, B., Taylor, W., Foster, F., A 100 Mhz B-scan ultrasound backscatter microscope. Ultrasound Imaging, 1989. 11: p. 95-105.
34. Pavlin, C., Harasiwicz, K., Sherar, M., Foster, F., Clinical use of Ultrasound Biomicroscopy. Ophthalmology, 1991. 98: p. 287-295.
35. Sherar, M.,Foster, F., The design and fabrication of high frequency transducer. Ultrasound Imaging, 1989. 11: p. 75-94.
36. Pavlin, C., Harasiwicz, K., Foster, F., Ultrasound biomicroscopy of anterior segment structures in normal and glaucomatous eyes. Am J Ophthalmol, 1992. 113: p. 381-389.
37. Iezzi, R., Rosen, R., Tello, C., Liebmann, J., Walsh, F., Ritch, R., Personal computer-based 3-dimensional ultrasound biomicroscopy of the anterior segment. Arch Ophthalmol, 1996. 114: p. 520-524.
38. Coleman, D., Silverman, R., Daly, S., Advances in ophthalmic ultrasound. Radiol Clin North Am, 1998. 36: p. 1073-1082.
39. Cusumano, A., Coleman, D., Silverman, R., Reinstein, D., Rondeau, M., Ursea, B., Daly, S., Three dimensional ultrasound imaging - clinical applications. Ophthalmology, 1998. 105: p. 300-306.
40. Stachs, O., Kirchhoff, A., Martin, H., Guthoff, R., 3-D Ultrasonic Imaging of the Ciliary Body Region.
41. Kirchhoff, A., Stachs, O., Guthoff, R., Three-dimensional ultrasound findings of the posterior iris region. Graefe's Arch Clin Exp Ophthalmol, 2001. 239: p. 968-971.
42. Stachs, O., Schneider, H., Stave, J., Guthoff, R., Potentially Accommodating Intraocular Lenses - An In Vitro and In Vivo Study Using Three-dimensional High-frequency Ultrasound. J Refract Surgery, 2005. 21(Jan/Feb 2005): p. 37-45.
43. Schneider, H., Stachs, O., Göbel, K., Guthoff, R., Changes of the accommodative amplitude and the anterior chamber depth after implantation of an accommodative intraocular lens. Graefe's Arch Clin Exp Ophthalmol, 2005. Aug 17: p. Epub ahaed of print.
44. Grasslin, H.,Bagley, E., Studies of peripheral blood vascular. Bull Johns Hopkins Hosp, 1953. 92: p. 47.
45. Hasenfratz, G., Echographische Befunde orbitaler Gefässanomalien bei conjunctivaler Kongestion als Leitsymptom. Fortschr Ophthalmol, 1986. 84: p. 275.
46. Radius, L.,Maumenee, A., Dilated episcleral vessels and open angle glaucoma. Am J Ophthalmol, 1978. 86: p. 31.
47. Ruprecht, K.,Naumann, G., Einseitiges sekundäres Offenwinkelglaukom bei idiopathisch dilatierten episkleralen Gefäßen. Klin Monatsbl Augenheilkd, 1984. 184: p. 23.
48. Jörgensen, J.,Guthoff, R., 24 cases of carotid cavernous fistulas: frequency, symptoms, diagnosis and treatment. Arch Ophthalmol Suppl (Copenh), 1985. 173: p. 67.
49. Feldon, S., Sigelman, J., Albert, D., Smith, T., Clinical manifestations of brawny scleritis. Am J Ophthalmol, 1978. 85: p. 781.
50. Bujara, K., von Domarus, D., Guthoff, R., Necrotic malignant melanoma of the choroid with unusual clinical, echgraphical and histological case study. Ophthalmologica, 1980. 180(4): p. 222-227.
51. Vedel-Jensen, N., Retinal grooves caused by pressure on the globe. Acta Ophthalmol, 1959. 37: p. 279.
52. Wolter, J., Parallel horizontal choroidal folds secondary to an orbital tumor. Am J Ophthalmol, 1974. 77: p. 669.
53. Norton, E., A characteristic fluorescein angiography patern in choroidal folds. Proc Roy Soc Med, 1969. 62: p. 119.
54. Winning, C., Fluorgraphy of choroidal folds, in 165th netherlands Ophthalmologic Society Meeting. 1973: The Hague. p. 436.
55. Newell, F., Choroidal folds. Am J Ophthalmol, 1973. 75: p. 930.
56. Hyvärien, L.,Walsh, F., Benign chorioretinal folds. Am J Ophthalmol, 1970. 70: p. 14.
57. Bird, A.,Sanders, M., Choroidal folds in association with papilloedema. Br J Ophthalmol, 1973. 57: p. 89.
58. Cappaert, W., Purnell, E., Frank, K., Use of B-scan ultrasound in the diagnosis of benign choroidal folds. Am J Ophthalmol, 1977. 84: p. 375.
59. Singh, G., Guthoff, R., Foster, F., Observations on long-term follow-up of posterior scleritis. Am J Ophthalmol, 1986. 101: p. 570.
60. Verbeek, A., Echographic findings in 36 patients with choroidal folds. Doc Ophthalmol Proc Ser, 1981. 29.
61. Phelps, C., Thompson, H., KC, O., The diagnosis and prognosis of atypical carotid cavernous fistula (red-eye-shunt syndrome). Am J Ophthalmol, 1982. 93: p. 423.
62. Rochels, R., Nover, A., Hackelbusch, R., Echographische Befunde und Differentialdiagnostik. Klin Monatsbl Augenheilkd, 1986. 188: p. 101.
63. Esslen, E.,Papst, W., Die Bedeutung der Elektromyography für die Analyse von Motilitätsstörungen der Augen. Bibl Ophthalmol, 1961. 57: p. 168.
64. Guthoff, R., Ultraschall in der ophthalmologischen Diagnostik. Ein Leitfaden für die Praxis. Bücherei des Augenarztes. Beihefte der "Klinischen Monatsblätter für Augenheilkunde", ed. M.H.-J. Naumann GOH, Hollwich F, Gloor B. Vol. 116. 1988, Stuttgart: Enke-Verlag. 182 Seiten.
65. Langenbucher, A., Huber, S., Nguyen, N., Seitz, B., Gusek-Schneider, G., Kuchle, M., measurement of accommodation after implantation of an accommodating posterior chamber intraocular lens. J Cat Refract Surgery, 2003. 29: p. 677-685.
66. Findl, O., Kiss, B., Petternel, V., Menapace, R., Georgopoulus, M., Rainer, G., Drexler, W., Intraocular lens movement caused by ciliary muscle contraction. J Cat Refract Surgery, 2003. 29: p. 669-676.
67. Findl, O., Kriechbaum, K., Menapace, R., Koeppl, C., Sacu, S., Wirtitsch, M., Buehl, W., Drexler, W., Laserinterferometric assessment of pilocarpine-induced movement of an accommodating intraocular lens: a randomized trial. Opthalmology, 2004. 111 (8): p. 1515-1521.

Prof. Dr. med. R. F. Guthoff, MD
Dr. rer. nat. Oliver Stachs, PhD
Universitäts-Augenklinik Rostock
Rostock, Germany

SELBSTSTÄNDIGKEITSERKLÄRUNG

Ich erkläre, dass ich die eingereichte Habilitationsschrift selbstständig und ohne fremde Hilfe verfasst habe, keine außer den von mir angegebenen Hilfsmittel und Quellen dazu verwendet habe und die den benutzten Werken inhaltlich und wörtlich entnommenen Stellen als solche kenntlich gemacht habe.

Rostock, den 15. Juni 2007